UNCLASSIFIED

AD NUMBER
AD877672
LIMITATION CHANGES
TO: **Approved for public release; distribution is unlimited.**
FROM: **Distribution authorized to U.S. Gov't. agencies and their contractors; Critical Technology; OCT 1970. Other requests shall be referred to U.S. Army Aviation Materiel Laboratories, Fort Eustis, VA 23604. This document contains export-controlled technical data.**
AUTHORITY
USAAMRDL ltr, 30 Jul 1971

THIS PAGE IS UNCLASSIFIED

(20)

AD

USAAVLABS TECHNICAL REPORT 70-48

REVERSE-FLOW TURBOSHAFT ENGINE STUDY

By

K. M. Johansen
W. H. Duncan

October 1970

U. S. ARMY AVIATION MATERIEL LABORATORIES
FORT EUSTIS, VIRGINIA

CONTRACT DAAJ02-69-C-0089 NEW

AIRESEARCH MANUFACTURING COMPANY OF ARIZONA
PHOENIX, ARIZONA

This document is subject to special export controls and each transmittal to foreign governments or foreign nationals may be made only with prior approval of U.S. Army Aviation Materiel Laboratories, Fort Eustis, Virginia 23604.

224

DISCLAIMERS

The findings in this report are not to be construed as an official Department of the Army position unless so designated by other authorized documents.

When Government drawings, specifications, or other data are used for any purpose other than in connection with a definitely related Government procurement operation, the United States Government thereby incurs no responsibility nor any obligation whatsoever; and the fact that the Government may have formulated, furnished, or in any way supplied the said drawings, specifications, or other data is not to be regarded by implication or otherwise as in any manner licensing the holder or any other person or corporation, or conveying any rights or permission, to manufacture, use, or sell any patented invention that may in any way be related thereto.

DISPOSITION INSTRUCTIONS

Destroy this report when no longer needed. Do not return it to the originator.

DEPARTMENT OF THE ARMY
HEADQUARTERS US ARMY AVIATION MATERIEL LABORATORIES
FORT EUSTIS, VIRGINIA 23604

This report was prepared by the AiResearch Division of the Garrett Corporation under the terms of Contract DAAJ02-69-C-0089. It consists of detailed cycle analyses of a unique three-spool reverse-flow turboshaft engine and a comparison of this configuration to a conventional two-spool cycle engine of comparable power.

The object of this contractual effort was to define the characteristics of the reverse-flow turboshaft engine in order to assess its capabilities, limitations, and potential as a primary power unit for future Army aircraft.

In general, it can be stated that the unrecuperated reverse-flow turboshaft engine offers no advantage over conventional turboshaft engines. The recuperated version appears to have some potential, although additional analysis of this configuration is required. The conclusions contained herein are concurred in by this Command.

Task 1G162204A01409
Contract DAAJ02-69-C-0089 NEW
USAAVLABS Technical Report 70-48
October 1970

REVERSE-FLOW TURBOSHAFT ENGINE STUDY

Final Report

By

K. M. Johansen

W. H. Duncan

Prepared by

AiResearch Manufacturing Company of Arizona
Phoenix, Arizona

for

U. S. ARMY AVIATION MATERIEL LABORATORIES
FORT EUSTIS, VIRGINIA

ABSTRACT

This report presents the results of a program conducted to investigate the characteristics of a three-spool turboshaft engine having an unconventional turbine arrangement. In this engine, called a three-spool reverse-flow turboshaft engine, the combusted air passes through the high-pressure (HP) turbine, then the power turbine, and finally through the low-pressure (LP) turbine. The performance, weight, envelope, and transient characteristics of this engine were compared to those of a more conventional two-spool turboshaft engine of comparable life and component technology. In addition, the suitability of the three-spool reverse-flow turboshaft engine for recuperation was assessed.

The results of the study indicated that the three-spool reverse-flow turboshaft engine provides better part-power specific fuel consumption (SFC) than the two-spool engine. However, the engine is sensitive to ambient temperature variations, and some of the performance advantage must be compromised by flat-rating the engine to minimize the hot-day power lapse. The flat-rated reverse-flow engine designed for this study produced 5 percent lower SFC at 60 percent power (4000 ft, static, standard-day conditions) than its two-spool counterpart. However, it is somewhat heavier, has a slightly larger envelope (length and diameter) and higher power-output speed, and requires approximately 3 seconds longer to accelerate from flight idle to 95 percent MRP.

The reverse-flow engine component arrangement is well suited for an integrated recuperator. Also, the part-power temperature and airflow of this engine result in approximately 18 percent lower cruise SFC than a comparable recuperated two-spool engine.

FOREWORD

The work described in this report was a joint effort by two divisions of The Garrett Corporation. The design and analysis of the three-spool reverse-flow turboshaft engine were conducted by the Torrance, California, division of AiResearch. The Phoenix Division of AiResearch was responsible for the analysis of the two-spool engine, as well as for overall program management.

The program was sponsored by the United States Army Aviation Materiel Laboratories under Contract DAAJ02-69-C-0089, Task 1G162204A01409. Mr. L. T. Burrows and Mr. P. Chesser of USAAVLABS were the technical monitors for the program.

BLANK PAGE

TABLE OF CONTENTS

TABLE OF CONTENTS - Continued

LIST OF ILLUSTRATIONS

LIST OF ILLUSTRATIONS - Continued

LIST OF ILLUSTRATIONS - Continued

LIST OF ILLUSTRATIONS - Continued

LIST OF ILLUSTRATIONS - Continued

LIST OF ILLUSTRATIONS - Continued

LIST OF ILLUSTRATIONS - Continued

LIST OF ILLUSTRATIONS - Continued

LIST OF TABLES

LIST OF SYMBOLS

A	Area, sq in.
C	Chord, in.
g	32.174 ft/sec^2
h	Enthalpy, Btu/lb
j	778.26 ft-lb/Btu
K	Constant
N	Rotational speed, rpm
P	Pressure
P/P	Pressure ratio
Q	Torque, ft-lb
R	Radius
S	LaPlace operator
T	Temperature, °F
t	Time, hr
U	Tangential velocity, ft/sec
W	Flow
ε	Recuperator effectiveness, %
δ	P/14.7
θ	(T + 460)/518.7
η	Efficiency
τ	Lead time constant

Subscripts

a	Air
ACT	Actual
AD	Adiabatic

AMB	Ambient
AVG	Average
B	Burner
C	Command
ca	Cooling air
CD	Compressor discharge
D	Difference
F	Fuel
g	Gas
gg	Gas generator
H	Hub
HP	High-pressure
l	Leakage
LP	Low-pressure
M	Mean
m	Metal
MAX	Maximum
MIN	Minimum
POLY	Polytropic
PT	Power turbine
Q	Torque
R	Rotor
REF	Reference

T	Tip
T-S	Total-to-static
T-T	Total-to-total
TD	Turbine discharge
X	Axial direction

1. INTRODUCTION

Projected Army aircraft propulsion requirements indicate a need for dependable lightweight turboshaft engines in the range of 500 to 2000 shaft horsepower. Part-power performance for helicopter propulsion systems in particular has become particularly important since the hot-day, altitude, and hover requirements imposed on these craft result in engine operation at low power settings for a significant portion of the normal mission.

To achieve engine performance commensurate with these military requirements, civil and military research and development efforts are being directed toward both component- and cycle-improvement studies. Preliminary studies with an unconventional component arrangement indicated that improved performance characteristics could be obtained for multi-engine helicopters where low part-power fuel consumption is of prime importance. In this engine (shown schematically in Figure 1), air is compressed in a two-spool compressor, combusted, and then passed in order through the HP turbine, power (free) turbine, and finally through the LP turbine. This arrangement, designated as a three-spool* reverse-flow turboshaft engine, is similar to the component arrangement used in the Model ATF3 Turbofan Engine currently under development by AiResearch Los Angeles, a division of The Garrett Corporation.

The objective of the analytical study reported herein was to investigate the operating characteristics of the three-spool reverse-flow turboshaft engine and to assess the inherent differences between this engine concept and a more conventional two-spool turboshaft engine (shown schematically in Figure 2) of comparable technology. The performance, transient characteristics, control requirements, weight, and envelope of the two engine configurations were compared. In addition, the suitability of the three-spool reverse-flow turboshaft engine for recuperation was also assessed.

For brevity in this report, the abbreviation "3S-RF-TSE" will be used for "three-spool reverse-flow turboshaft engine" and the "two-spool turboshaft engine" will be abbreviated as "2S-TSE."

The engines selected for this study were designed with the same life and component technology. Moreover, both were initially designed to operate at maximum turbine inlet temperature (TIT) at military rated power (MRP) for sea-level,

* Sometimes designated "two-and-a-half-spool" rather than "three-spool."

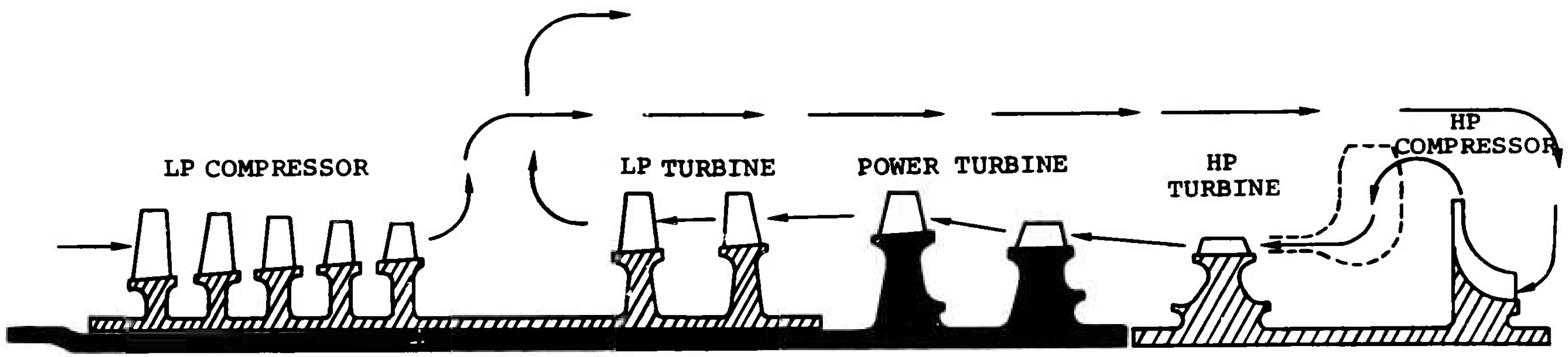

Figure 1. Three-Spool, Reverse-Flow Turboshaft Engine.

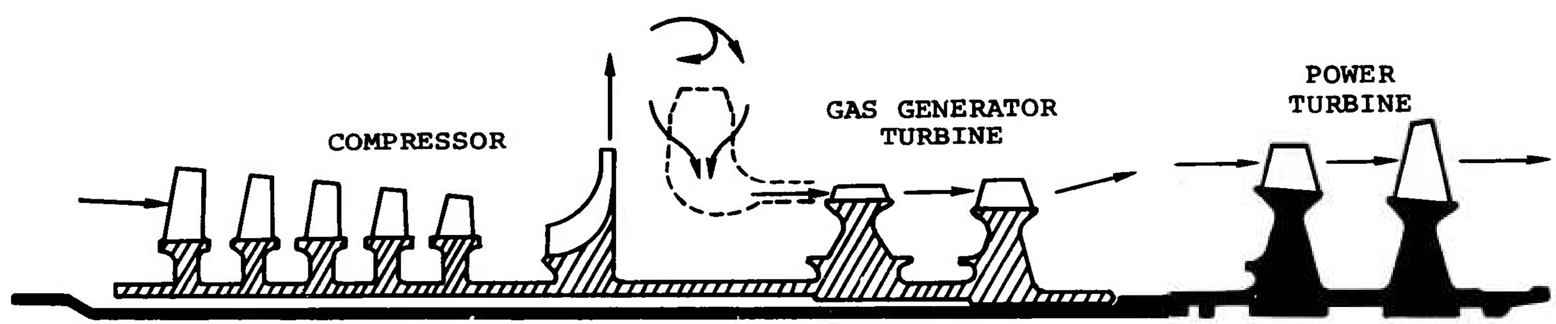

Figure 2. Two-Spool Turboshaft Engine.

static, standard-day conditions. However, as the study progressed and the unique throttling characteristics of the 3S-RF-TSE were defined, the following changes were incorporated:

1. The design-point of both engines was changed to 4000-foot, static, 95°F-day conditions in order to minimize the hot-day power lapse of the 3S-RF-TSE.

2. The rotating speed of the 3S-RF-TSE high-pressure (HP) spool was reduced by 10 percent to extend its life to a level comparable with that of the 2S-TSE, since the initial assumptions used to evaluate turbine life (i.e., part-power temperature, rotating speed, etc.) were shown to be invalid.

The sequence of events described in this report parallels the study as it was conducted. A flow diagram illustrating the individual tasks of the study is shown in Figure 3. Subsequent sections of this report describe the activities conducted to fulfill these tasks and the results of the analysis.

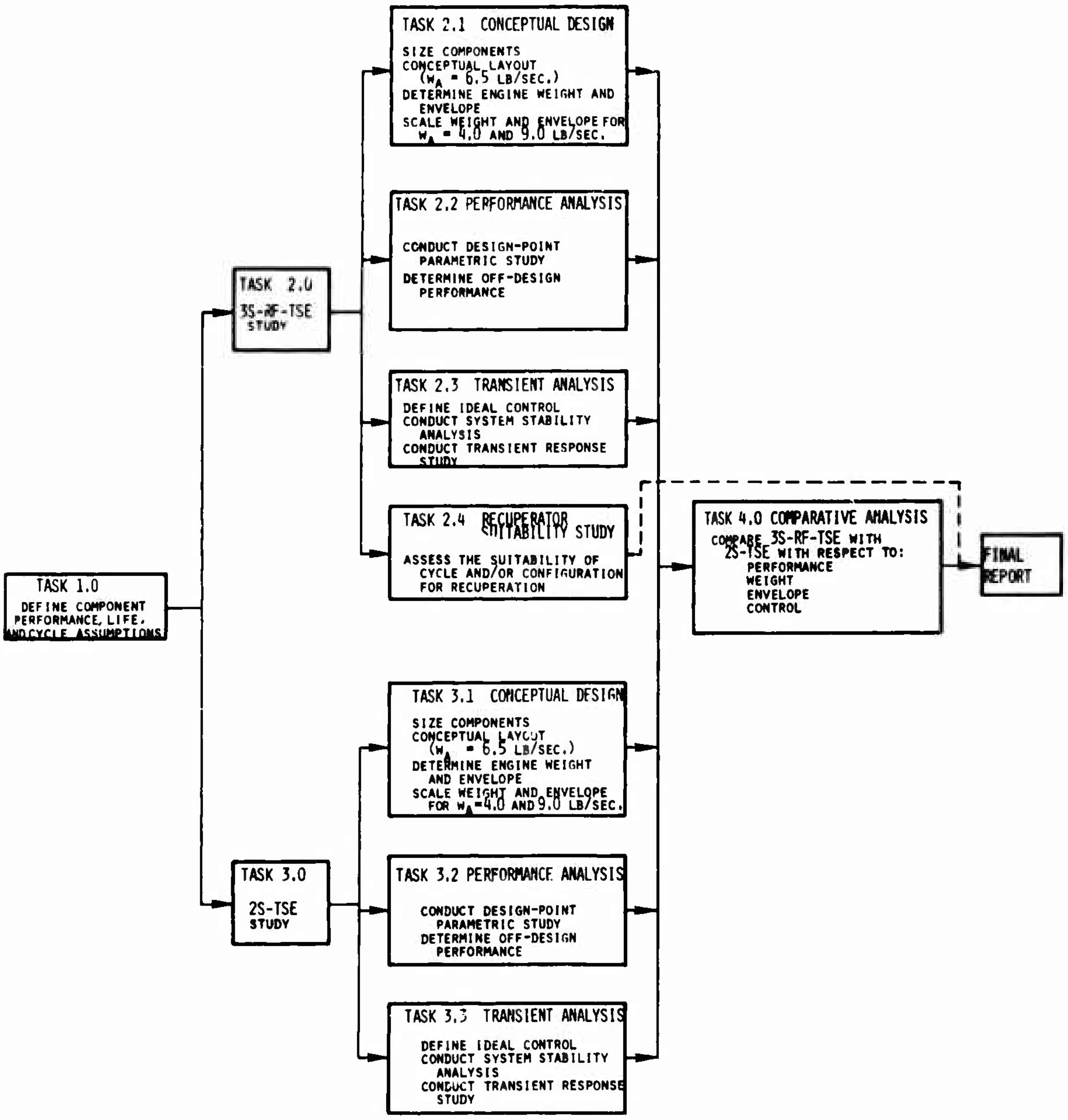

Figure 3. Flow Diagram of Tasks for Reverse-Flow Turboshaft Engine Study.

2. COMMON ENGINE TECHNOLOGY

The comparison of the 3S-RF-TSE and the 2S-TSE was based on equivalent engine life and component technology. The technology used, including compressor and turbine performance, turbine material properties, and turbine cooling effectiveness, was projected to represent levels attainable for small engines following a 3-year development program (i.e., approximately 1972). The component technology and the cycle assumptions used for initial performance and design studies are discussed in the following paragraphs.

2.1 INITIAL DESIGN-POINT SELECTION

Based on preliminary cycle performance studies, a cycle pressure ratio (P/P) of 16 and a turbine inlet temperature (TIT) of 2400°F were selected for both engines. This combination of TIT and P/P represent technology development 3 years hence as stipulated at the outset of the study and, as will be shown later by the results of the final cycle performance studies, a compromise between maximum specific shaft horsepower and minimum specific fuel consumption (SFC). An engine airflow of 6.5 pounds per second was used for sizing the engine layouts and establishing component performance.

2.2 COMPRESSOR TECHNOLOGY

The compressor configuration and nondimensional off-design performance maps used for the 3S-RF-TSE were scaled and modified (to account for size) versions of those used for the Model ATF3 Turbofan Engine. This configuration consists of a five-stage axial LP compressor and a single-stage centrifugal HP compressor. Because of the relative location of these compressors (see again Figure 1), an annular inter-compressor duct connects the LP compressor and the HP compressor. A similar compressor configuration (five-stage axial plus a single-stage centrifugal) was used for the single-spool gas generator of the 2S-TSE.

Efficiencies and P/P's of the axial and centrifugal compressors were selected to reflect the capability and limitations imposed by specific speed, stress, and inlet conditions available for each spooling arrangement. Compressor performance and design data for both engines are presented in Table I. These performance data are also indicated on Figure 4, which shows compressor adiabatic efficiency versus P/P with lines of constant polytropic efficiency. Design-point performance of other compressors is also indicated on this figure for comparison purposes.

TABLE I. COMPRESSOR PERFORMANCE SUMMARY		
	3S-RF-TSE	2S-TSE
Five-Stage Axial Compressor		
P/P	6.0	6.4
N_{ACT}, rpm	34,560	40,800
U_T, ft/sec	1265	1240
Inlet hub-to-tip ratio, R_H/R_T	0.73	0.61
η_{POLY}, %	88.3	87.5
η_{AD}, %	84.1	82.8
Single-Stage Centrifugal Compressor		
P/P	2.67	2.5
N_{ACT}, rpm	75,000	40,800
U_T, ft/sec	1725	1620
Inducer hub-to-tip ratio, R_H/R_T	0.54	0.692
η_{POLY}, %	85.7	85.2
η_{AD}, %	83.5	83.1
Overall Compressor		
P/P	15.55	16
η_{POLY}, %	87.4	88.0
η_{AD}, %	79.3*	80.0

* Efficiency is based on inlet and exit conditions and therefore includes the effects of the inter-compressor duct pressure loss and temperature rise.

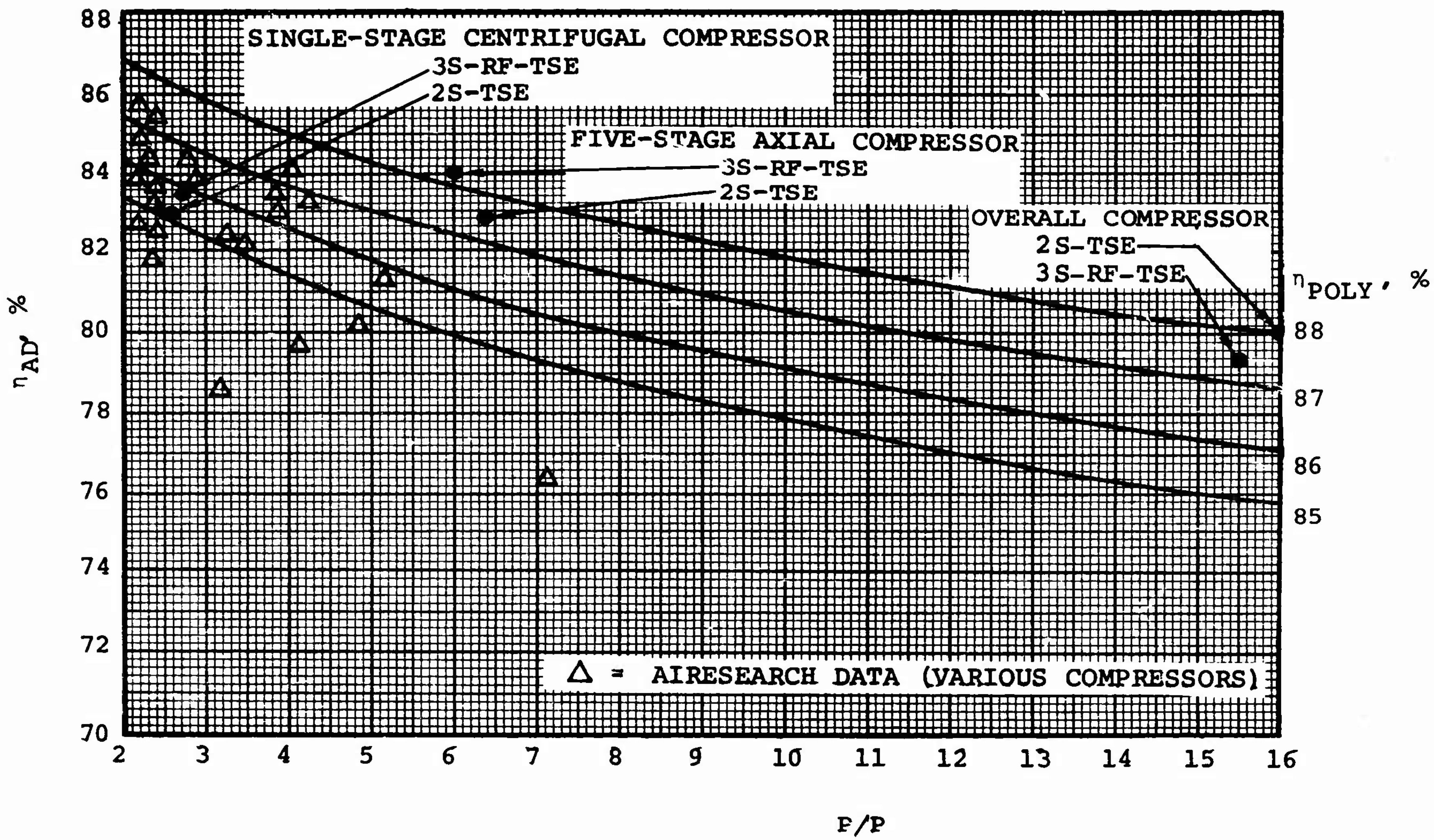

Figure 4. Compressor Technology.

The following items are of interest from Figure 4:

1. Since polytropic efficiency is somewhat indicative of compressor technology, it can be noted that the axial compressor performance reflects the advanced state of the art for these small flow compressors, with polytropic efficiencies greater than 87 percent. However, the inlet conditions and specific-speed restrictions imposed on the centrifugal compressors limit the polytropic efficiencies of these compressors to levels comparable to the current state of the art, as indicated by the other compressor data shown.

2. Efficiencies of the individual compressor components are higher for the 3S-RF-TSE because each rotating group is free to rotate at whatever speed will provide the optimum compressor and/or turbine efficiency (limited only by stress considerations). The compressors on the 2S-TSE are, of course, coupled, which requires a compromise in speed by each compressor component in order to provide for the highest overall compressor performance.

3. Even though the performance of the individual compressor components is higher for the 3S-RF-TSE, the overall compressor performance is penalized by the pressure drop in the inter-compressor duct and by the temperature rise that results as the flow passes over the hot section. Thus, the overall compressor efficiency is 0.7 point lower than that of the 2S-TSE compressor.

A definition of compressor surge margin was required for the transient and off-design studies. The surge margin definition used for these studies is expressed in Equation (1).

$$\text{Surge margin} = \left(\frac{(P/P)_{\text{surge}} \times \left(W_a \frac{\sqrt{\theta}}{\delta}\right)_{\text{operating}}}{(P/P)_{\text{operating}} \times \left(W_a \frac{\sqrt{\theta}}{\delta}\right)_{\text{surge}}} \right)_{\frac{N}{\sqrt{\theta}}} -1.0 \leq 0.04 \qquad (1)$$

where P/P = compressor P/P

$W_a \frac{\sqrt{\theta}}{\delta}$ = corrected flow

$\frac{N}{\sqrt{\theta}}$ = corrected speed

2.3 COMBUSTOR TECHNOLOGY

Combustor technology used for the study is summarized in Table II. The radial temperature profile (referenced to the turbine inlet) is shown in Figure 5.

A slightly higher compressor discharge Mach number for the 3S-RF-TSE (M_{CD} = 0.187 versus 0.172 for the 2S-TSE) resulted in a combustor pressure drop of 4.7 percent compared to 4.0 percent for the 2S-TSE.

TABLE II. COMBUSTOR TECHNOLOGY SUMMARY

	3S-RF-TSE	2S-TSE
$\Delta P/P$, %	4.7	4.0
η, %	99.0	99.0
Pattern factor* (Circumferential)	0.16	0.16

* Pattern factor = $\dfrac{T_{MAX} - T_{AVG}}{T_{AVG} - T_{CD}}$

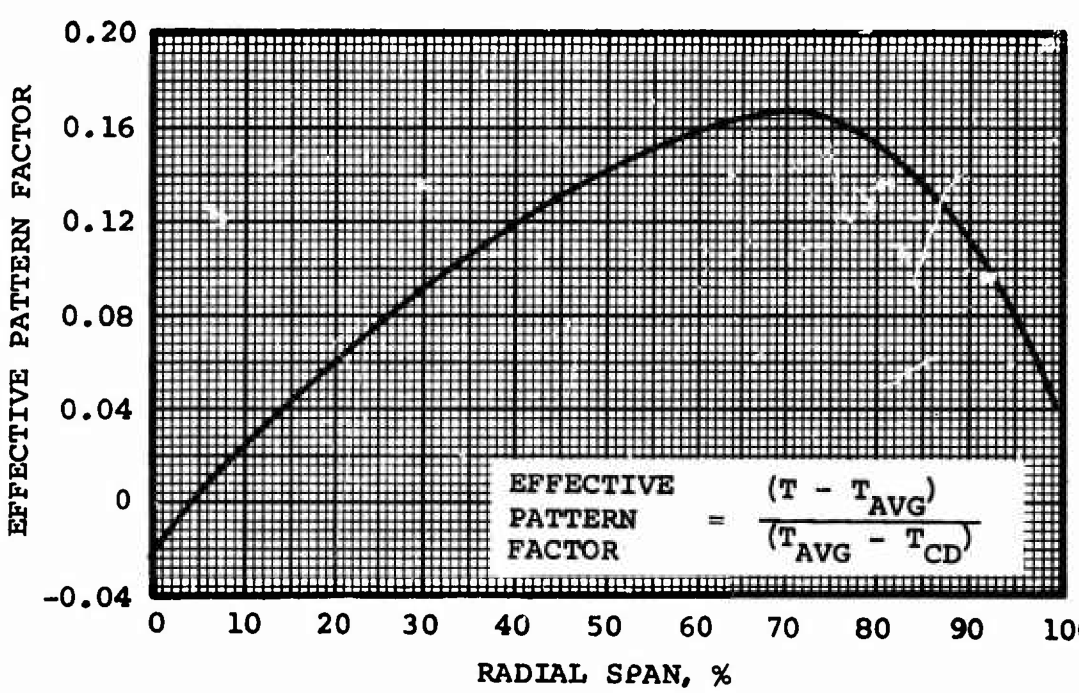

Figure 5. TIT Radial Profile.

2.4 TURBINE TECHNOLOGY

The turbine flow paths and aerodynamic design-point performance were obtained from computerized techniques based on AiResearch and NASA correlations.* Efficiency levels predicted by the correlations account for blading losses only (aerodynamic efficiency) and do not include the losses attributable to rotor-tip clearance and divergence within the stage. Thus, the aerodynamic efficiencies from the correlations were modified by the use of Equations (2) and (3) to account for rotor-tip clearance losses and divergence, respectively.

$$\eta_{\substack{\text{with}\\ \text{clearance}}} = \eta_{\substack{\text{without}\\ \text{clearance}}} \left(1.0 - \frac{R_T}{R_M} \times \frac{\text{clearance}}{(R_T - R_M)} \times K\right) \qquad (2)$$

NOTE:
1. With unshrouded blades, K = 1.7 - 2.0. With shrouded blades, K = 1.0. Thus, shrouded blades are penalized less by clearance, but their base level of efficiency (without clearance) is usually lower.
2. The effect of clearance should be applied to each stage to adequately account for reheat.

$$\eta_{\substack{\text{with}\\ \text{divergence}}} = \eta_{\substack{\text{without}\\ \text{divergence}}} \left(1.077 - 0.077 \frac{A_{exit}}{A_{inlet}}\right) \qquad (3)$$

where A_{exit} = stage exit annulus area, sq in.

A_{inlet} = stage inlet annulus area, sq in.

A summary of the turbine design and performance data is presented in Table III. A two-stage LP turbine was required to drive the LP compressor. Thus, the turbine section of the 3S-RF-TSE contains five axial turbine stages compared to four axial stages for the 2S-TSE turbine. The extra turbine stage, as well as the lower expansion ratio, resulted in a 1.8-percent higher overall turbine efficiency for the 3S-RF-TSE. A more detailed description of the turbine design philosophy is presented in Section 3, Conceptual Design Studies.

*Stewart, Warner L., Warren J. Whitney, and Robert Y, Wong, <u>A Study of Boundary Layer Characteristics of Turbomachine Blade Rows and Their Relation to Overall Blade Loss</u>, ASME Trans., J. of Basic Engr., Paper No. 59-A-23; 1959.

TABLE III. TURBINE PERFORMANCE SUMMARY

Turbine Component	3S-RF-TSE First Stage	3S-RF-TSE Second Stage	2S-TSE First Stage	2S-TSE Second Stage
<u>HP Turbine*</u>				
Inlet corrected flow, $W_a \frac{\sqrt{\theta}}{\delta}$ (lb/sec)	0.922	-	0.903	-
N_{ACT}, rpm	75,000	-	40,800	40,800
Stator aspect ratio, $\frac{R_T - R_H}{C_X}$	0.56	-	0.43	0.62
Rotor blade height $(R_T - R_H)$, in.	0.400	-	0.400	0.700
Rotor tip clearance, in.	0.015	-	0.015	0.015
Rotor hub-to-tip ratio, R_H/R_T	0.795	-	0.902	0.831
Stage P/P	1.81	-	2.07	2.07
Stage divergence $(A_{exit} - A_{inlet})/A_{inlet}$	0.23	-	0.11	0.48
Velocity ratio/stage, $U_M/\sqrt{2gJ\Delta h}$	0.67	-	0.61	0.61
η_{T-T}, %	87.9	-	-	85.0**
Maximum allowable disk stress, psi	80,000	-	80,000	80,000
<u>Power Turbine</u>				
Inlet corrected flow, $W_a \frac{\sqrt{\theta}}{\delta}$ (lb/sec)	1.645	-	3.43	-
N_{ACT}, rpm	46,000	46,000	34,450	34,450
Stator aspect ratio, $\frac{R_T - R_H}{C_X}$	0.75	2.34	1.30	2.30
Rotor hub-to-tip ratio, R_H/R_T	0.75	0.70	0.72	0.59
Stage P/P	1.71	1.71	1.87	1.87
Velocity ratio/stage, $U_M/\sqrt{2gJ\Delta h}$	0.63	0.65	0.65	0.68
η_{T-T}, %	-	89.7**	-	92.2**
<u>LP Turbine</u>				
Inlet corrected flow, $W_a \frac{\sqrt{\theta}}{\delta}$ (lb/sec)	4.56	-	-	-
N_{ACT}, rpm	34,560	34,560	-	-
Stator aspect ratio, $\frac{R_T - R_H}{C_X}$	2.66	3.50	-	-
Rotor hub-to-tip ratio, R_H/R_T	0.675	0.545	-	-
Stage P/P	1.57	1.57	-	-
Velocity ratio/stage, $U_M/\sqrt{2gJ\Delta h}$	0.70	0.70	-	-
η_{T-T}, %	-	91.90**	-	-
<u>Overall</u>				
η_{T-T}, %	91.0		89.3	

*Data applies to the gas generator turbine of the 2S-TSE.
**Combined two-stage efficiency.

2.5 ENGINE LIFE AND TURBINE COOLING FLOW

Both engines were designed for a minimum life of 5000 hours with the mission profile shown in Table IV. An accumulative damage law [Equation (4)] was used to transform this mission profile into an equivalent time at MRP for evaluating turbine cooling-flow requirements.

TABLE IV. MISSION PROFILE

MRP (%)	Percent Engine Life at This (%) Power
100	10
75	15
60	60
35	10
5 (idle)	5

$$\text{Equivalent time} = \text{minimum engine life} \times \text{LIFE}_{MRP} \times \sum_{i=1}^{n} \frac{k_i}{\text{LIFE}_i} \qquad (4)$$

where

Minimum engine life = 5000 hours

LIFE_{MRP} = stress-rupture life at MRP

k_i = portion of mission $\frac{\%}{100}$ required for each step of the mission profile

LIFE_i = stress-rupture life at each step of the mission profile

Several iterations were required to finally evaluate the equivalent life and cooling flow. Part-power cycle performance data were necessary to determine the cycle parameters affecting life (stress and temperatures) at each step in the mission profile. Also, special considerations were required to minimize the hot-day power lapse for the 3S-RF-TSE (discussed in Section 4.3).

The calculation procedure used for evaluating equivalent life at MRP and turbine cooling flow is outlined in Paragraph 2.5.1. TIT radial profile, cooling effectiveness correlations, and stress-rupture properties used for these calculations are presented in Figures 5, 6, and 7, respectively. The resulting cooling-flow requirements for the two engines are presented in Table V.

TABLE V. TURBINE COOLING-FLOW REQUIREMENTS

	3S-RF-TSE (% W_a)	2S-TSE (% W_a)
First vane, W_{ca}	2.0	2.0
First blade, W_{ca}	3.0	2.8
Second vane, W_{ca}	1.2	1.2
Second blade, W_{ca}	0.8	1.6
Seals, disks, and shrouds, W_{ca}	3.2	3.2
TOTAL	10.2	10.8

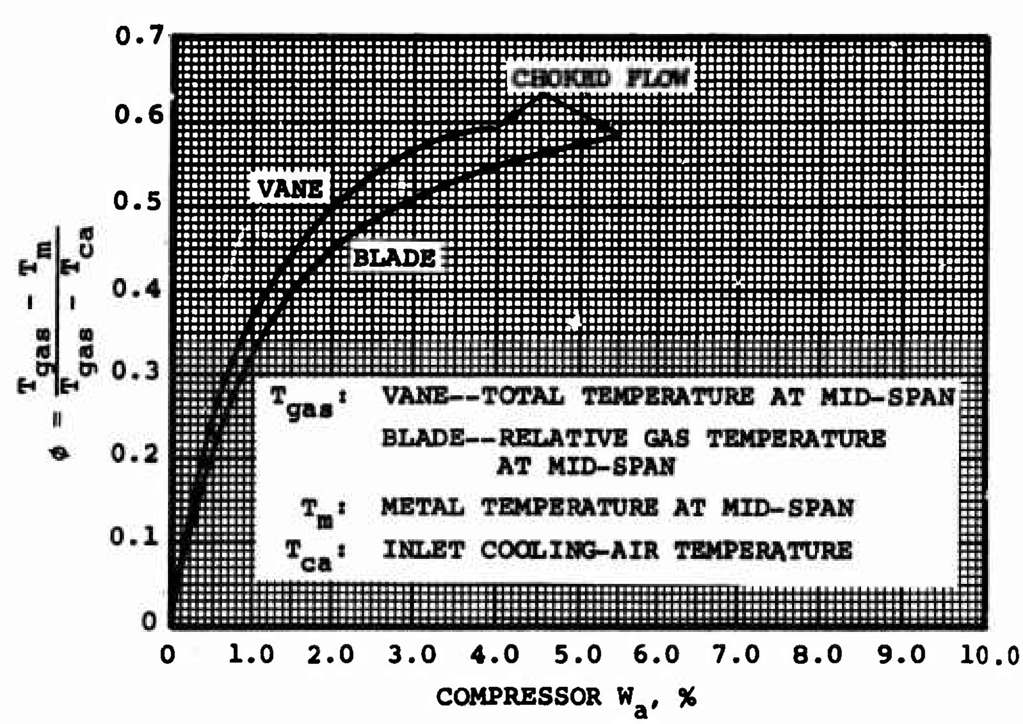

Figure 6. Vane and Blade Cooling Requirements.

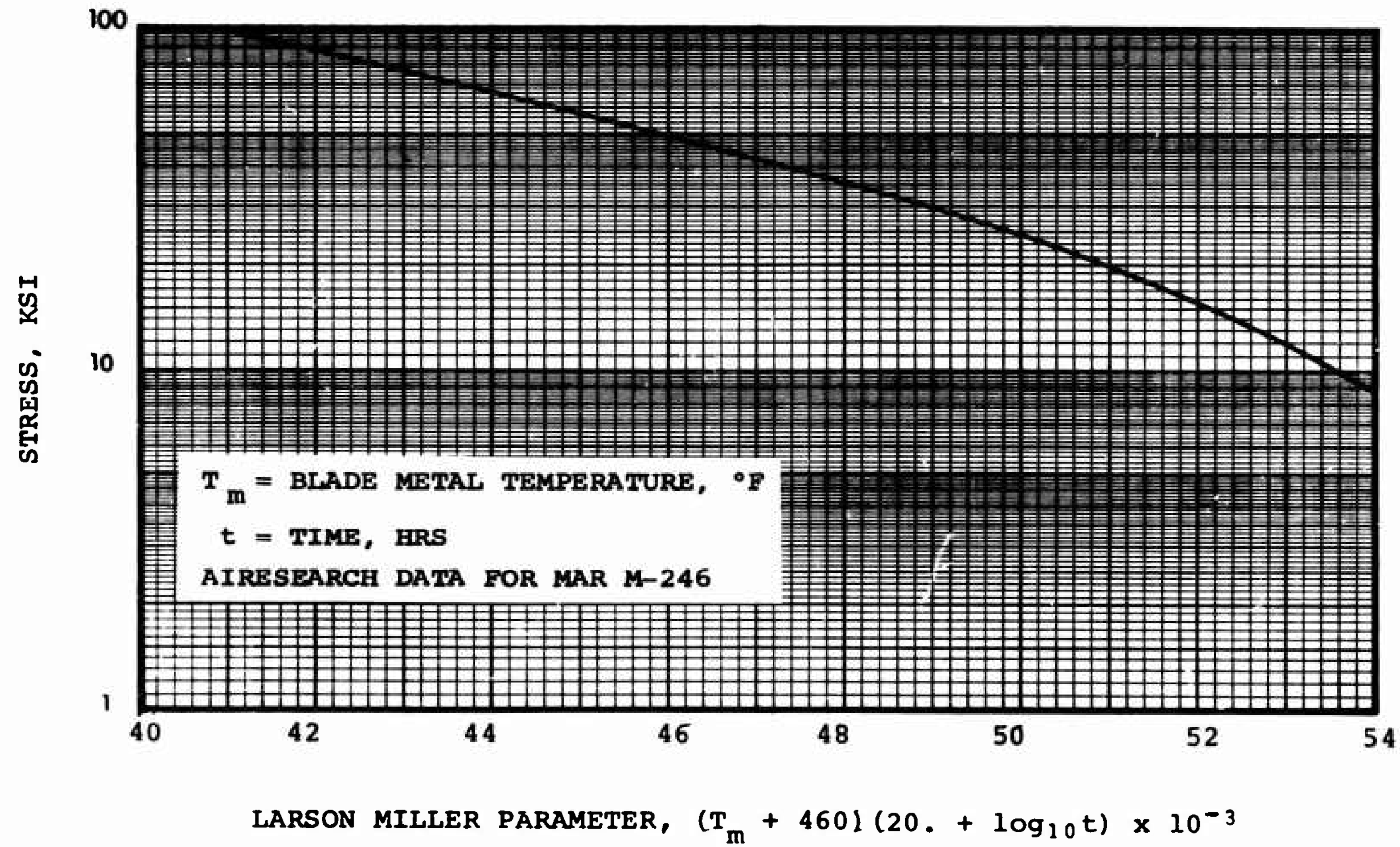

Figure 7. Turbine Blade Stress-Rupture Properties.

2.5.1 Engine Life Calculation Procedure

The steps for evaluating equivalent life at MRP and turbine cooling flow are as follows:

1. Define the following:

   $\left.\begin{array}{l}\text{TIT}\\ \text{P/P}\\ \text{Compressor speed}\\ \text{Gas generator speed}\end{array}\right\}$ at MRP

   Turbine geometry

   Stress-rupture properties

   Maximum stator metal temperature = 1800°F

   TIT radial profile

   Correlation of cooling effectiveness (ϕ)* versus cooling flow

2. Estimate the equivalent life at MRP based on the mission profile.

3. Calculate cooling flow (first pass) for rotors based on an assumed equivalent life.

4. Estimate a total turbine cooling flow and calculate off-design performance to define the following at each step in the mission profile:

   TIT

   T_{CD}

   Rotor blade stress

5. Determine rotor metal temperature at each step in the mission profile using the cooling flow at MRP.

6. Based on the metal temperature from Step 5 and the stress from Step 4, determine a new equivalent life at MRP using Equation (4).

7. Determine cooling flow in stators, rotors, shrouds, disks, and seals (approximately) for the new equivalent life.

8. Iterate from Step 3 for final cooling flow and equivalent life.

$$*\phi = \frac{T_{gas} - T_m}{T_{gas} - T_{ca}}$$

3. CONCEPTUAL DESIGN STUDIES

3.1 LAYOUT

Conceptual engineering design drawings prepared for the 3S-RF-TSE and the 2S-TSE are presented in Figures 8 and 9, respectively. Manufacturing and mechanical limitations are, of course, inevitably associated with small, high-temperature, high P/P gas turbine engines. Thus, the conceptual design studies that were conducted for these engines are intended primarily to indicate weight, envelope, and a general mechanical feasibility of the engine concepts.

Rotating components were sized for sea-level, static, standard-day conditions, TIT = 2400°F, P/P = 16, and airflow = 6.5 pounds per second. Compressor and turbine geometry and speeds were selected to provide optimum component performance within the framework of the basic flow path.

Compressor design features are indicated in Table I. The inlet hub-to-tip ratio on the 3S-RF-TSE axial compressor is somewhat higher than for the 2S-TSE (0.73 and 0.61, respectively) because the LP turbine that drives the compressor has a large diameter and thus requires a low speed to avoid excessive stress. Backward-swept blades were employed on the centrifugal compressors to extend their range and provide the required speed match with the turbine. Somewhat higher leakage is encountered with the 3S-RF-TSE in order to thrust-balance the LP spool. As the air flows through the inner compressor duct, its temperature increases by 12 degrees as a result of heat transfer from the hot combustor/turbine section. In addition, it encounters a 3.0-percent loss in total pressure.

The characteristics of the 3S-RF-TSE compressor are such that the surge margin available is adequate for all throttle settings and transient conditions without the assistance of either variable geometry or bleed. Variable stator geometry, however, was required for the 2S-TSE compressor. A cursory study indicated that a 15-degree closure below 90 percent speed would yield satisfactory surge-margin characteristics.

Combustor volume was selected to provide restart capability to an altitude of 25,000 feet. Modular designs were employed on both engines to permit access to the hot section to facilitate inspection and component replacements. Vaporizer-type fuel nozzles are illustrated on the 2S-TSE layout and an atomizer-type nozzle on the 3S-RF-TSE.

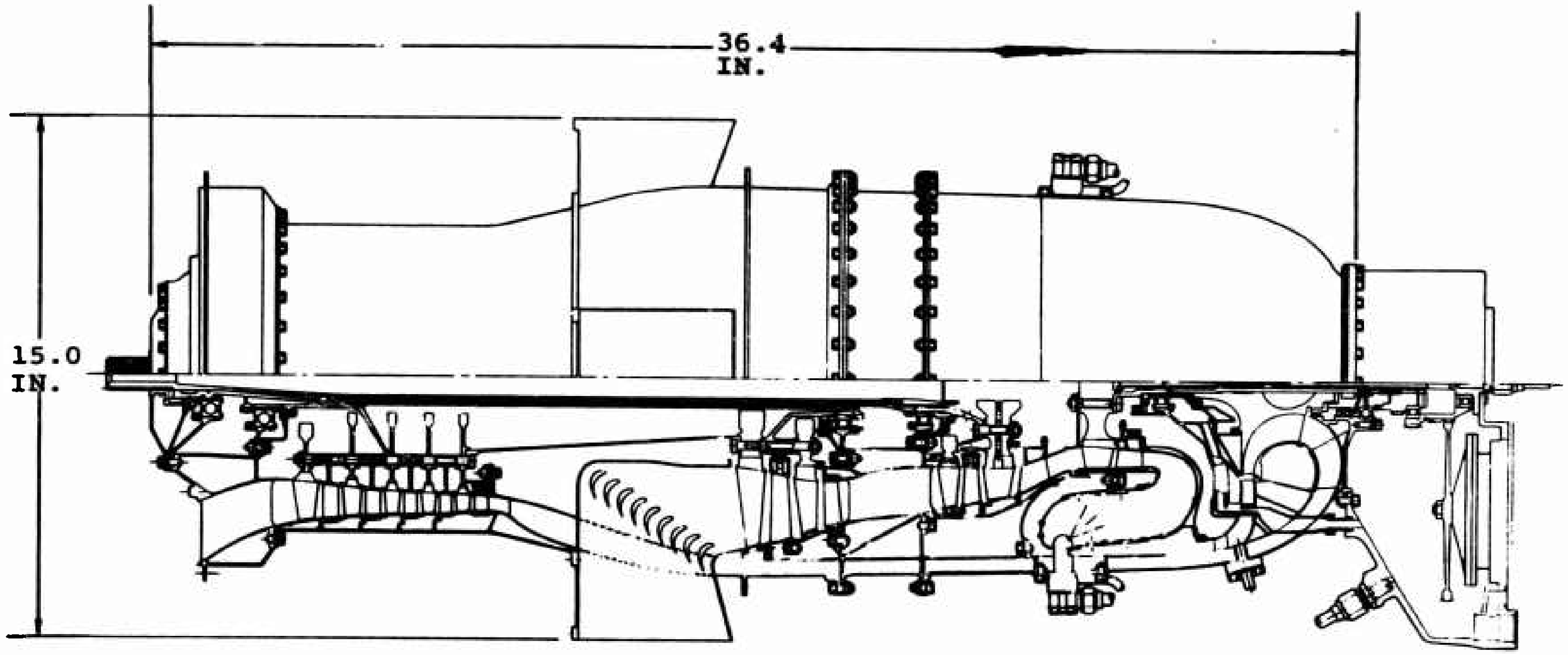

Figure 8. Conceptual Layout, 3S-RF-TSE.

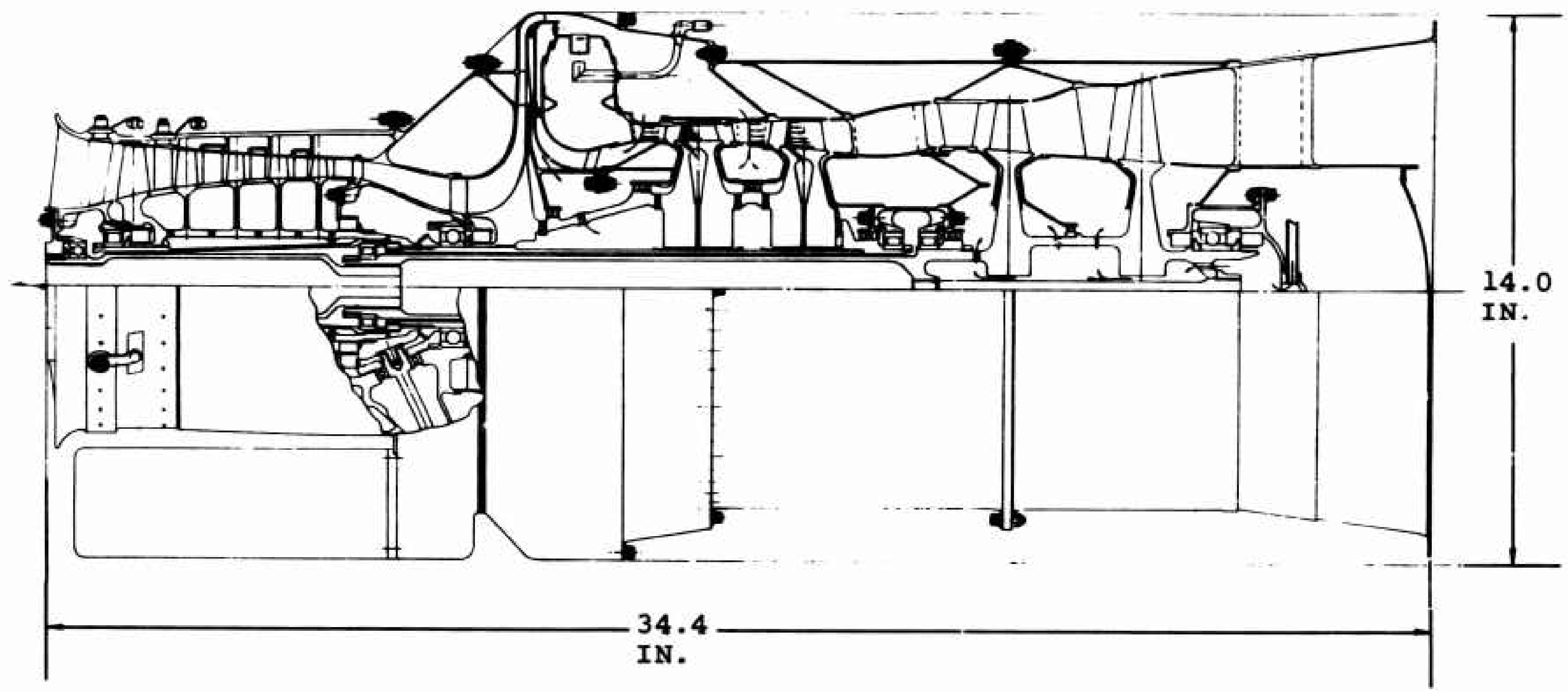

Figure 9. Conceptual Layout, 2S-TSE.

The combination of low airflow and high cycle P/P results in a small annulus for the HP turbine, and tip-clearance effects severely penalize performance. A minimum blade height of 0.400 inch was used, along with a tip clearance of 0.015 inch. For the 2S-TSE, where large disk bores were required for the concentric power shaft, split fabricated HP turbine disks were employed with internal passages for blade cooling. An allowable tangential disk stress of 80,000 psi was assumed for both designs.

The turbines were designed around the constant mean-line concept. Appropriate speeds, diameters, and blade chord lengths were selected to produce acceptable values of aspect ratio, hub-tip ratio, etc., as previously delineated in Table III.

A higher power-spool speed was selected for the 3S-RF-TSE (46,000 rpm versus 34,450 rpm for the 2S-TSE) in order to select a diameter for optimum transition between the HP and the LP turbines

In order to minimize the divergence loss through the power turbine second stage for the 2S-TSE, an interstage diffuser was employed. Even though it created a 1.5-inch increase in the length of the engine, it was deemed advisable in order to obtain the quoted performance.

Particular attention was required for the design of the exhaust diffuser and turning cascade in the 3S-RF-TSE. To minimize the total pressure loss, the low-velocity LP turbine exit flow is accelerated through the cascade from a Mach number of 0.35 to 0.45. The flow is then decelerated to the exhaust-diffuser exit through four rectangular ducts with a half-divergence angle of 7 degrees. This design provides for a dynamic pressure recovery of 0.60 and a total pressure loss of 4.5 percent (compared to 0.5 and 3.8 percent, respectively, for the 2S-TSE diffuser).

Both layouts provide for power extraction at the forward end of the engine. Because of diametral restrictions imposed by the gas generator spool, inner shaft bearings were required on the 2S-TSE to provide acceptable critical-speed characteristics on the power shaft. The critical-speed characteristics of the 3S-RF-TSE were found to be acceptable without inner shaft bearings.

The control, starter, pumps, etc., are driven by, and thus are located aft of, the HP spool on the 3S-RF-TSE. For the 2S-TSE, these components are driven by a tower shaft from the gas generator spool and situated around the axial compressor without affecting the engine envelope. A somewhat similar arrangement could, of course, have been adopted for the 3S-RF-TSE, but only at the expense of engine diameter and mechanical complexity.

3.2 WEIGHT AND ENVELOPE

Engine weight and envelope were determined from the conceptual layouts. Bare engine weight (dry, without accessories, control, etc.) was determined by multiplying the volume of each component by the density of an appropriate material. Geometrically similar (scaled) layouts were prepared for engines having airflows of 4.0 and 9.0 pounds per second. Based on these layouts, engine weight and envelope over this range of airflows were determined. The results (shown in Figure 10) indicate that the 3S-RF-TSE is somewhat larger and heavier than the selected 2S-TSE configuration having the same airflow.

While the envelope differences are small, the weight of the 3S-RF-TSE is greater than that of its two-spool counterpart, with some of the weight increase attributable to (a) the bearing and support requirements for the third spool, (b) the additional turbine stage required for the LP turbine, and (c) the annular inner compressor duct.

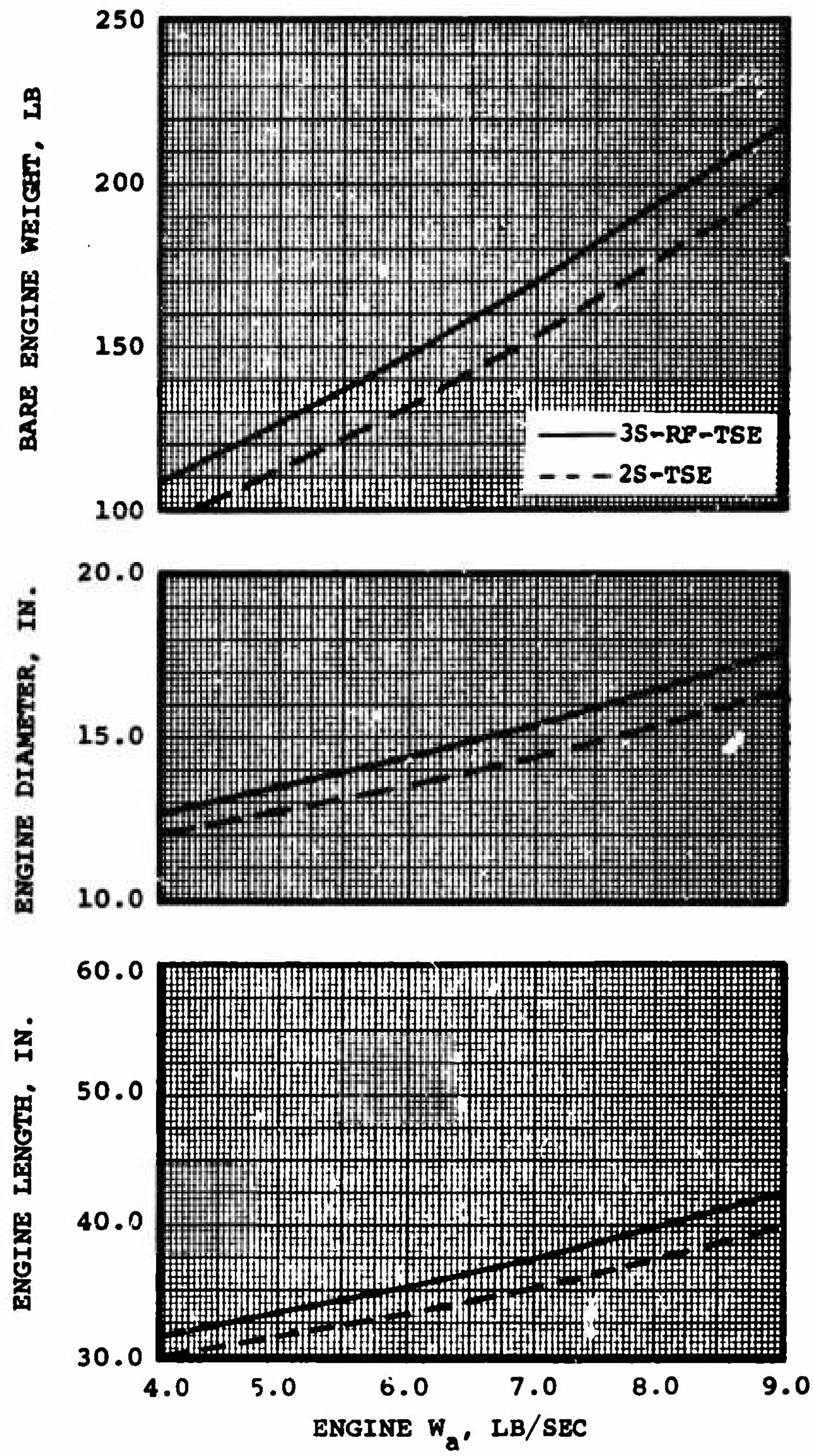

Figure 10. Bare Engine Weight, Diameter, and Length Versus Airflow.

4. PERFORMANCE

Based on the technology and assumptions presented in Section 2, parametric cycle performance studies were conducted for the two engine configurations. The final design point was selected to optimize part-power performance while minimizing hot-day power lapse. Off-design performance studies were conducted for various ambient conditions to determine the effects of throttling, altitude, flight speed, and ambient temperature. An in-depth study of the reverse-flow cycle thermodynamics was conducted to explain the unique performance characteristics that result from an engine having the component arrangement.

4.1 CYCLE PERFORMANCE STUDIES

Parametric cycle performance studies were conducted for the two engine configurations representative of the 4.0- to 9.0-pound-per-second airflow range covering cycle P/P's of 10.0 to 20.0 and TIT's from 2000°F to 2500°F. The following assumptions were used for these parametric studies:

1. Standard, sea-level, static conditions
2. Compressor efficiencies (polytropic) = constant
3. Turbine efficiencies (adiabatic) = constant
4. Total pressure and leakage losses = constant
5. Turbine cooling flow = f(P/P and TIT)
6. For the 3S-RF-TSE LP compressor and HP compressor, P/P's were varied as shown in Table VI.

TABLE VI. COMPRESSOR P/P VARIATION FOR CYCLE STUDIES

$(P/P)_{cycle}$	$(P/P)_{LP\ compressor}$	$(P/P)_{HP\ compressor}$
10.0 - 16.0	3.67 - 6.0	2.67 (constant)
16.0 - 20.0	6.0 (constant)	2.67 - [illegible].33

Component performance, duct losses, assumptions, etc., used for these studies are presented in Table VII.

TABLE VII. CYCLE ASSUMPTIONS

	3S-RF-TSE	2S-TSE
Inlet		
W_a, lb/sec	6.5	6.5
Pressure drop, $\Delta P/P$ (%)	0	0
Axial Compressor		
P/P	3.67 - 6.0	5.07 - 6.72
η_{POLY}, %	88.3	87.5
Inner Compressor Duct		
Pressure loss, $\Delta P/P$ (%)	2.9	-
Temperature rise, ΔT (°F)	12.0	-
Centrifugal Compressor		
P/P	2.67 - 3.33	1.97 - 2.98
η_{POLY}, %	85.7	85.2
Overall Compressor		
P/P	10.0 - 20.0*	10.0 - 20.0
W_1, % W_a	3.0	1.5
Combustor		
Pressure drop, $\Delta P/P$ (%)	4.7	4.0
$\eta_{[illegible]}$, %	99.0	99.0
[illegible]l LHV,** Btu/lb	18,400	18,400
H[illegible] Turbine		
η_{T-T}, %	87.9	85.1
TIT, °F	2000 - 2500	2000 - 2500
Turbine Duct		
Pressure drop, $\Delta P/P$ (%)	2.0	2.0
Power Turbine		
η_{T-T}, %	89.7	92.2
LP Turbine		
η_{T-T}, %	91.9	-

TABLE VII - Continued		
	3S-RF-TSE	2S-TSE
Exhaust Duct		
Pressure drop, $\Delta P/P$ (%)	4.10	3.80
Exhaust nozzle, P/P	1.06	1.02
Mechanical Losses		
Accessories, bearings, etc., hp	9.75	9.75

*$P/P = (P/P)_{LP\ compressor} \times (P/P)_{HP\ compressor}$.
**Lower heating value.

The results of the MRP parametric studies for the 3S-RF-TSE and the 2S-TSE are shown in Figures 11 and 12, respectively. These figures present specific shaft horsepower versus SFC for lines of constant-cycle P/P and TIT. For comparison, the envelope of the 3S-RF-TSE parametric study from Figure 11 is superimposed on that of the 2S-TSE in Figure 12. While the results are relatively coincident because of the comparable component technology used for the two engines, the 2S-TSE MRP performance is somewhat better (displaced toward lower SFC and higher specific shaft horsepower) at lower P/P's because of inherently lower pressure losses and thrust-balance leakage than in the 3S-RF-TSE. The shapes of the constant-temperature and P/P lines are different for the two engines because of increasing significance of the unique losses in each cycle. For example, consider a constant temperature line (TIT = 2000°F) with varying cycle P/P from Figure 12.

As will be explained in Paragraph 4.3, the 3S-RF-TSE configuration requires a higher exhaust diffuser P/P than does the 2S-TSE [$(P/P)_{exhaust}$ = 1.06 and 1.02, respectively]. The unavailable energy tied up in the higher exhaust diffuser P/P (held constant for this parametric cycle study) represents a greater portion of the total compressor work at the low cycle P/P.

As a result of this type of phenomenon, the 3S-RF-TSE displays somewhat different characteristics and, in fact, suggests a different optimum cycle P/P for minimum SFC. However, as was indicated previously, at a TIT of 2400°F, the P/P of 16.0 represents a reasonable compromise between minimum SFC and maximum specific shaft horsepower for both engines.

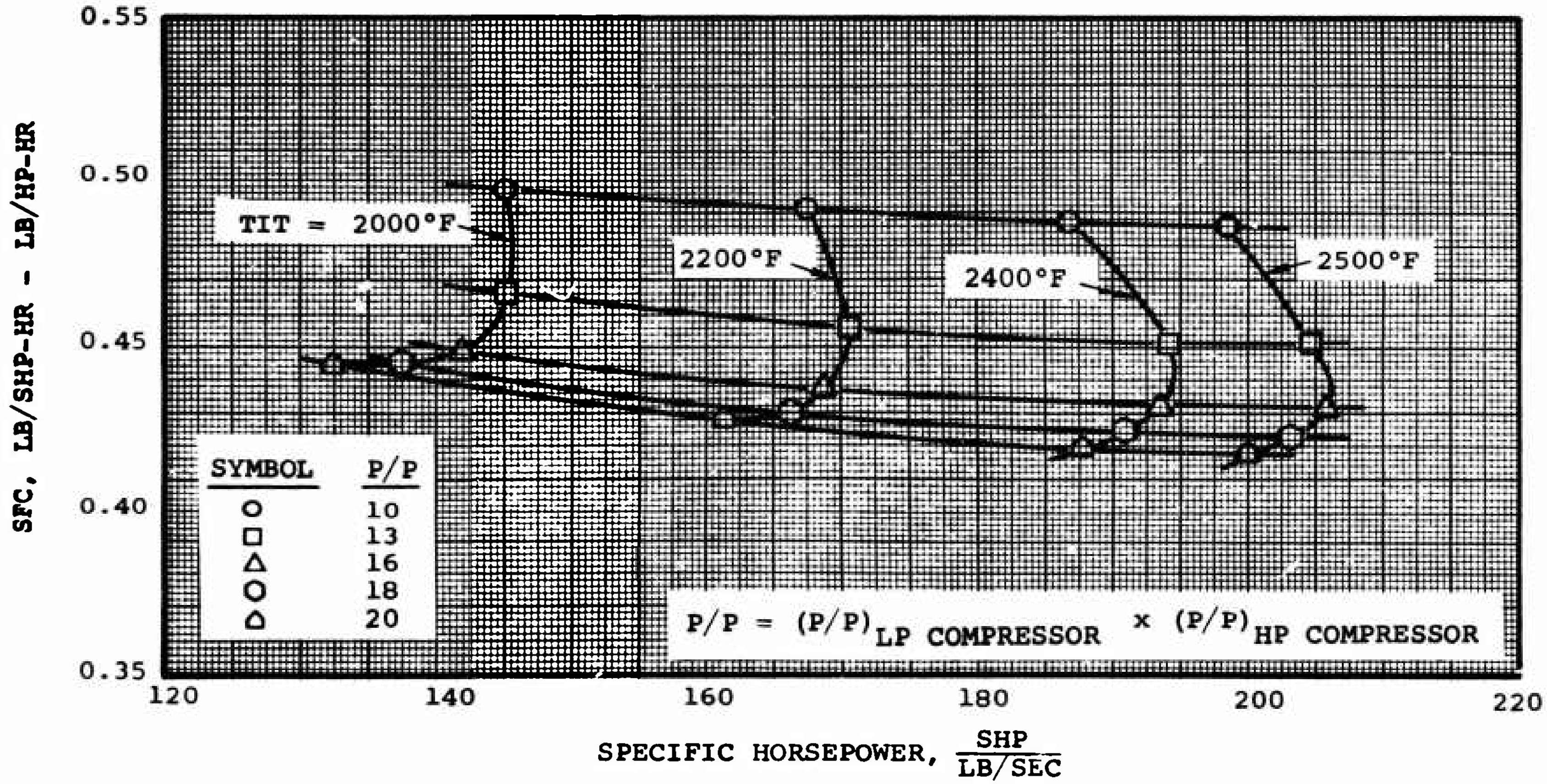

Figure 11. Parametric Performance Study for 3S-RF-TSE Configuration.

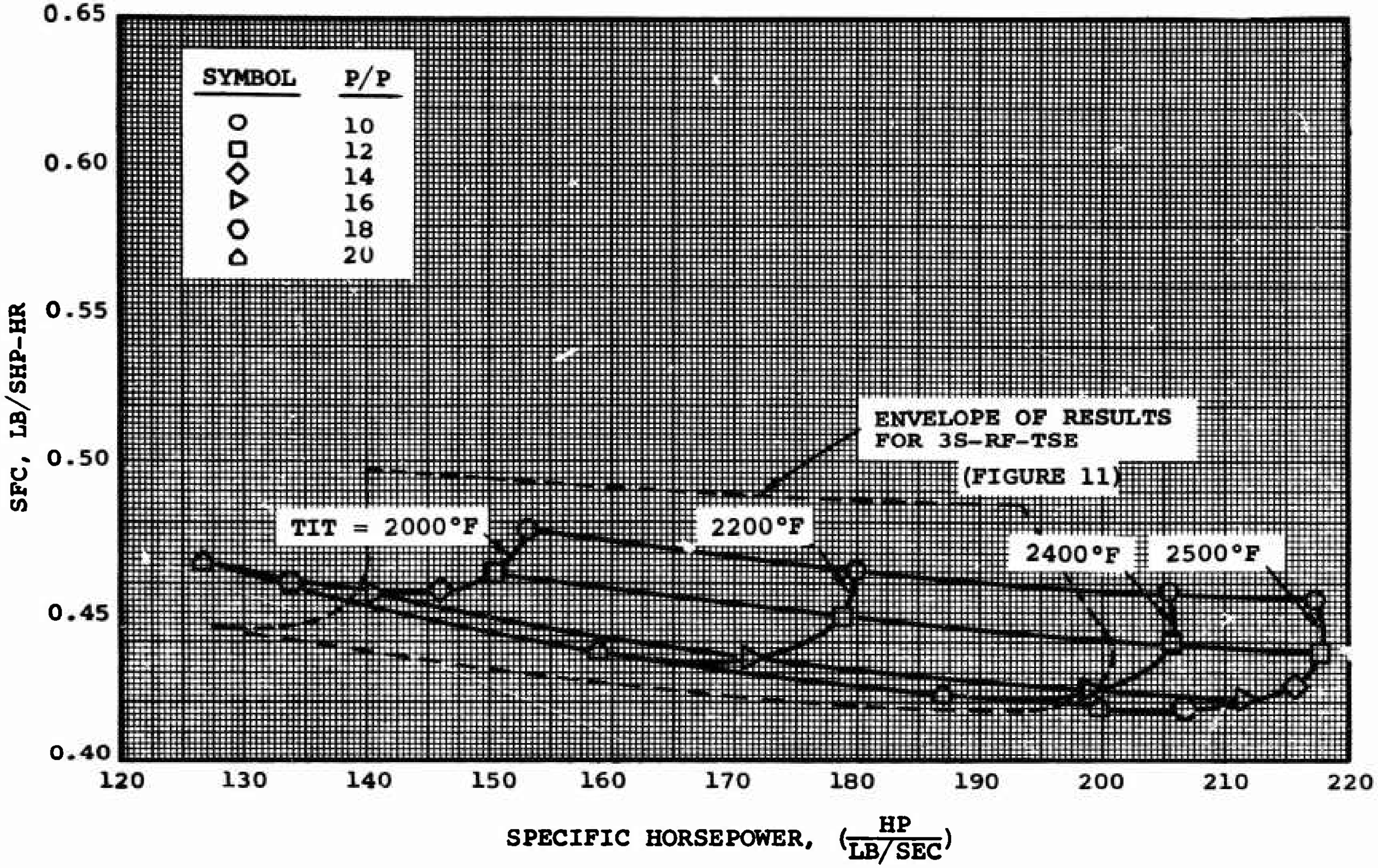

Figure 12. Parametric Performance Study for 2S-TSE Configuration.

4.2 OFF-DESIGN PERFORMANCE CHARACTERISTICS

One of the primary objectives of the study was to demonstrate low part-power SFC for both engines. Previous studies have shown that for the conventional 2S-TSE, significant part-power performance improvement can be obtained by selecting a match point for the compressors and turbines such that their peak aerodynamic efficiencies occur at part power. Of course, this technique imposes a penalty on the SFC and shaft horsepower at MRP for a given TIT. In order to make the part-power SFC of the 2S-TSE as competitive as possible (without the complexity of such devices as variable turbine geometry), the components were optimized at approximately 60 percent MRP, as shown in Figure 13.

Typical behavior of the 3S-RF-TSE off-design compressor and turbine efficiencies are shown in Figure 14. Analysis has shown that no improvement can be made in off-design cycle performance for this engine by optimizing the components for 60 percent power in lieu of maximum power. Both compressors operate with relatively constant efficiency between MRP and 60 percent power. Relatively constant stage loading from MRP down to 60 percent power (discussed later in detail) results in constant efficiency for the HP turbine and power turbine and only 1/2-percent point drop in LP turbine efficiency at 60 percent power.

Off-design performance (SFC and shaft horsepower) of the two engine configurations is shown in Figure 15. Also shown is the estimated off-design performance of the 2S-TSE with the components optimized at MRP. As the preliminary studies had shown, the part-power SFC of the 3S-RF-TSE is approximately 5 percent lower than the more conventional 2S-TSE, even with the latter optimized at 60 percent MRP. A study of the cycle thermodynamics showed the improved performance to be a result of the turbine arrangement on the 3S-RF-TSE and that off-design operating characteristics of the engine were unlike those of the more conventional turbine cycles. The most notable characteristics of the 3S-RF-TSE cycle during part-throttle operation from MRP to 60 percent power are that:

1. It drops rapidly in engine airflow.

2. It produces high power turbine specific work.

3. It holds relatively constant component efficiencies.

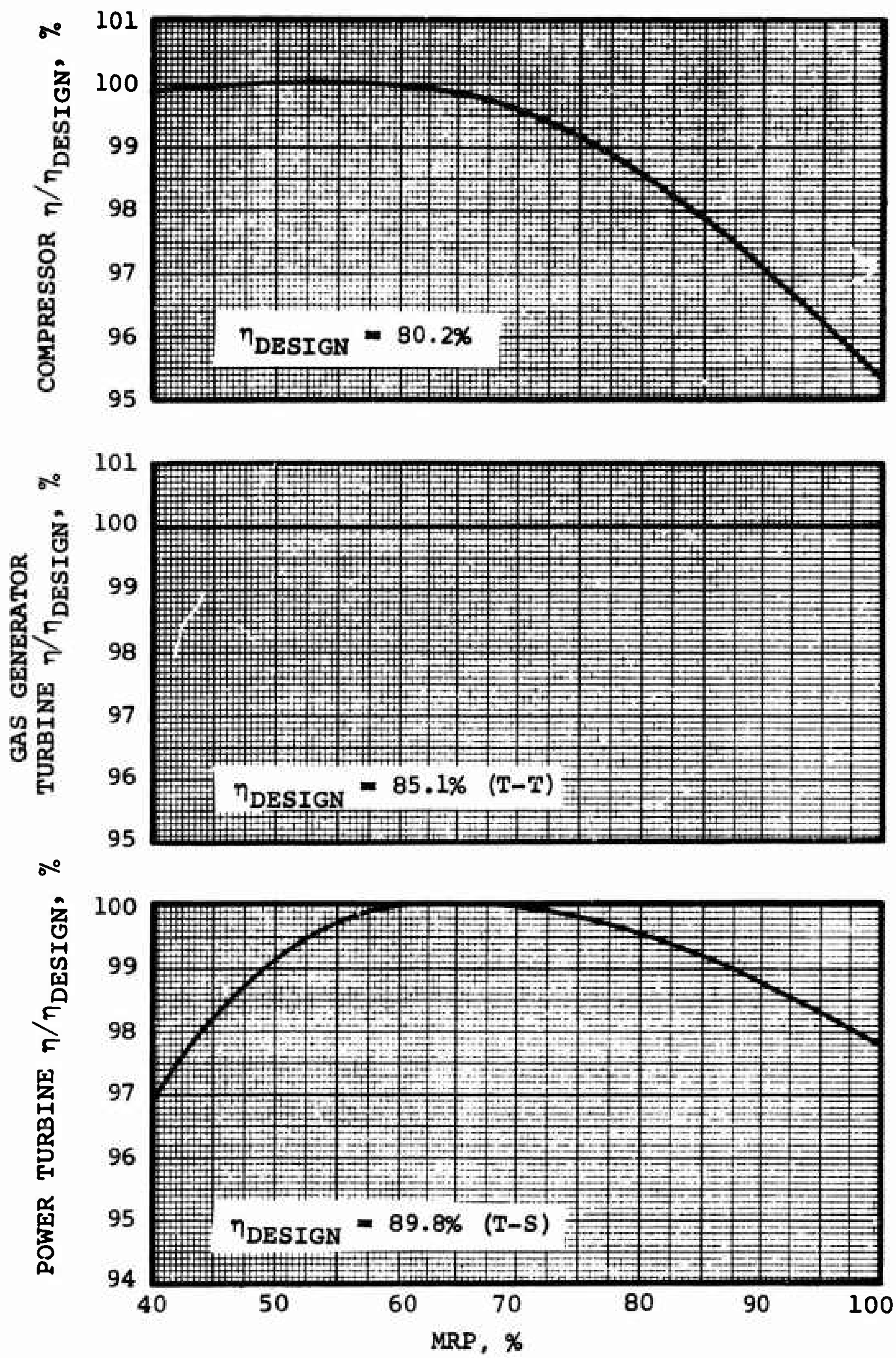

Figure 13. Off-Design Compressor and Turbine Efficiency for 2S-TSE.

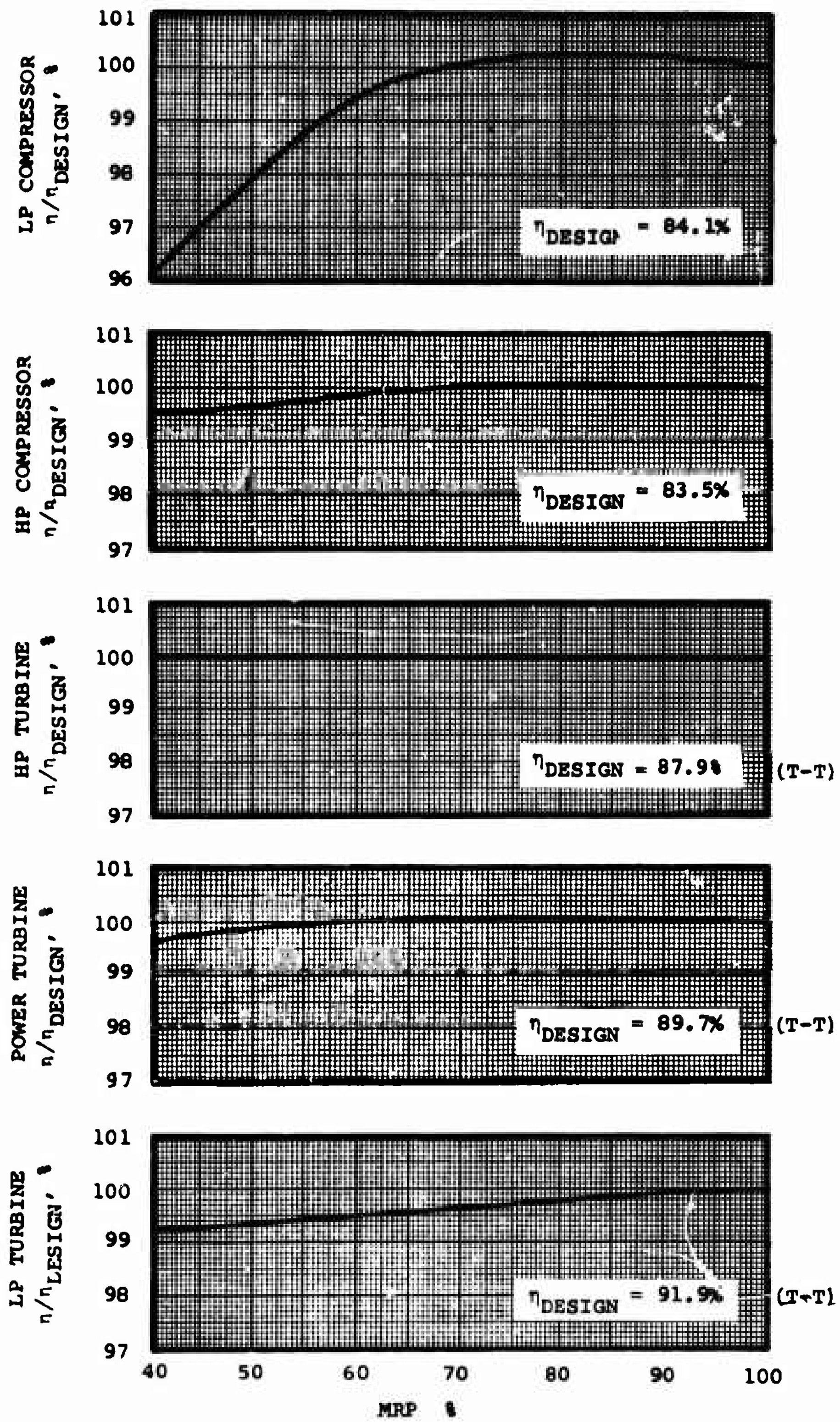

Figure 14. Off-Design Compressor and Turbine Efficiency for 3S-RF-TSE.

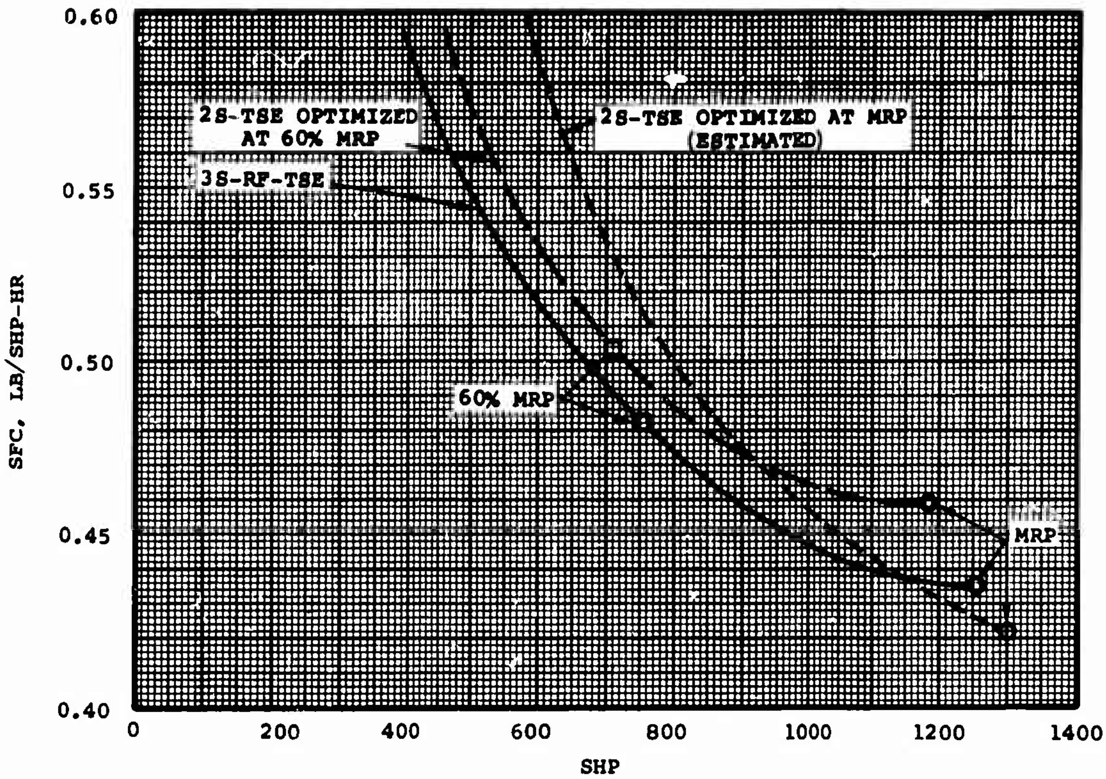

Figure 15. Off-Design Performance Using Initial Design Point.

The characteristics of the 3S-RF-TSE cycle can be most easily explained by investigating the behavior of the turbines during part-throttle conditions, as presented in the following subparagraphs. The performance data presented in the following discussions were determined for sea-level, static, standard-day conditions unless defined differently.

4.2.1 Engine Airflow

As in conventional free-turbine engines, a slight drop in TIT below its MRP value produces a small decrease in HP spool speed, which thus reduces cycle P/P. As shown in Figure 16, the HP turbine and power turbine P/P remain constant as the engine is throttled; but the LP turbine, being last in line and, therefore, discharging into the unchoked exhaust diffuser, drops rapidly in P/P. This reduces the power available to the LP compressor, which therefore drops in speed, reducing both engine airflow and cycle P/P. This further reduces LP turbine P/P and speed. Figure 17 shows that for a given part-power throttle setting (percent MRP), the 3S-RF-TSE airflow is significantly lower than for the 2S-TSE. Small changes in TIT thus cause large changes in LP spool speed (illustrated in Figure 18) and engine airflow.

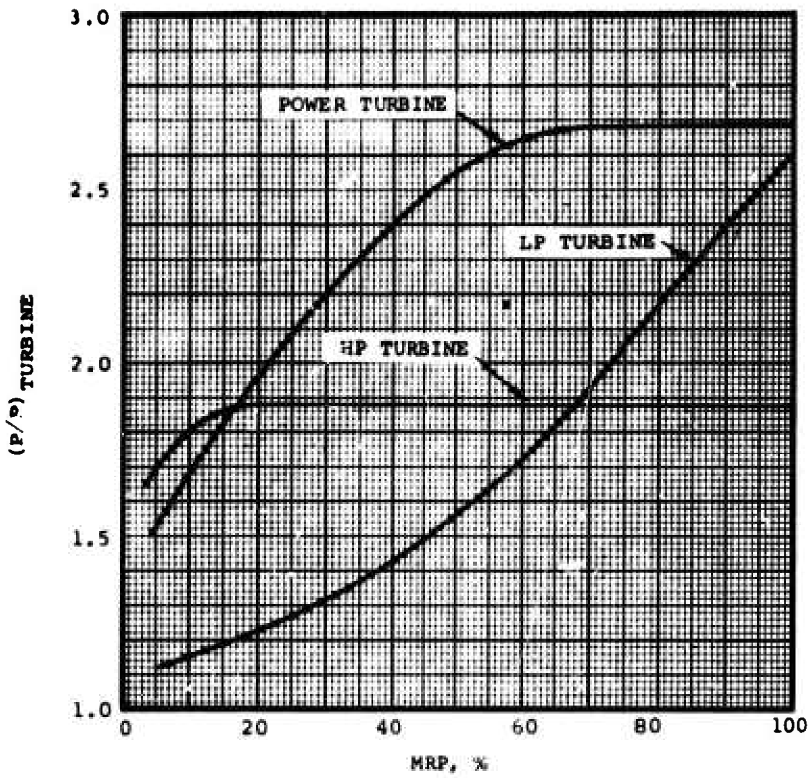

Figure 16. Turbine P/P Versus SHP, 3S-RF-TSE.

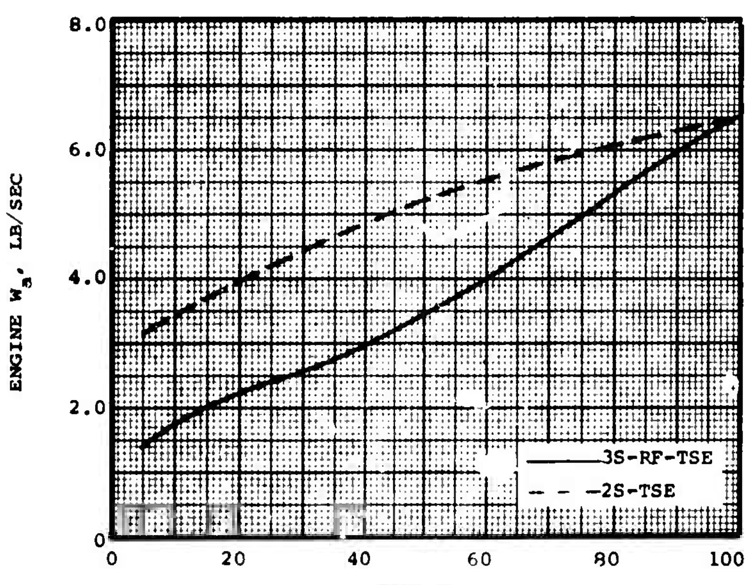

Figure 17. Engine Airflow Versus Percent Power.

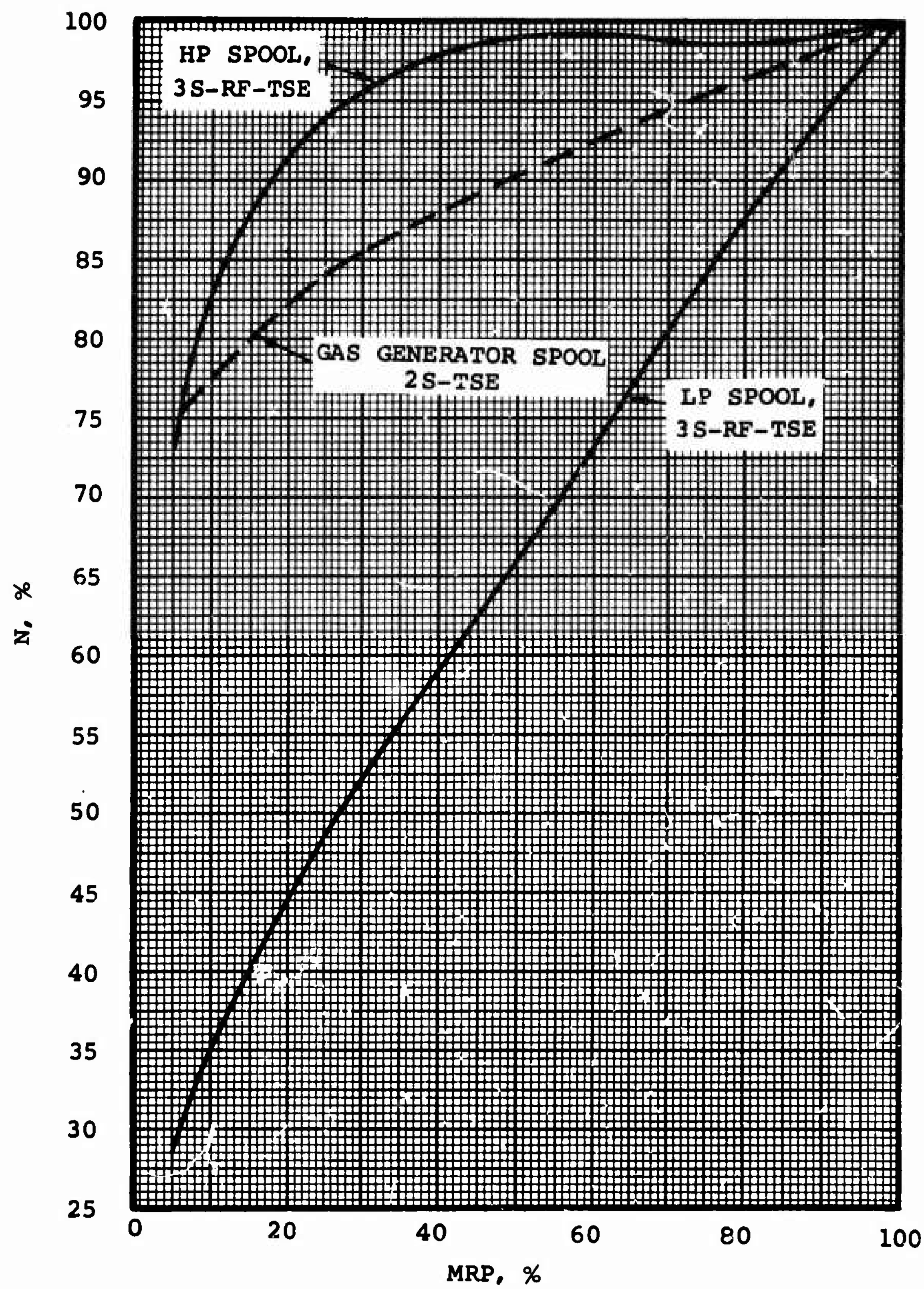

Figure 18. Spool Speed Versus Percent Power.

4.2.2 Power Turbine Specific Work

While the airflow of the 3S-RF-TSE drops rapidly while throttling down in power, the power turbine and HP turbine specific work remains high because the TIT and P/P seen by these turbines remains essentially constant.

The TIT of a conventional cycle decreases as the engine is throttled, as shown in Figure 19, because airflow drops more slowly than fuel flow and, thus, the fuel-air ratio decreases. The more rapid reduction of airflow in the 3S-RF-TSE is manifested in relatively constant fuel-air ratio and TIT, again as shown in Figure 19.

Referring again to Figure 16, notice that the P/P of the power turbine remains constant from MRP to approximately 60 percent power, at which time the orifice into which it discharges (the LP turbine) becomes unchoked. Similarly, the HP turbine P/P remains constant almost down to idle.

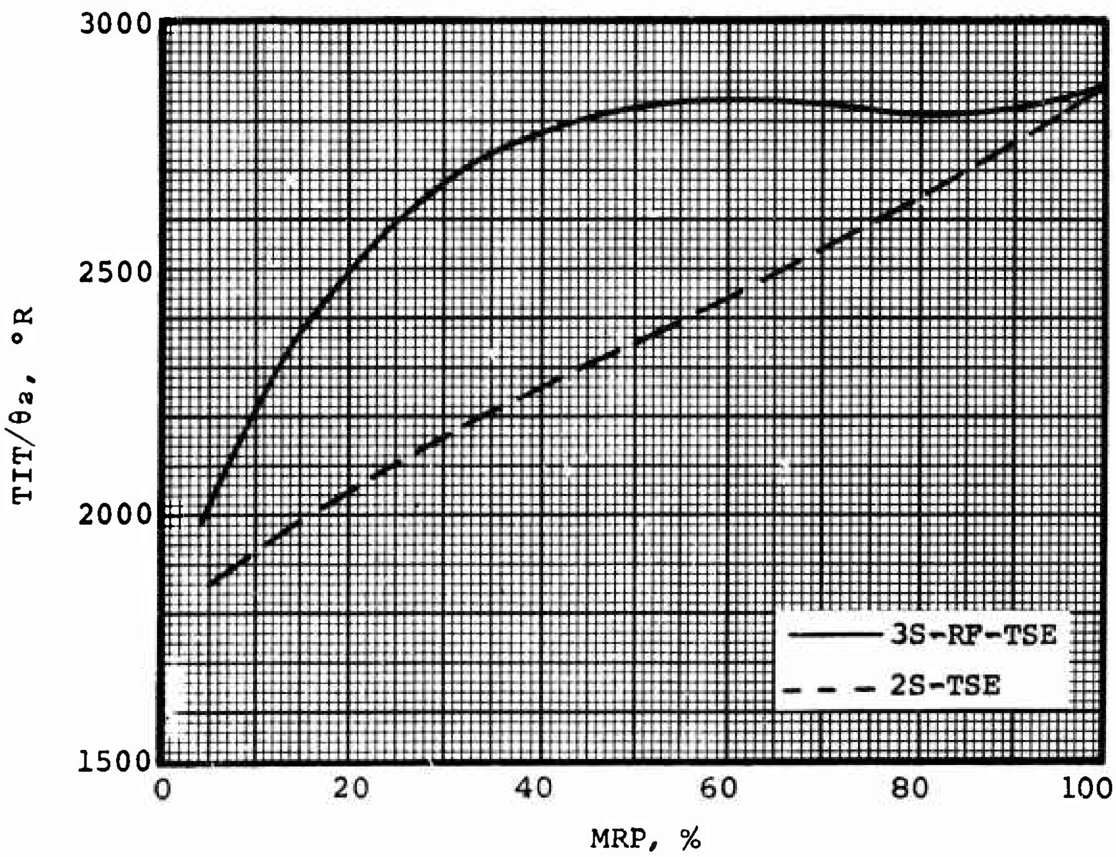

Figure 19. TIT/θ_2 Versus Percent Power.

With a constant TIT and P/P, the HP turbine produces constant specific work and discharge temperature. The same is true for the power turbine, which therefore drops only slightly in specific work from MRP to 60 percent power. Part-power specific work of the 3S-RF-TSE is compared to the more conventional 2S-TSE in Figure 20. The anticipated deficiency in power for the 3S-RF-TSE, because of lower airflow, is offset by higher than usual power turbine specific work.

4.2.3 Component Efficiencies

The three spools in conjunction with the turbine arrangement on the 3S-RF-TSE provide for relatively constant component efficiencies (compressors and turbines) from MRP to 60 percent power (see again Figure 14). Both compressors operate with relatively constant efficiency between MRP and 60 percent MRP. This matching is enabled because the compressors are on separate spools and the operating line remains in the maximum efficiency regime.

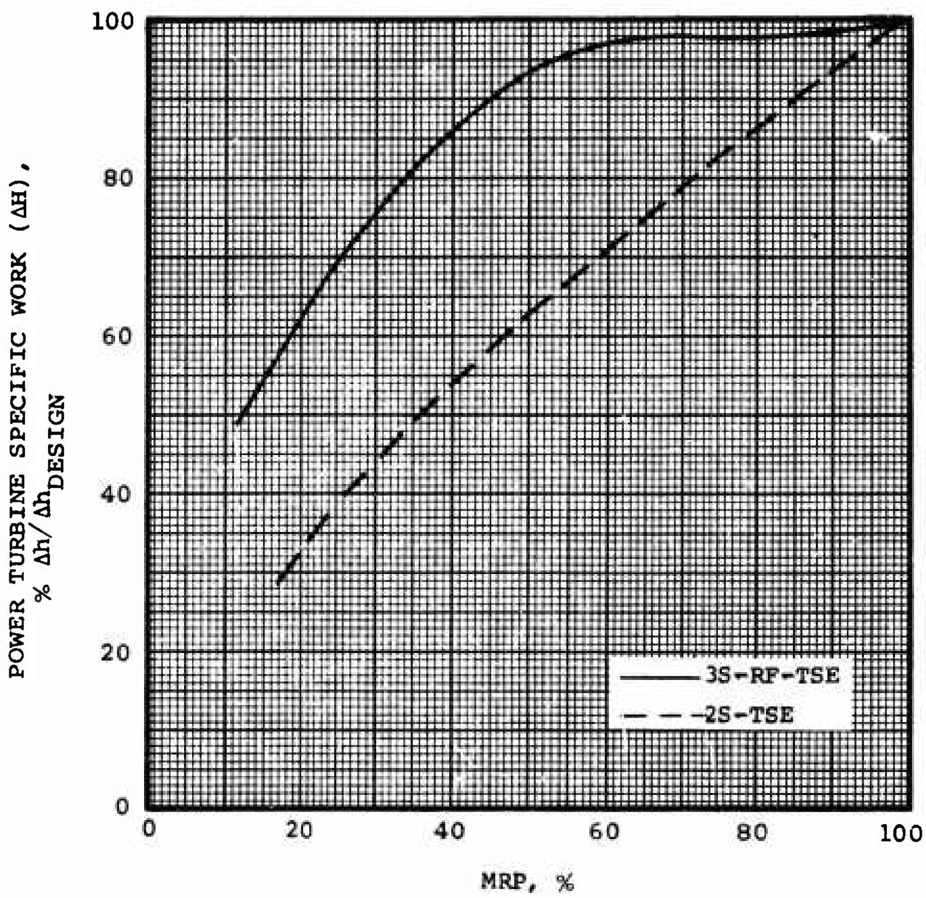

Figure 20. Power Turbine Specific Work Versus Percent Power.

The 3S-RF-TSE power turbine holds constant velocity ratio* and therefore efficiency because of its constant spool speed (as required for the study) and specific work. Conversely, for the 2S-TSE, the decreasing power turbine specific work coupled with constant speed changes the velocity ratio and efficiency. However, since design point velocity ratio occurs at part power, efficiency increases as the engine is throttled toward 60 percent power from MRP.

Like the gas generator turbine in the 2S-TSE with decreasing engine power, the 3S-RF-TSE LP turbine offsets decreasing specific work with lower spool speed. This results in only 1/2-percent drop in efficiency at 60 percent power. The 3S-RF-TSE HP turbine maintains constant specific work and spool speed at part power, resulting in constant velocity ratio and efficiency.

4.3 HOT-DAY POWER-LAPSE CHARACTERISTICS

Off-design TIT characteristics can be conveniently displayed on a plot of temperature ratio (TIT/θ_2) versus corrected output horsepower (see again Figure 19). To hold constant TIT/θ_2 as the ambient temperature is increased, approximately a 25-degree increase in actual TIT is needed for every 5-degree increase in ambient temperature. Thus, the 3S-RF-TSE, providing relatively constant TIT/θ_2 from MRP to 60 percent power, reaches the actual TIT limit (2400°F) with only a small increase in ambient temperature when designed with the maximum allowable TIT at MRP, sea level, static, standard-day conditions. Conventional cycles require a lower part-power TIT/θ_2 for a given output power because they throttle less quickly in airflow.

The 3S-RF-TSE can approach the TIT/θ_2 characteristics of the conventional cycle by either of the following techniques:

1. Designing the engine with increased exhaust diffuser P/P, reducing the lapse of the LP compressor and therefore decreasing the required TIT/θ_2 at part throttle.

2. Decreasing the design-point TIT while maintaining the same cooling flow. This is called "flat" rating the engine and will permit an increase in the actual TIT on a hot day to mitigate the decrease in temperature ratio.

---

*Velocity ratio = $\dfrac{U_M}{\sqrt{2gJ\Delta h}}$

Off-design temperature characteristics of several engines designed for various TIT's* and $(P/P)_{exhaust}$ are superimposed on a curve of TIT/θ_2 versus corrected horsepower in Figure 21. Line A-B on this figure indicates the maximum allowable TIT (2400°F) for the most restrictive operating condition within the flight spectrum specified for this study--i.e., 4000 feet, 95°F, zero knots. As will be shown later, an engine designed to provide maximum horsepower at this flight condition will provide optimum performance for the other flight conditions.

Off-design performance of the engines from Figure 21 is shown in Figure 22 for comparison with the structural design point [TIT = 2400°F, $(P/P)_{exhaust}$ = 1.06]. Consider first the engine with a reduced temperature [TIT = 2250°F, $(P/P)_{exhaust}$ = 1.06]; the design-point horsepower is reduced 12.8 percent and the SFC is increased 2.54 percent. On the other hand, comparing the engine with the higher $P/P_{exhaust}$ [TIT = 2400°F, $(P/P)_{exhaust}$ = 1.26] to the structural design point shows that the horsepower penalty is about the same as for the previous case (12 percent) but the SFC is increased by 13.6 percent. This comparison of these three engines is summarized in Table VIII.

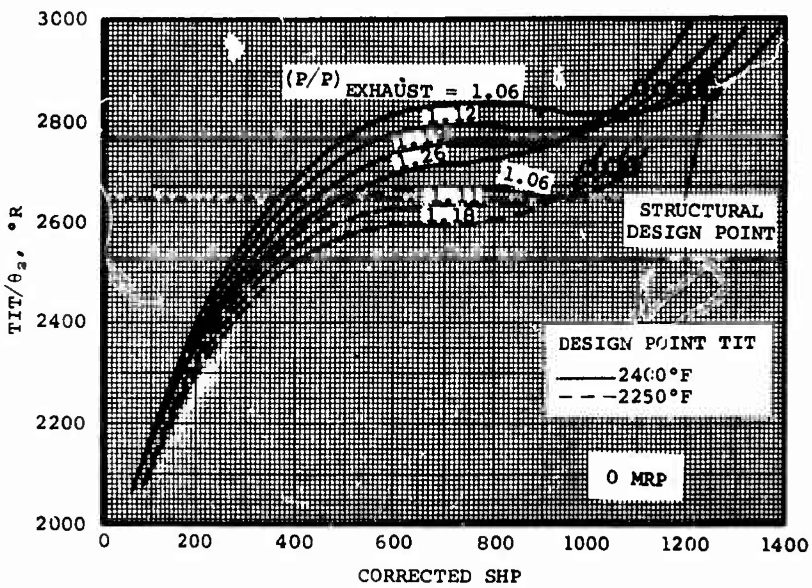

Figure 21. Off-Design TIT/θ_2 Characteristics of Several 3S-RF-TSE.

*The flat-rated engines shown are rated on $N_2\sqrt{\theta_2}$ until the TIT limit of 2400°F is reached.

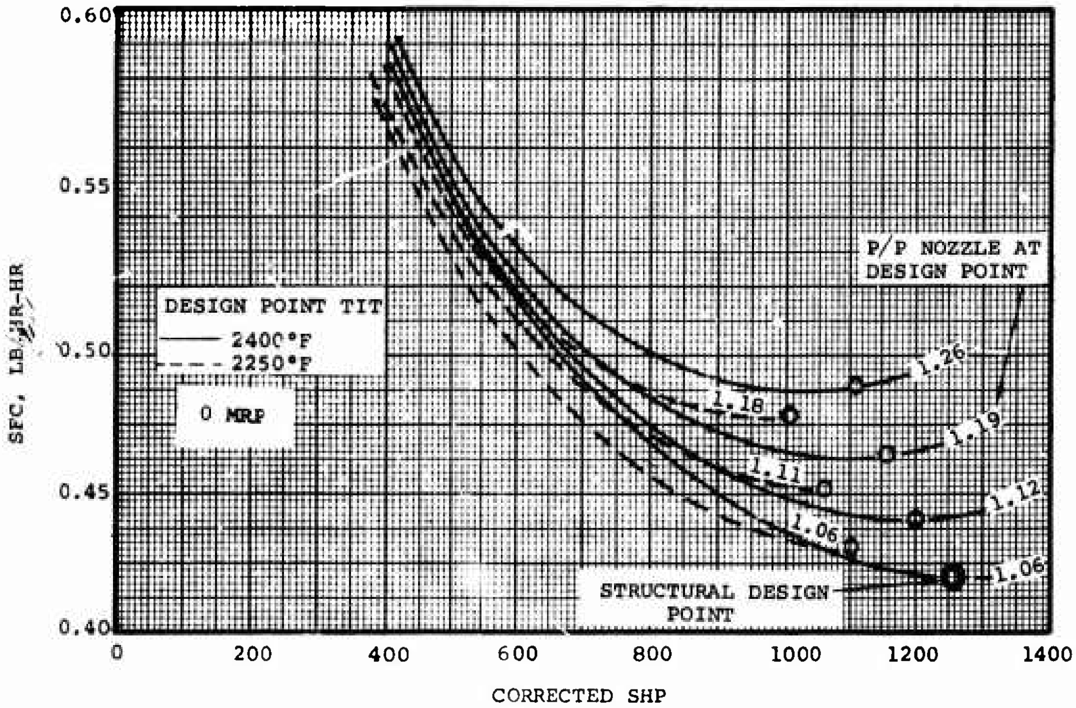

Figure 22. Off-Design Performance Characteristics of Several 3S-RF-TSE's.

TABLE VIII. DESIGN-POINT PERFORMANCE AND POWER-LAPSE IMPROVEMENT

Solution	Design Point (TIT)	Design Point $(P/P)_{exhaust}$	ΔHP (%)	ΔSFC (%)	Power-Lapse Characteristics
1	2860°R	1.06	0	0	Poor
2	2710°R	1.06	-12.8	+2.54	Good
3	2860°R	1.26	-12.0	+13.6	Fair

Hot-day power-lapse characteristics for these three engines are presented in Figure 23. The original engine [TIT = 2400°F, $(P/P)_{exhaust}$ = 1.06] falls off a power "cliff" on a 70°F day at 4000 ft. With TIT = 2400°F and $(P/P)_{exhaust}$ = 1.26, the power discontinuity is eliminated, but the horsepower available on a 95°F day at 4000 feet is approximately half the standard-day power. The third and most desirable solution is to flat-rate the engine by designing it with a lower TIT (2250°F) and low $(P/P)_{exhaust}$, and then increasing TIT on a hot day to maintain horsepower.

In summary, the engine with design point TIT = 2250°F and nozzle P/P = 1.06 produces the most desirable hot-day power-lapse characteristics, with a minimum penalty in cycle performance (minus 12.8 percent in horsepower and plus 2.54 percent in SFC). The original engine can be operated up to an ambient temperature of 69°F at 4000 feet without a significant performance penalty at maximum power. For hotter days, the design-point TIT should be lowered approximately 25 degrees for every 5°F increase in ambient temperature, to provide room for increasing TIT on a hot day without exceeding the maximum TIT limit of 2400°F.

As a result of this analysis, and to improve the hot-day power-lapse characteristics of the 3S-RF-TSE, the design point of the two engines was changed to provide for maximum TIT at MRP, 4000 feet, static, 95°F day conditions. Part power TIT/θ_2 of the two engines at sea level, static, standard-day conditions is shown in Figure 24 (a revision to Figure 19).

Having then selected a new design point, and with the part-power TIT and HP-spool speed characteristics defined by the preceeding analyses, the 3S-RF-TSE turbine life was re-evaluated to ensure comparability with the 2S-TSE. As shown in Table IX, the 3S-RF-TSE falls well within the design requirement for life at each power setting specified by the duty cycle. However, according to the previously given accumulative damage law, Equation (4), the 3S-RF-TSE has an equivalent time at MRP of 2860 hours--comprising 57.2 percent (2860 hours/5000 hours) of the mission. This compares with an equivalent time at an MRP of approximately 510 hours, or 10 percent of the mission for the 2S-TSE.

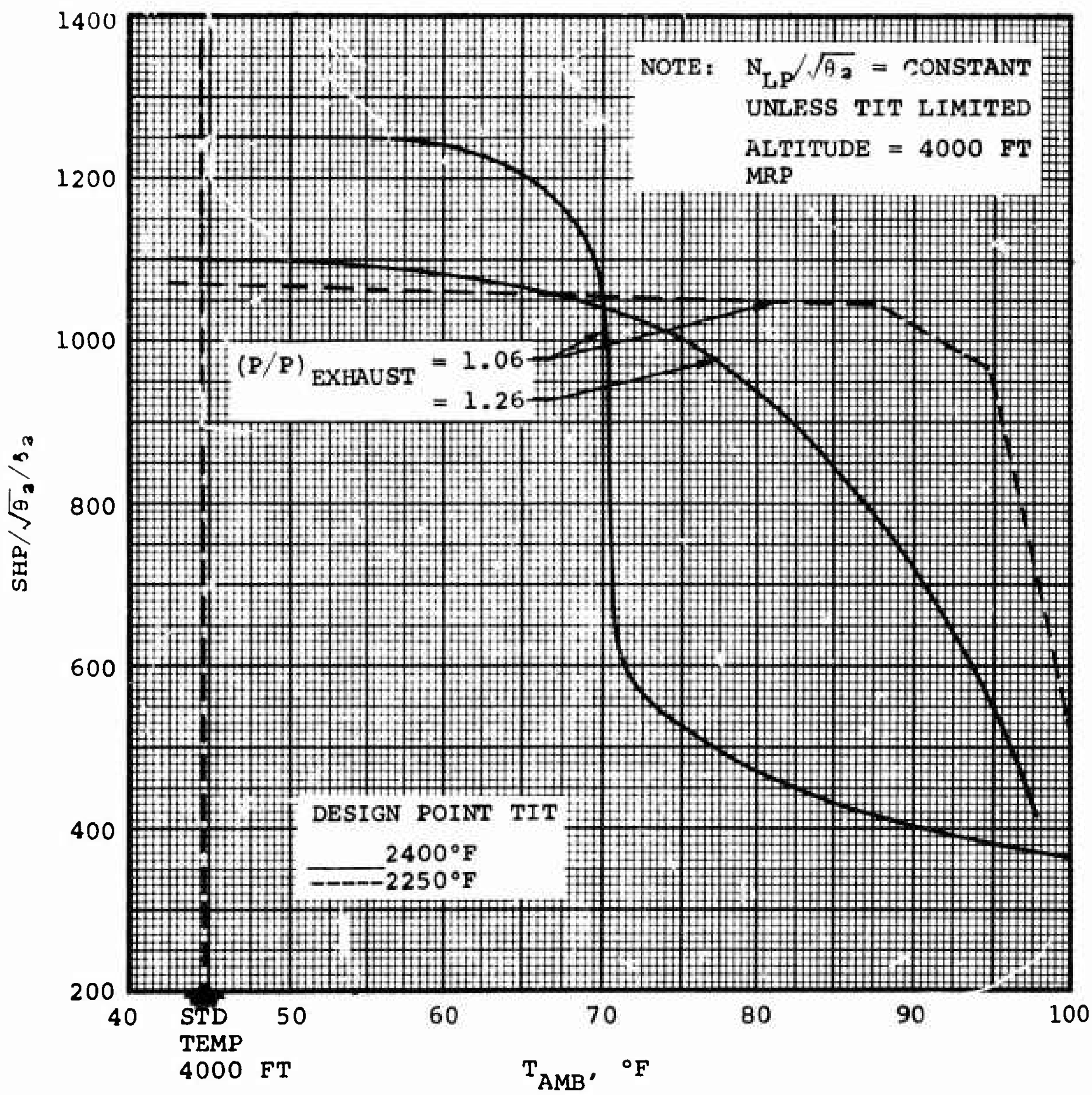

Figure 23. Hot-Day Power-Lapse Characteristics of Several 3S-RF-TSE'S.

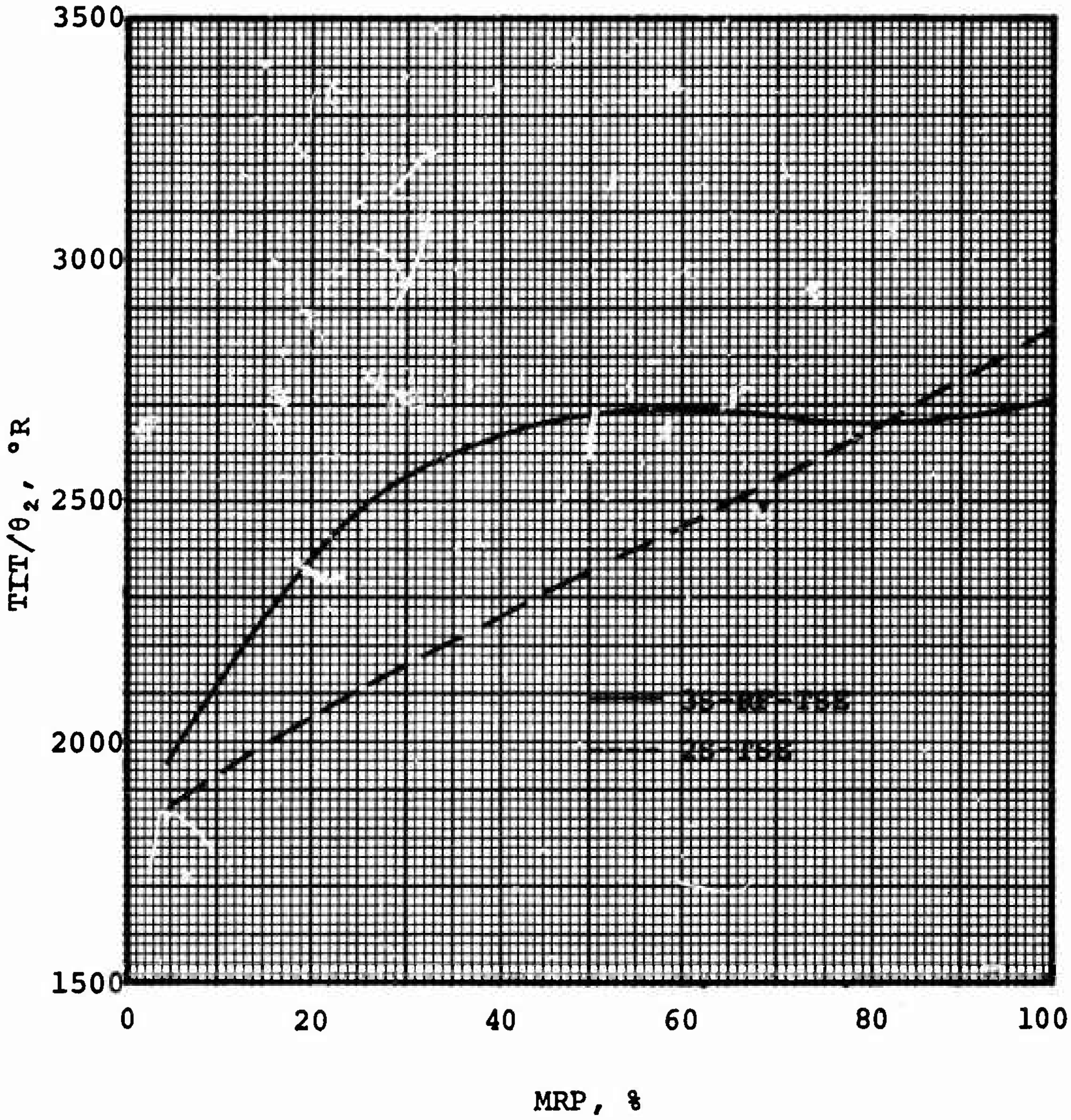

Figure 24. TIT/θ_2 Versus Percent Power (Revised From Figure 19 for New Design Point).

TABLE IX. ENGINE LIFE AND EQUIVALENT TIME AT MRP				
Power Setting	Mission Time* (%)	Life Required (hr)	Life Available 3S-RF-TSE (hr)	2S-TSE (hr)
MRP	10	500	3160	708
75%	15	750	6410	1.78×10^5
60%	60	3000	4910	∞
35%	10	500	2.51×10^4	∞
5%	5	250	∞	∞

*Total mission time = 5000 hours.

Operating 5.72 times as long as the 2S-TSE during the mission with high temperatures and stresses, the 3S-RF-TSE high-temperature components should thus be designed for 5.72 times the absolute life. Additional safety margin (comprising less than 5 percent mission time) may be introduced to account for (a) increased TIT on a hot day to minimize power lapse (the life analysis was made for an engine with maximum standard day TIT = 2250°F, with TIT increased to a maximum of 2400°F on a hot day), and (b) flexibility (i.e., ambient temperature >95°F on a hot day; the selected 3S-RF-TSE will not encounter the power "cliff" up to 95°F (see again Figure 23). Any subsequent increase in ambient temperature over 95°F must be countered with an increase in TIT--25°F for every 5°F increase in ambient temperature).

Several options were available for extending the life of the 3S-RF-TSE turbine. A cursory calculation indicated that the turbine life could be extended by a factor of 10 by reducing the HP-spool design speed by 10 percent (from 75,000 rpm to 67,000 rpm). Reducing the backward-sweep angle on the HP compressor blades produces the same pressure rise and efficiency at the lower rotational speed. The lower speed also results in a one-point decrease in the HP turbine efficiency as a result of the reduced velocity ratio. The performance penalty for these changes is 1/2 percent in SFC and horsepower. The performance data and comparisons presented in the following sections of this report are based in this revised design.

4.4 FLIGHT-SPEED POWER-LAPSE CHARACTERISTICS

Based on the preliminary data available prior to this study, it appeared that, because of variation in operating characteristics of the 3S-RF-TSE with flight speed, there exists a unique design (a specific cycle P/P, TIT, and exhaust diffuser P/P) to optimize for each flight speed specified for the mission. Detailed analyses, however have shown that one engine design can provide optimum performance for all flight speeds. To arrive at this conclusion, two methods were investigated for engine optimization at different flight speeds:

1. Varying design-point TIT and exhaust diffuser P/P.
2. Rematching components to improve efficiency at higher flight speeds.

4.4.1 Varying TIT and Exhaust Diffuser P/P

The previous analysis (see Paragraph 4.3) has shown that superior performance is achieved by minimizing design-point exhaust diffuser P/P and maximizing design-point TIT (see again Figures 21 and 22). Therefore, only changes in TIT with constant exhaust-diffuser P/P equal to approximately 1.06 will be diagnosed.

Shown in Figure 25 is the variation in corrected TIT versus corrected horsepower with flight speed and design-point TIT. Superimposed on the curves are lines of constant maximum allowable corrected TIT (TIT = 2400°F, ambient temperature = 95°F). For constant corrected horsepower, the required corrected TIT drops faster than maximum allowable corrected TIT with increased flight speed, shown again in Figure 26. This is because the ram pressure effect is greater than the ram temperature effect. Therefore, the most restrictive operating condition is hot day, zero flight speed. During off-design operation, while holding constant actual TIT, the engine with increasing flight speed will not experience the power lapse encountered by the engine operating with constant actual TIT and increasing ambient temperature. As shown in Figure 25, the engine is overdesigned at higher flight speeds; i.e., performance could be improved at higher flight speeds by raising the design point TIT. However, this could be done only at the expense of a power lapse at lower flight speeds.

In summary, a unique design-point TIT (and therefore one engine design) provides optimum overall performance for all flight speeds because (a) performance improves with increasing flight speed and (b) power lapse must be avoided at lower flight speeds.

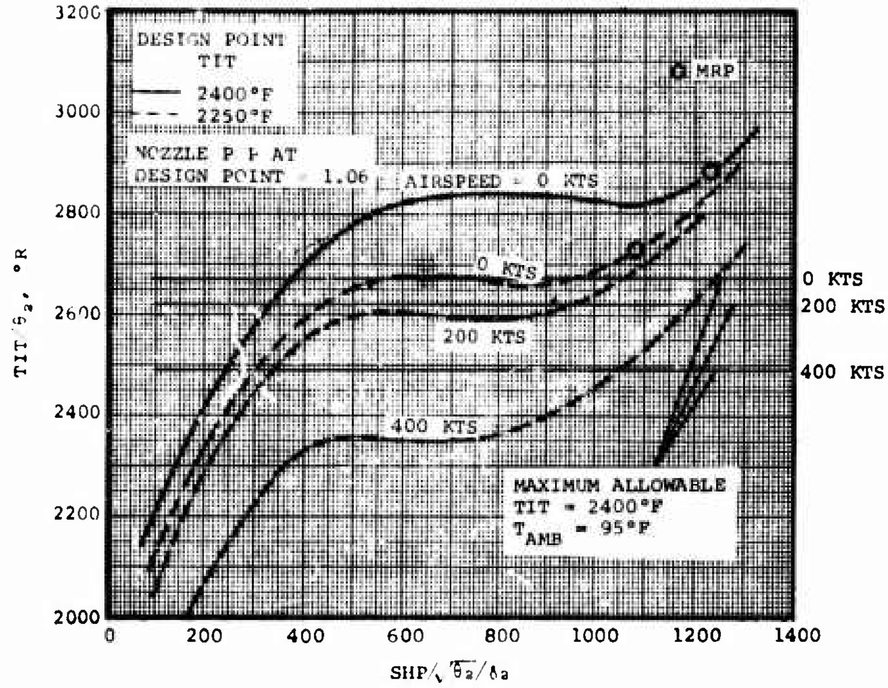

Figure 25. TIT/θ_2 Versus Corrected Shaft Horsepower for Varying Flight Speed.

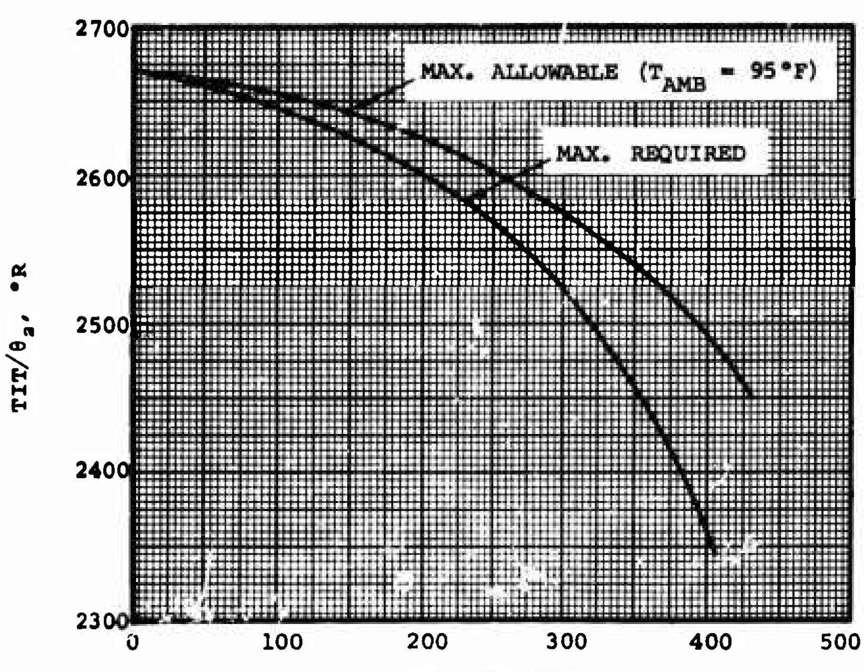

Figure 26. TIT/θ_2 Versus Airspeed for 3S-RF-TSE.

4.4.2 Rematching Components

Compressors and turbines could be rematched to provide improved off-design efficiency at higher flight speeds. Figures 27 and 28 show the variation in component off-design efficiency, between the low- and high-speed flight, for an engine optimized for low-speed flight.

Both compressors can be rematched by selecting the turbine nozzle area needed to shift the 400-knot operating lines to the position of the zero-knot operating lines. The turbines would be redesigned to provide maximum velocity ratio at 400 knots. As summarized in Table X, compressor and turbine efficiency can be slightly improved by optimizing for 400 knots. However, an influence coefficient study shows that this results in only 0.59 percent improvement in SFC at MRP and 0.64 percent lower SFC at 60 percent power.

It was therefore concluded that no significant cycle performance improvement can be obtained by rematching the components for the high-speed condition.

TABLE X. PERFORMANCE DIFFERENCES AT 400 KNOTS BY REMATCHING COMPONENTS

	MRP (% Points)	60% Power (% Points)
$\Delta\eta_{LP}$ COMPRESSOR	-0.2	+0.5
$\Delta\eta_{HP}$ COMPRESSOR	+1.5	0
$\Delta\eta_{HP}$ TURBINE	0	0
$\Delta\eta_{PT}$	0	0
$\Delta\eta_{LP}$ TURBINE	+0.15	+0.35
ΔSFC	-0.59 (%)	-0.64 (%)

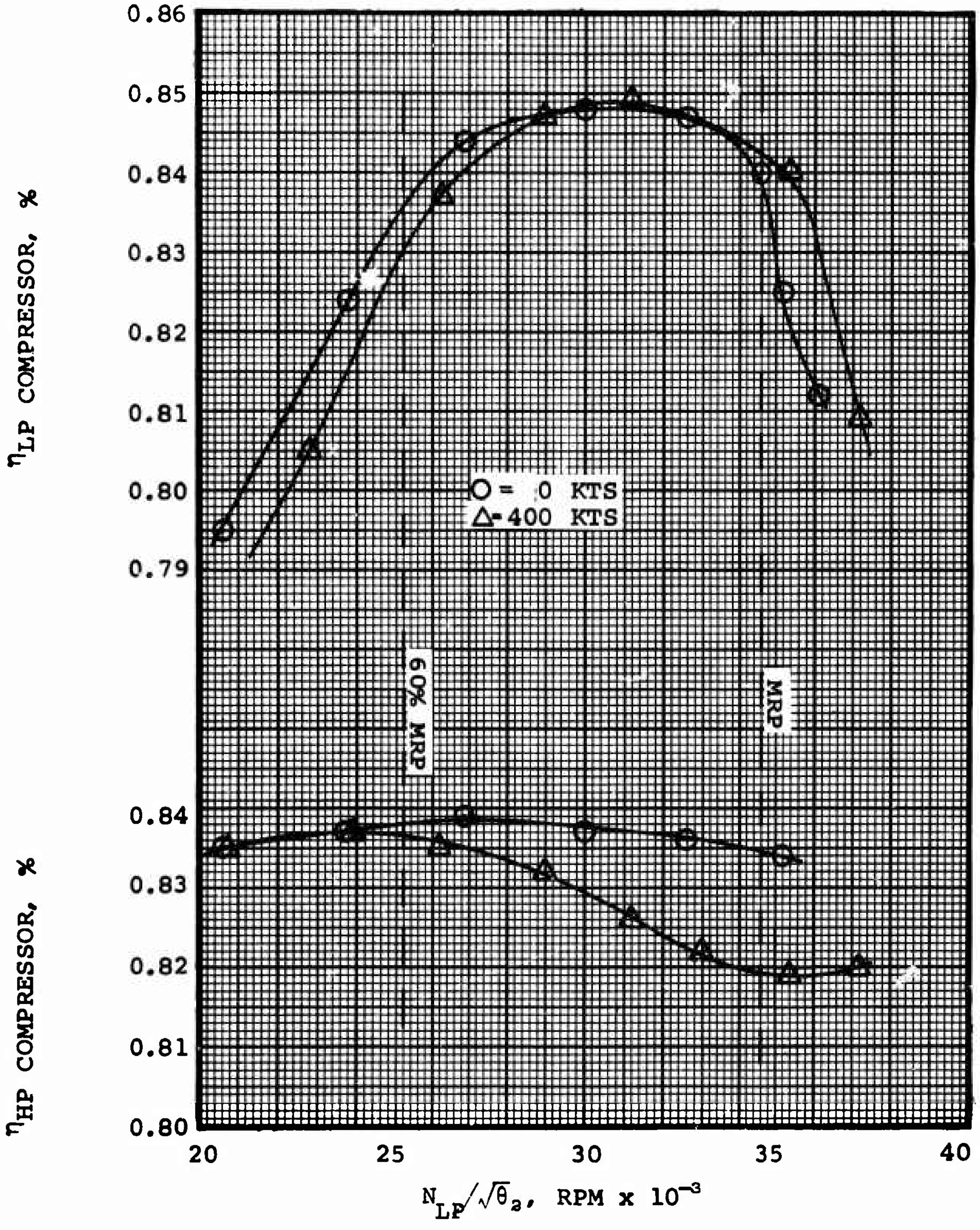

Figure 27. Compressor Efficiency Versus Corrected LP Spool Speed for 3S-RF-TSE.

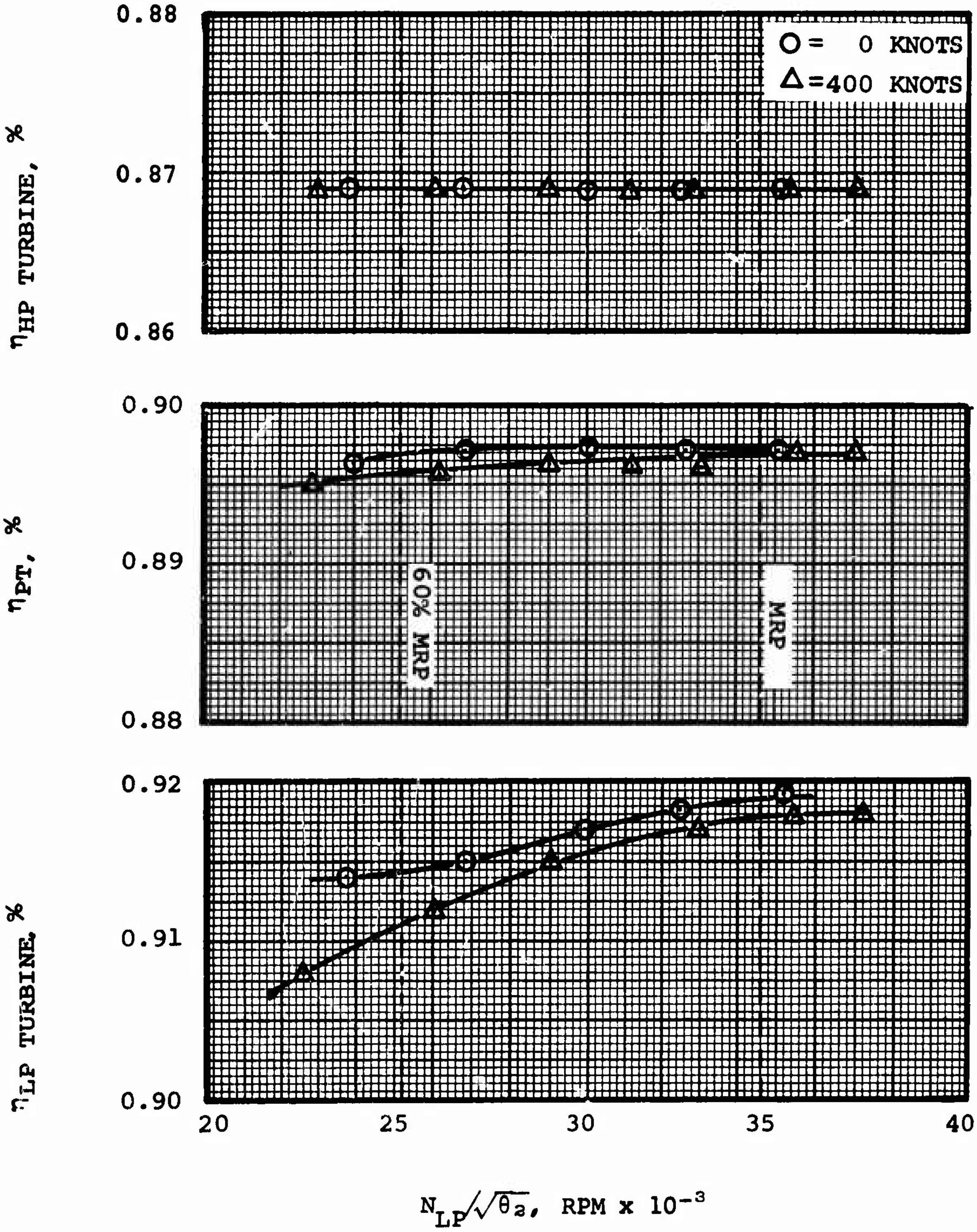

Figure 28. Turbine Efficiency Versus Corrected LP Spool Speed for 3S-RF-TSE.

4.5 OFF-DESIGN PERFORMANCE DATA

4.5.1 3S-RF-TSE Performance Data

Off-design performance was determined for the 3S-RF-TSE at the various throttle, altitude, airspeed, and temperature conditions delineated in Table XI. The data are presented in Appendix I. For each of the operating conditions specified in Table XI, the following parameters are presented to illustrate the off-design performance of the engine:

Shaft horsepower
SFC
Engine airflow
TIT
LP spool speed
HP spool speed
LP compressor P/P
HP compressor P/P
Cycle P/P (including inter-compressor duct loss)

TABLE XI. OFF-DESIGN OPERATING CONDITIONS

Altitude (ft)	Airspeed (kts)	Ambient Temperature	Power Setting (% MRP)
0	0 to 400	Std	100, 60, 45, 30, 5
4000	0 to 400	Std	100, 60, 45, 30, 5
6000	0 to 400	Std	100, 60, 45, 30, 5
10,000	0 to 400	Std	100, 60, 45, 30, 5
15,000	0 to 400	Std	100, 60, 45, 30, 5
20,000	0 to 400	Std	100, 60, 45, 30, 5
25,000	0 to 400	Std	100, 60, 45, 30, 5
4000	0 to 400	95°F	100, 60, 45, 30, 5
6000*	0	95°F	100

*These data are presented in Table XIV in Appendix I.

During the evaluation of off-design (steady-state) operation, the following guidelines and limitations were followed:

1. Power turbine spool speed = 100 percent (constant)

2. Maximum TIT = 2400°F. This limit was attained only during hot-day operation.

3. Maximum corrected LP spool speed $(N_{LP}/\sqrt{\theta_2})$ = 100 percent (34,600 rpm). Thus, as will be discussed in Section 5, the engine is rated on corrected LP spool speed with a TIT limit of 2400°F.

4. Minimum steady-state surge margin = 5 percent. This steady-state limit was stipulated in order to provide surge range (above the 4-percent minimum) for transients. This 5-percent limit was not encountered for any steady-state operating point within the flight spectrum examined.

5. Maximum LP and HP spool speeds (actual) encountered were 105 percent (36,300 rpm) and 103 percent (69,000 rpm), respectively, occurring at MRP, 4000 feet, 95°F.

4.5.2 2S-TSE Performance Data

In order to provide a basis for evaluating the off-design operating characteristics of the 3S-RF-TSE, off-design performance data were determined for the 2S-TSE at the same operating conditions (Table XI). The performance data for this engine are presented in Appendix II. The following parameters are presented to indicate the off-design characteristics of this engine:

Shaft horsepower
SFC
Engine airflow
Cycle P/P
Gas generator speed

The following guidelines and limitations were observed:

1. Power turbine spool speed = 100 percent (constant)

2. The engine was rated on TIT as follows (anticipating a gas generator spool speed override if necessary):

MRP	=	2400°F
60% MRP	=	1980°F
45% MRP	=	1845°F
30% MRP	=	1695°F
5% MRP (idle)	=	1400°F

3. Maximum gas generator spool speed (actual) encountered was 41,180 rpm (100.9 percent) occurring at MRP, 4000 feet, 95°F, 400 knots. This overspeed is insignificant, and a gas generator spool speed was not required.

4.6 PERFORMANCE SCALING

The performance studies that have been discussed previously were conducted with an airflow of 6.5 pounds per second for both engines. A cursory study was made to determine the variation of component performance over the range of airflows from 4.0 to 9.0 pounds per second. Influence coefficients were then used to determine MRP performance (shaft horsepower and SFC) over this range of airflows for performance scaling.

Compressor adiabatic efficiency was found to vary as shown in Figure 29, and HP turbine and gas generator turbine efficiency varied as indicated in Figure 30. LP turbine and power turbine efficiencies were assumed unchanged over this range of airflows.

The resulting MRP performance of the two engines from 4.0 to 9.0 pounds per second is indicated in Figure 31.

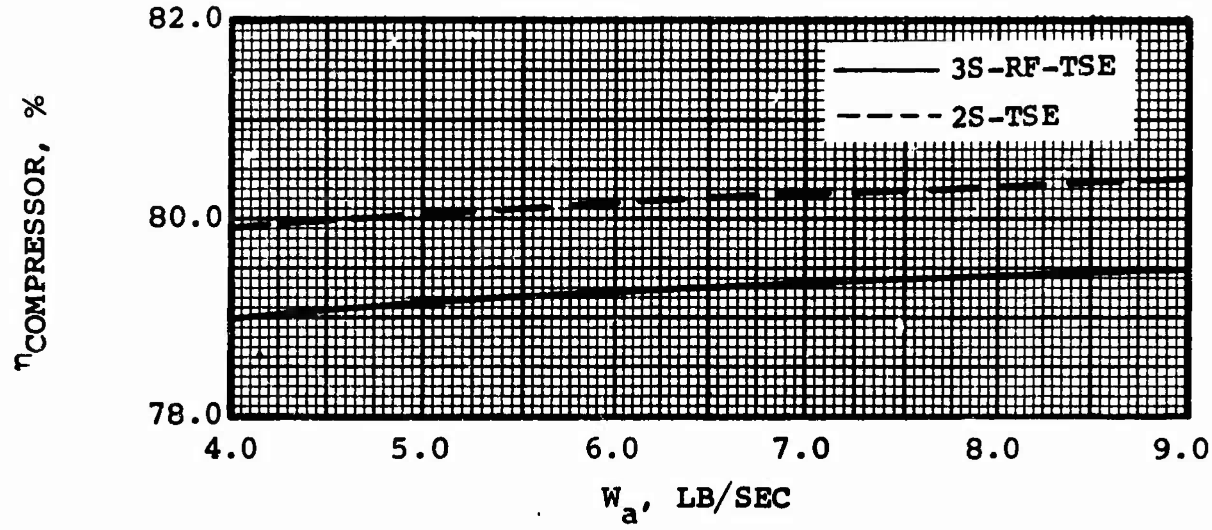

Figure 29. Compressor Adiabatic Efficiency Versus Airflow.

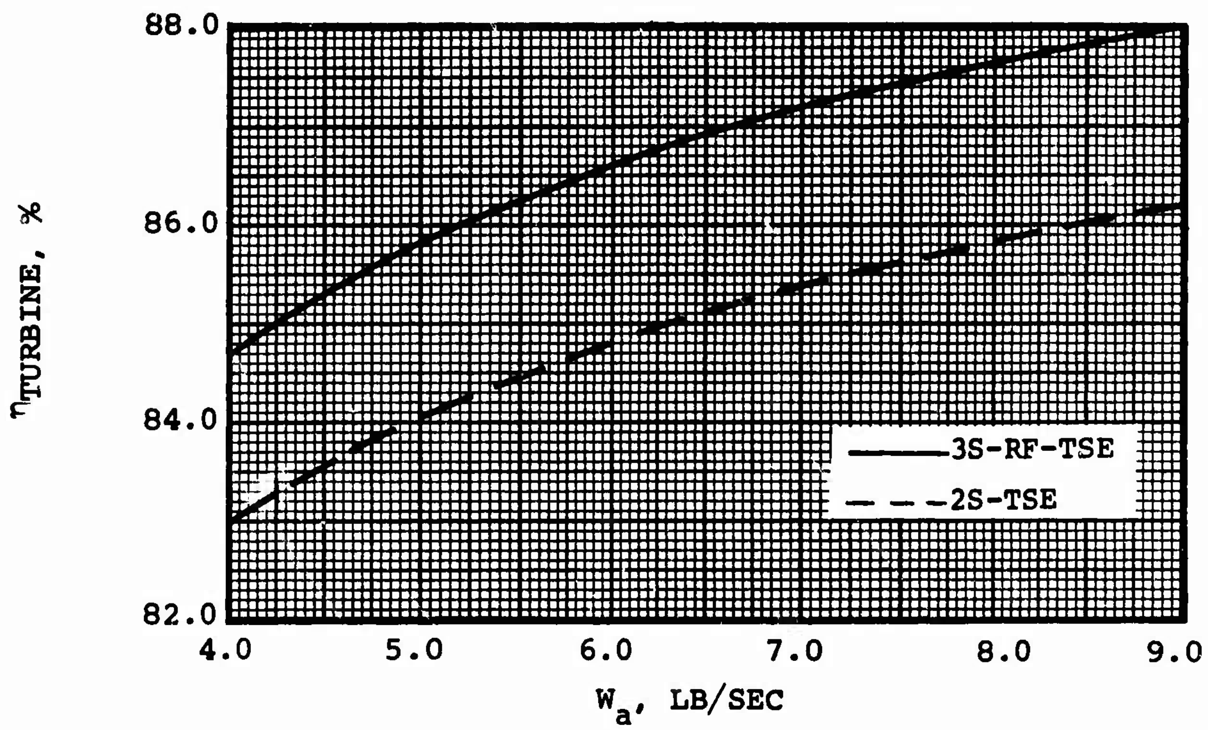

Figure 30. HP Turbine Efficiency Versus Airflow.

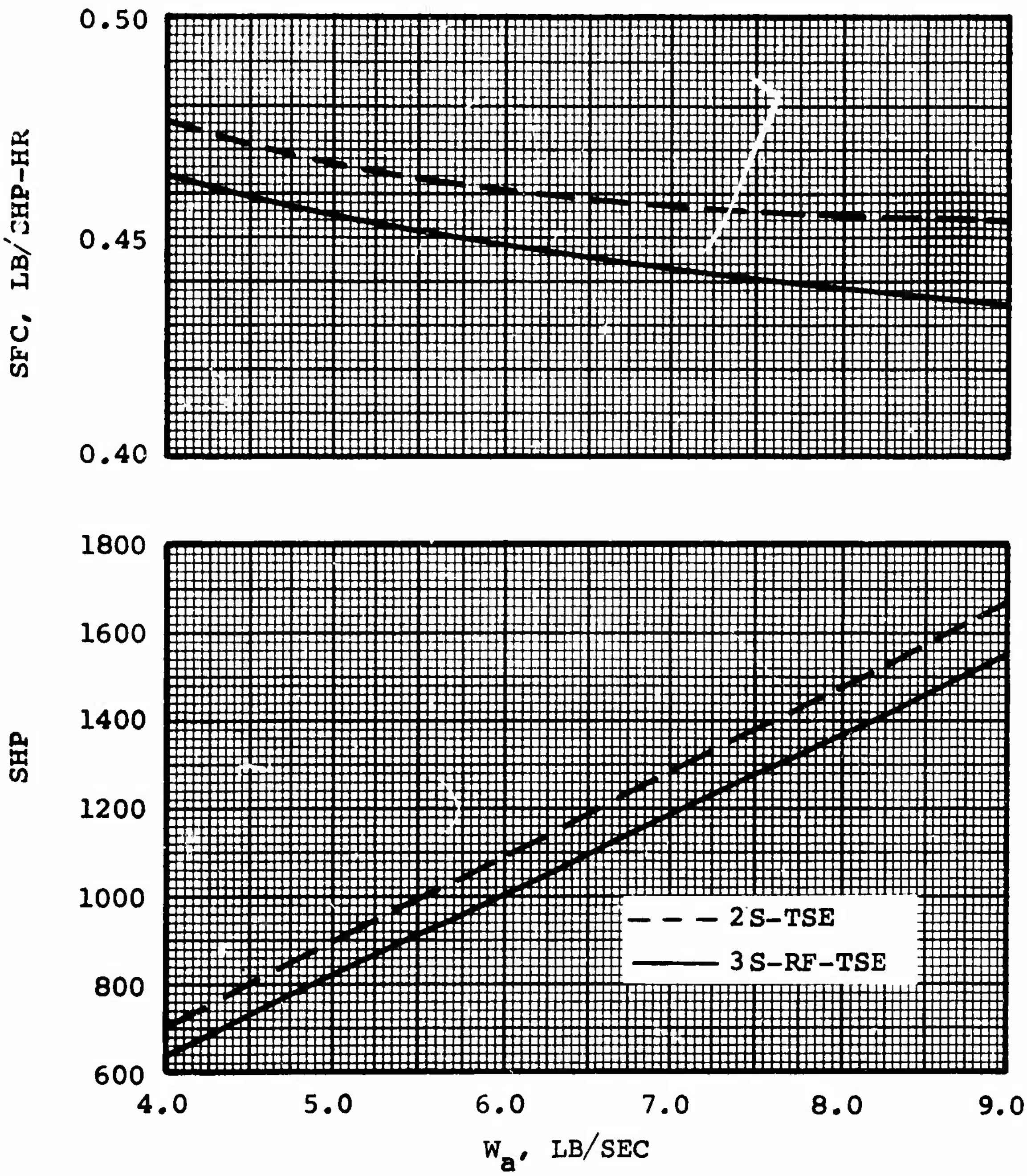

Figure 31. Performance Scaling Curves.

5. CONTROL AND TRANSIENT STUDIES

Control and system response and stability analyses were conducted for the two engine configurations. Features of a feasible control system for the 3S-RF-TSE are discussed. System stability and transient characteristics of the two engines were determined by use of digital and analog computer simulations of the engine/control systems.

5.1 CONTROL REQUIREMENTS

5.1.1 3S-RF-TSE Control

Figure 32 illustrates the basic control configuration selected for the 3S-RF-TSE. The objectives of this system are (a) to produce steady-state droop-free control of power turbine speed; (b) to present the pilot with a four-position power-control lever corresponding to engine off, engine start, idle control, and maximum power; and (c) to further provide surge-free engine operation with rapid collective-pitch transients in increasing and decreasing power directions.

In this system, the power lever generates two reference levels: HP spool speed and fuel flow. The commanded parameter value is compared to the actual value, and each difference is passed to a "lowest wins" logic network. This network compares the magnitude and sign of two or more inputs and transmits that signal which results in the lowest engine fuel flow. The output of the "lowest wins" is passed to the fuel-delivery system, which increases or decreases fuel flow to reduce the error to zero. The "lowest wins" network receives additional difference signals from a power turbine speed-control loop and from a TIT control loop.

A conceptual schematic of the fuel-metering section is presented in Figure 33. The design is such that for zero input current, the OPEN and CLOSE pressures applied to the actuating piston are equal. For a positive input current, the OPEN pressure exceeds the CLOSE pressure; and for a negative input current, the opposite applies. A shaped plunger would be connected directly to the actuating piston; thus, the insertion of this plunger into a throttle area is controlled directly by the actuating piston position. A constant pressure drop is maintained across the throttle area by the bypass regulator; hence, fuel flow is a direct function of both actuator position and the plunger profile.

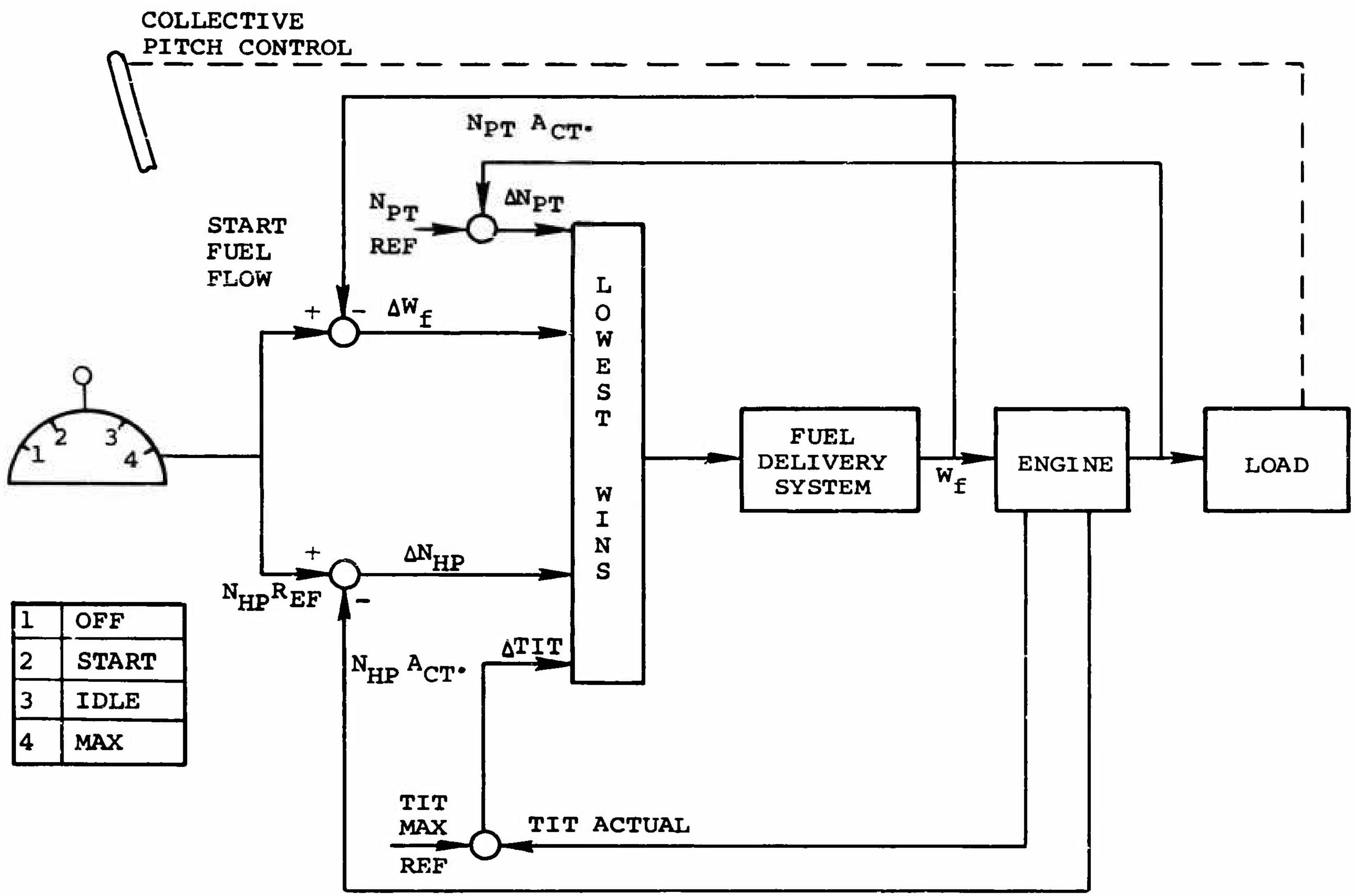

Figure 32. Basic Control Configuration for the 3S-RF-TSE.

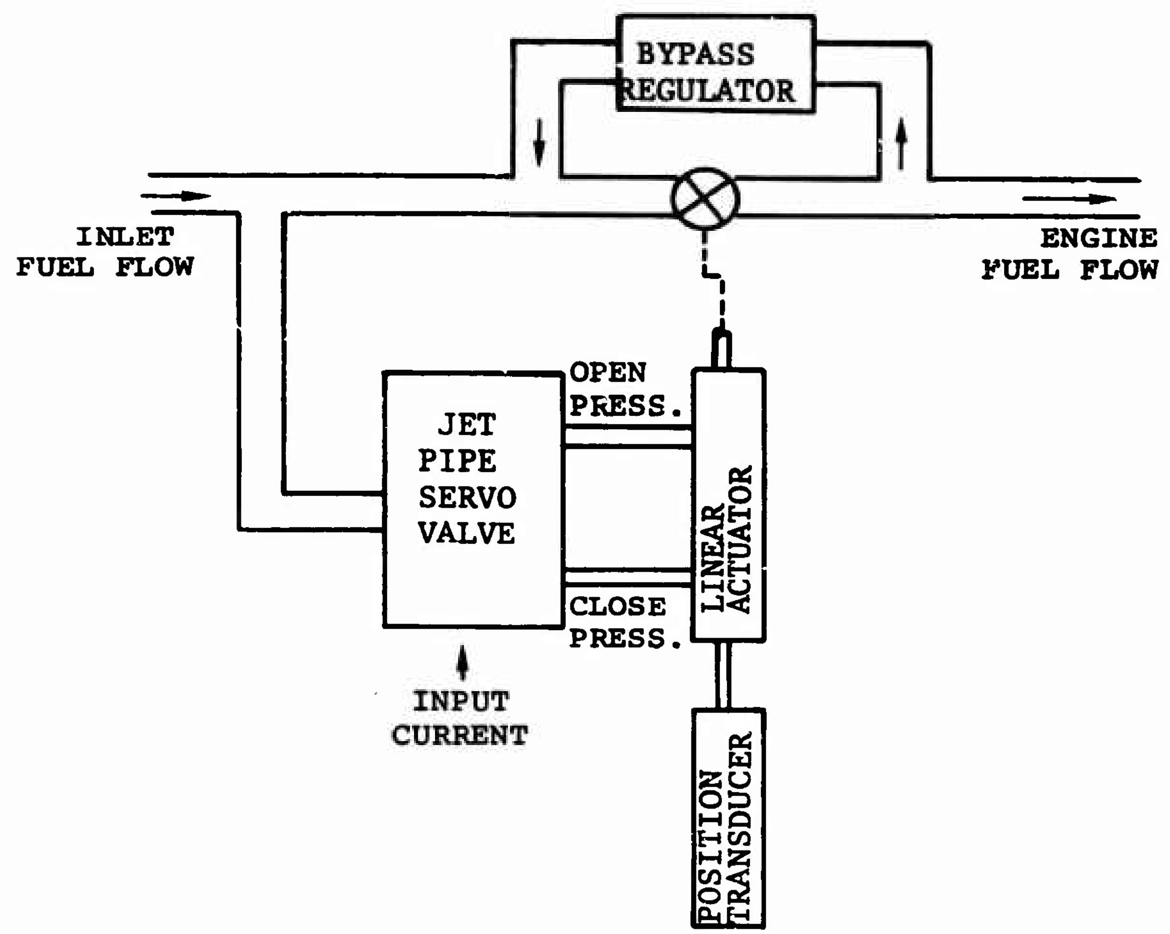

Figure 33. Schematic of Fuel Metering System.

The use of an integrating control system, while offering strong advantages in operating accuracy, presents some difficulty during engine start. Clearly, if the start is attempted under control of a speed governor, the metering valve will position for the maximum fuel flow. For this reason, a position feedback transducer is coupled to the throttle actuator and start-flow is specified as a throttle position. Figure 34 illustrates a characteristic plot of HP spool speed versus valve position, the shape being obtained by control of the plunger profile previously described. Clearly, with the engine off, HP spool speed, power turbine speed, and TIT will be below their respective reference levels and will all correspond to fuel-increase inputs to the "lowest wins" block of Figure 32. As the engine start cycle is initiated, fuel pressure will be applied to the throttle control actuator which, in turn, will slew to the reference position shown in Figure 34. On completion of the start sequence, the HP spool speed will accelerate toward the value corresponding to the start-throttle position. This, however, is somewhat higher than the start reference speed and, as actual speed approaches reference speed, control will revert to speed governing.

Figure 35 illustrates a typical profile of HP spool speed and power turbine speed for minimum and maximum rotor load conditions. Advancing the power lever to the idle position increases the valve position command to maximum fuel flow and the HP spool speed command reference to idle. The value of idle HP spool speed is selected such that, with minimum collective pitch, the steady-state power turbine speed exceeds 100 percent. As the power turbine attempts to accelerate to

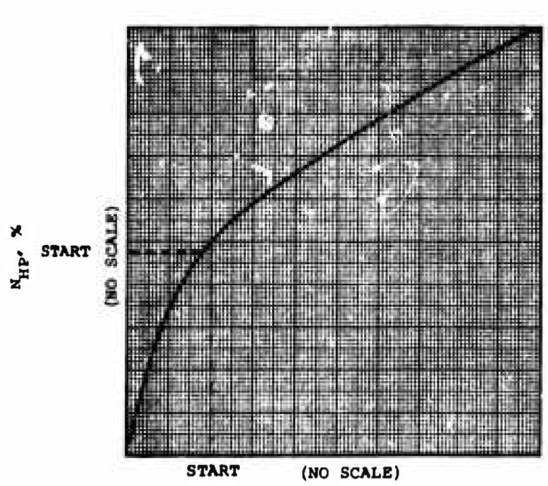

Figure 34. Characteristic HP Spool Speed Versus Fuel Metering Valve Position.

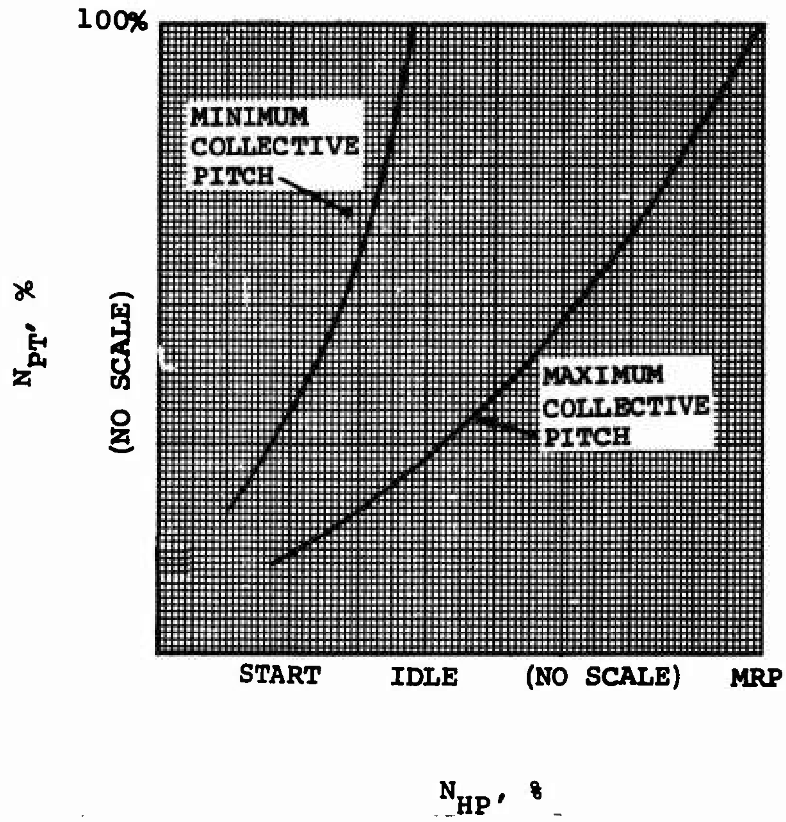

Figure 35. A Typical Profile of HP Spool Speed Versus Power Turbine Speed for Maximum and Minimum Rotor Load.

a speed greater than 100 percent, control reverts to the power turbine speed governor. The power lever may now be advanced to the maximum power position, which results in the HP spool limit speed reference corresponding to 100 percent power turbine speed with maximum collective pitch. Steady-state control of the engine between idle power and maximum power is now exclusively a function of collective pitch, power turbine speed being maintained at 100 percent and free from droop.

Control of overfueling margin was shown to be free of surge-margin constraints during engine acceleration transients. Thus, the only transient constraint is TIT. The control schematic of Figure 32 includes this control function. Similarly, engine control during deceleration was shown to be primarily a function of constraining the deceleration rate of corrected HP spool speed as a function of corrected LP spool speed. Implementation of this control is shown in Figure 36. In this case, a "highest wins" logic block is interposed between the "lowest wins" and the fuel system. LP compressor

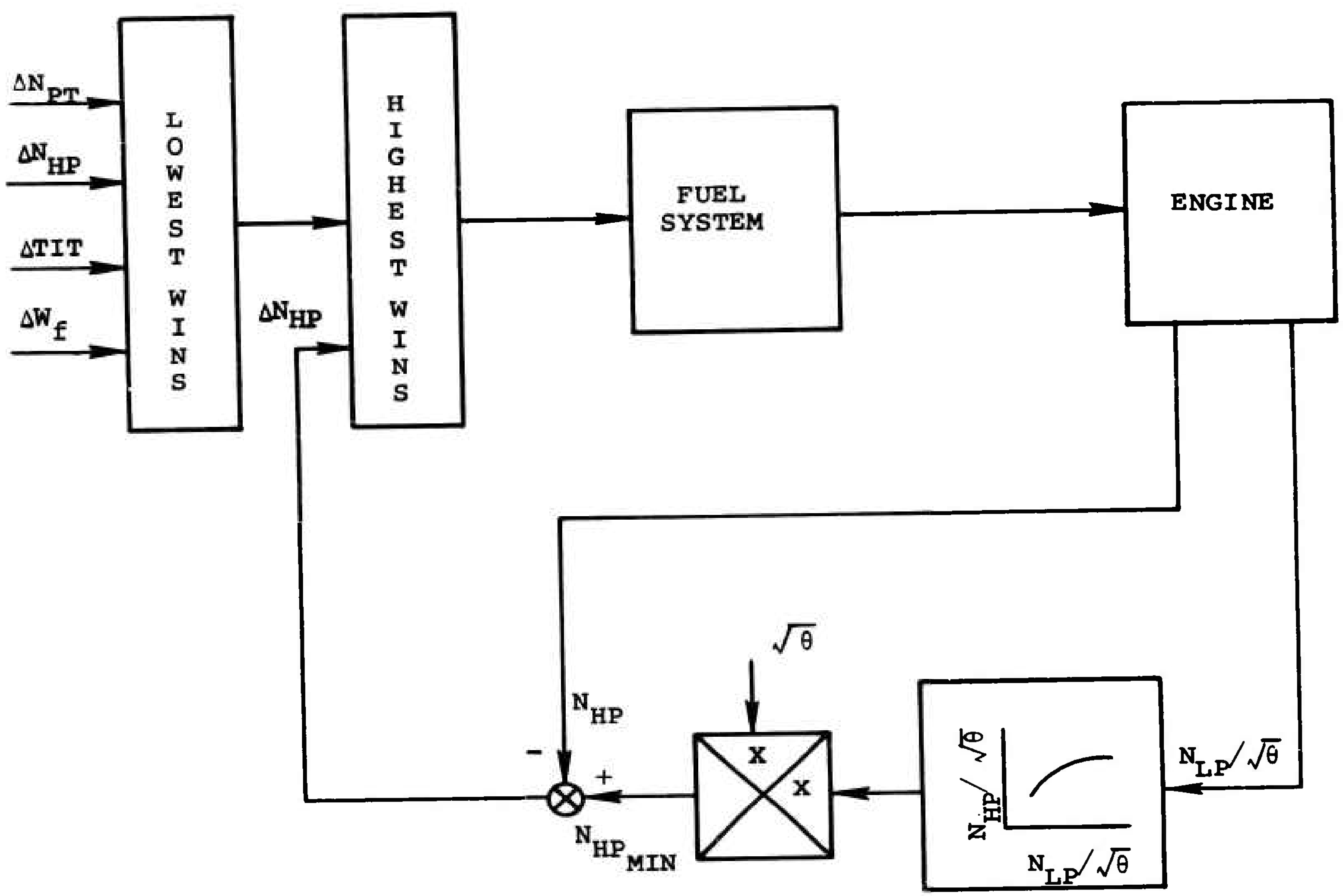

Figure 36. Deceleration Control Schematic for 3S-RF-TSE.

speed, corrected to inlet temperature, is entered into a function generator, the output of which corresponds to minimum HP spool speed, corrected to inlet temperature. This minimum HP spool speed is multiplied by $\sqrt{\theta_2}$ and then compared to physical spool speed. If the spool speed attempts to fall below the minimum allowable, the action of the "highest wins" block prevents further defueling and thereby prevents the engine from entering surge conditions.

5.1.2 2S-TSE Control

The control system for the 2S-TSE consists of (a) an acceleration schedule to avoid surge and turbine overtemperature, (b) a deceleration schedule to prevent lean-combustor blowout, (c) a gas generator speed governor, and (d) a power turbine speed governor. Figure 37 is a block diagram showing the functional aspects of the control. The maximum schedule is fuel flow to compressor discharge P/P versus gas generator speed. Although not indicated on the diagram, the scheduled ratio is corrected, as is gas generator speed. It was found that lean-combustor blowout could be avoided by scheduling a constant minimum corrected ratio. It was assumed for the purposes of this study that the variable-geometry actuation is of such a rate that it was always positioned to allow this scheduling.

The power turbine governor resets the gas generator governor to increase or decrease gas generator speed to accommodate changes in rotor load. The system is designed to maintain power turbine speed for changes in load. Because of proportional control, there will be some droop of power turbine speed. The control gains were chosen from the stability study to give good transient characteristics and reasonable power turbine droop (less than 3 percent). It was not the purpose of this study to optimize a control; therefore, the control parameters that do not affect transient acceleration and deceleration times were not considered.

A linear mathematical engine/rotor model for the 2S-TSE was generated based on steady-state unbalanced torque data. Except for the acceleration and deceleration schedules, the fuel control has a negligible effect on the transient results for the large changes in rotor load that were considered.

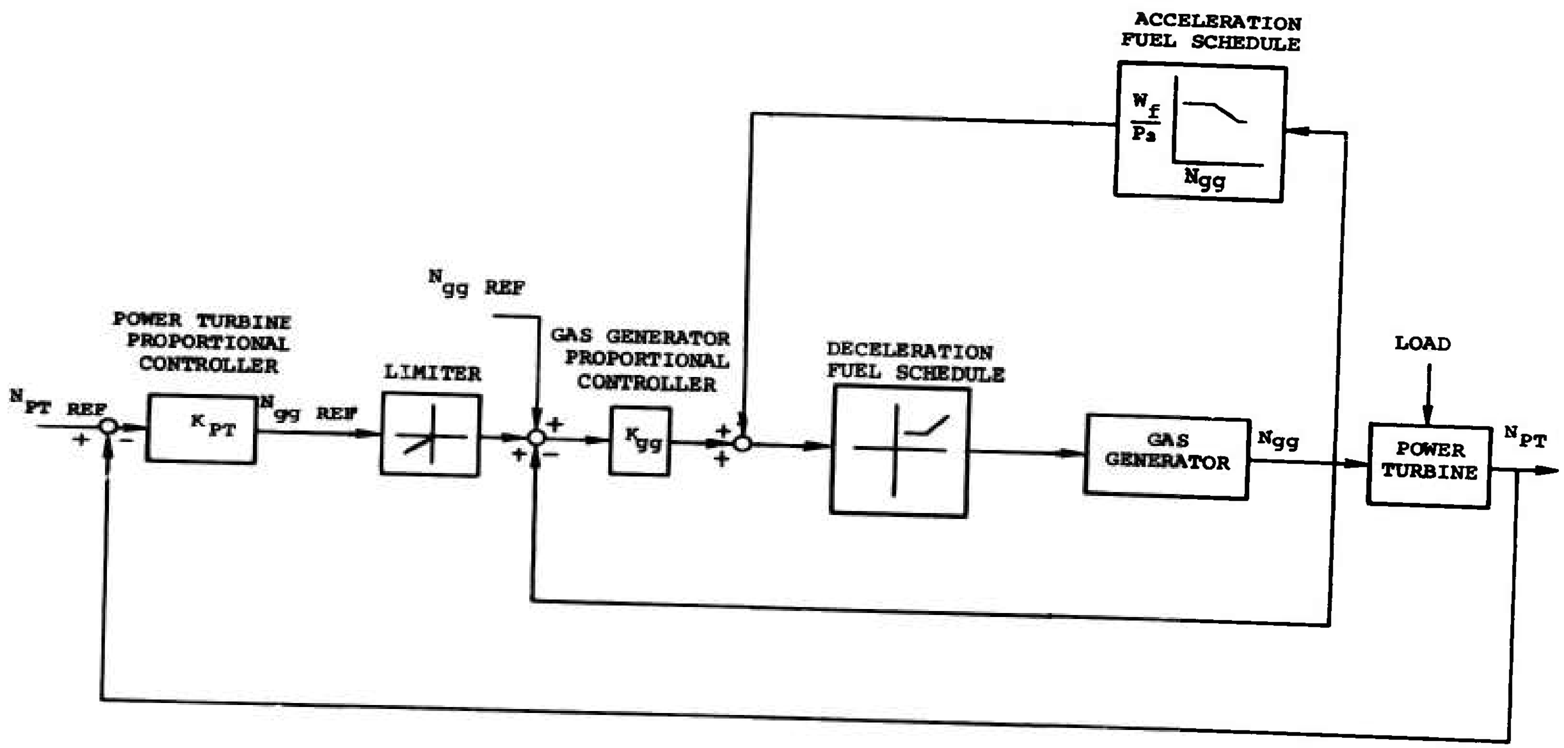

Figure 37. Functional Block Diagram for Control Used for the 2S-TSE.

5.2 POWER MANAGEMENT

As with other conventional turboshaft engines, the 2S-TSE is rated on TIT with a gas generator speed override. As shown in Figure 38, the turbine arrangement for the 3S-RF-TSE causes unconventional variation in turbine temperature with engine power. In many instances, more than one value of horsepower is produced for a given TIT, which eliminates TIT as a power-rating parameter.

Since a relatively constant off-design power turbine specific work is maintained, the 3S-RF-TSE throttles almost entirely with LP compressor airflow. Therefore, LP spool corrected speed ($N_{LP}/\sqrt{\theta_2}$) was chosen for the engine rating parameter because of:

1. The close correlation between corrected LP spool speed and engine airflow,
2. The accuracy of speed measurement, and
3. The unique value of corrected LP spool speed that exists for each power setting.

Figure 39 shows corrected LP spool speed versus corrected horsepower with lines of constant flight speed. The curves are nondimensionalized to include all altitudes and ambient temperature variations. The LP spool speeds selected to represent the various throttle settings are indicated on this figure.

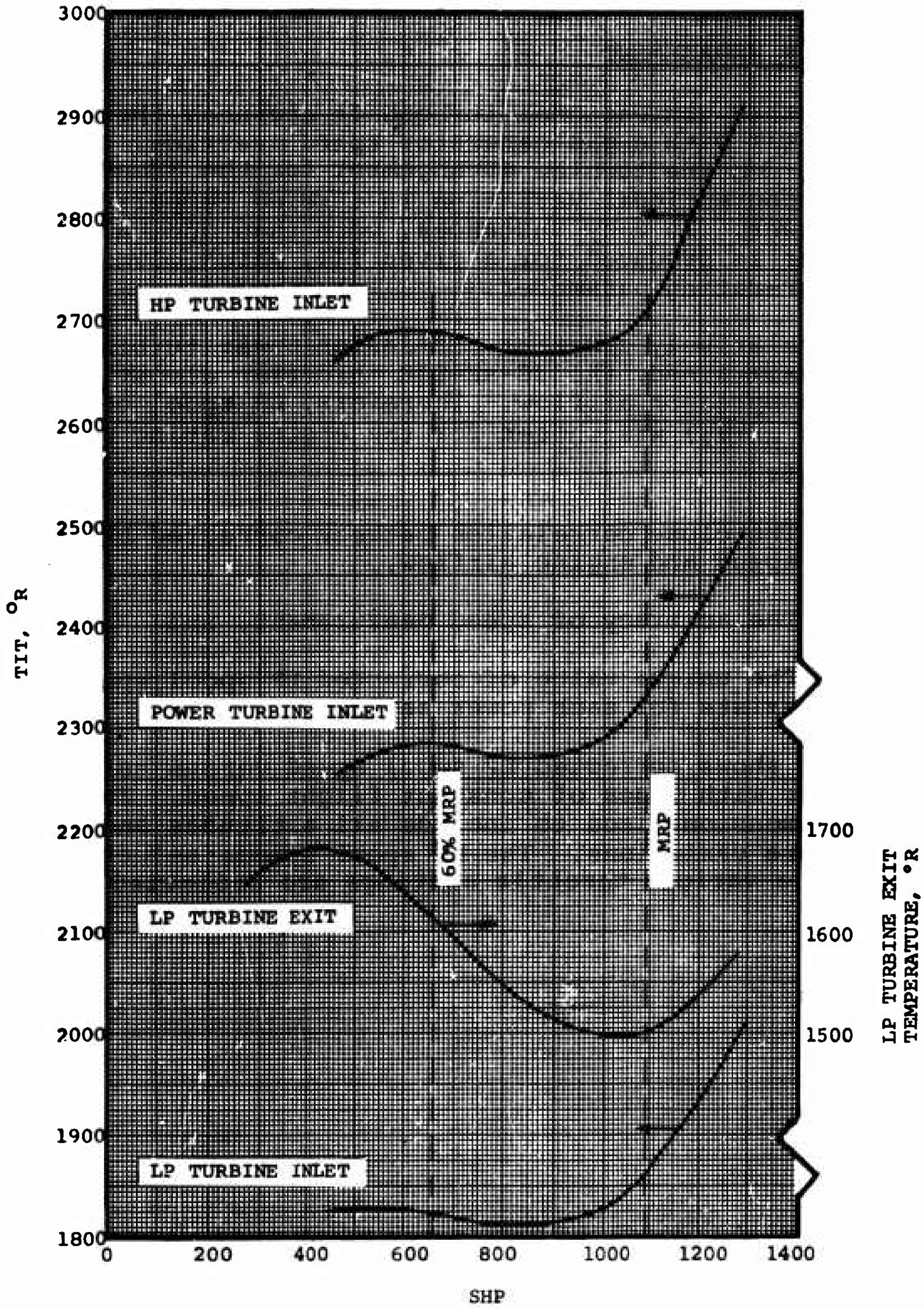

Figure 38. TIT Versus Shaft Horsepower for 3S-RF-TSE.

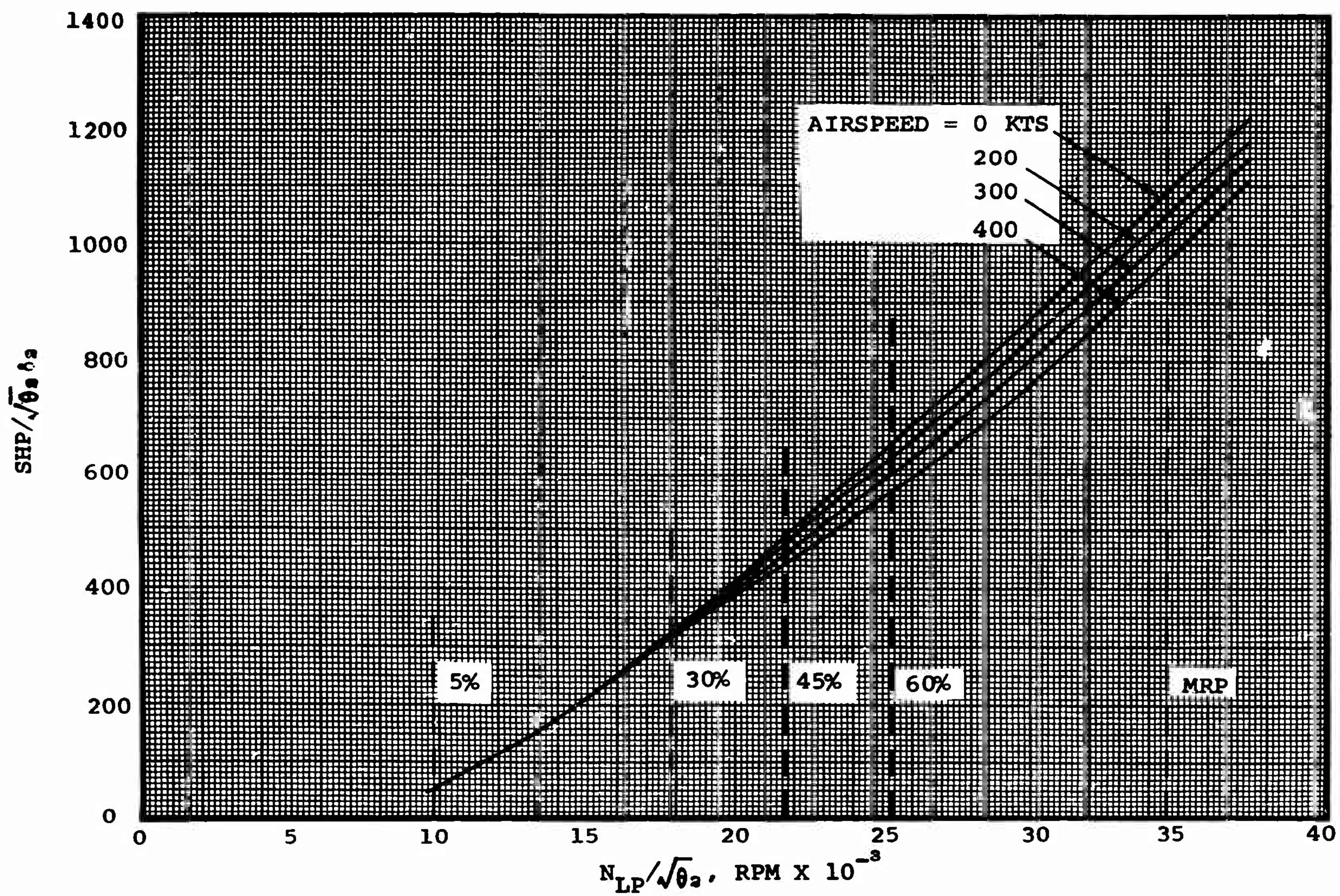

Figure 39. Corrected Shaft Horsepower Versus Corrected LP Spool Speed for 3S-RF-TSE.

5.3 STABILITY ANALYSIS

Conventional Bode plot techniques were employed to demonstrate engine/control-system stability for both engine configurations. The technique utilized was to disconnect the rotor load and dynamics from the engine model and then to input a step change in rotor load.

A linear engine/load model was prepared for the 3S-RF-TSE since the digital thermodynamic model used for assessment of acceleration and deceleration characteristics is nonlinear.

A block diagram of the fuel control, engine, and rotor load in linearized transfer function form is presented in Figure 40. Selection of fuel control gain (K_F) and lead-time-constant (τ) values was accomplished by conventional frequency-response techniques, the final values being 2.0 and 0.65, respectively.

Verification of the resulting linear model was achieved by comparing its response with the nonlinear model when subjected to a 5-percent fuel-flow step at MRP. Figure 41 illustrates the response of both models and shows good agreement.

Figure 42 illustrates the Bode plot for the system with the feedback signal disconnected. The system is stable as indicated by the 130-degree phase margin (arrows in Figure 42).

In order to verify closed-loop stability, the linear model was mechanized in digital form with use of the IBM Continuous System Modeling Program (CSMP) in the IBM 1130 Computer. Conditions were initiated at rotor speed = 100 percent and rotor load = 60 percent, after which rotor load was stepped to 100 percent. The transient response of the system is represented in Figure 43 and demonstrates a well-ordered control action. Maximum power turbine droop during the transient is constrained to 0.45 percent.

A similar stability analysis was conducted for the 2S-TSE with use of the linear engine/load model developed for the transient study. The 270-degree phase margin implied for this engine on the Bode plot of Figure 44 assures open-loop stability. A perturbation analysis of the closed-loop system was conducted on the analog computer (comparable to the CSMP technique used for the 3S-RF-TSE). Again, well-ordered system response to a step change in rotor load is indicated in Figure 45.

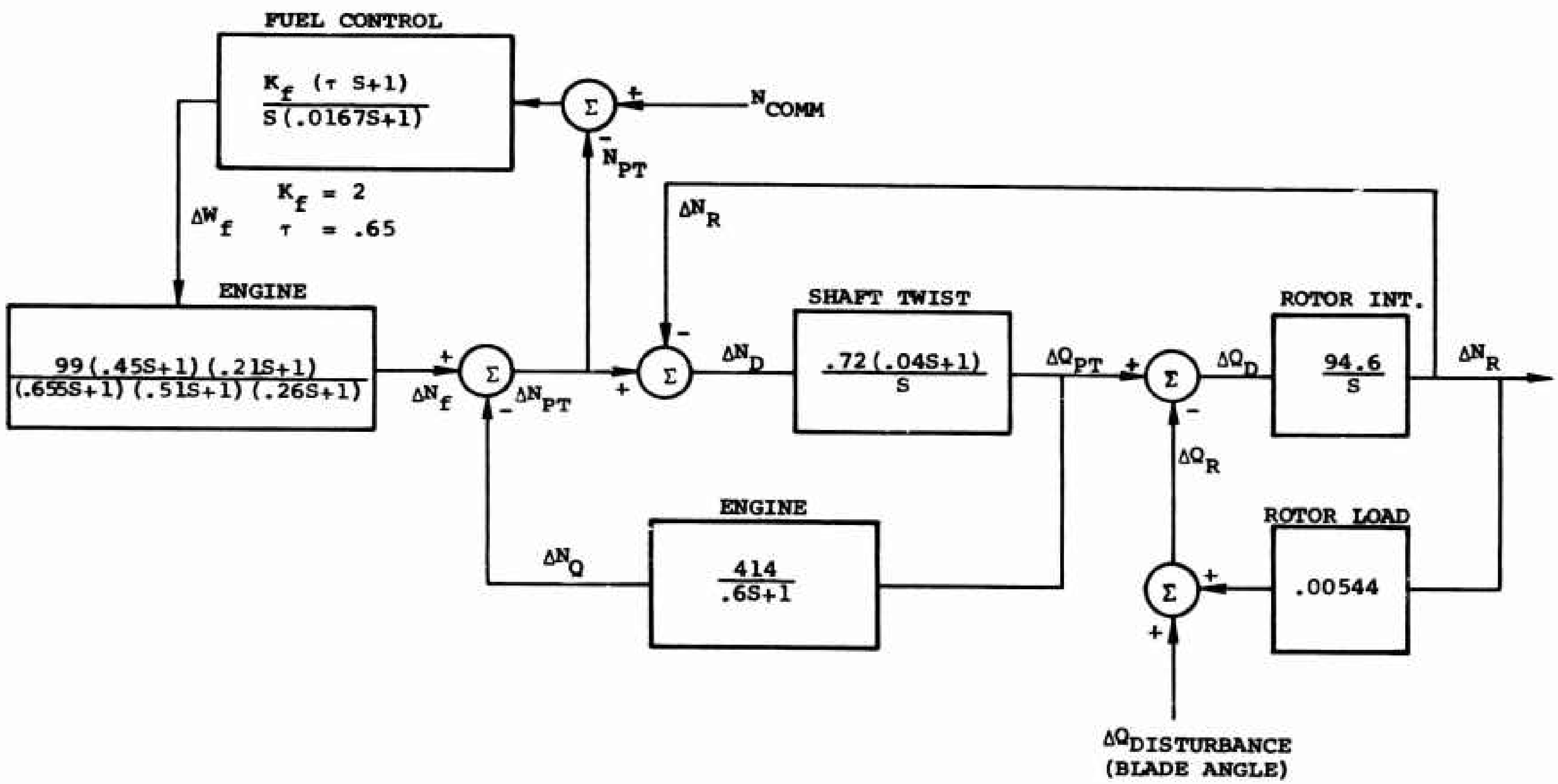

Figure 40. Block Diagram of Linear Transfer Function Mode for 3S-RF-TSE.

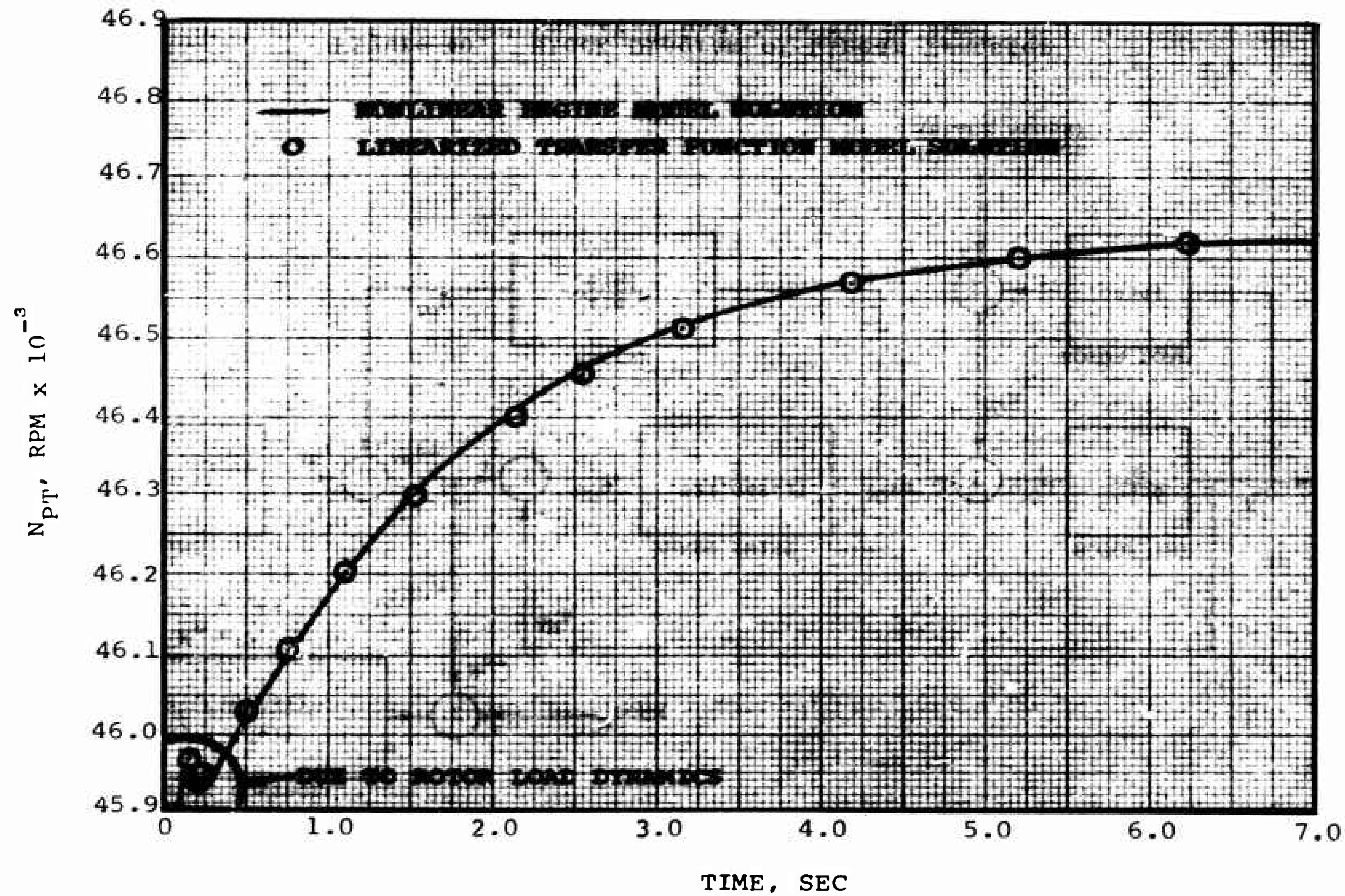

Figure 41. Comparison of Transient Response for Both Linear and Nonlinear Engine Models.

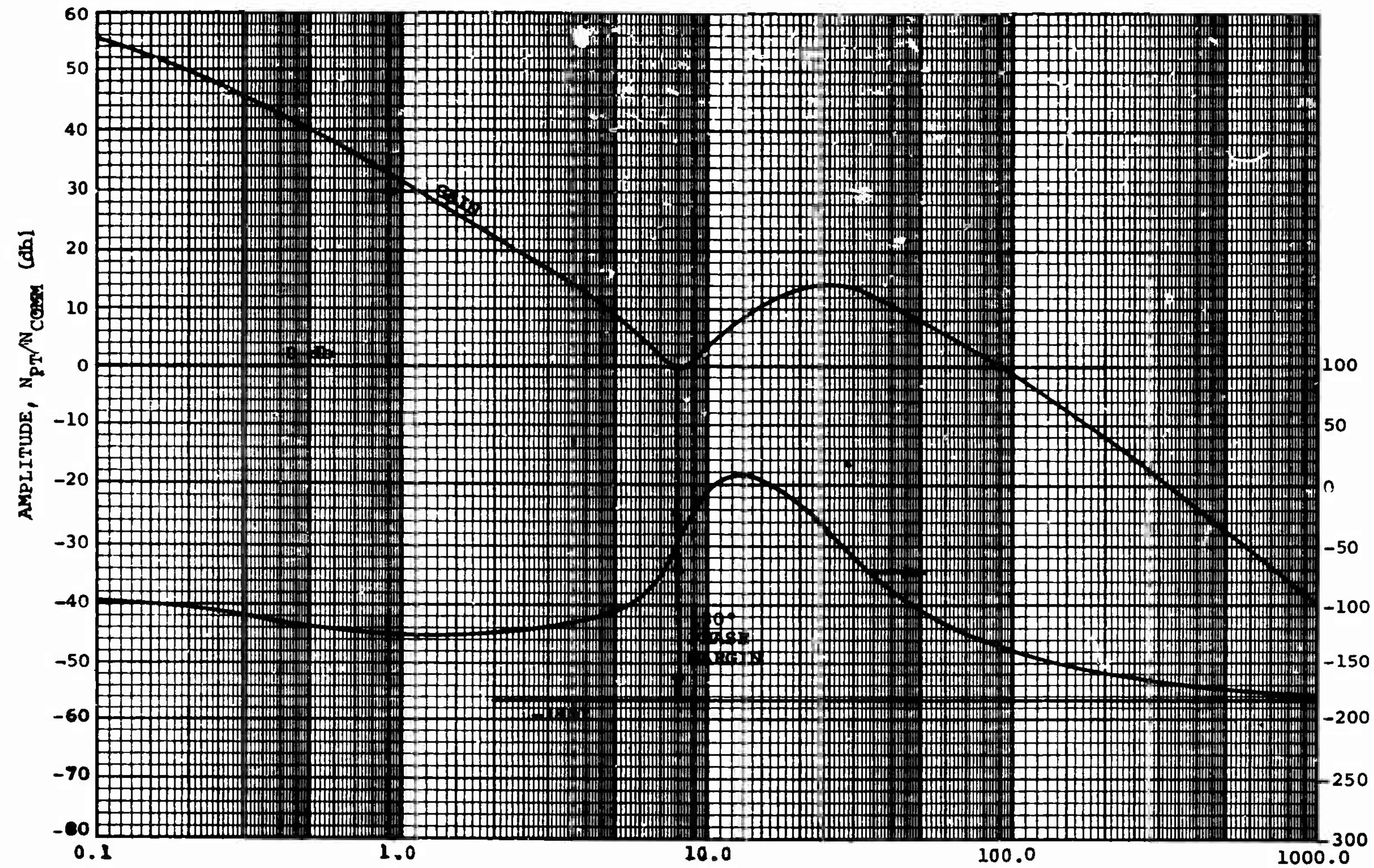

Figure 42. Bode Plot Illustrating Open-Loop Stability of 3S-RF-TSE.

TIME, SEC	ΔW_f, LB/HR			$\Delta N_{TURBINE}$, RPM
0.000	0.0000	0.0000	0.0000	0.0000
0.050	42.2808	0.0000	0.0000	-40.3253
0.100	110.1602	0.0000	0.0000	-96.7949
0.150	164.6865	0.0000	0.0000	-144.7991
0.200	253.7273	0.0000	0.0000	-182.7133
0.250	309.2356	0.0000	0.0000	-206.2295
0.300	346.7837	0.0000	0.0000	-213.9524
0.350	365.1782	0.0000	0.0000	-207.0088
0.400	365.8311	0.0000	0.0000	-188.0039
0.450	351.9893	0.0000	0.0000	-160.6406
0.500	327.9238	0.0000	0.0000	-126.8594
0.550	298.2178	0.0000	0.0000	-96.3906
0.600	267.1426	0.0000	0.0000	-66.3203
0.650	238.2344	0.0000	0.0000	-40.8574
0.700	214.0488	0.0000	0.0000	-21.3047
0.750	196.0713	0.0000	0.0000	-8.0458
0.800	184.7959	0.0000	0.0000	-0.7539
0.850	179.9682	0.0000	0.0000	1.4590
0.900	180.3086	0.0000	0.0000	-0.1758
0.950	184.7764	0.0000	0.0000	-4.3008
1.000	191.7676	0.0000	0.0000	-9.6250
1.050	199.8545	0.0000	0.0000	-15.0195
1.100	207.8067	0.0000	0.0000	-19.6289
1.150	214.6807	0.0000	0.0000	-22.9219
1.200	219.8926	0.0000	0.0000	-24.6172
1.250	223.1572	0.0000	0.0000	-24.7188
1.300	224.5029	0.0000	0.0000	-23.4141
1.350	224.1602	0.0000	0.0000	-21.0391
1.400	222.5098	0.0000	0.0000	-17.9344
1.450	219.9983	0.0000	0.0000	-14.6133
1.500	217.0606	0.0000	0.0000	-11.3047
1.550	214.1143	0.0000	0.0000	-8.3203
1.600	211.4756	0.0000	0.0000	-5.5955
1.650	209.3467	0.0000	0.0000	-3.9844
1.700	207.9438	0.0000	0.0000	-2.7393
1.750	206.9905	0.0000	0.0000	-2.0547
1.800	206.7051	0.0000	0.0000	-1.8320
1.850	206.9004	0.0000	0.0000	-1.9453
1.900	207.4277	0.0000	0.0000	-2.2578
1.950	208.1504	0.0000	0.0000	-2.6484
2.000	208.9209	0.0000	0.0000	-3.0313
2.050	209.6553	0.0000	0.0000	-3.3281
2.100	210.2490	0.0000	0.0000	-3.4805
2.150	210.6748	0.0000	0.0000	-3.4383
2.200	210.9043	0.0000	0.0000	-3.3555
2.250	210.9561	0.0000	0.0000	-3.1016
2.300	210.8565	0.0000	0.0000	-2.7517
2.350	210.6436	0.0000	0.0000	-2.3328
2.400	210.3741	0.0000	0.0000	-1.9961
2.450	210.0733	0.0000	0.0000	-1.6172
2.500	209.7903	0.0000	0.0000	-1.2969
2.550	209.5361	0.0000	0.0000	-1.0195
2.600	209.3418	0.0000	0.0000	-0.8242

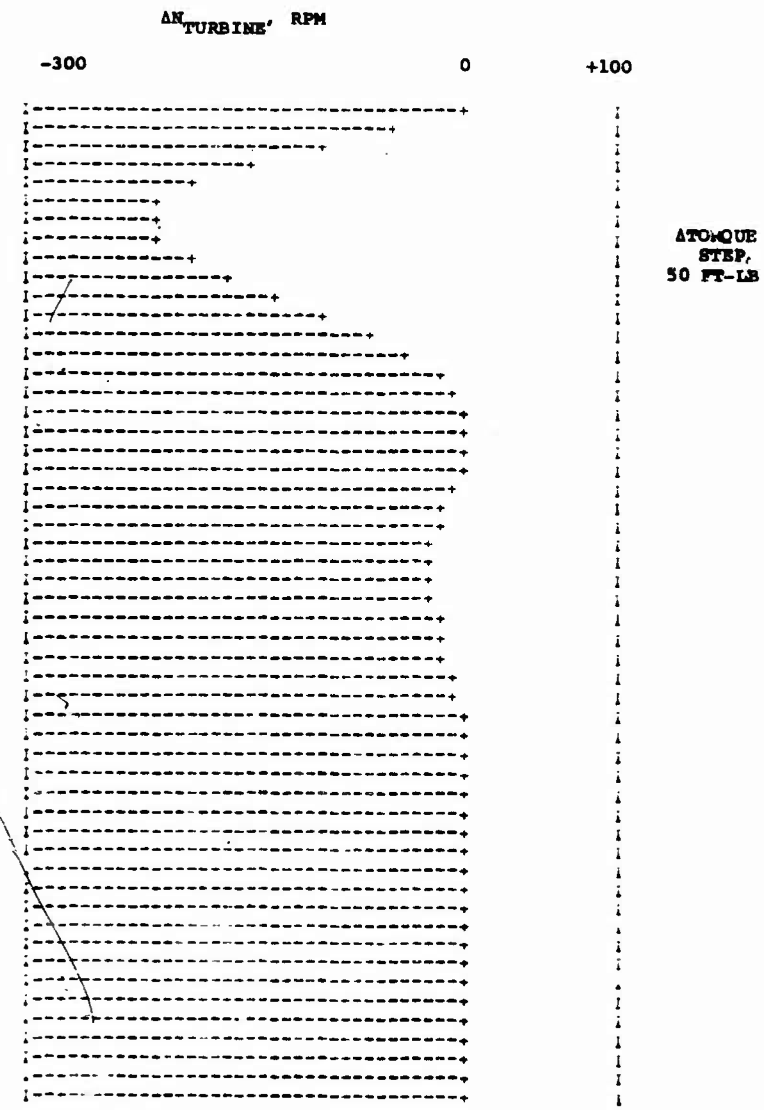

Figure 43. CSMP Data Showing Closed-Loop Stability of 3S-RF-TSE.

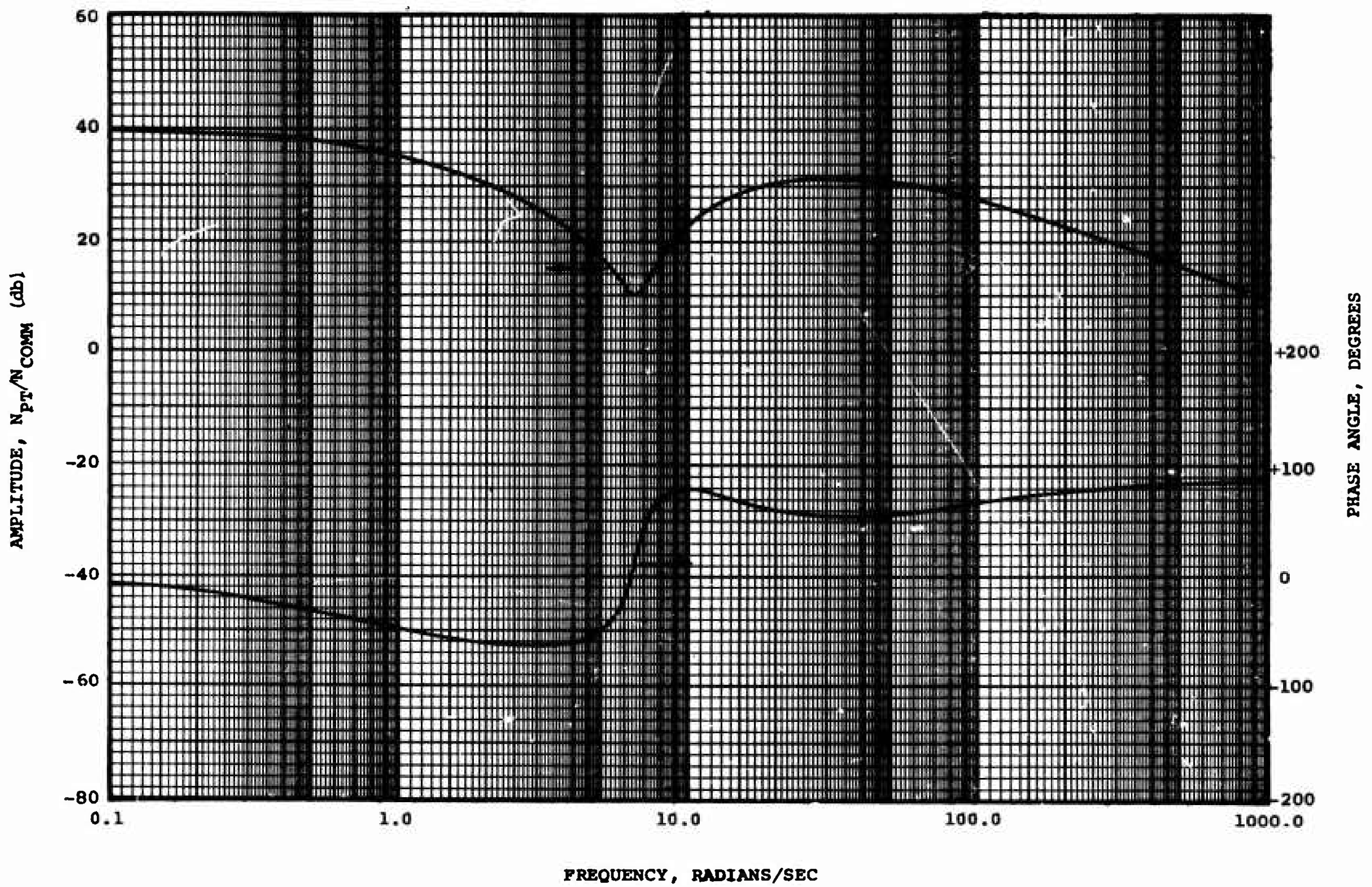

Figure 44. Bode Plot Illustrating Open-Loop Stability of 2S-TSE.

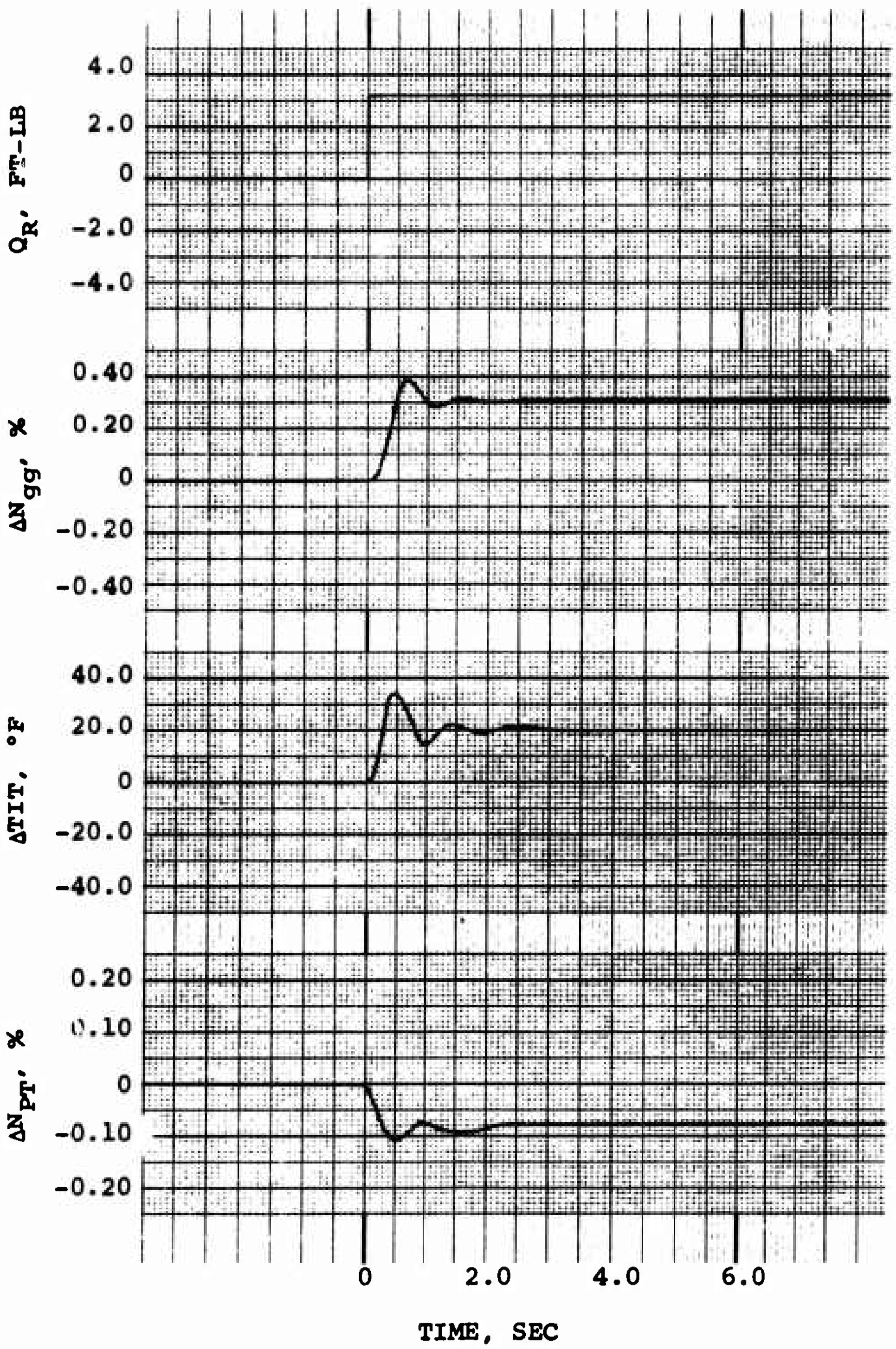

Figure 45. Analog Perturbation Study Showing Closed-Loop Stability of 2S-TSE.

5.4 ENGINE TRANSIENT ANALYSIS

5.4.1 Assumptions

The following assumptions were used for the transient analysis of both engines.

1. Load application (collective) from idle to MRP in 1.0 second (linear).

2. Transient overtemperature limit - 100°F (to 2500°F).

3. Minimum compressor surge margin from nominal surge - 4 percent [see Equation (2) for surge margin definition].

4. Reflected gearbox characteristics as defined by Figure 46.

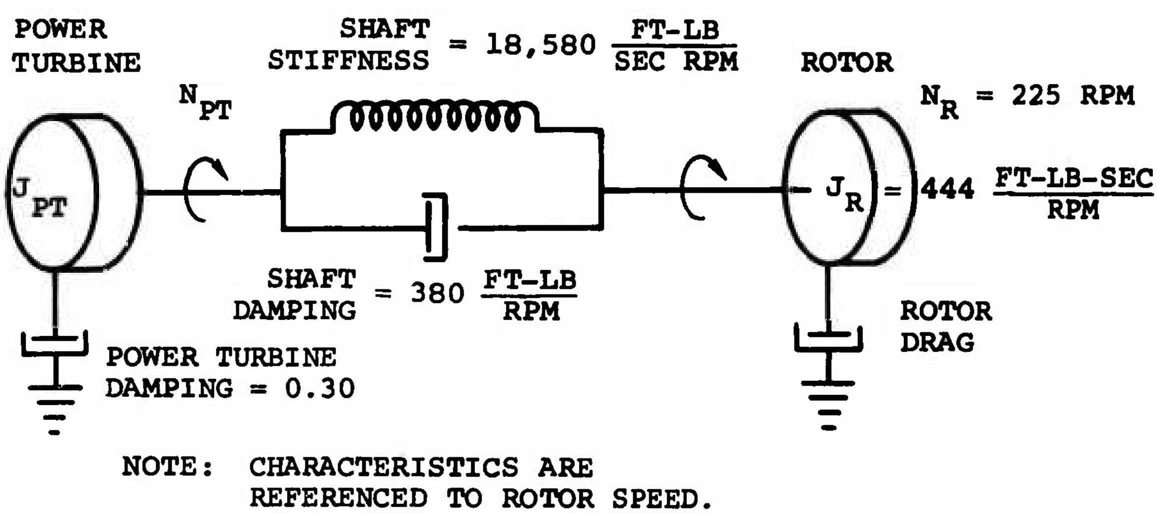

Figure 46. Schematic of Reflected Gearbox Characteristics Used for Transient Study.

5.4.2 Transient Analysis for 3S-RF-TSE

The transient characteristics of the 3S-RF-TSE were determined by using a computerized thermodynamic model of the engine and an ideal control system. The primary limitation in engine overfueling was TIT, since surge margin for both the HP compressor and LP compressor were in excess of the 4-percent limit.

Transient characteristics were determined by the flight conditions defined in Table XII. Results of the acceleration study are presented in Figure 47, which shows the time required for the engine to reach 95 percent MRP when accelerated from various initial horsepower points. From this figure it can be concluded that acceleration response time is increased with

1. Decreasing flight speed
2. Increasing altitude
3. Increasing ambient temperature

TABLE XII. TRANSIENT CONDITIONS FOR THE 3S-RF-TSE STUDY

Day	Altitude (ft)	Flight Speed (kts)	Transient
Std	0	0, 200, 400	Accel from idle to MRP
Std	0	0, 200, 400	Accel from 30% to MRP
Std	0	0, 200, 400	Accel from 60% to MRP
Std	0	0, 200, 400	Decel from MRP to idle
Std	0	0, 200, 400	Decel from MRP to 60%
Std and 95°F	4000	0 and 400	Accel from idle to MRP
Std and 95°F	4000	0 and 400	Decel from MRP to idle
Std	10,000	0 and 400	Accel from idle to MRP
Std	10,000	0 and 400	Decel from MRP to idle

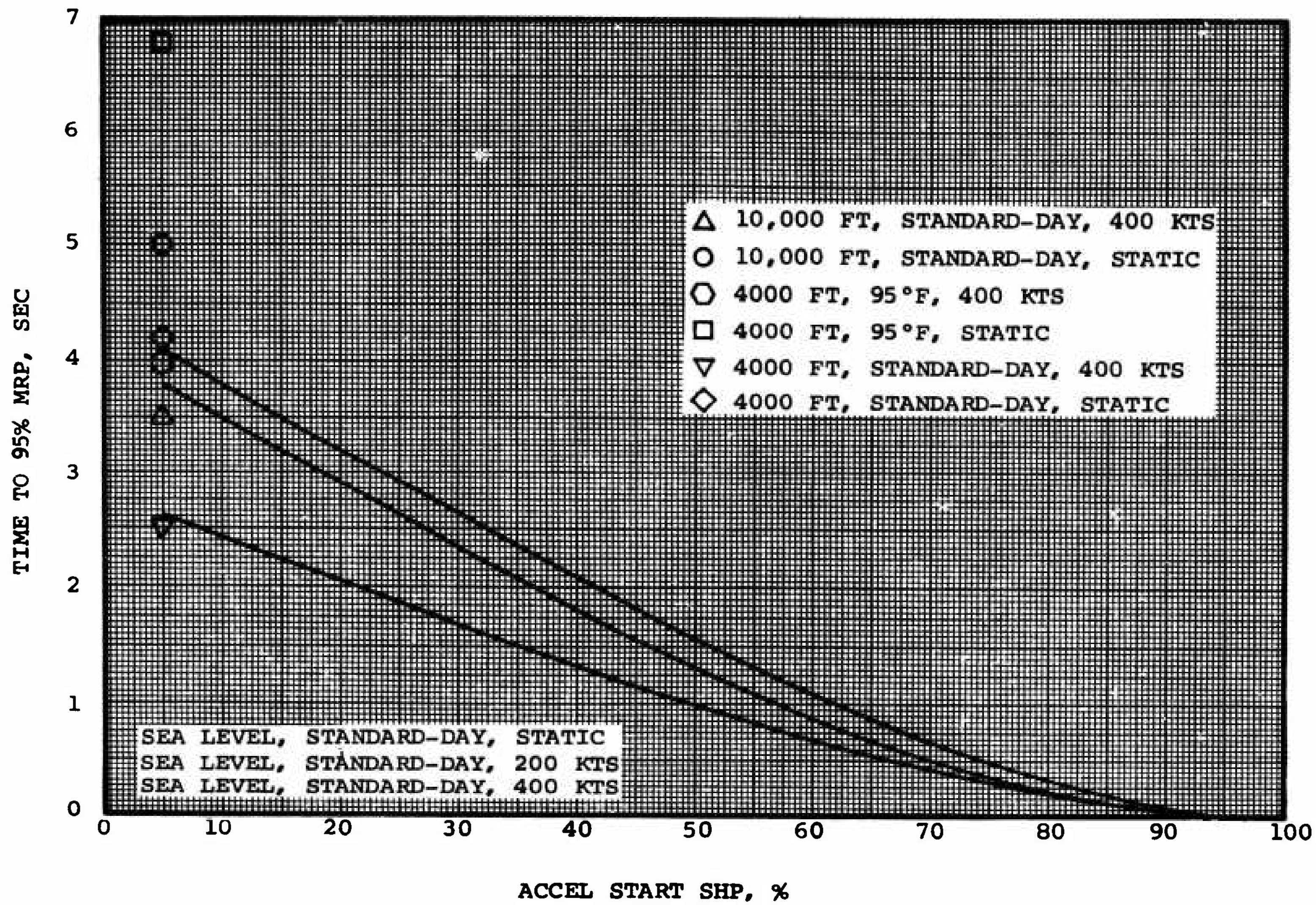

Figure 47. Acceleration Characteristics of 3S-RF-TSE.

Figure 48 indicates the results of the deceleration study, showing the time required to traverse 95 percent of the power-demand change when decelerated from MRP. From this figure it can be concluded that deceleration time is increased with

1. Increasing flight speed

2. Increasing altitude

3. Increasing ambient temperature (negligible effect)

Figures 49 and 50 demonstrate the relative behavior of the three spool speeds, TIT, and output torque, during a sea-level static acceleration and deceleration, respectively.

During the analysis it became evident that, when starting from low initial horsepower, power turbine droop conditions would result through the acceleration (refer to Figure 49). Two of the ground rules established for the study (i.e., 2500°F maximum acceleration TIT and a load-ramp time of 1 second from idle to MRP) had a significant effect on this droop. In order to preserve the comparative compatibility between the two engine studies, these ground rules were not changed, and the data presented include these effects. However, in retrospect, it was apparent that several variations of these ground rules, as well as other devices, could have been employed to counteract the droop condition.

For example, consider the fixed TIT limit. The 3S-RF-TSE has an inherent acceleration handicap, since it is essentially throttled by reduction of airflow rather than TIT, this being a characteristic of the turbine arrangement and the mechanism by which its good part-power performance is obtained (see Paragraph 4.2). The airflow at idle for the 2S-TSE is approximately 50 percent of its MRP airflow, while the 3S-RF-TSE idle airflow is only 20 percent of its MRP value. Figure 51 illustrates a plot of power turbine droop as a function of airflow at the start of the transient and shows that the droop increases significantly as the airflow decreases below 50 percent of its MRP airflow.

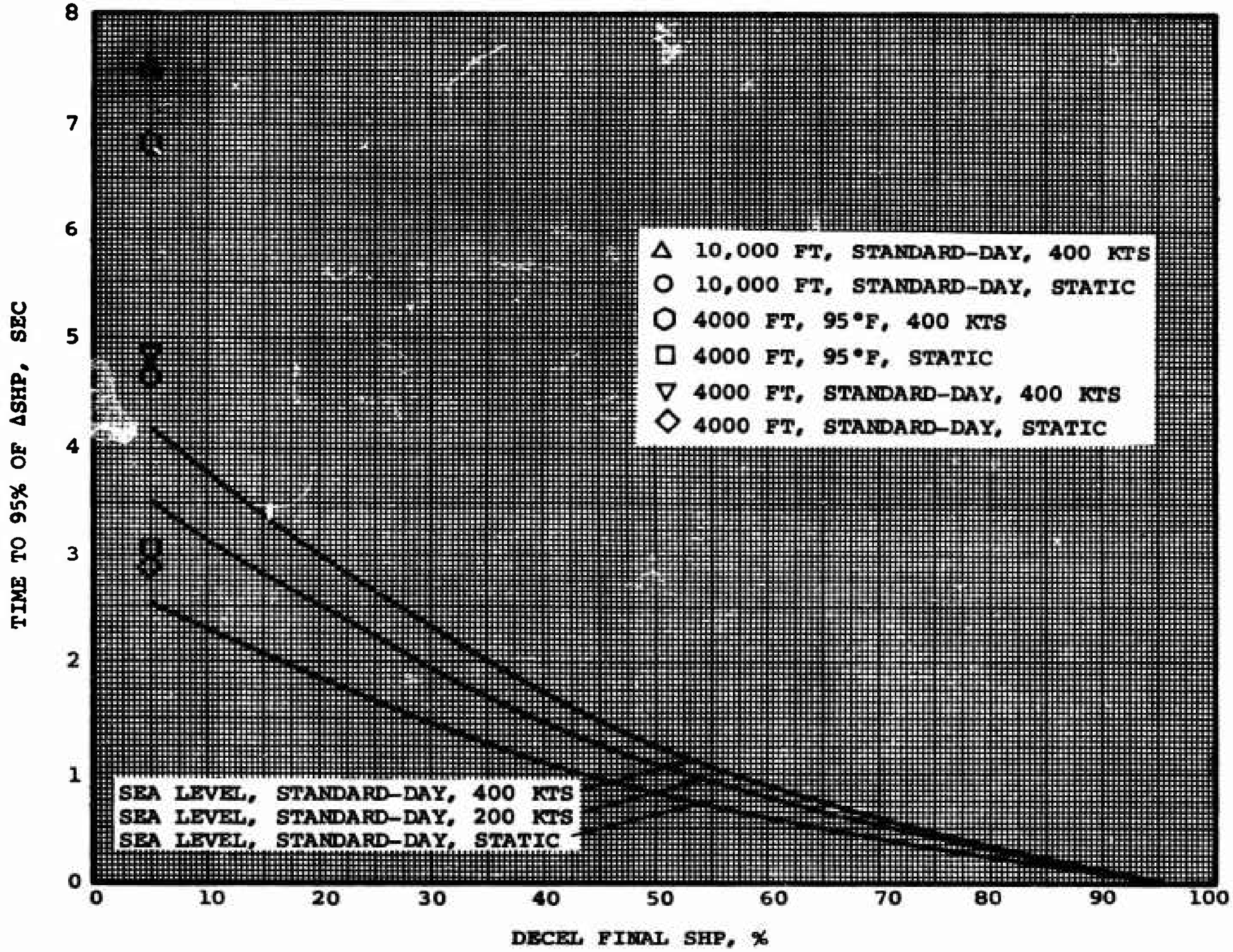

Figure 48. Deceleration Characteristics of 3S-RF-TSE.

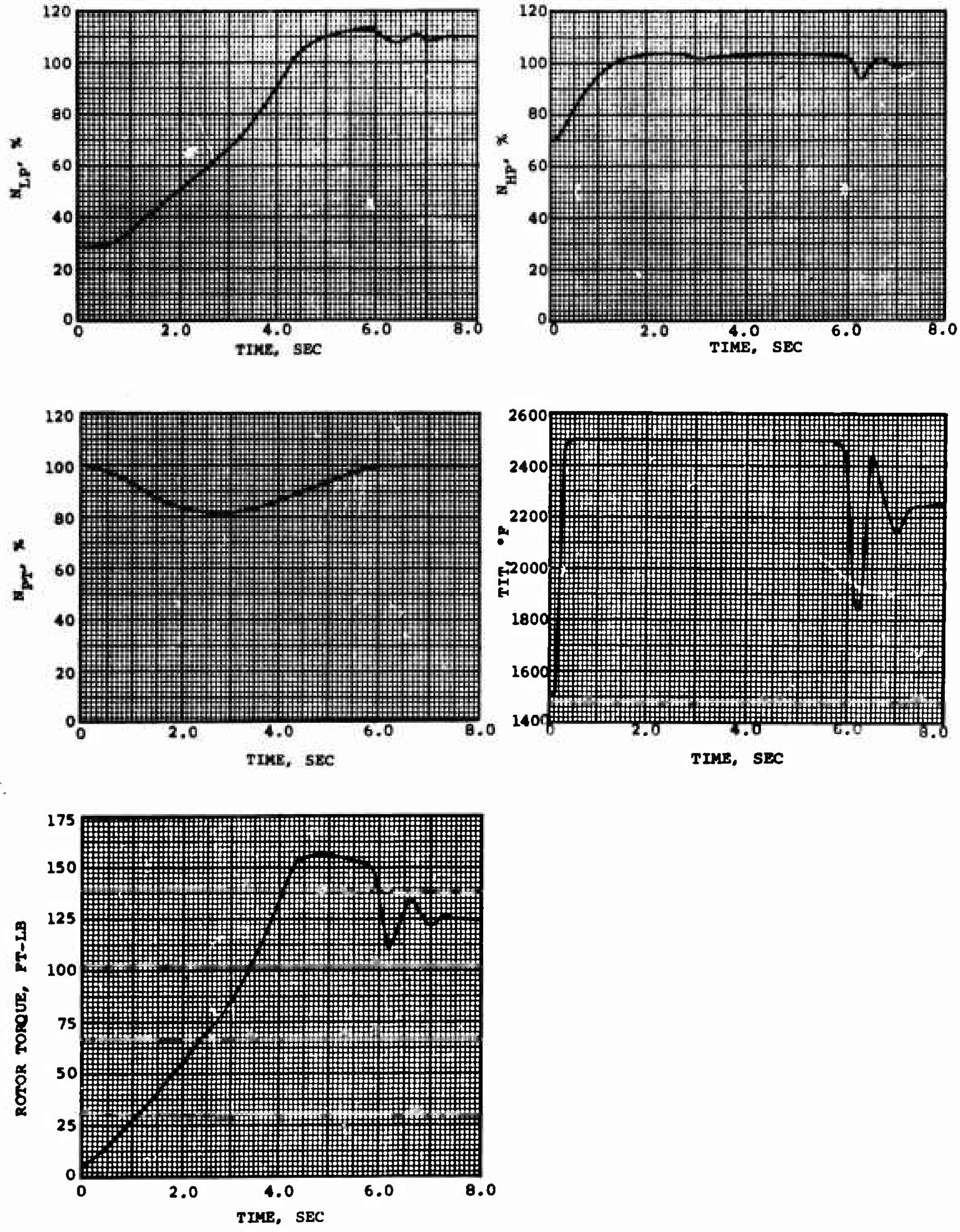

Figure 49. HP and LP Compressor and Power Turbine Speed, TIT, and Output Torque Versus Time for Acceleration of 3S-RF-TSE.

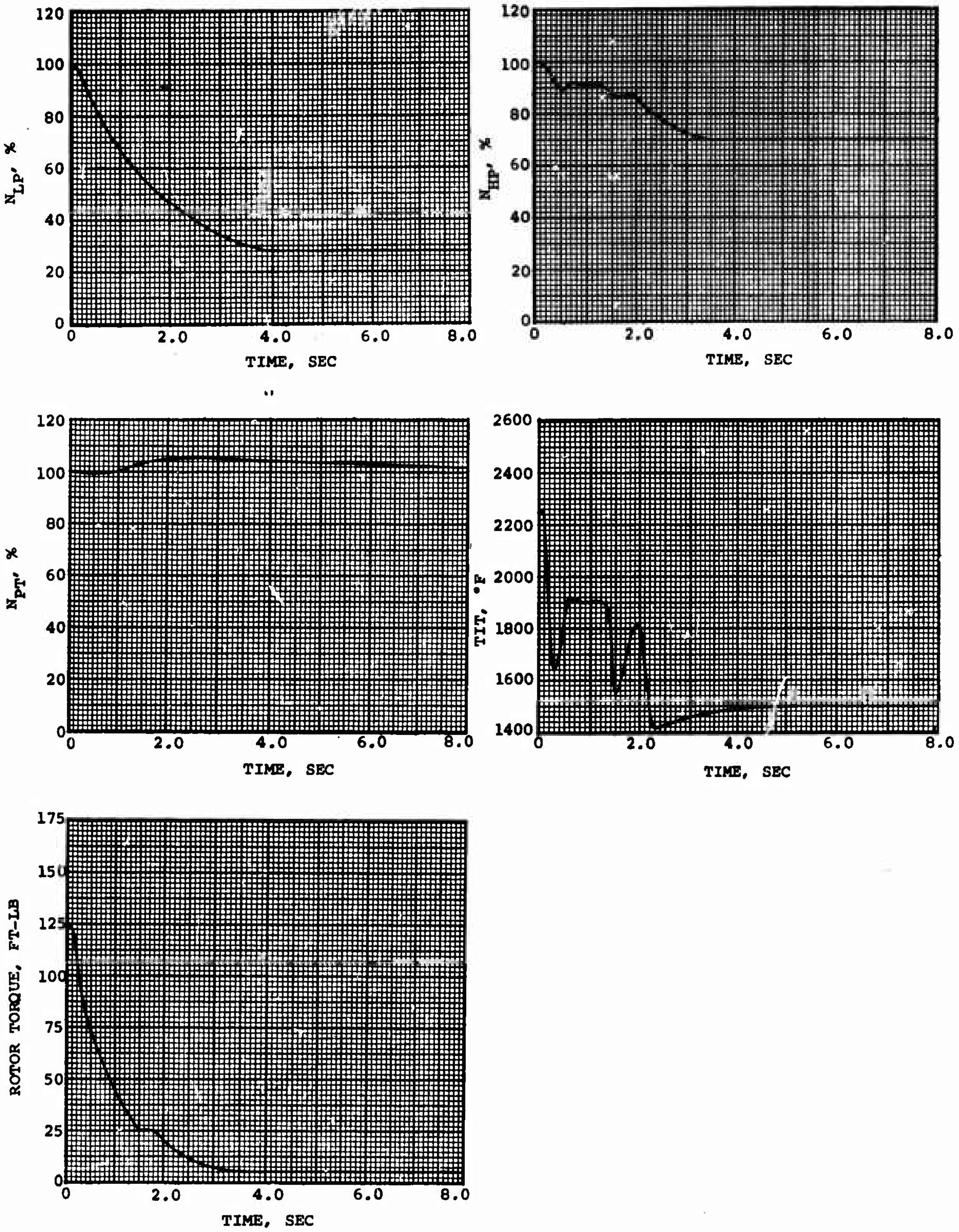

Figure 50. HP and LP Compressor and Power Turbine Speed, TIT, and Output Torque Versus Time for Deceleration of 3S-RF-TSE.

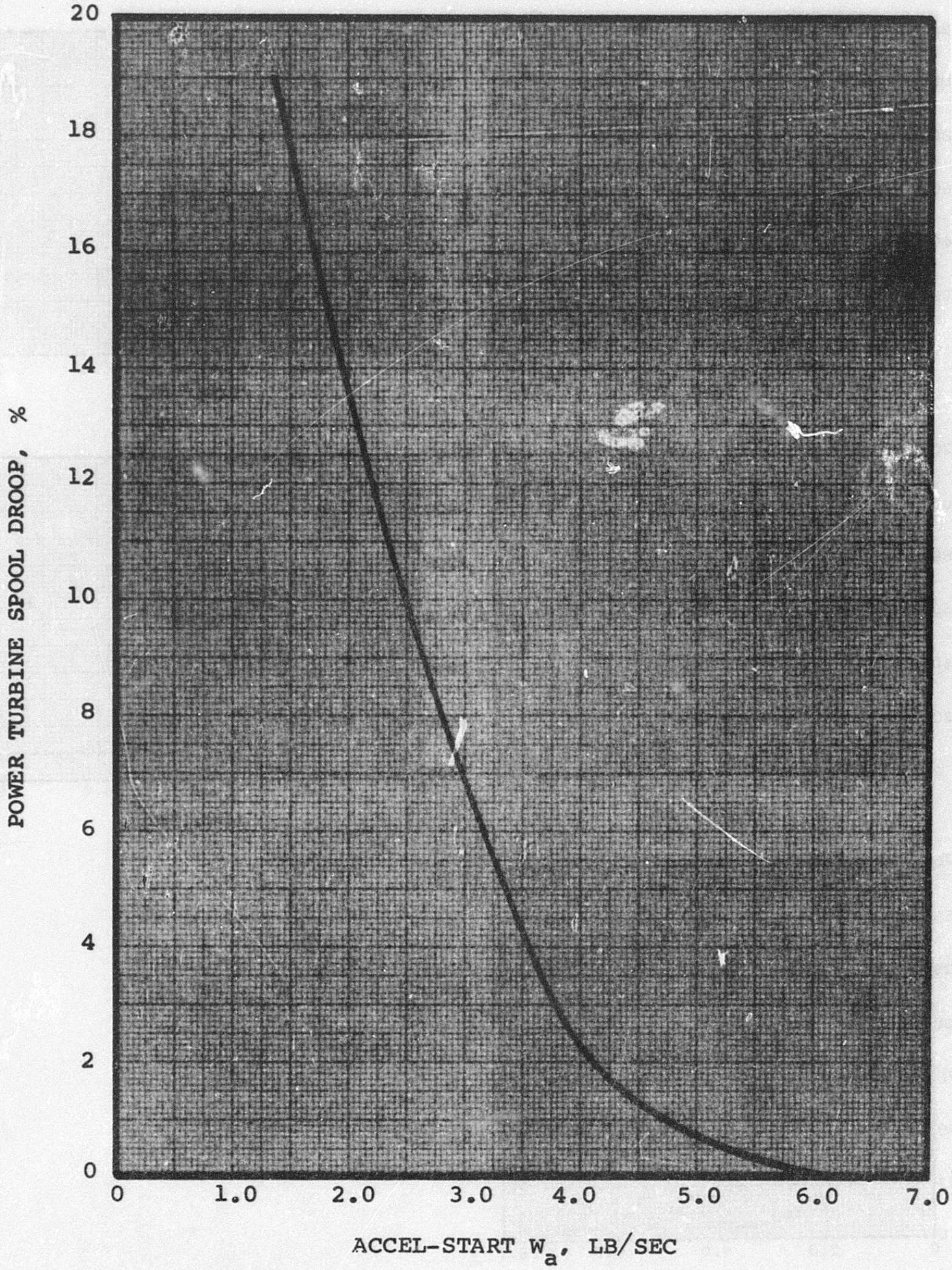

Figure 51. Power Turbine Droop Versus Initial Airflow.

Since both airflow and ΔTIT (between idle and 2500°F) contribute to the excess torque available to sustain the power turbine and accelerate the LP compressor, the same fixed TIT for both engines imposes an additional burden on the 3S-RF-TSE. It is apparent that the droop that results from the low airflow at idle with the 3S-RF-TSE could be mitigated by providing a higher maximum TIT at these lower airflow conditions and that the temperature increase could be a function of the LP spool speed. Figure 52 illustrates a candidate TIT versus corrected LP spool speed schedule.

Other techniques that could be employed to reduce the droop and possibly increase the transient response rate of the 3S-RF-TSE are:

1. Variable turbine geometry.
2. A limiter between the collective pitch control stick and rotor blade angle actuator such that for low airflow conditions, the collective pitch demand rate is reduced.
3. Some form of load anticipator such as collective-pitch reset of the power turbine governor to reset the gas generator governor when the collective pitch control stick is moved rather than waiting to sense the power turbine droop.
4. Power transfer from the power shaft to the LP spool to increase the airflow.

These investigations were considered to be beyond the scope of this study but would be essential for optimizing the transient characteristics of the 3S-RF-TSE.

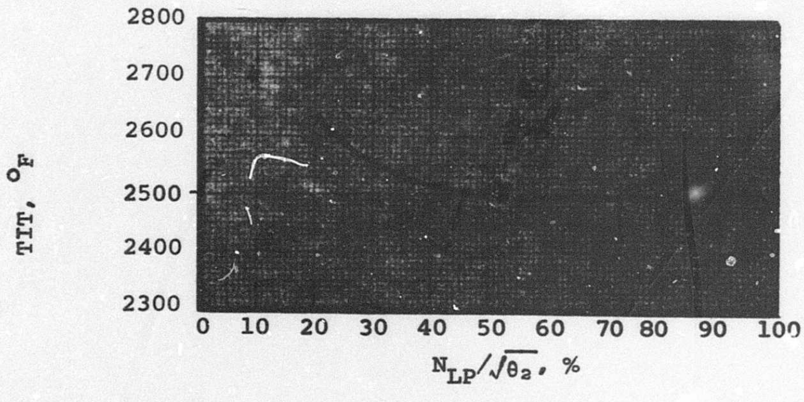

Figure 52. Candidate TIT Versus Corrected LP Spool Speed.

5.4.3 Transient Analysis for 2S-TSE

Figure 53 shows the acceleration characteristics of the 2S-TSE from idle (5 percent MRP) to MRP for the sea-level, standard-day, static case. The gas generator spool accelerated from 74.7 percent speed (IDLE) to 100 percent speed (MRP) in approximately 1.6 seconds. The power turbine speed dropped from 102.8 percent to 100.0 percent speed, and 95 percent MRP was attained within 1.3 seconds. A transient speed excursion to 97.7 percent was noted during the acceleration. Transient response of other engine or control parameters--TIT, fuel flow, and gas generator torque--is included in the figure.

Figure 54 shows the deceleration characteristics of the engine from MRP to idle for sea-level, standard-day, static. The curves show the same information as in the acceleration case. The gas generator spool speed drops down to within 0.5 percent of its steady-state value in 1.65 seconds.

The results of the acceleration and deceleration study for other initial throttle settings are summarized for the sea-level, standard-day, static conditions in Figure 55.

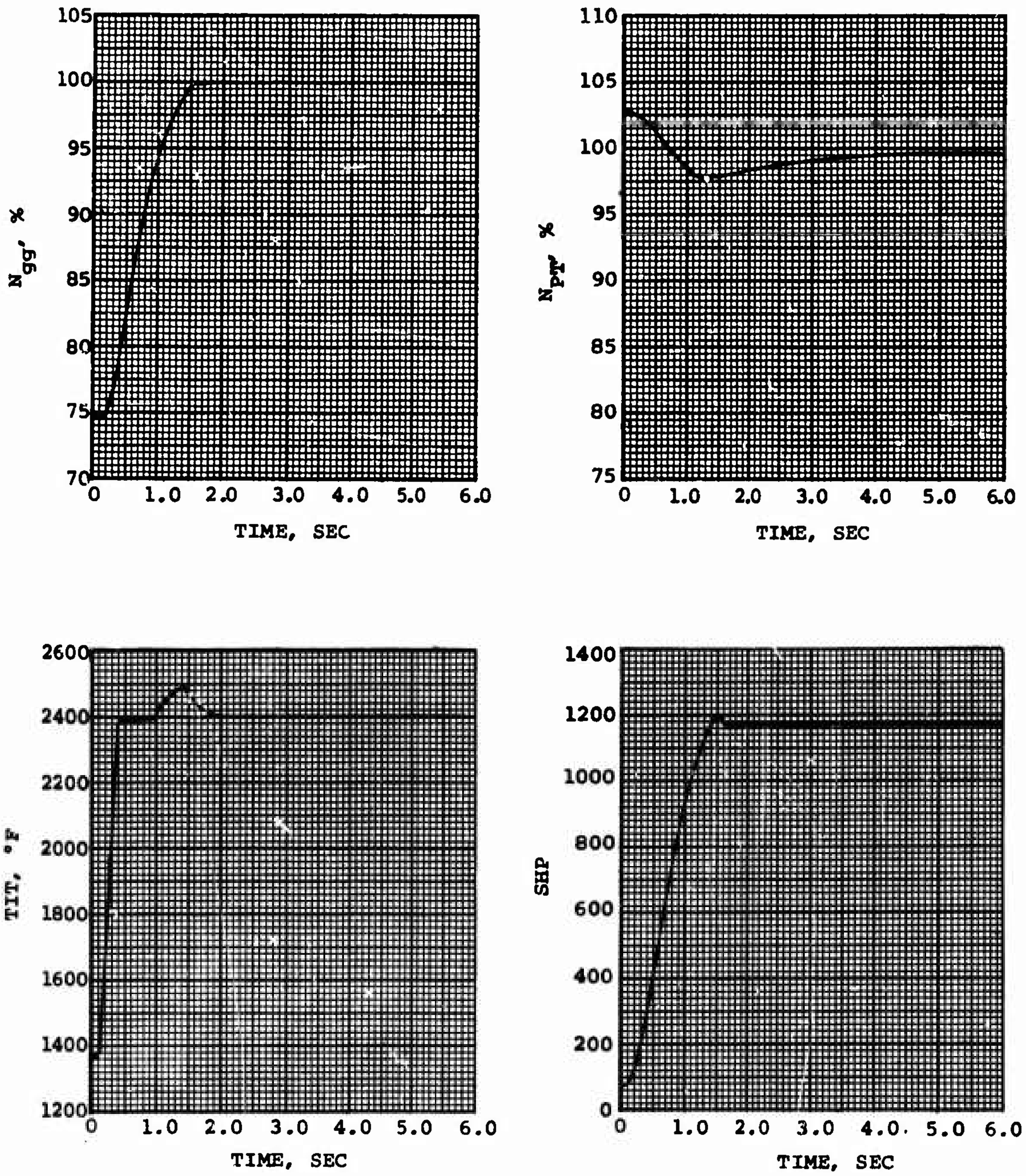

Figure 53. Gas Generator and Power Turbine Speed, TIT, and Output Power Versus Time for Acceleration of 2S-TSE.

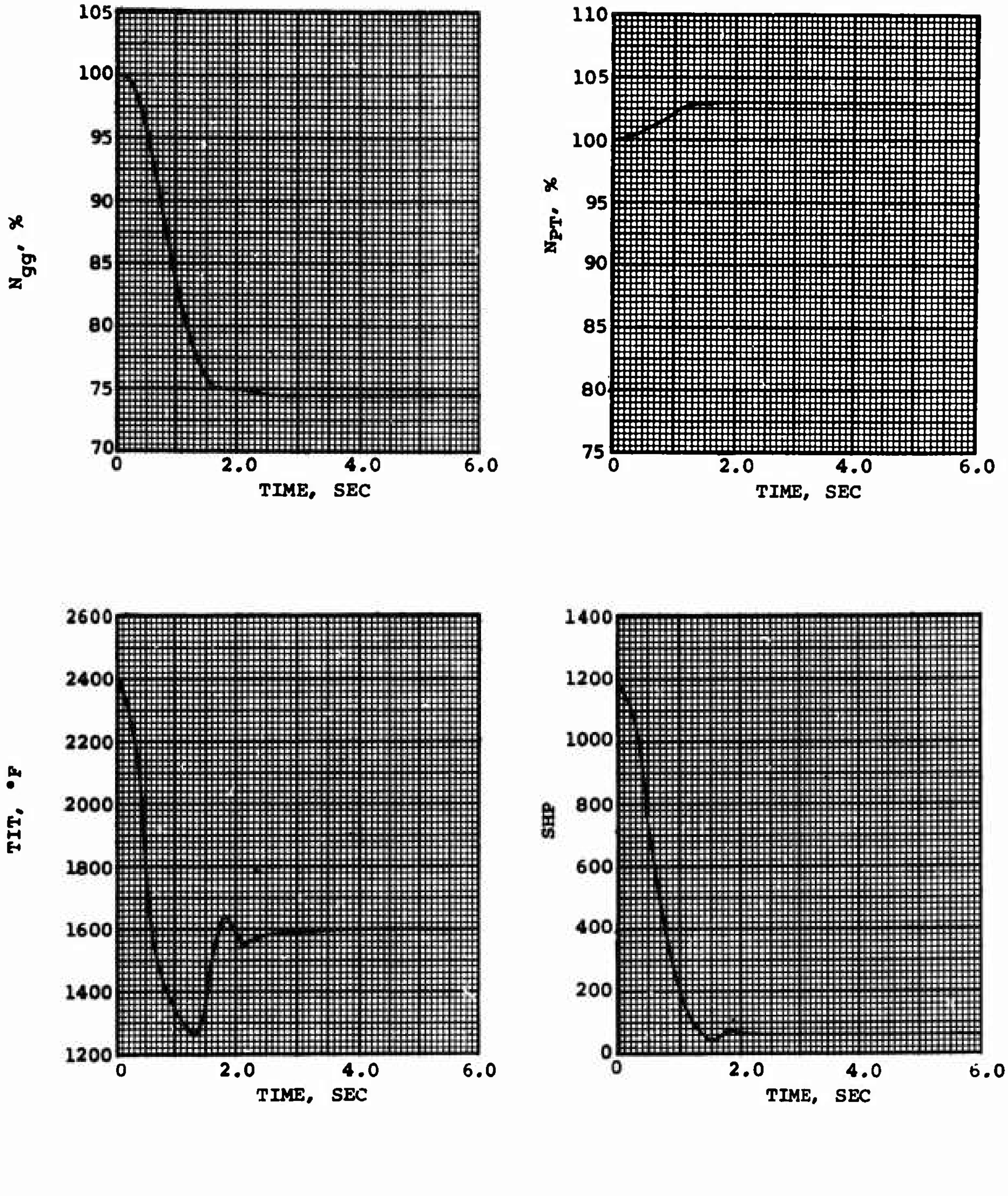

Figure 54. Gas Generator and Power Turbine Speed, TIT, and Output Power Versus Time for Deceleration of 2S-TSE.

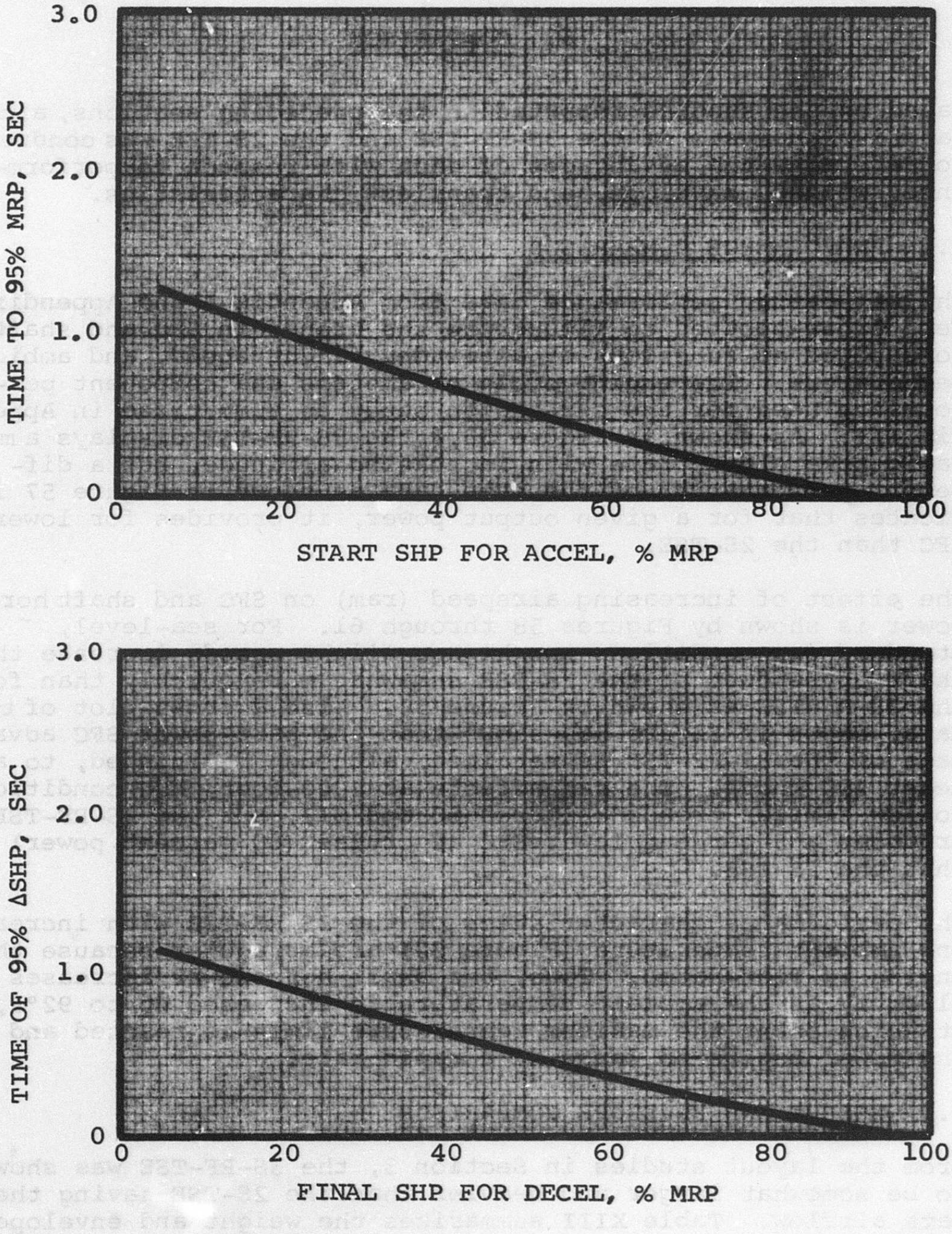

Figure 55. Results of Acceleration and Deceleration Study for 2S-TSE.

6. COMPARISON

Based on the studies reported in the preceding sections, a comparative analysis of the 3S-RF-TSE and the 2S-TSE was conducted to determine the advantages of each with respect to performance, weight, envelope, and transient characteristics.

6.1 PERFORMANCE COMPARISON

The off-design performance data from Appendix I and Appendix II were cross-plotted to illustrate the trends in SFC and shaft horsepower as functions of altitude, flight speed, and ambient temperature. The engine cycle parameters and component performance used for the off-design study is summarized in Appendix III. As shown in Figure 56,* the 3S-RF-TSE displays a more rapid power-lapse rate with increasing altitude, but a different presentation of the same data as shown in Figure 57 indicates that for a given output power, it provides for lower SFC than the 2S-TSE.

The effect of increasing airspeed (ram) on SFC and shaft horsepower is shown by Figures 58 through 61. For sea-level, standard-day conditions the higher flight speeds increase the shaft horsepower of the 2S-TSE somewhat more quickly than for the 3S-RF-TSE as shown by Figure 58. Also a cross-plot of this data, shown in Figure 59, shows that the part-power SFC advantage of the 3S-RF-TSE is retained, although diminished, to at least 400 knots. The ram effects at 4000-foot, 95°F conditions follow similar trends (Figures 60 and 61), but the 3S-RF-TSE produces a 5-percent lower SFC at cruise (60 percent power) than the 2S-TSE.

The performance characteristics of the 3S-RF-TSE with increasing ambient temperature (Figure 62) are irregular because the engine is flat-rated. Thus, the shaft horsepower increases slightly as the ambient temperature is increased up to 92°F, at which point the maximum temperature limit is reached and the power begins to lapse at a rapid rate.

6.2 WEIGHT AND ENVELOPE COMPARISON

From the layout studies in Section 3, the 3S-RF-TSE was shown to be somewhat larger and heavier than the 2S-TSE having the same airflow. Table XIII summarizes the weight and envelope differences between the two engines.

*Because different power-rating schemes were used (Section 5.2), the part-power lines shown on Figures 56, 58, and 60 indicate the percentage of shaft power available at the specispecified conditions rather than percentage of MRP.

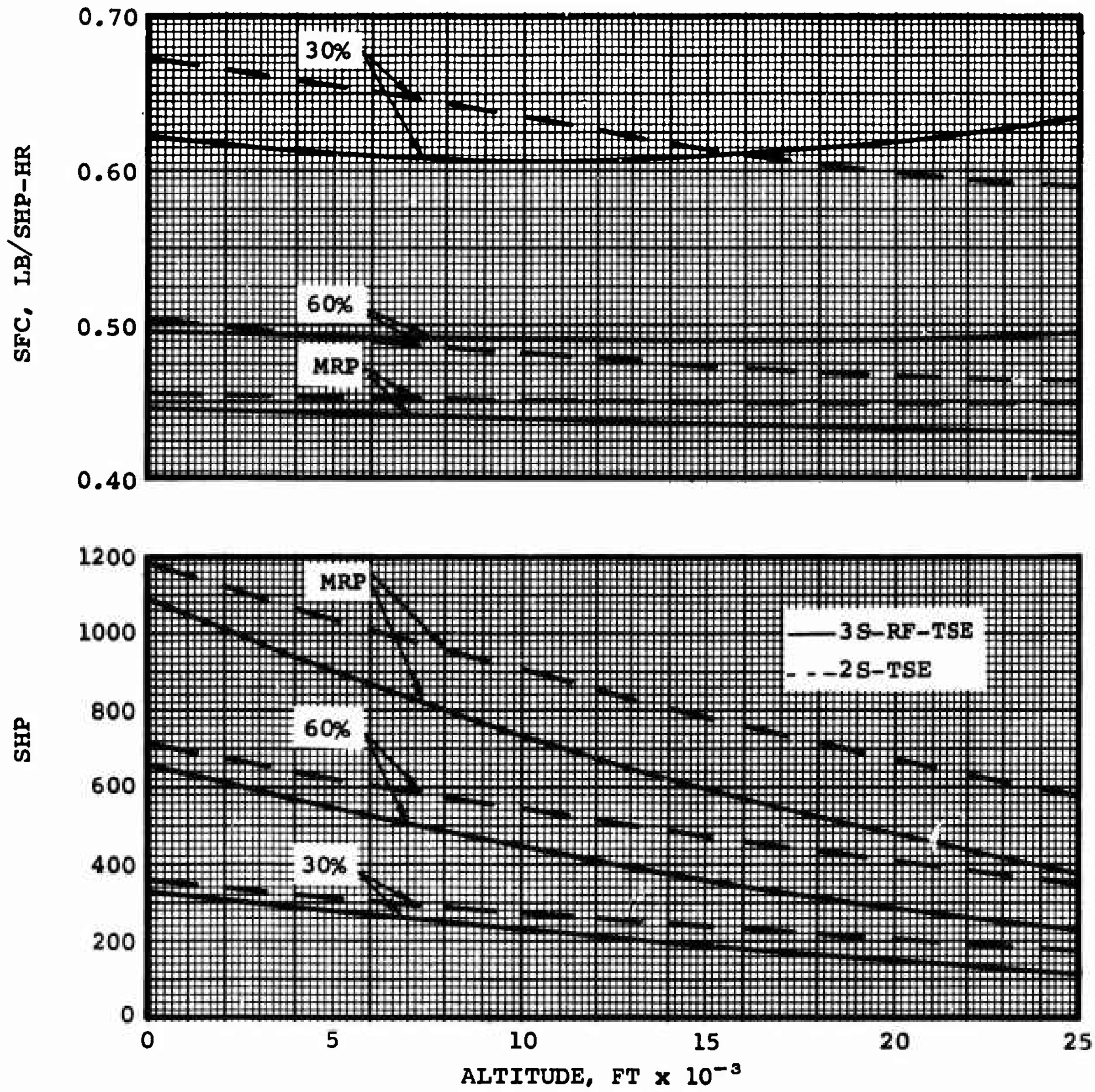

Figure 56. Comparison of SFC and Shaft Horsepower Versus Altitude (Static, Standard-Day Conditions).

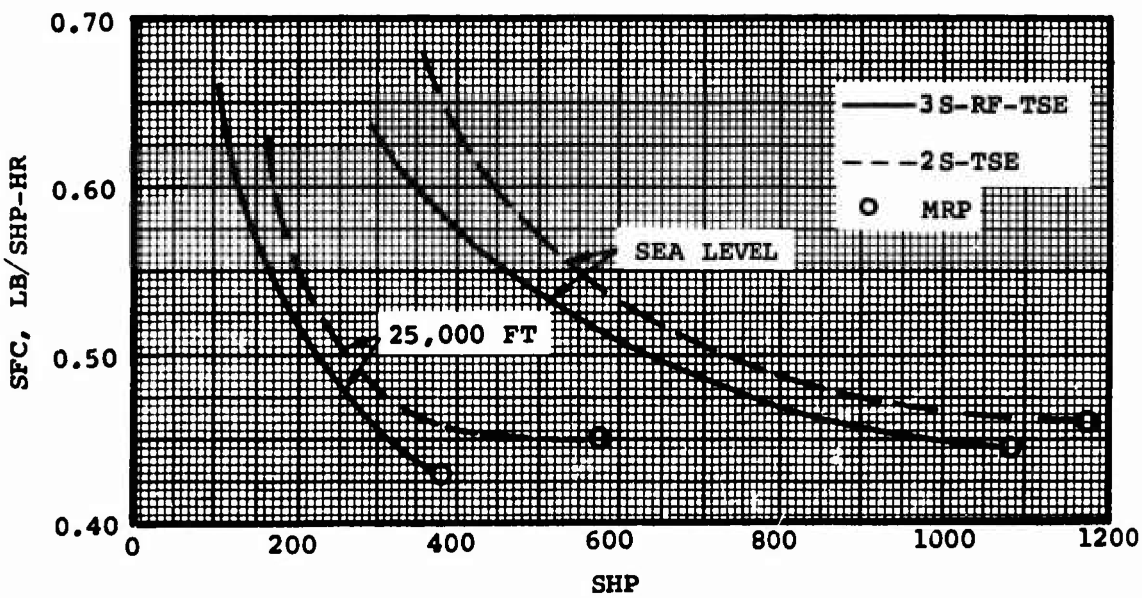

Figure 57. Comparison of SFC Versus Shaft Horsepower at Sea Level and 25,000 Feet (Static, Standard-Day Conditions).

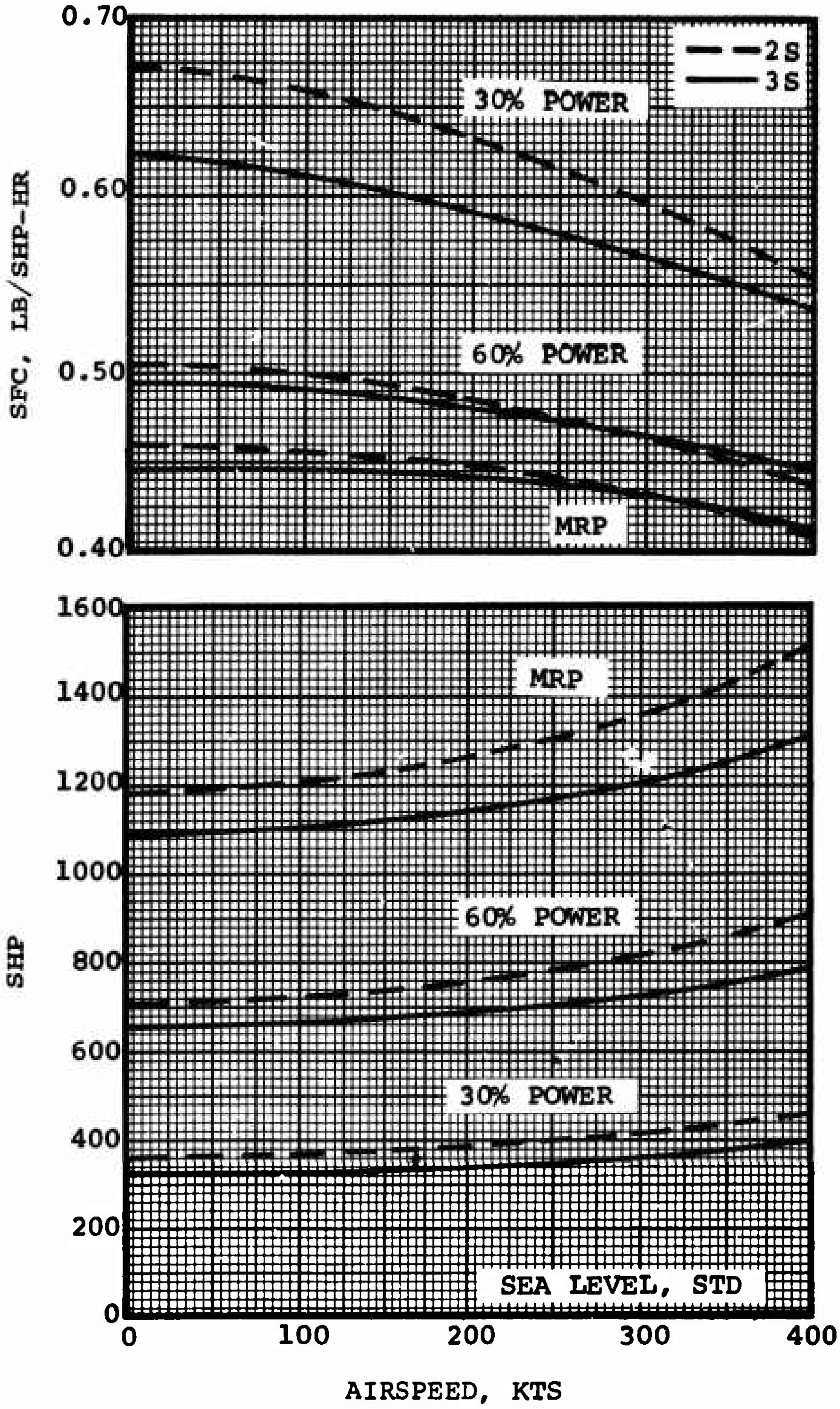

Figure 58. Comparison of SFC and Shaft Horsepower Versus Airspeed (Sea-Level, Standard-Day Conditions).

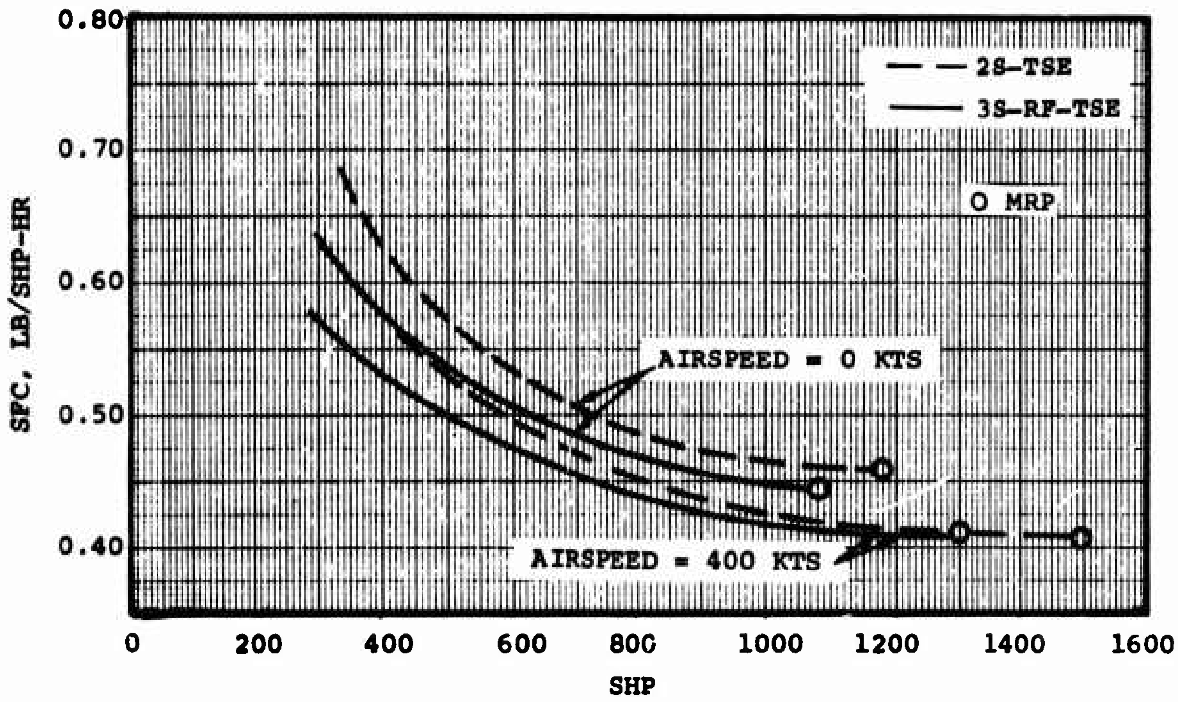

Figure 59. Comparison of SFC Versus Shaft Horsepower for Airspeeds of 0 and 400 Knots.

TABLE XIII. BARE ENGINE WEIGHT AND ENVELOPE COMPARISON

Engine	Engine Airflow (lb/sec)	Engine Weight (lb)	Engine Diameter (in.)	Engine Length (in.)
3S-RF-TSE	6.5	159	15.0	36.4
2S-TSE	6.5	143	14.0	34.4
Difference: (Percent)	0	11	7	6

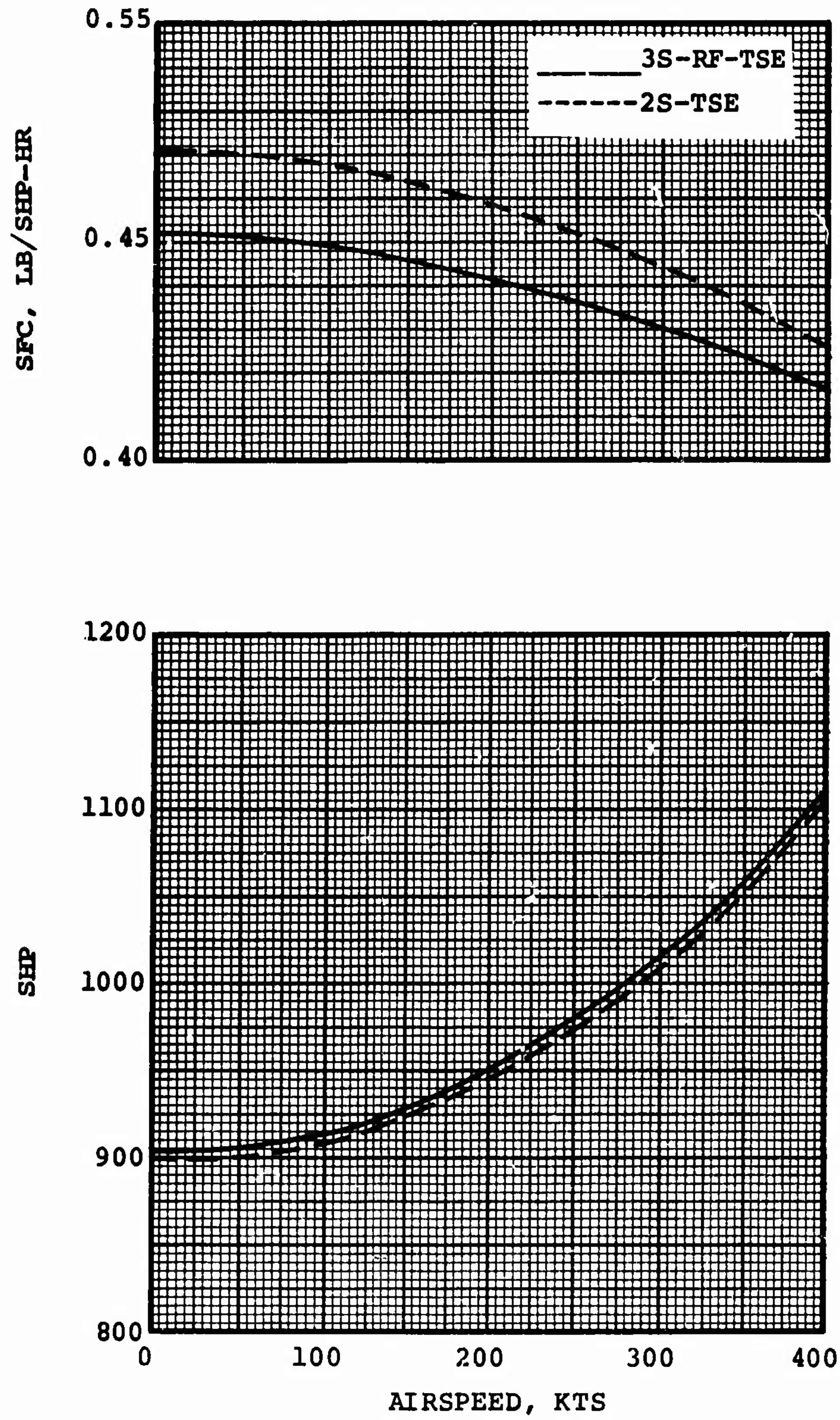

Figure 60. Comparison of SFC and Shaft Horsepower Versus Airspeed at 4000 Feet, 95°F, MRP.

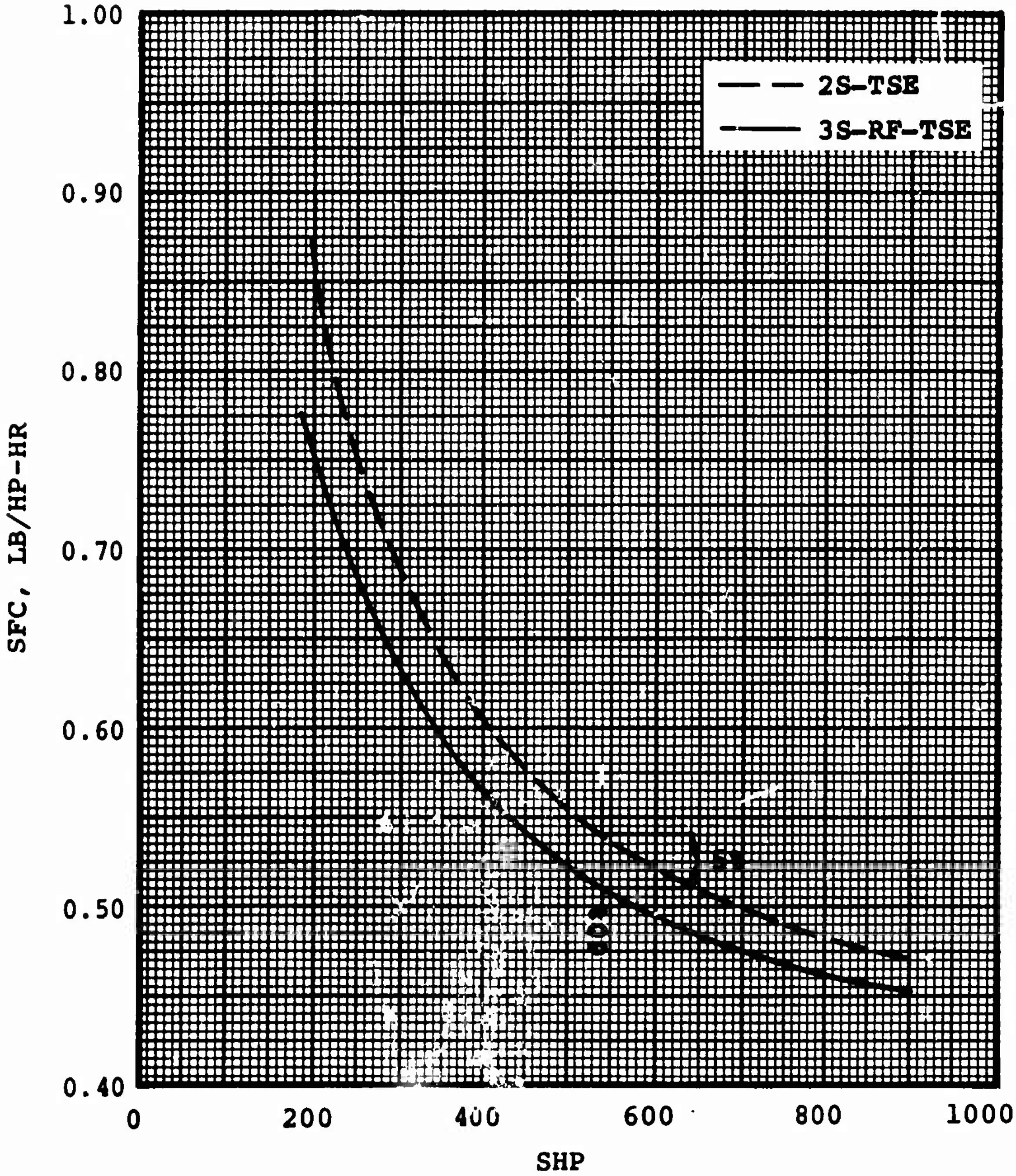

Figure 61. Comparison of SFC Versus Shaft Horsepower at 4000 Feet, Static, 95°F-Day Conditions.

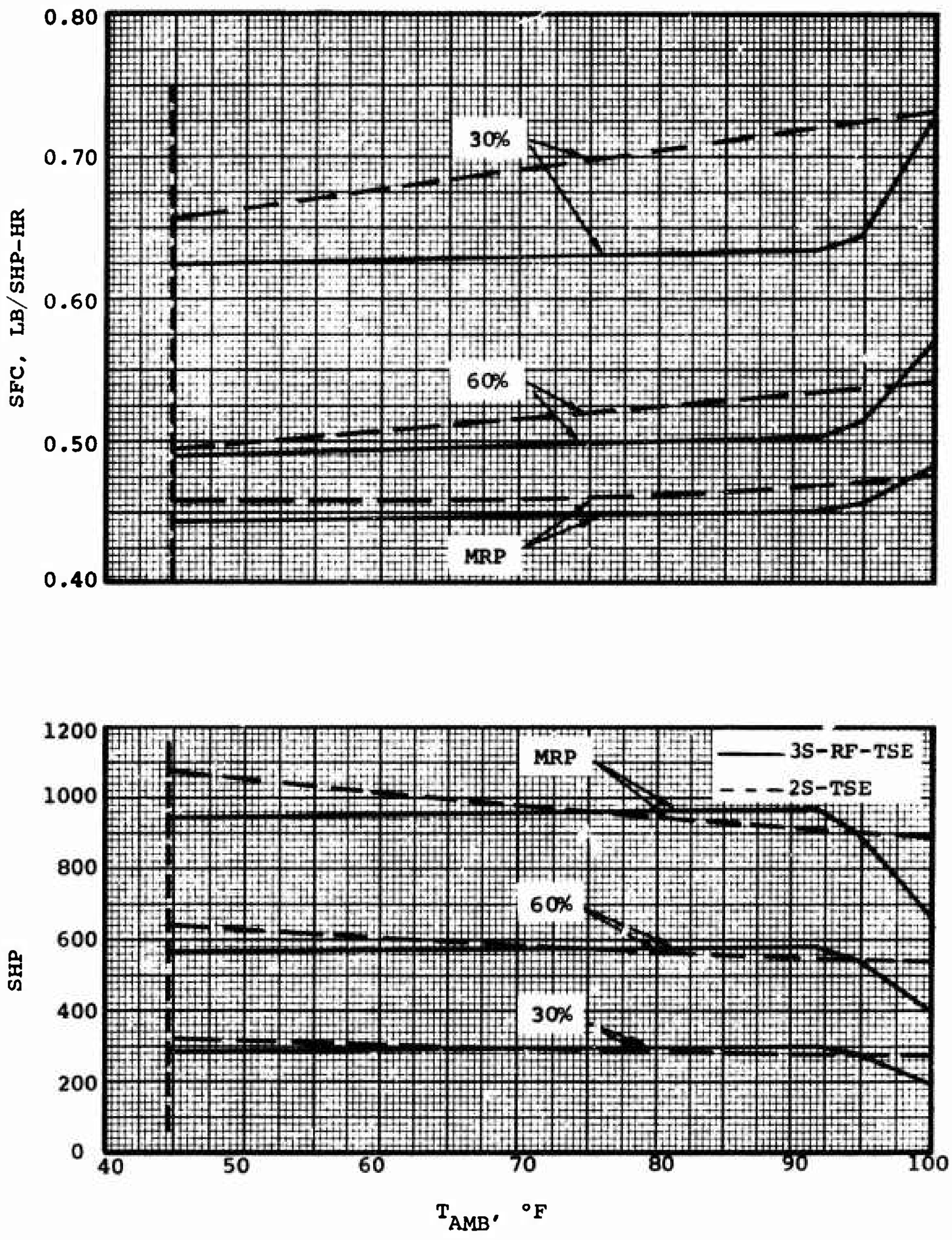

Figure 62. Comparison of SFC and Shaft Horsepower Versus Ambient Temperature.

6.3 TRANSIENT COMPARISON

A comparison of the transient characteristics of the two engines is presented in Figure 63, which shows the time required for each engine to reach 95 percent MRP when accelerated from various initial horsepower points. The more rapid response by the 2S-TSE is primarily a result of its higher part-power airflow. Several techniques and devices are available that could reduce the response time of the 3S-RF-TSE (discussed in Section 5.4.2).

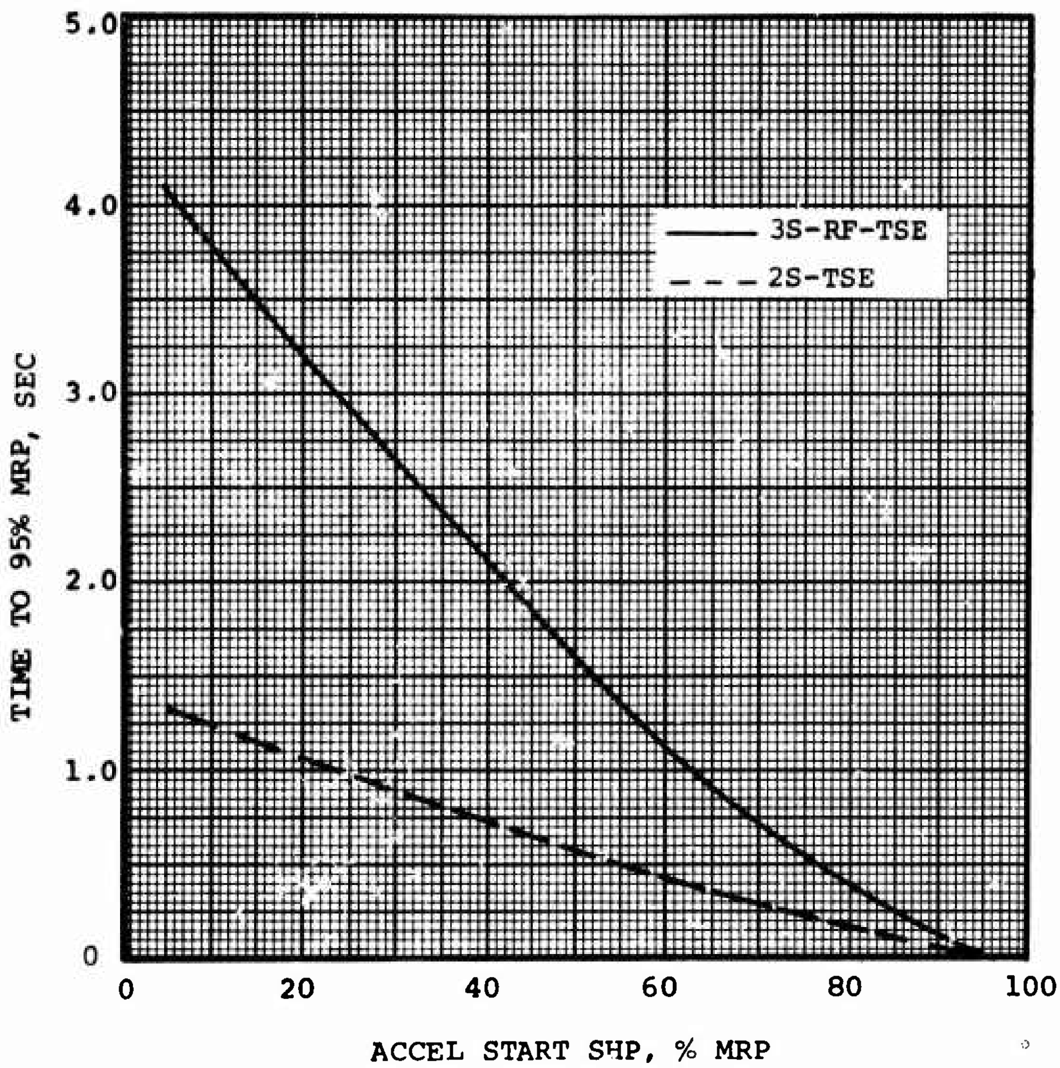

Figure 63. Comparison of Acceleration Characteristics.

7. RECUPERATOR SUITABILITY STUDY

The suitability of the 3S-RF-TSE for recuperation was assessed and compared to the more conventional 2S-TSE configuration. The cursory study that was conducted investigated the suitability of integrating the recuperator into the flow path and the part-power performance.

7.1 RECUPERATOR INTEGRATION

A typical recuperator arrangement for the 3S-RF-TSE is shown schematically in Figure 64. The flow path of the 3S-RF-TSE is well suited for recuperator integration because:

1. The maximum diameter for the unrecuperated 3S-RF-TSE is set by the exhaust-diffuser length needed to minimize cycle exit total pressure loss. Therefore, a concentric recuperator around the turbine/combustor section would require only a nominal increase in engine diameter.

2. The proximity of the turbine exhaust gas and compressor discharge air could reduce the required ducting and, thus, reduce recuperator ΔP and weight addition.

7.2 PART-POWER RECUPERATED ENGINE PERFORMANCE

For a given recuperator installation, the part-power effectiveness is inversely proportional to the airflow and gas flow per unit area. Therefore, recuperator effectiveness tends to increase as an engine is throttled because the airflow is reduced. However, since the airflow for the 3S-RF-TSE is reduced more rapidly than for the 2S-TSE (see again Figure 17), the part-power recuperator effectiveness is expected to be higher for the 3S-RF-TSE.

Again, for a given recuperator installation, the energy available for recuperation is directly proportional to the average temperature (T_{AVG}) of the hot (turbine exhaust) gas and the cold (compressor discharge) air. The part power T_{AVG} for both the 3S-RF-TSE and the 2S-TSE is shown in Figure 65. The T_{AVG} for the 3S-RF-TSE is lower at MRP because it was designed with 150°F lower TIT (flat-rated) but has essentially the same compressor discharge temperature. However, the part-power T_{AVG} for the 3S-RF-TSE increases rapidly as the engine is throttled (primarily because it holds an almost

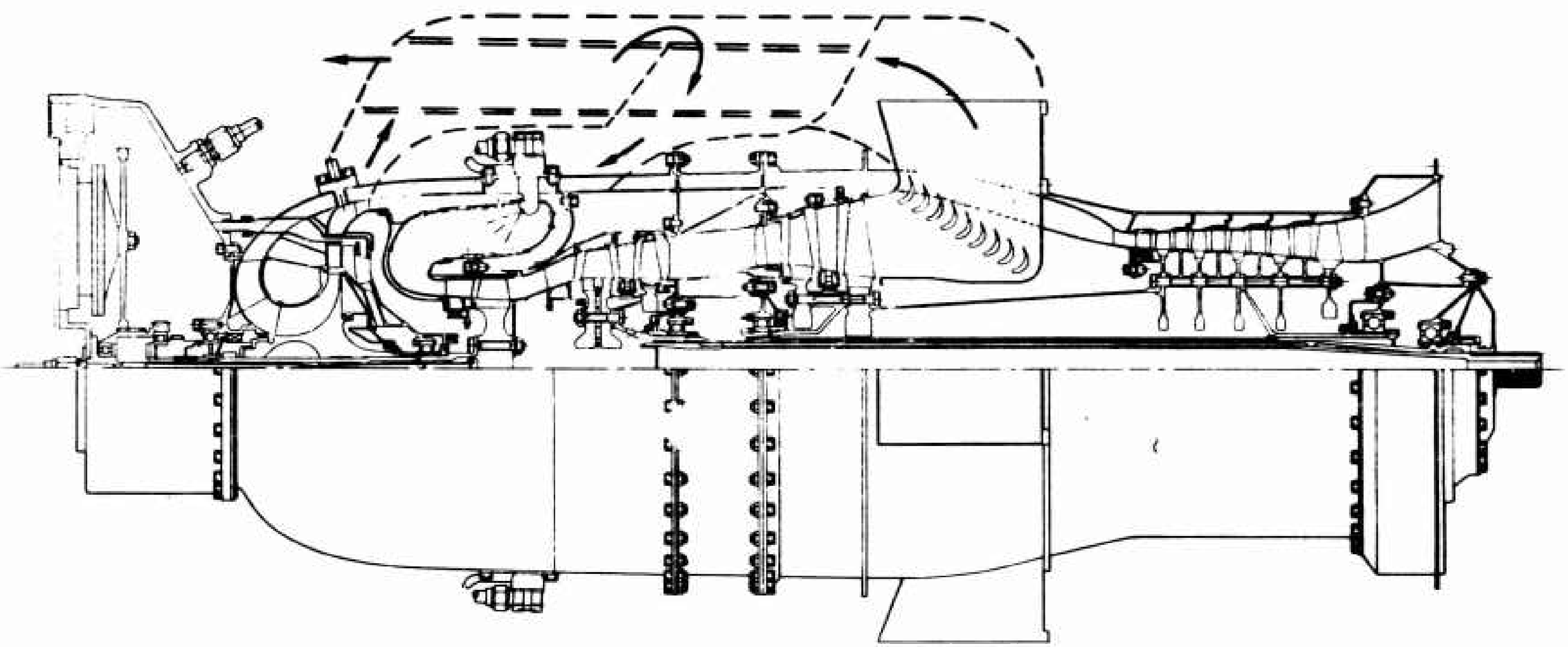

Figure 64. Schematic of Typical Recuperator Arrangement for 3S-RF-TSE.

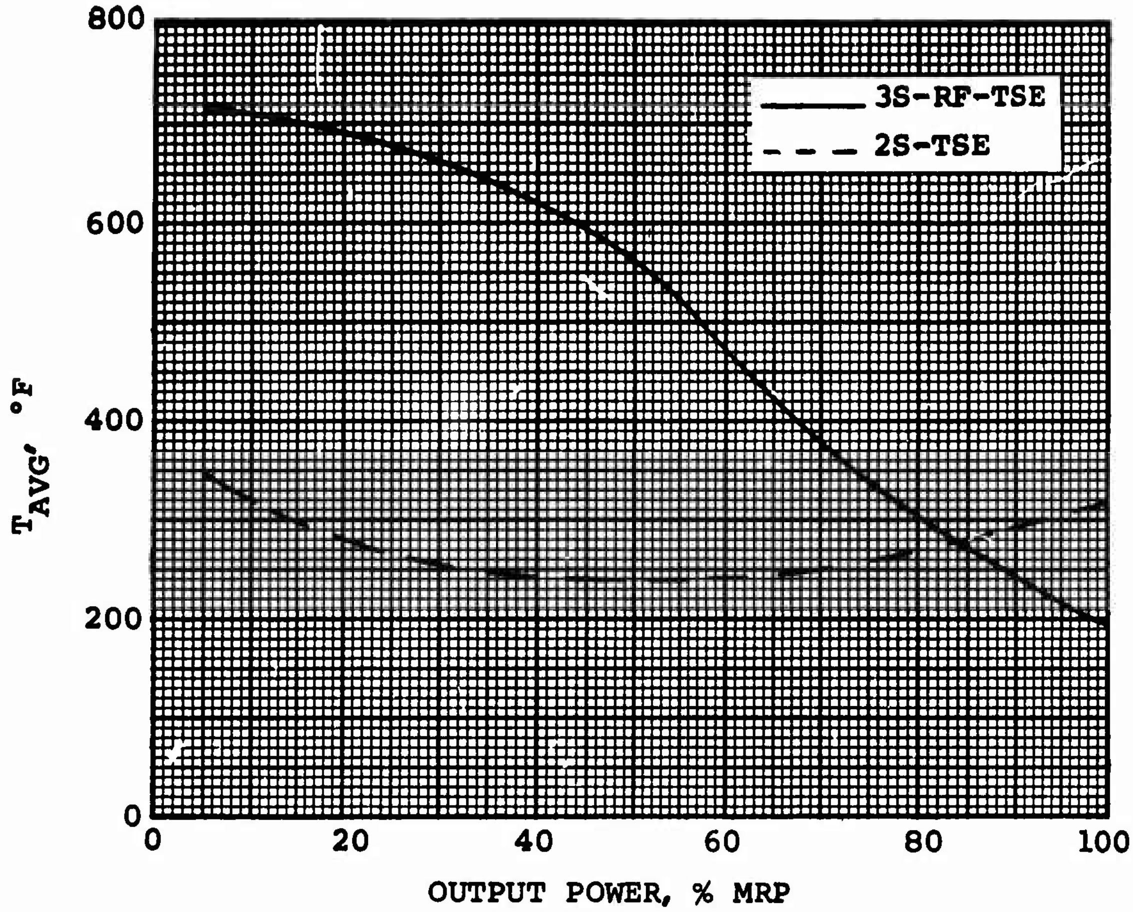

Figure 65. T_{AVG} Versus Percent MRP for 2S-TSE and 3S-RF-TSE.

constant TIT). The part-power T_{AVG} for the 2S-TSE remains relatively constant.

The recuperated 3S-RF-TSE would therefore receive the benefit of both higher T_{AVG} and lower airflow to provide improved part-power SFC. These trends were quantitatively evaluated by including recuperator effects (ϵ = 75 percent, $\Delta P/P$ = 6 percent) into the cycle calculations for both engines.

As expected, recuperator effectiveness is improved for both cycles as the engines are throttled. However, as shown by Figure 66, the improvement that results with the 3S-RF-TSE is considerably greater than for the 2S-TSE. More significantly, the comparison of part-power SFC shown in Figure 67 indicates a lower SFC at the cruise condition (i.e., 60 percent MRP) than at 100 percent MRP for the 3S-RF-TSE.

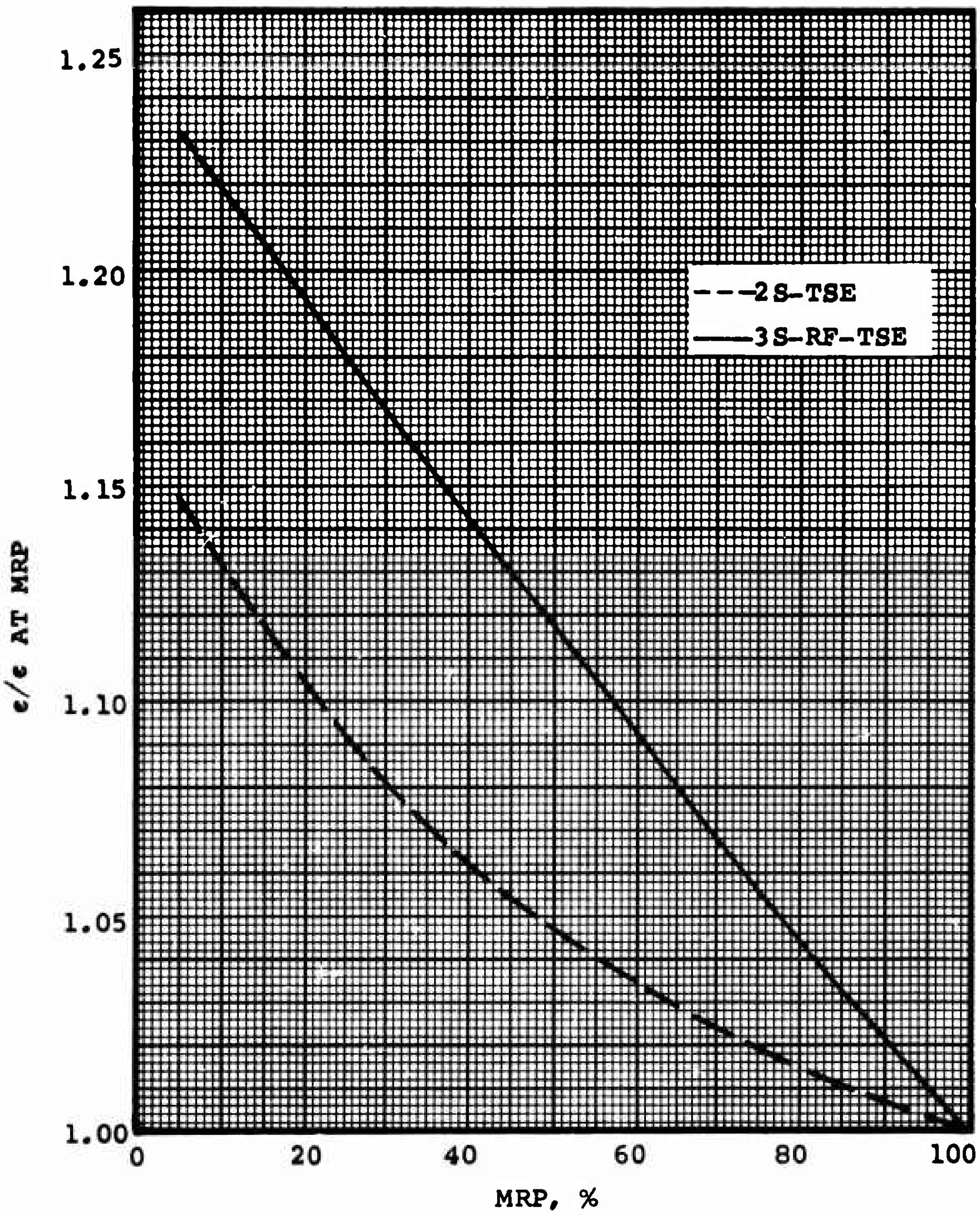

Figure 66. Recuperator Effectiveness Versus Output Power for 2S-TSE and 3S-RF-TSE.

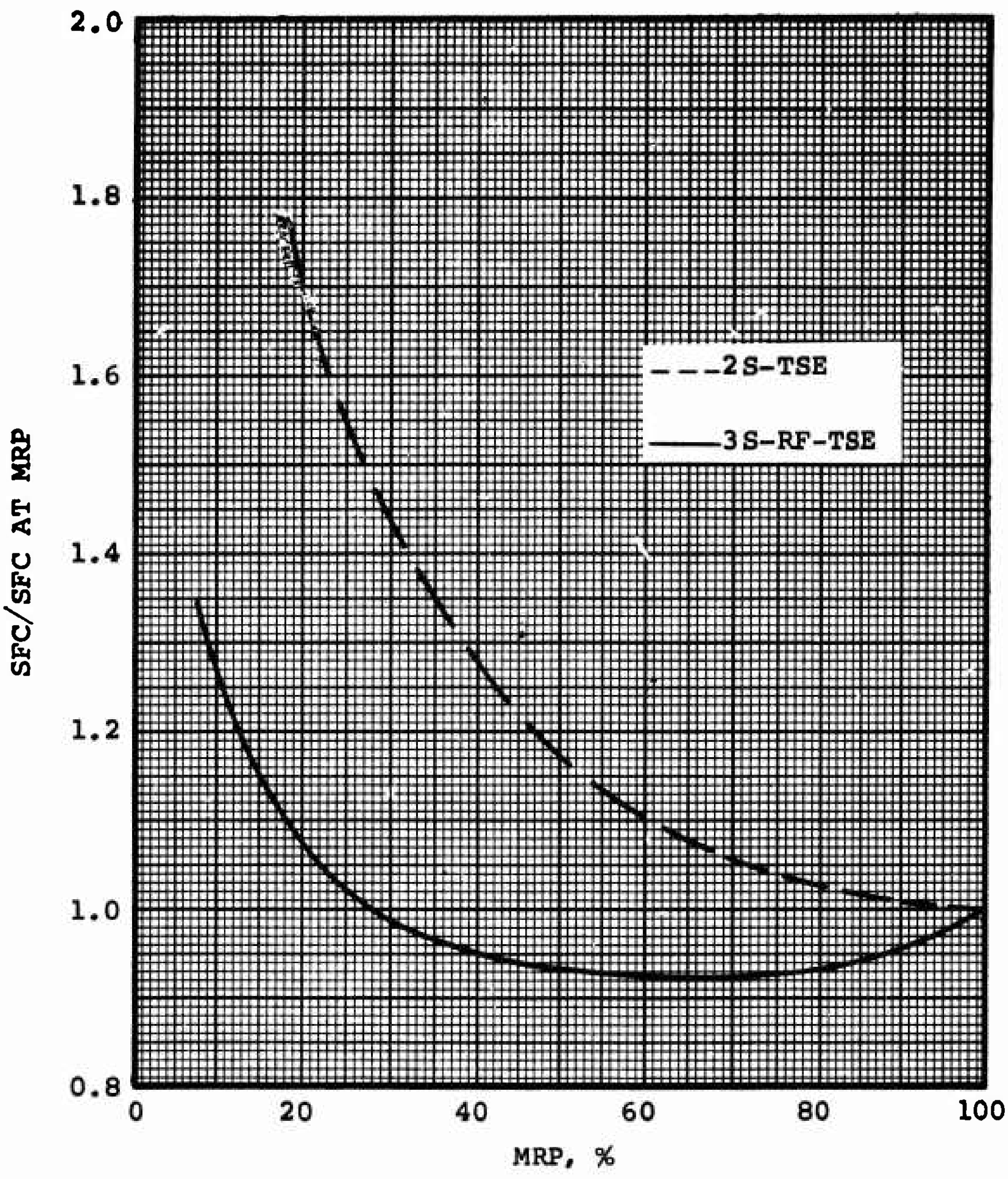

Figure 67. SFC Versus Output Power for Recuperated 2S-TSE and 3S-RF-TSE.

It is important also to note that for TIT in the range of 2250°F and a recuperator effectiveness in the range of 65 to 75 percent, the optimum cycle P/P for minimum SFC would fall between 8:0 and 12:0. A quantitative evaluation of recuperator performance would require a new selection of compressor P/P and efficiency, as well as a new compressor design, which would undoubtedly result in a new compressor configuration. Such an evaluation was considered to be beyond the scope of this study.

Thus, while this study made no attempt to optimize either the recuperator or the cycle, these results indicate a distinct performance advantage for a recuperated version of the 3S-RF-TSE.

8. CONCLUSIONS

As a result of the analyses conducted during this study, it was concluded that the combination of three spools and the "reverse-flow" turbine arrangement provides for the following engine characteristics:

1. All compressors and turbines of the 3S-RF-TSE operate close to their optimum efficiency over a wide range of powers. This fact, coupled with relatively constant power turbine specific work, indicates that as much as 5 percent lower SFC is produced at cruise (4000-foot, static, 95°F-day conditions) by a 3S-RF-TSE than by a comparable 2S-TSE.

2. Power is sensitive to ambient temperature variations. The 3S-RF-TSE maintains a relatively constant TIT ratio (TIT/θ_2) as the engine is throttled. When designed with the maximum allowable TIT at MRP on a standard day, the engine reaches its actual TIT limit with only a slight increase in ambient temperature. Further increases in ambient temperature must be countered by a reduction in TIT/θ_2, which will produce a significant hot-day power lapse. The most desirable hot-day power-lapse characteristics are obtained by lowering the design-point TIT or flat-rating the engine.

3. The engine will not encounter a flight speed power lapse similar to the hot-day power lapse discussed above because the ram pressure effect is greater than the ram temperature effect. The most restrictive operating condition is hot day, zero flight speed. Performance could be improved at higher flight speeds by raising the design-point TIT but, in so doing, an unacceptable power lapse would result at the lower flight speeds.

4. Because the engine maintains a high TIT and drops rapidly in airflow as the engine is throttled, the unbalanced (or excess) torque available for acceleration is considerably less than for a more conventional 2S-TSE. As a result, the 2S-TSE can accelerate from low throttle settings to MRP in approximately one-third of the time required by the 3S-RF-TSE (1.3 and 4.1 seconds, respectively).

5. When compared to a 2S-TSE with the same output power, the flat-rated 3S-RF-TSE has a somewhat larger envelope and is approximately 11 percent heavier.

6. The component arrangement and cycle of the 3S-RF-TSE is well suited for recuperation. The recuperator can be integrated into the flow path with only a nominal increase in engine diameter (frontal area) and ducting (weight). The cycle temperatures (compressor and turbine discharge) and airflow characteristics produce as much as an 18-percent lower SFC at 60 percent power than a comparable recuperated 2S-TSE.

7. The power turbine spool speed (and, thus, the ungeared output shaft speed) is higher for the 3S-RF-TSE (46,000 rpm compared to 34,500 rpm for the 2S-TSE) in order to provide a power turbine diameter that can be readily integrated between the HP and the LP turbine with high efficiency and with minimum interturbine duct losses.

9. RECOMMENDATIONS

In order to determine the net effect of the lower SFC and higher engine weight, computerized helicopter mission studies should be conducted. Also, various schemes for reducing the transient time of the engine should be investigated.

Because the cycle is well suited for recuperation, more detailed studies should be conducted to optimize this cycle for a recuperator. The lower cycle pressure ratio that would accompany a recuperated engine cycle would reduce the bare engine weight, as well as some of the losses.

APPENDIX I
3S-RF-TSE PERFORMANCE TABLE AND CURVES

TABLE XIV. 3S-RF-TSE PERFORMANCE DATA AT 6000 FEET, 95°F, MRP

Parameter	Values
TIT	2400°F
$N_{LP}/\sqrt{\theta_2}$	31,800 rpm
SHP	838 hp
SFC	0.458 lb/shp-hr
WA	4.76 lb/hr
P/P_{LP}	5.58
P/P_{HP}	2.70
CYCLE P/P	14.50
N_{LP}	32,900 rpm
N_{HP}	68,900 rpm

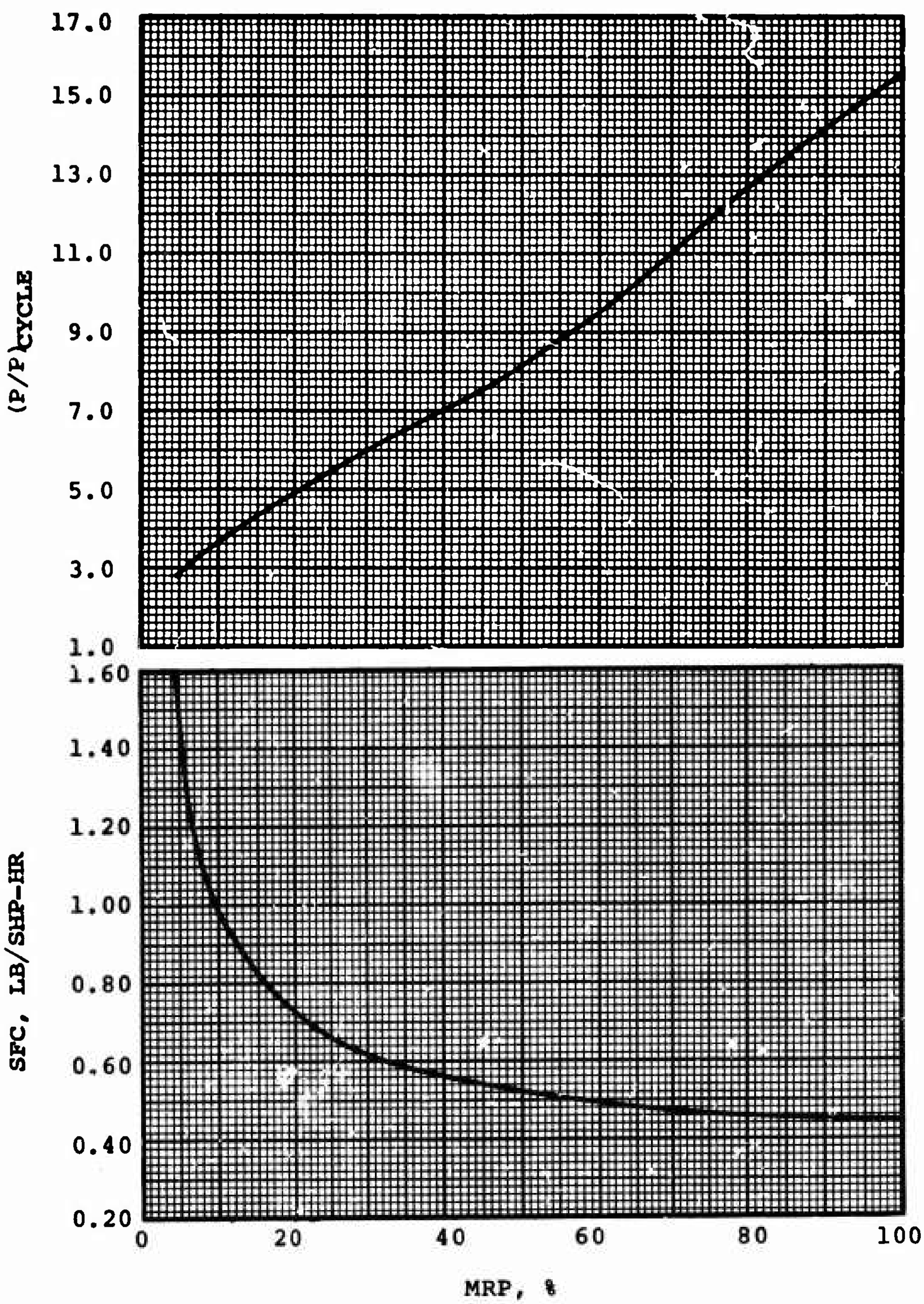

Figure 68. Cycle P/P and SFC Versus Percent MRP for 3S-RF-TCE at Sea-Level, Static, Standard-Day Conditions.

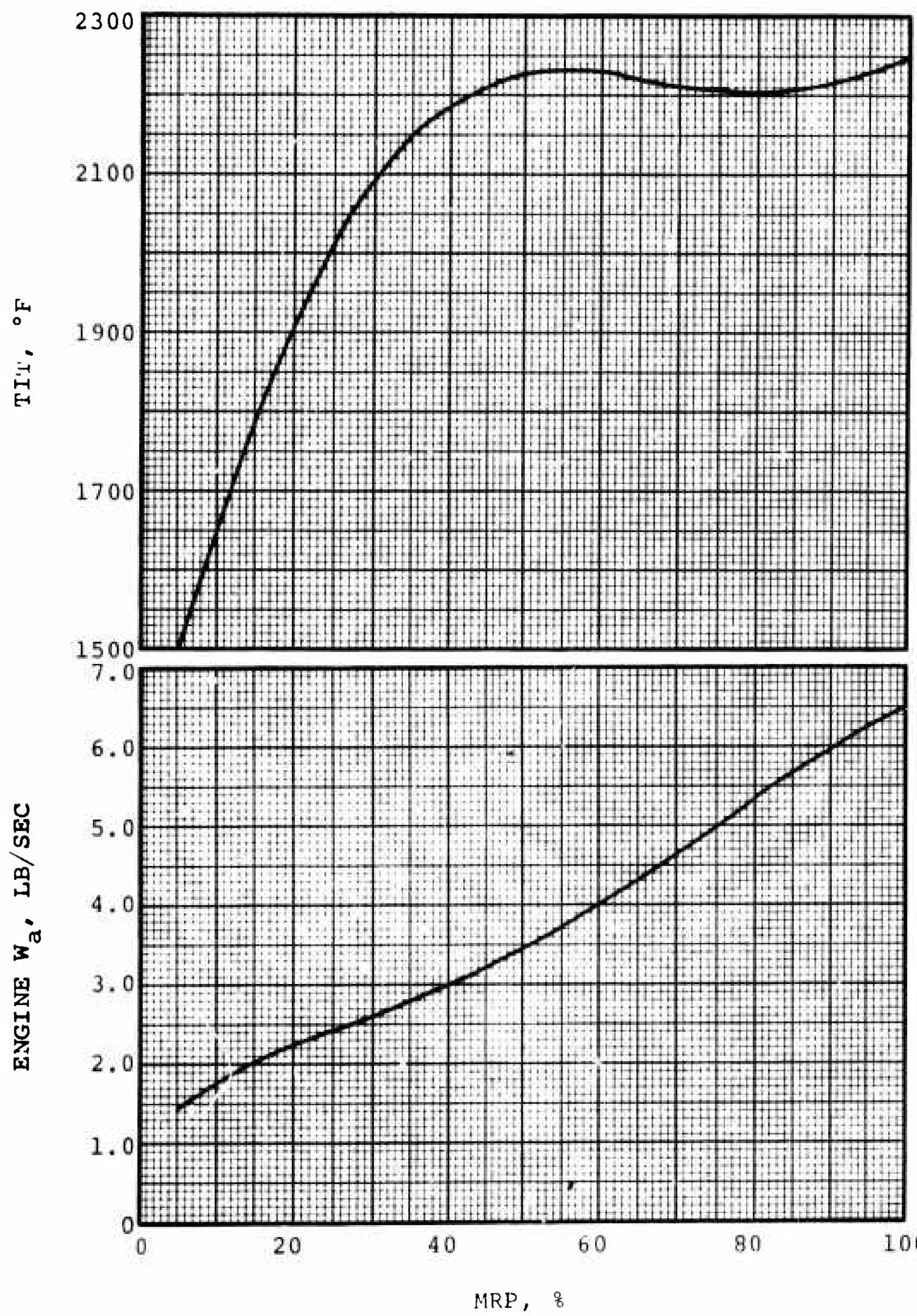

Figure 69. TIT and Airflow Versus Percent MRP for 3S-RF-TSE at Sea-Level, Static, Standard-Day Conditions.

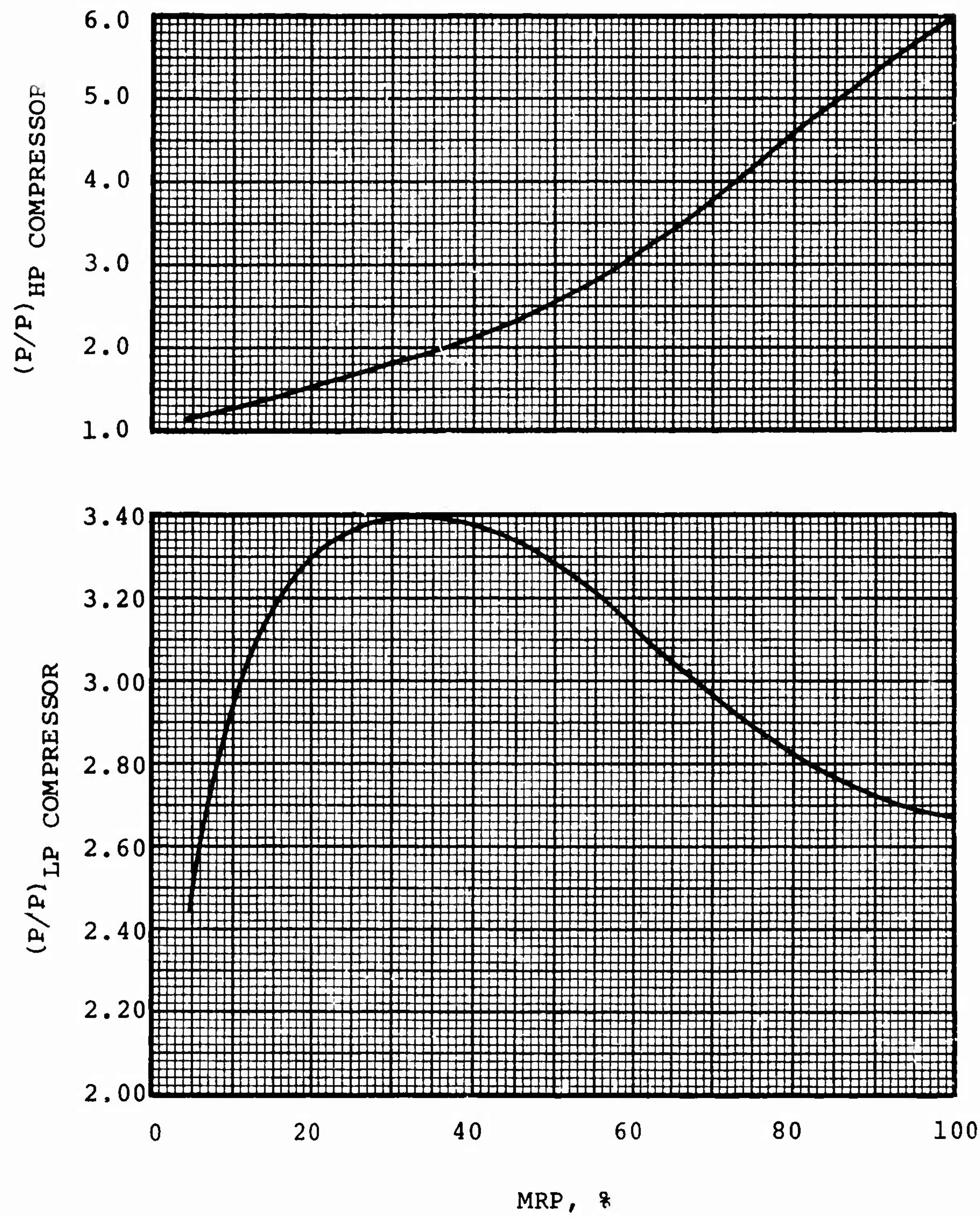

Figure 70. LP and HP Compressor P/P Versus MRP for 3S-RF-TSE at Sea-Level, Static, Standard-Day Conditions.

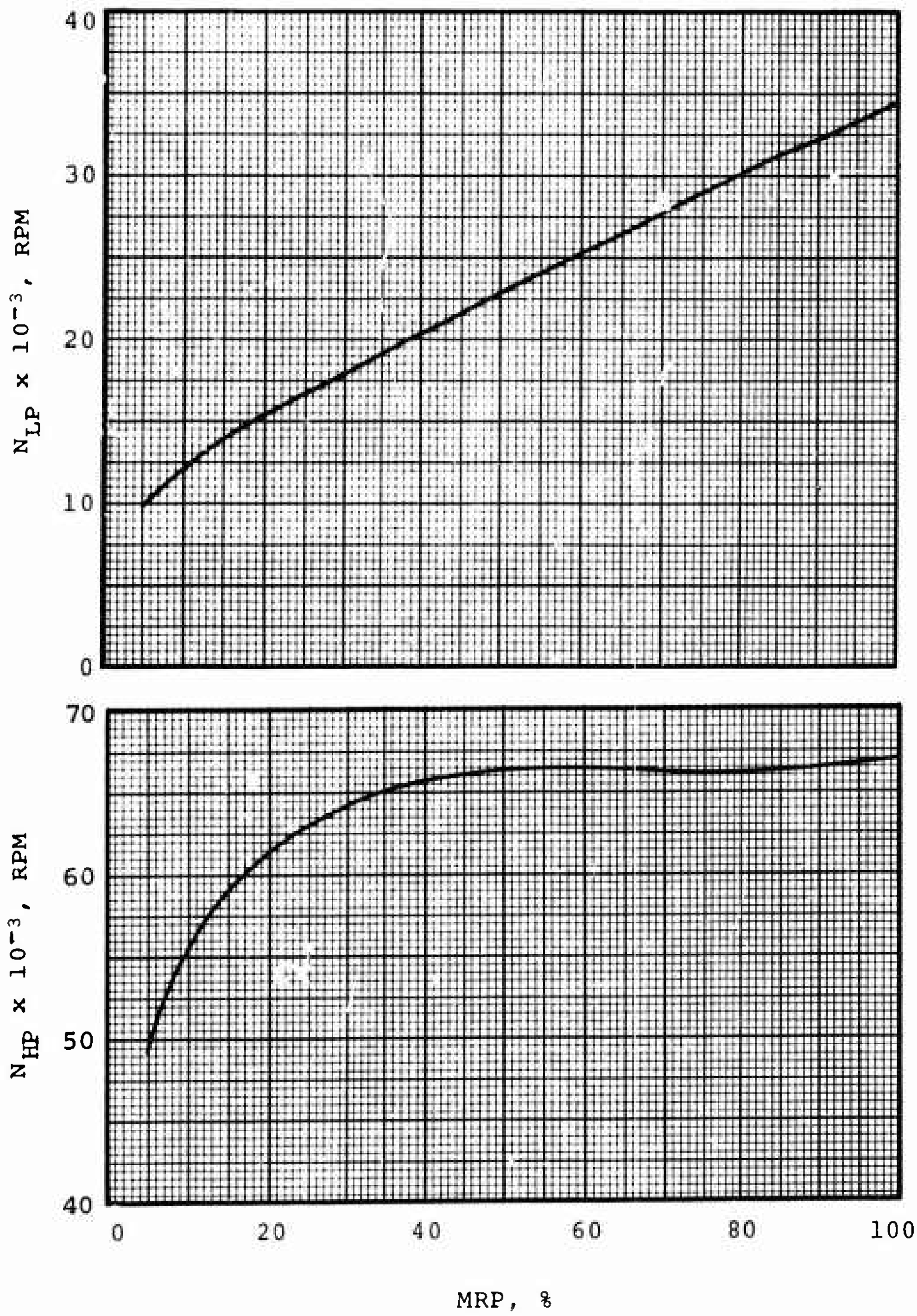

Figure 71. LP Spool Speed and HP Spool Speed Versus Percent MRP for 3S-RF-TSE at Sea-Level, Static, Standard-Day Conditions.

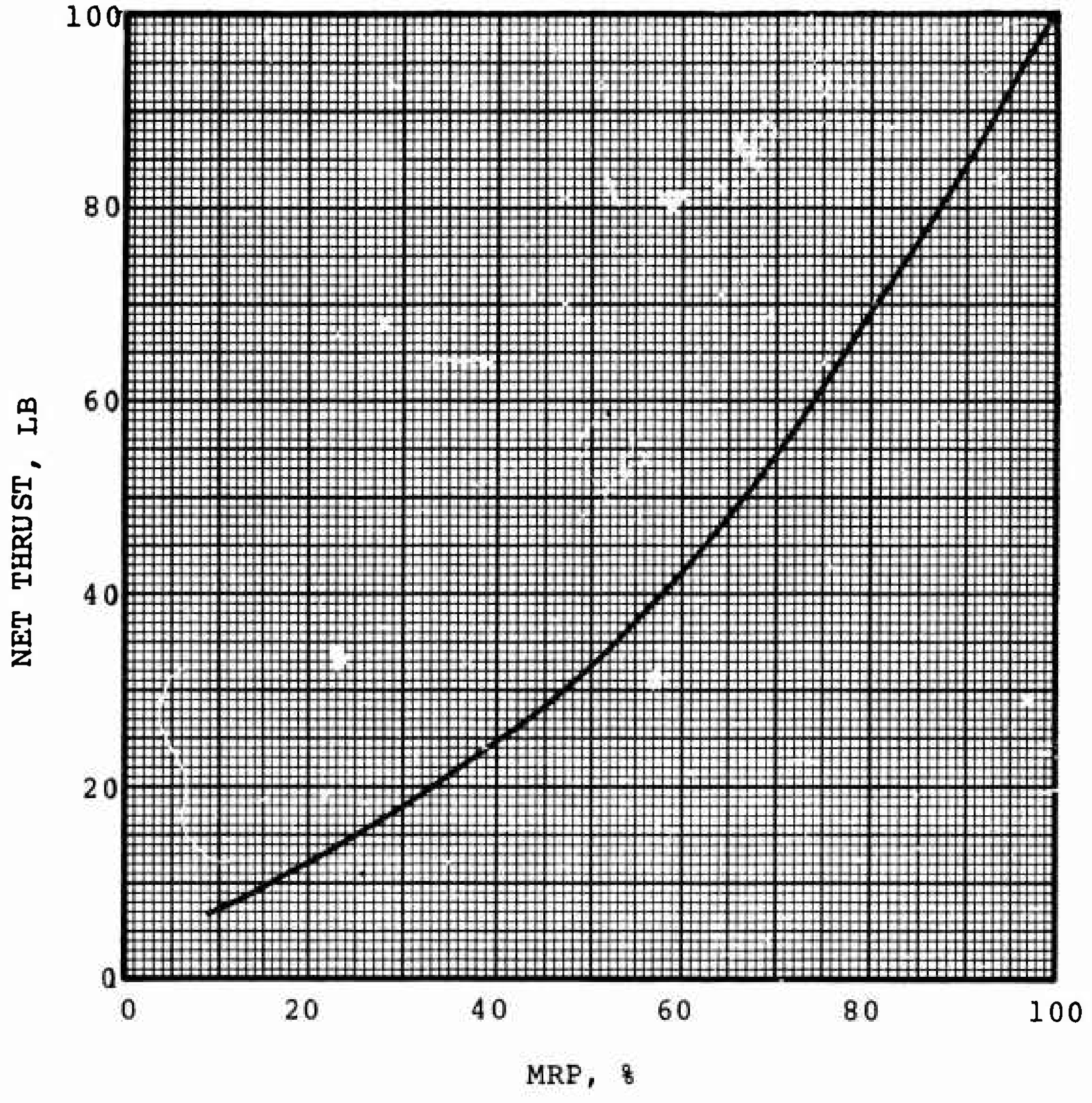

Figure 72. Net Thrust Versus Percent MRP for 3S-RF-TSE at Sea-Level, Static, Standard-Day Conditions.

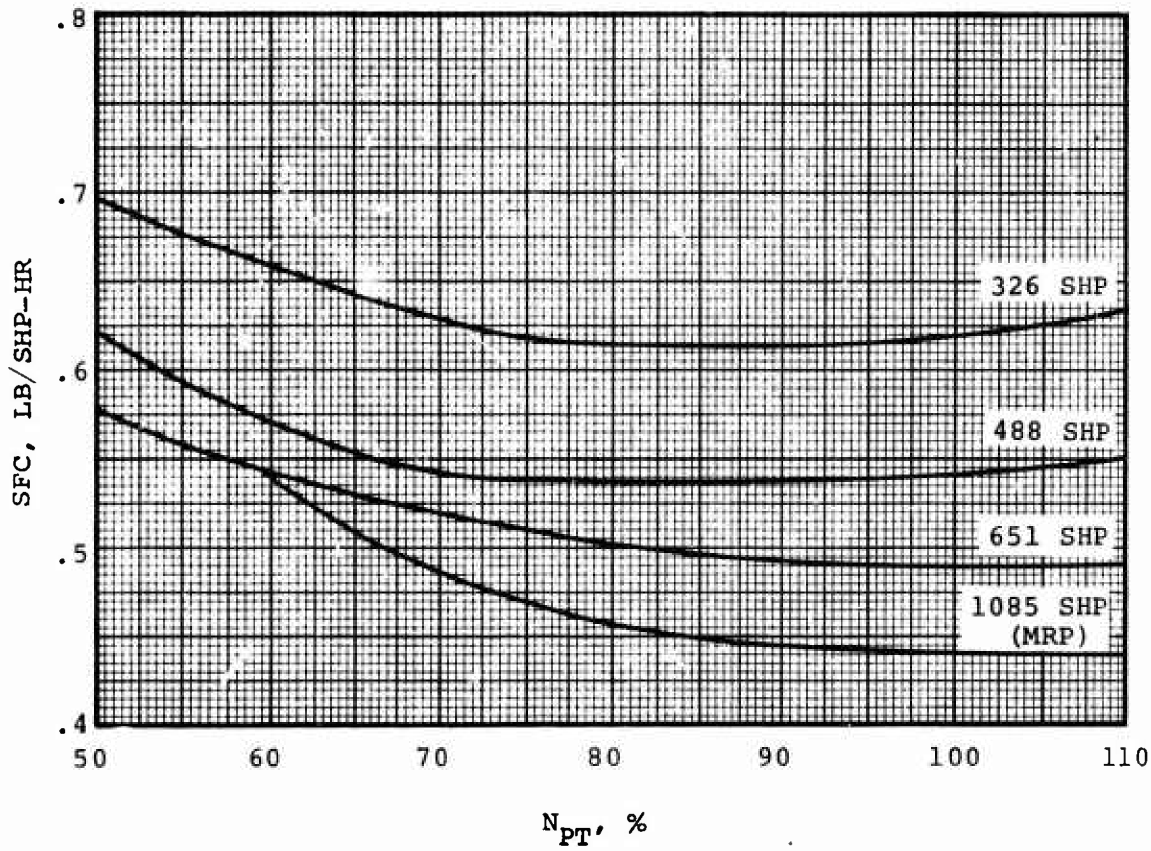

Figure 73. SFC Versus Percent Power Turbine Speed for 3S-RF-TSE at Sea-Level, Static, Standard-Day Conditions.

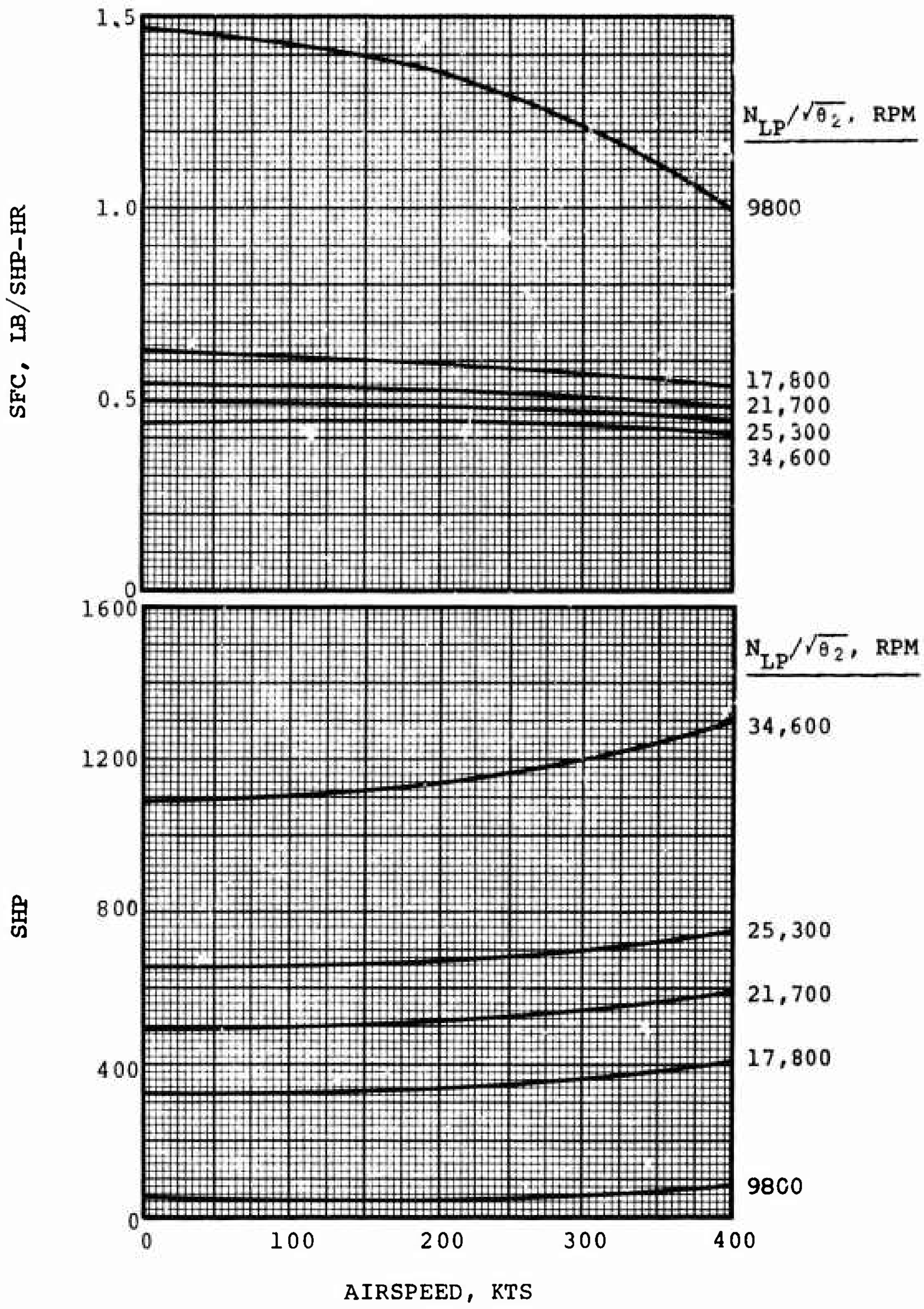

Figure 74. SFC and Shaft Horsepower Versus Airspeed for 3S-RF-TSE at Sea-Level, Standard-Day Conditions.

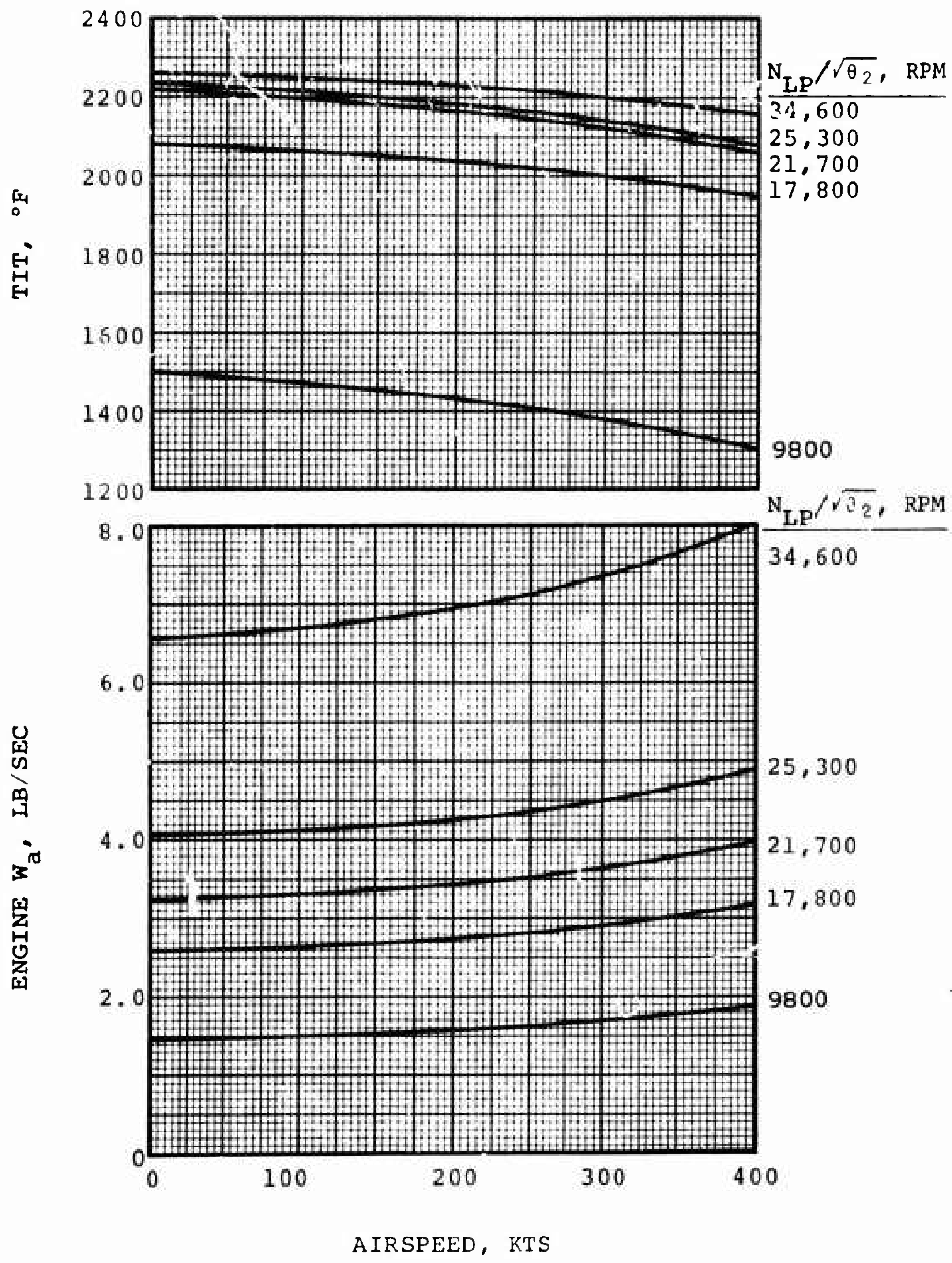

Figure 75. TIT and Airflow Versus Airspeed for 3S-RF-TSE at Sea-Level, Standard-Day Conditions.

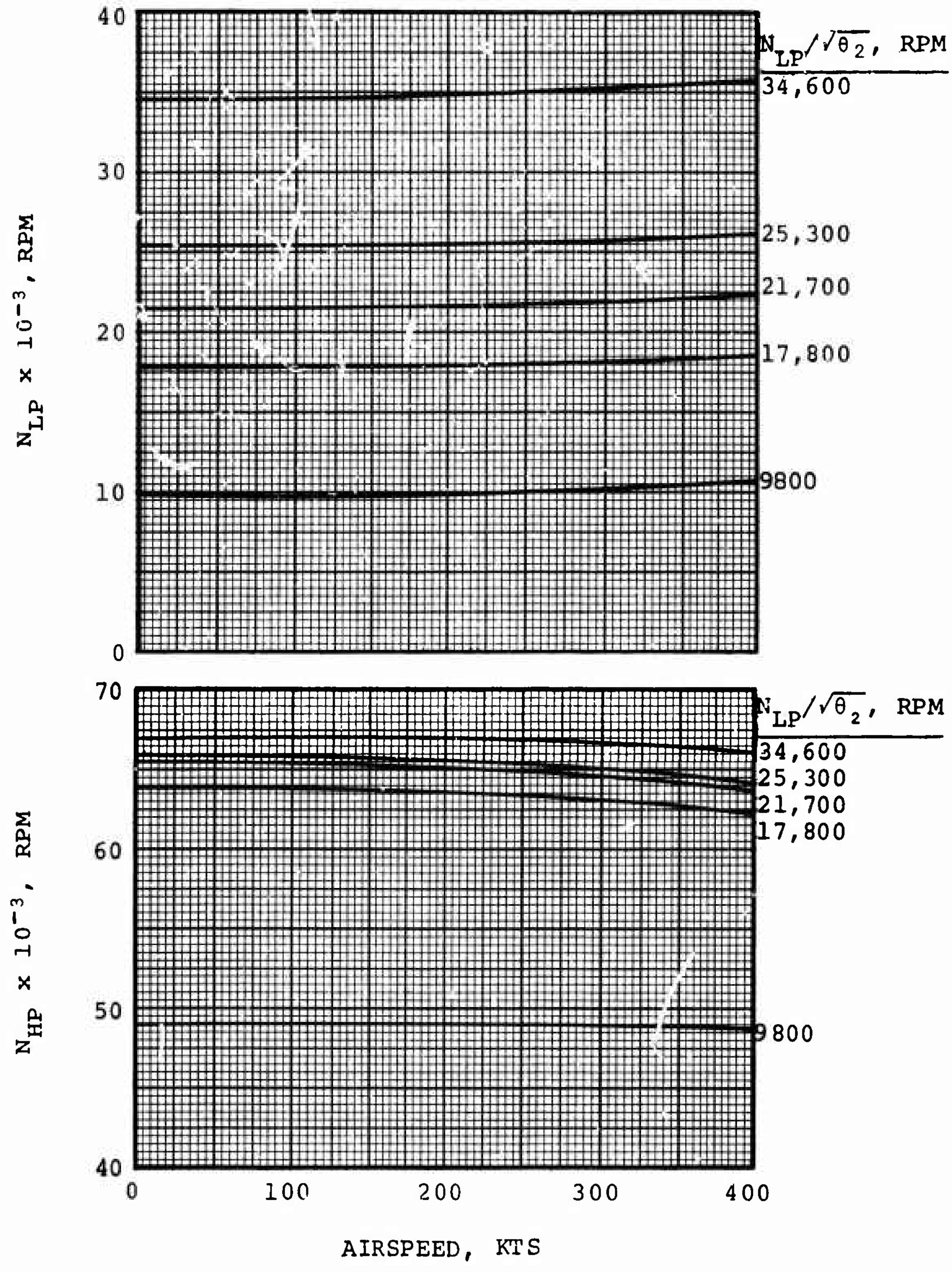

Figure 76. LP Spool Speed and HP Spool Speed Versus Airspeed for 3S-RF-TSE at Sea-Level, Standard-Day Conditions.

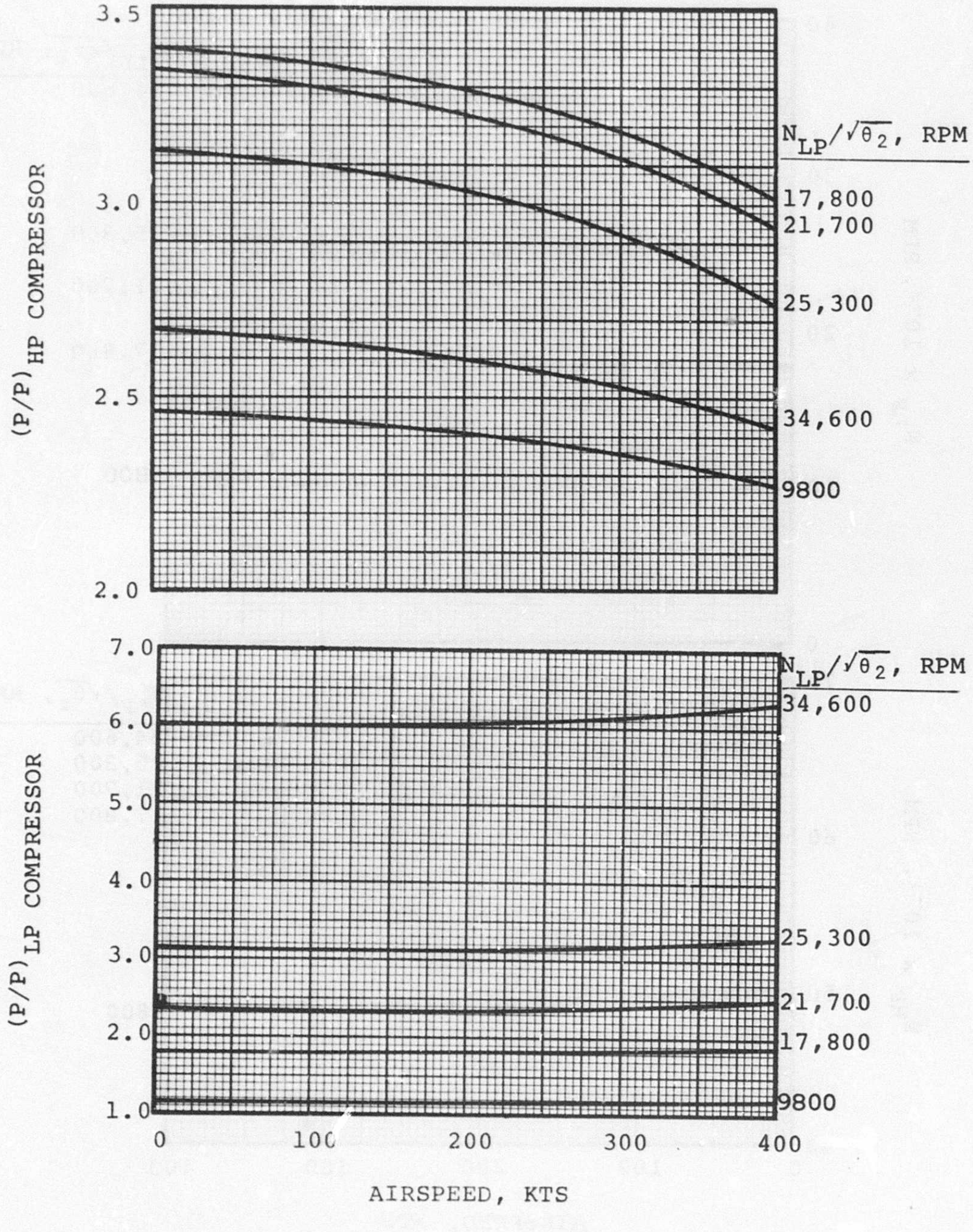

Figure 77. HP and LP Compressor P/P Versus Airspeed for 3S-RF-TSE at Sea-Level, Standard-Day Conditions.

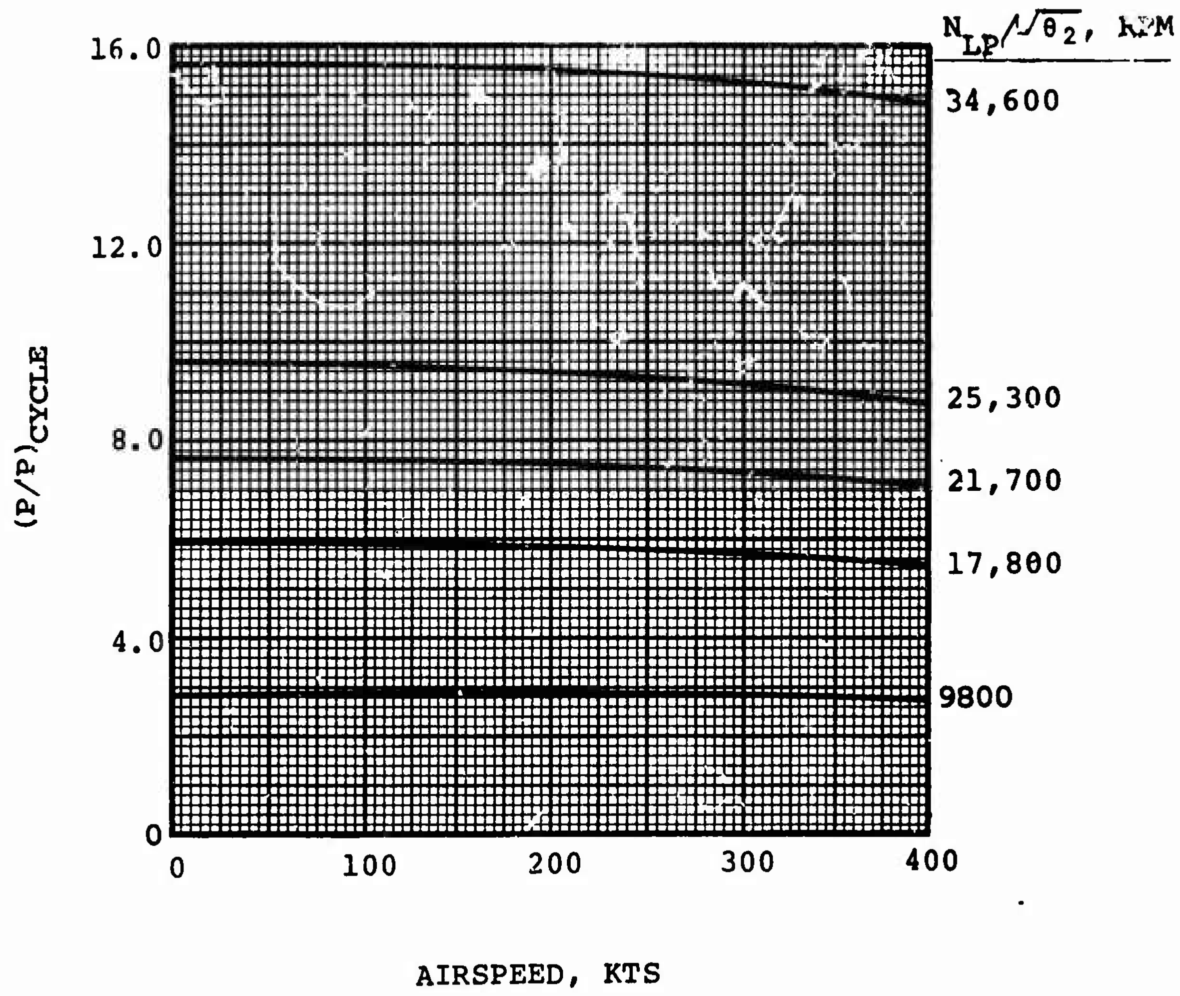

Figure 78. Cycle P/P Versus Airspeed for 3S-RF-TSE at Sea-Level, Standard-Day Conditions.

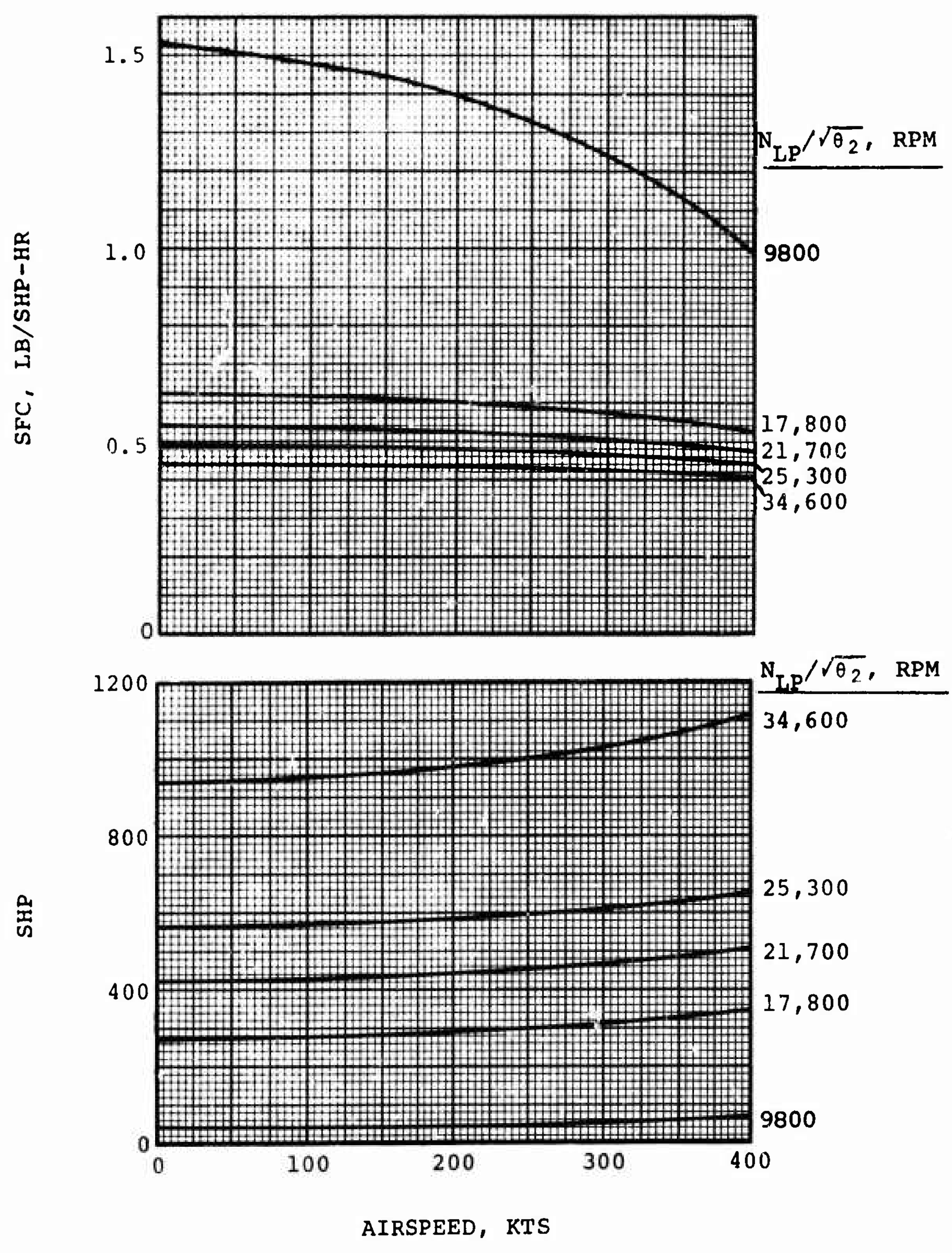

Figure 79. Shaft Horsepower and SFC Versus Airspeed for 3S-RF-TSE at 4000 Feet, Standard-Day Conditions.

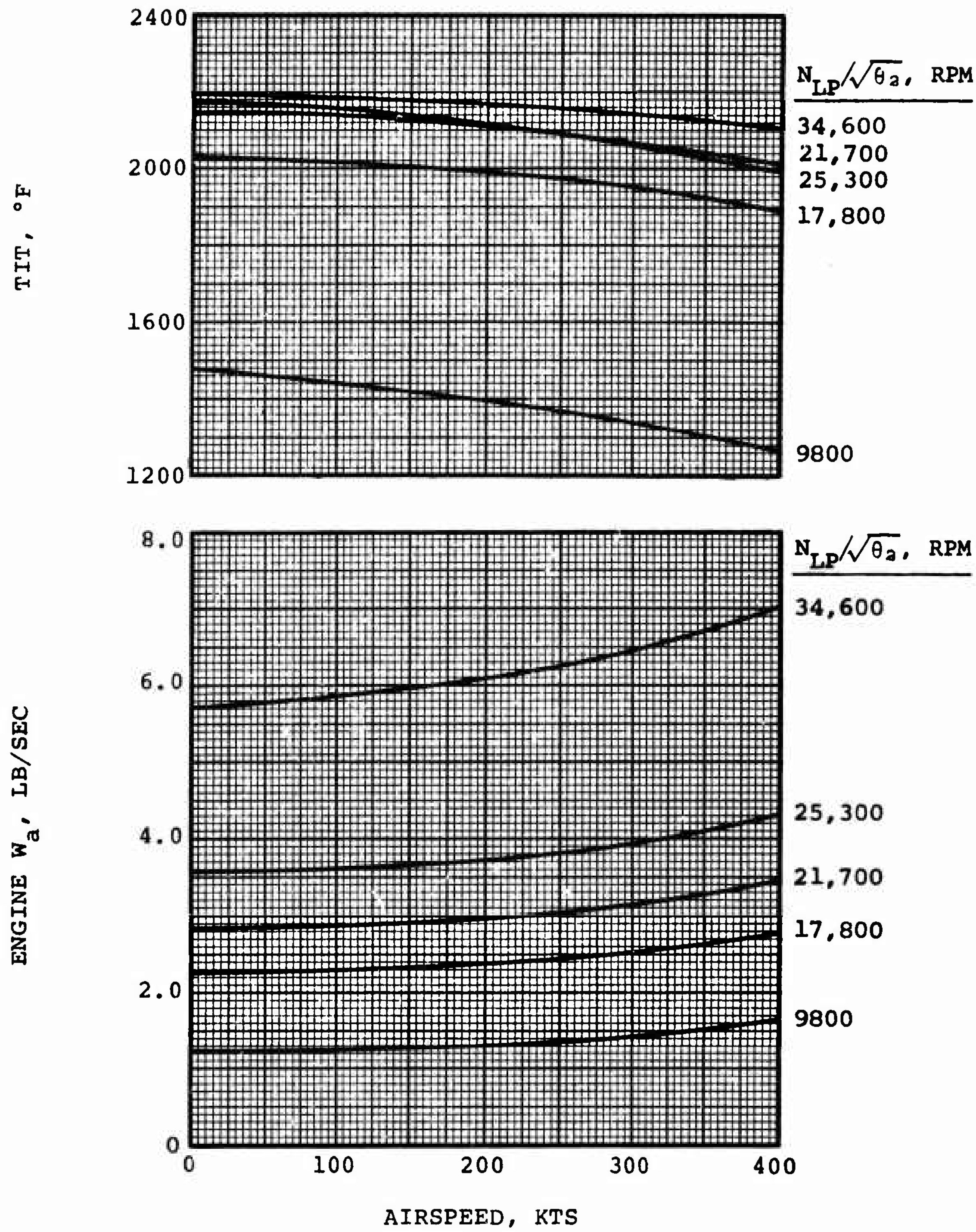

Figure 80. Airflow and TIT Versus Airspeed for 3S-RF-TSE at 4000 Feet, Standard-Day Conditions.

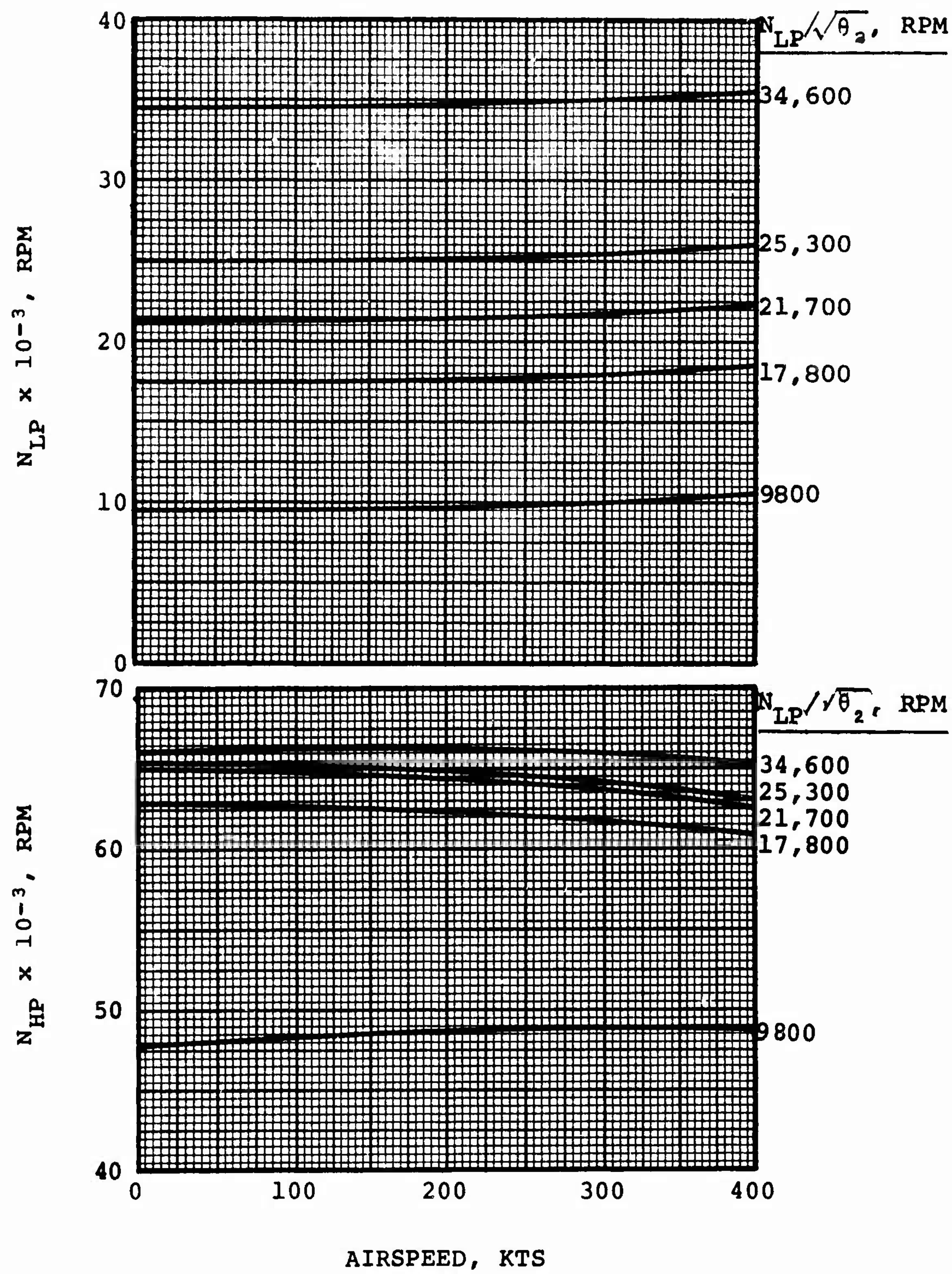

Figure 81. HP and LP Spool Speed Versus Airspeed for 3S-RF-TSE at 4000 Feet, Standard-Day Conditions.

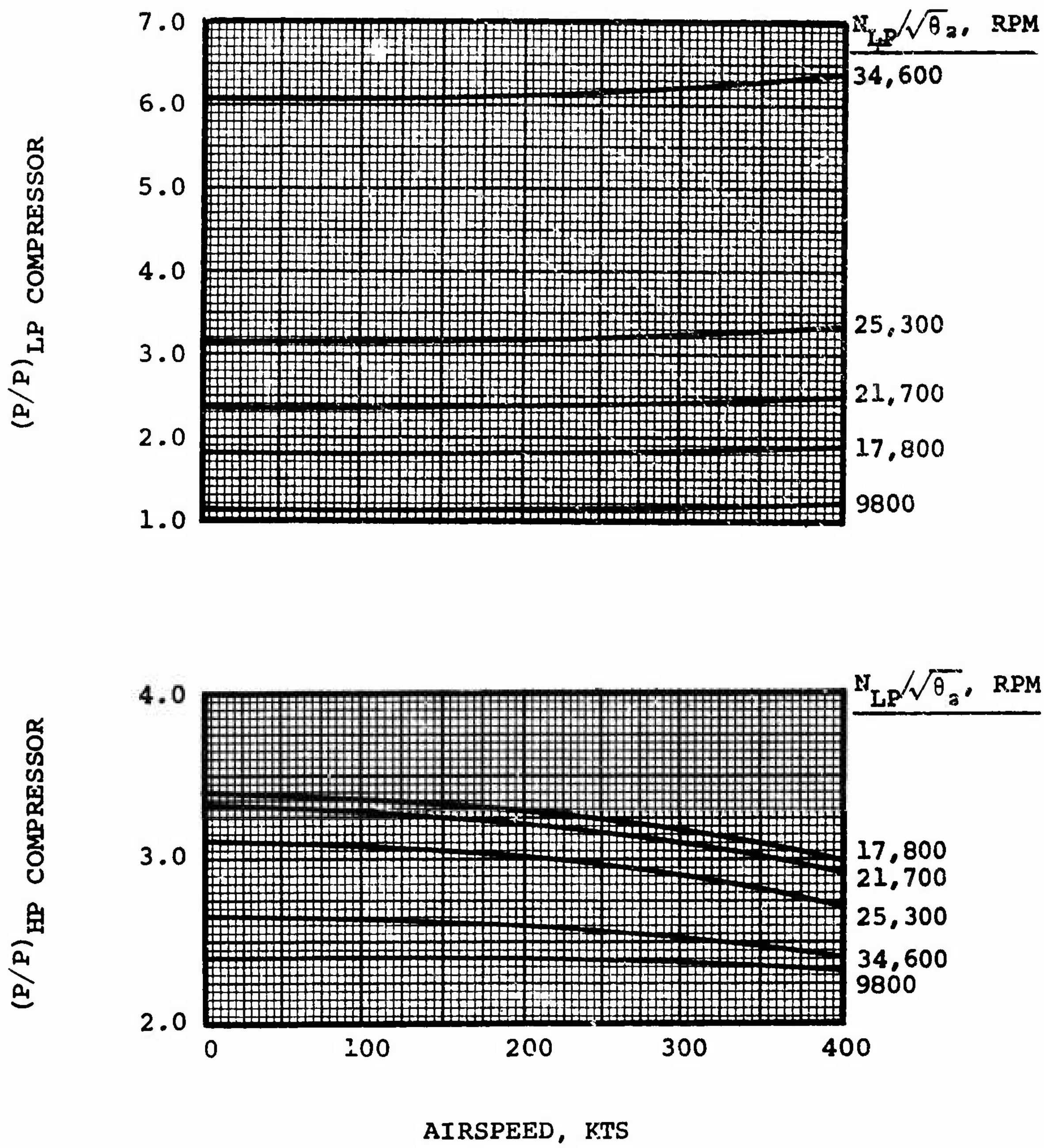

Figure 82. HP and LP Compressor P/P Versus Airspeed for 3S-RF-TSE at 4000 Feet, Standard-Day Conditions.

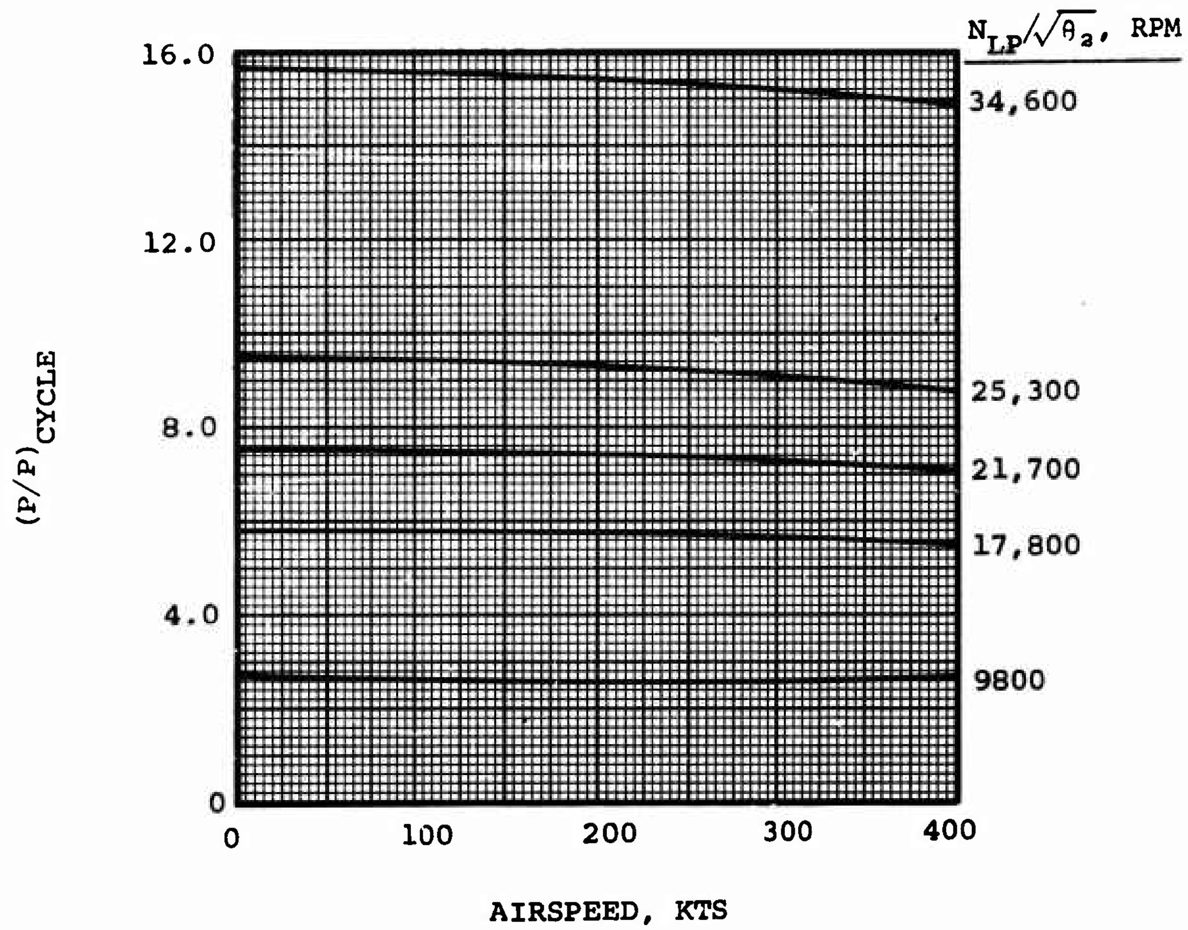

Figure 83. Cycle P/P Versus Airspeed for 3S-RF-TSE at 4000 Feet, Standard-Day Conditions.

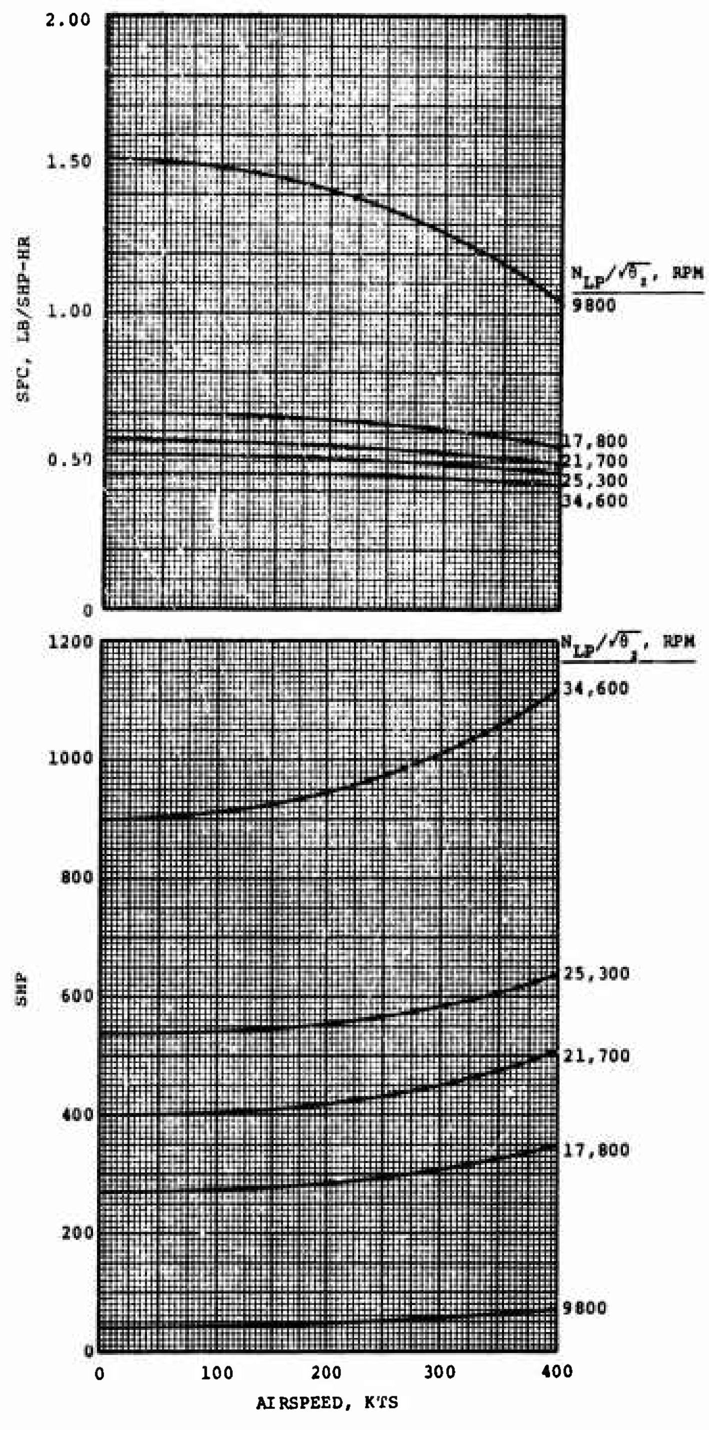

Figure 84. Shaft Horsepower and SFC Versus Airspeed for 3S-RF-TSE at 4000 Feet, 95°F-Day Conditions.

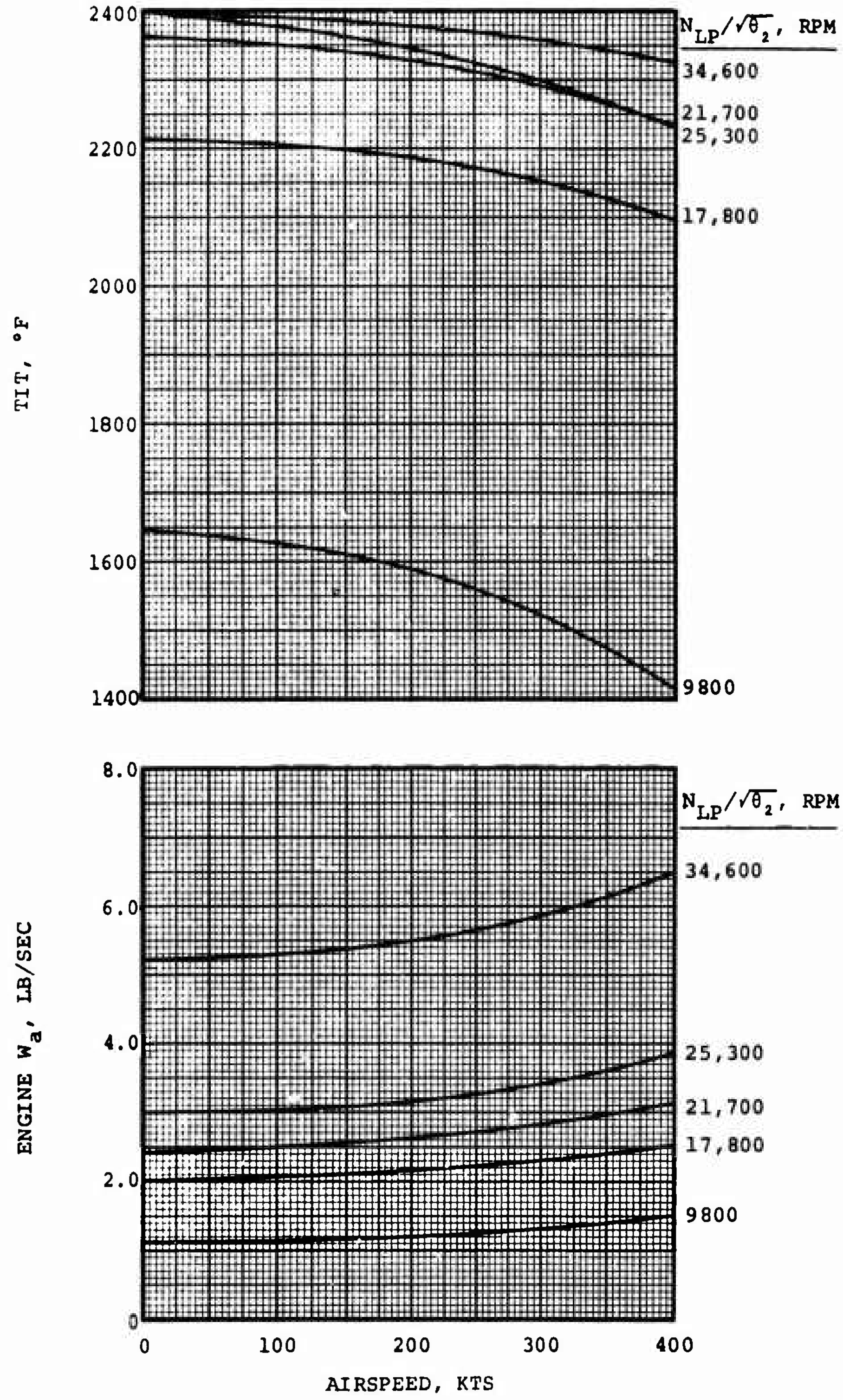

Figure 85. Engine Airflow and TIT Versus Airspeed for 3S-RF-TSE at 4000 Feet, 95°F-Day Conditions.

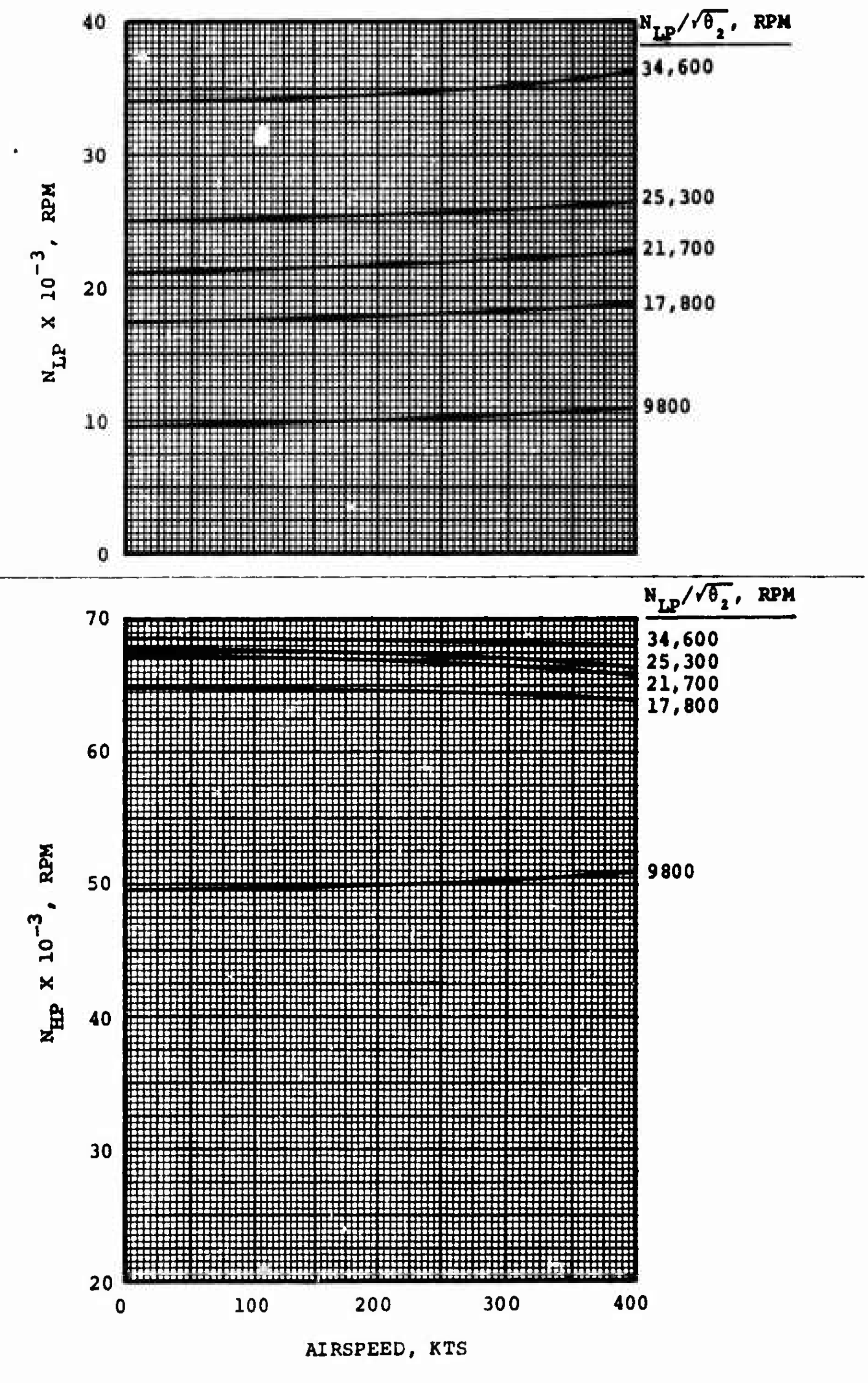

Figure 86. HP and LP Spool Speeds Versus Airspeed for 3S-RF-TSE at 4000 Feet, 95°F-Day Conditions.

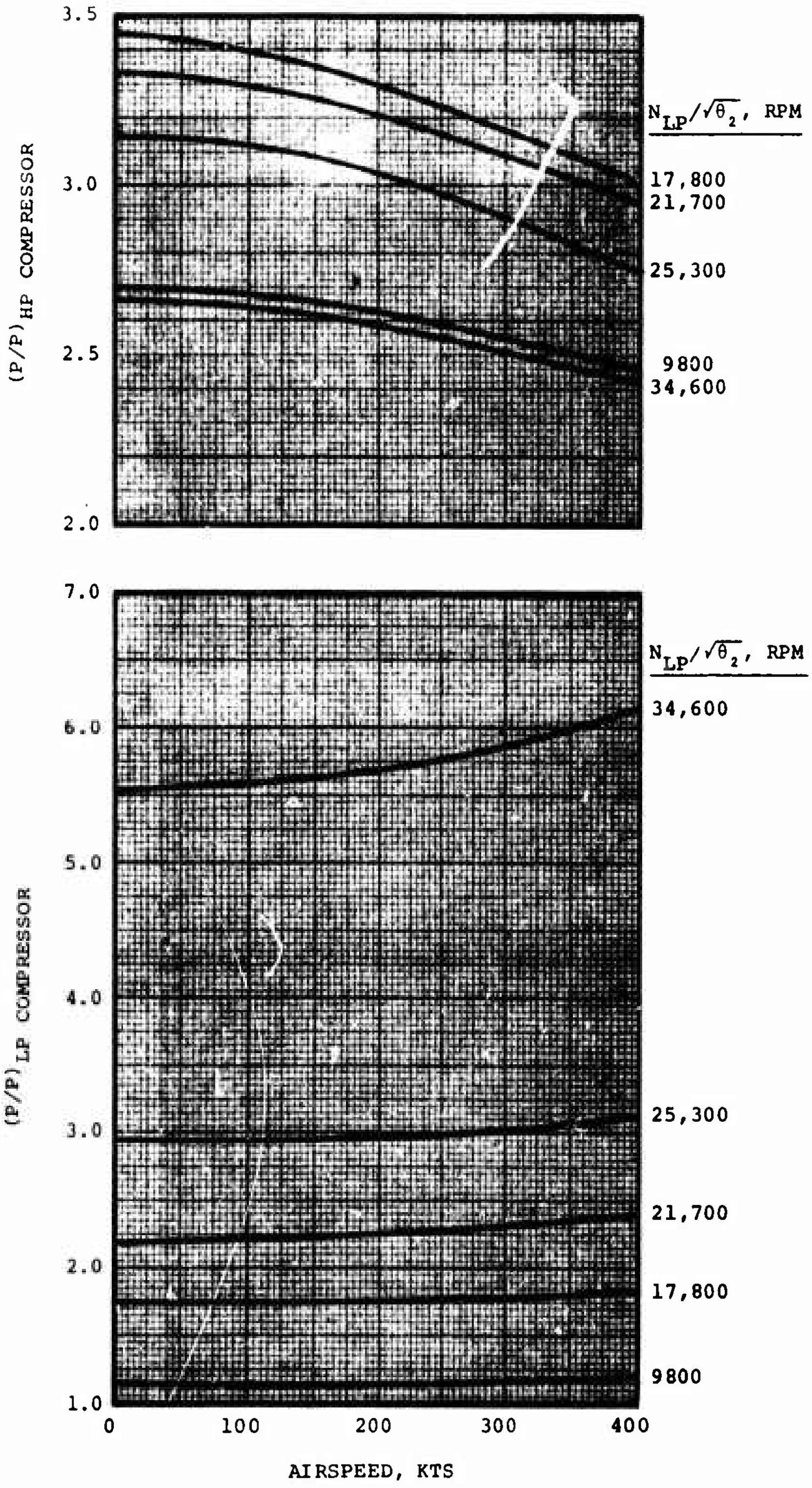

Figure 87. LP and HP Compressor P/P Versus Airspeed for 3S-RF-TSE at 4000 Feet, 95°F-Day Conditions.

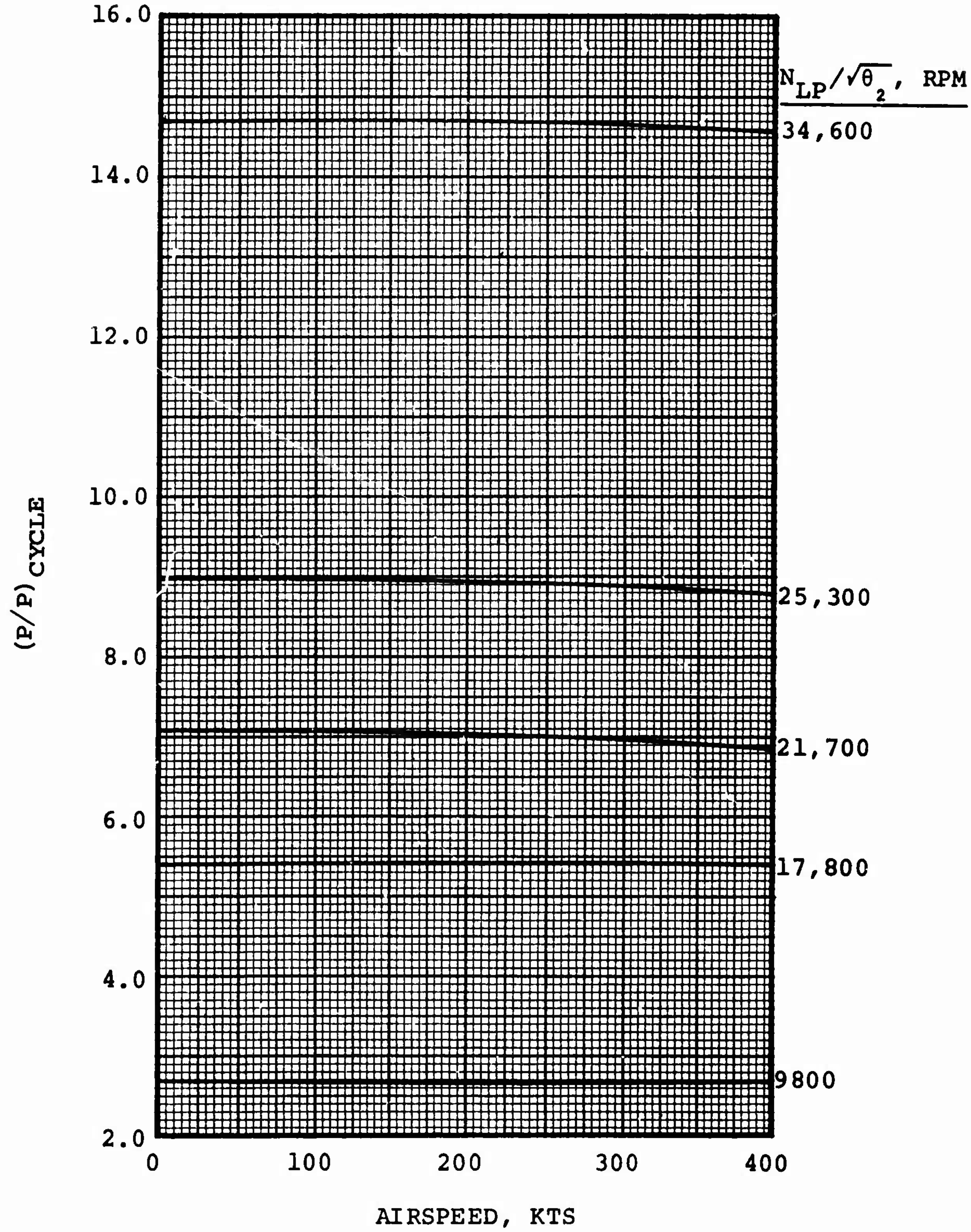

Figure 88. Cycle P/P Versus Airspeed for 3S-RF-TSE, at 4000 Feet, 95°F-Day Conditions.

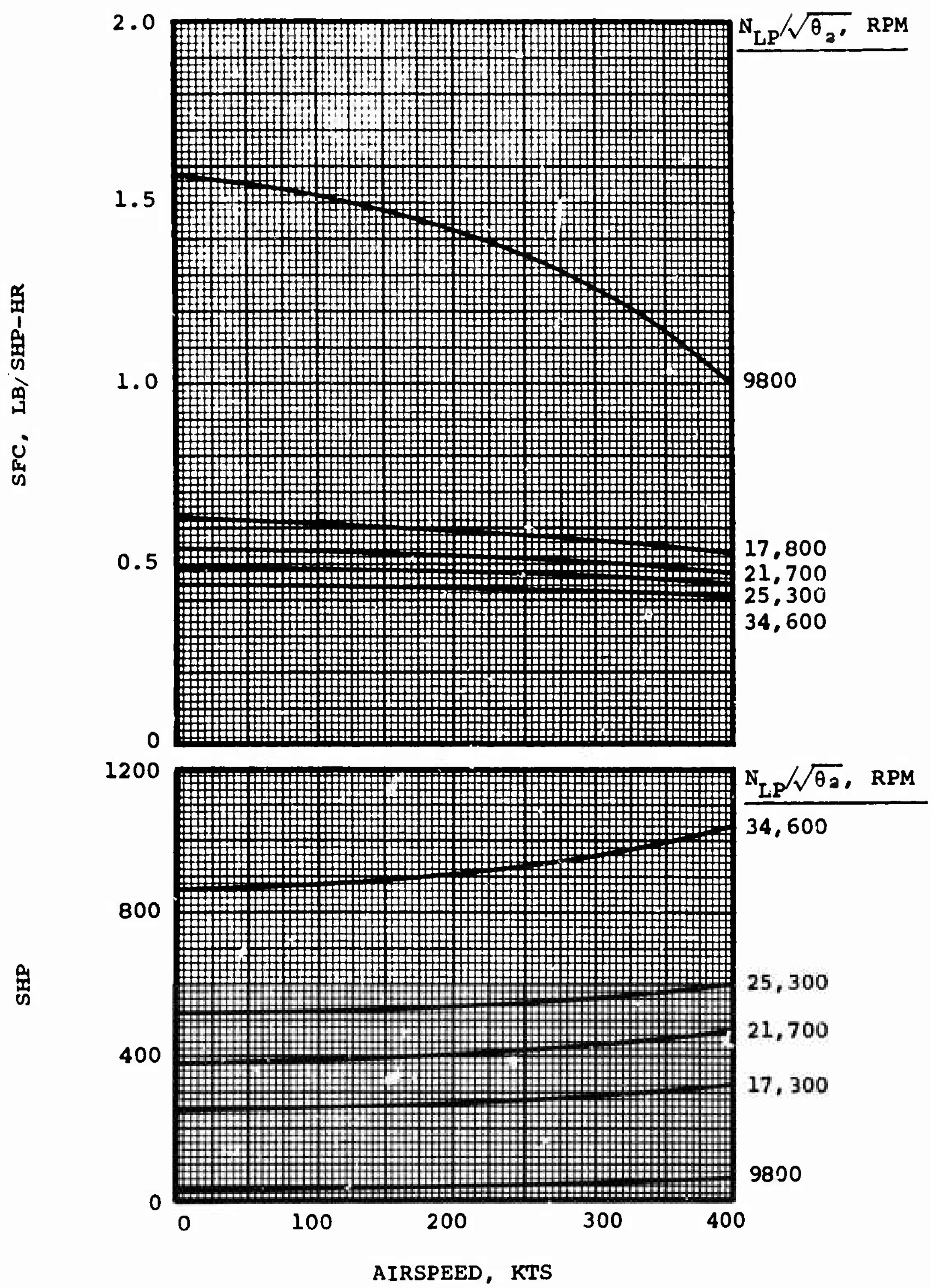

Figure 89. Shaft Horsepower and SFC Versus Airspeed for 3S-RF-TSE at 6000 Feet, Standard-Day Conditions.

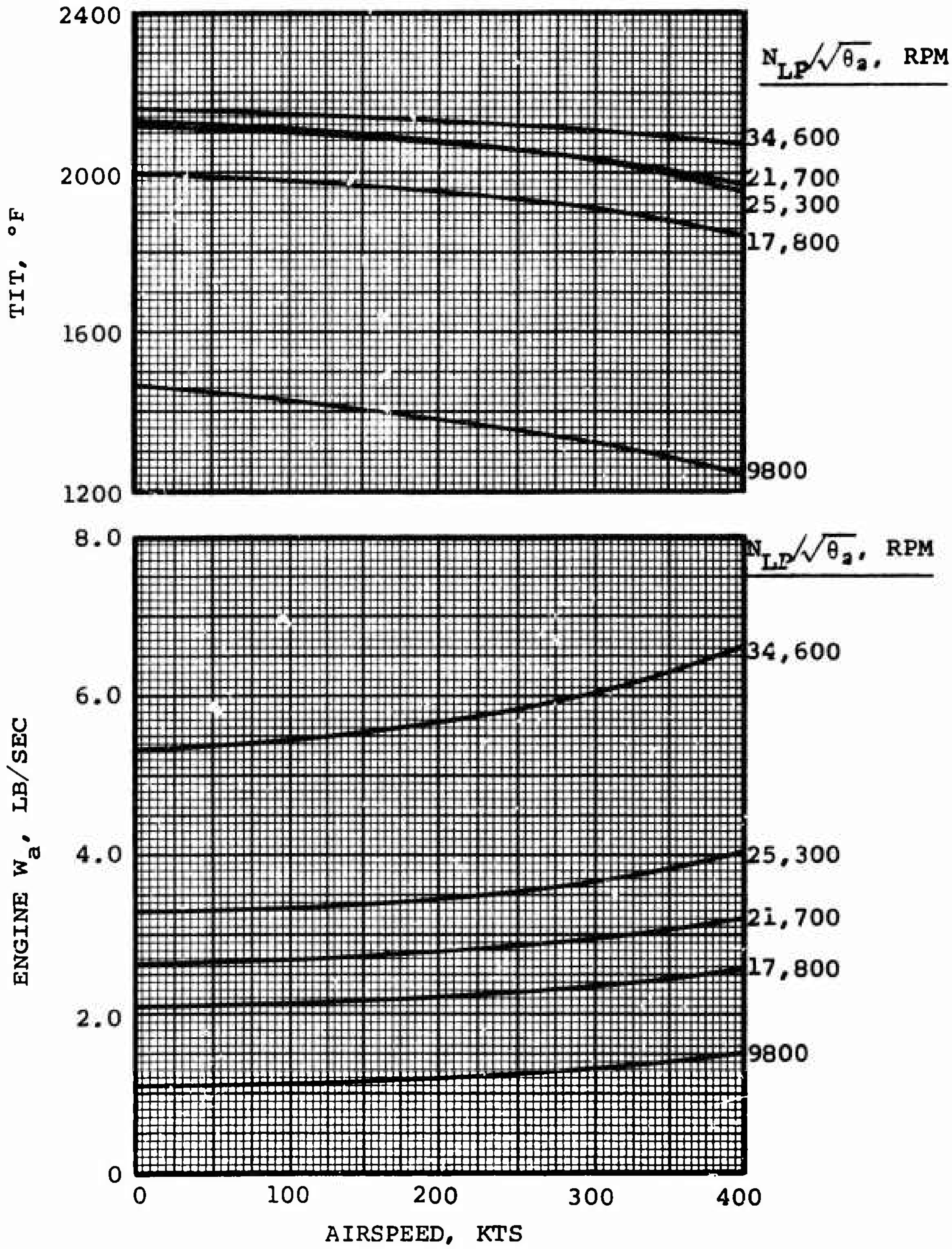

Figure 90. Engine Airflow and TIT Versus Airspeed for 3S-RF-TSE at 6000 Feet, Standard-Day Conditions.

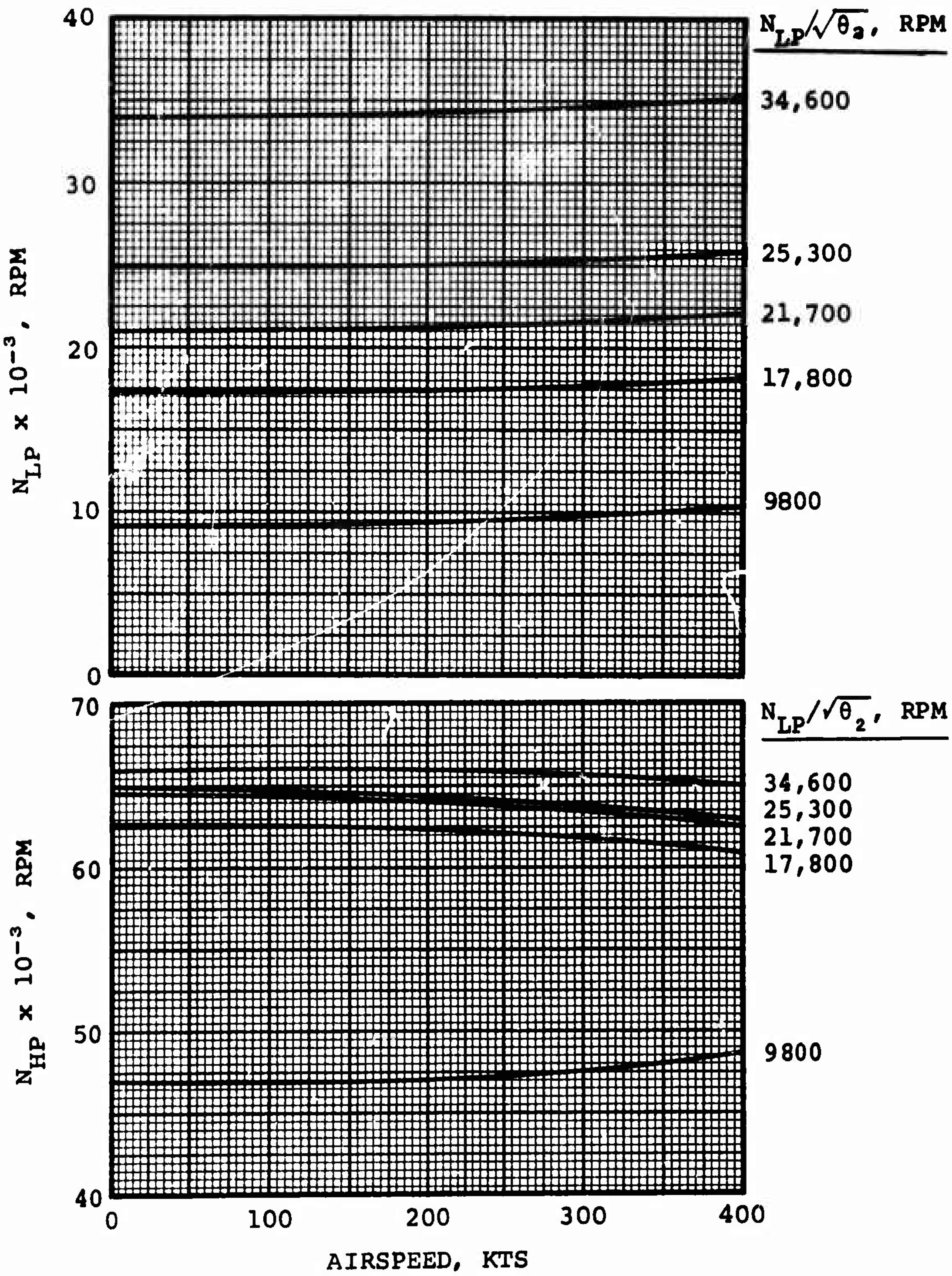

Figure 91. HP and LP Spool Speed Versus Airspeed for 3S-RF-TSE at 6000 Feet, Standard-Day Conditions.

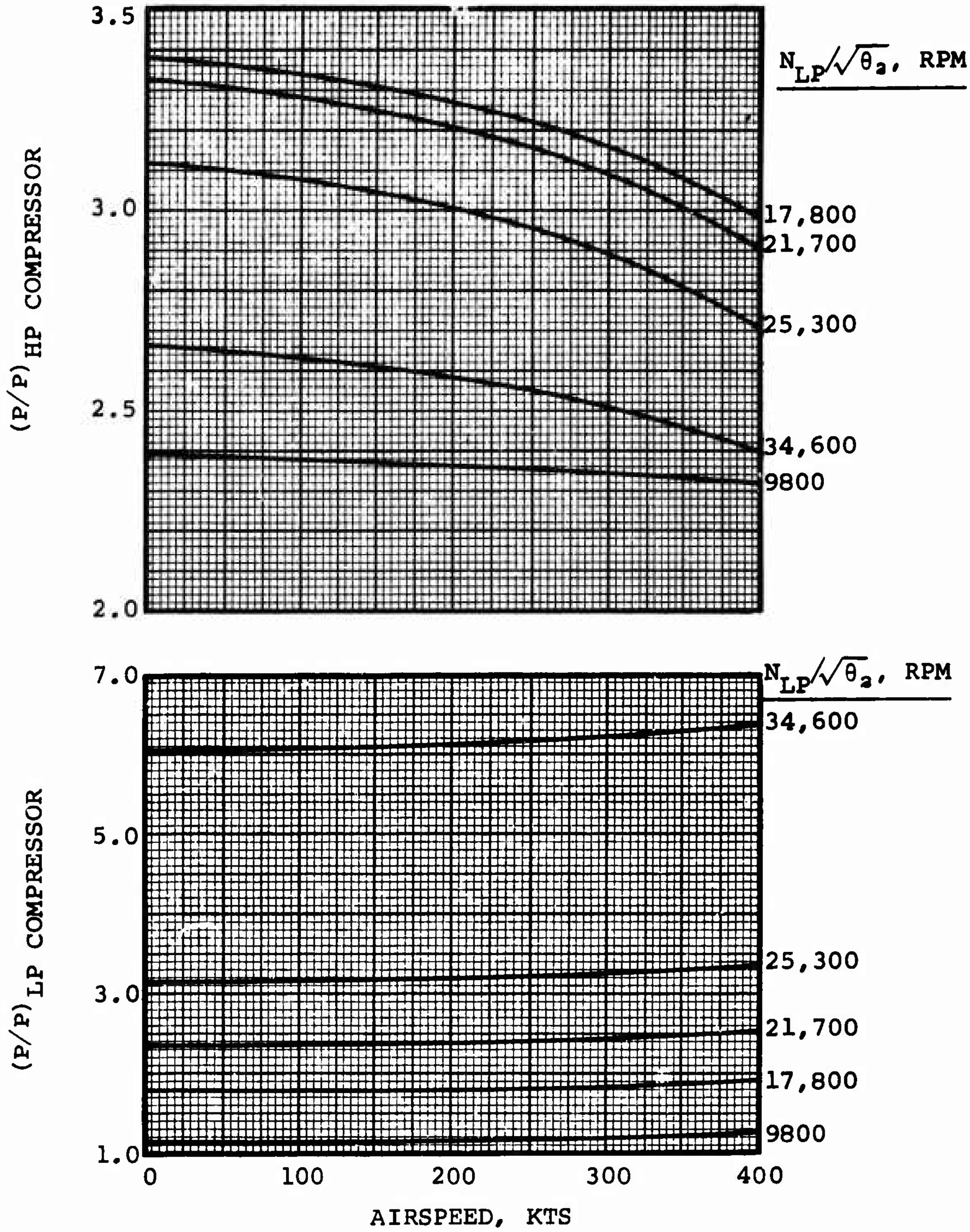

Figure 92. LP and HP Compressor P/P Versus Airspeed for 3S-RF-TSE at 6000 Feet, Standard-Day Conditions.

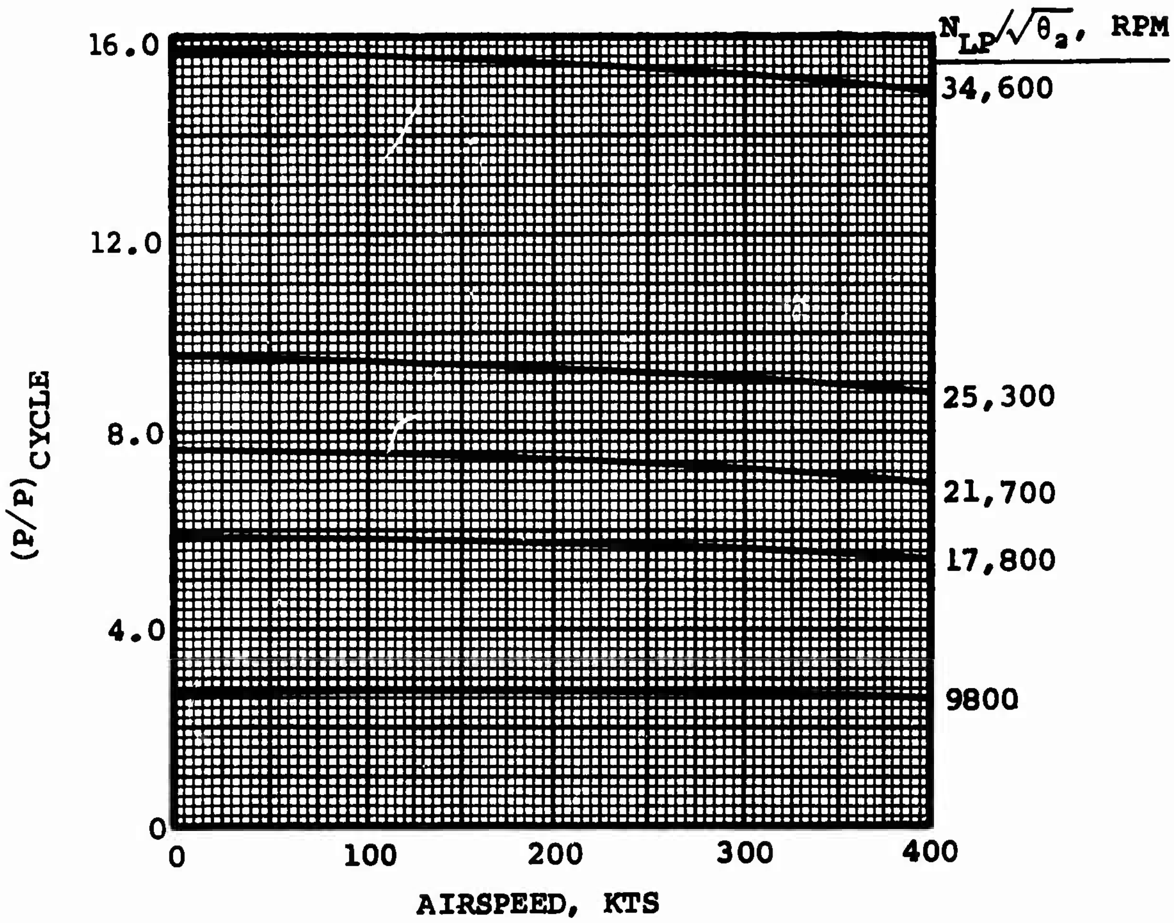

Figure 93. Cycle P/P Versus Airspeed for 3S-RF-TSE at 6000 Feet, Standard-Day Conditions.

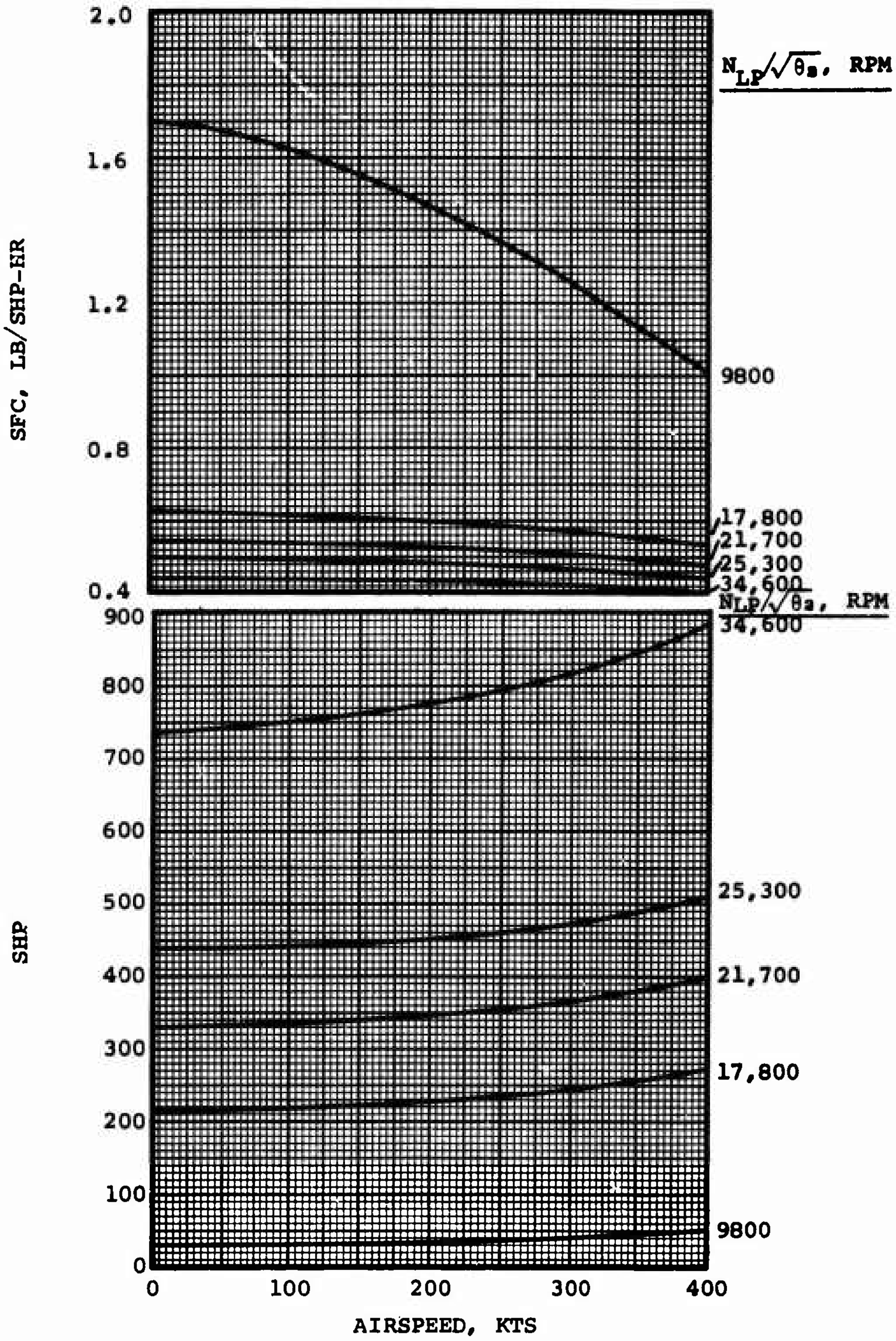

Figure 94. Shaft Horsepower and SFC Versus Airspeed for 3S-RF-TSE at 10,000 Feet, Standard-Day Conditions.

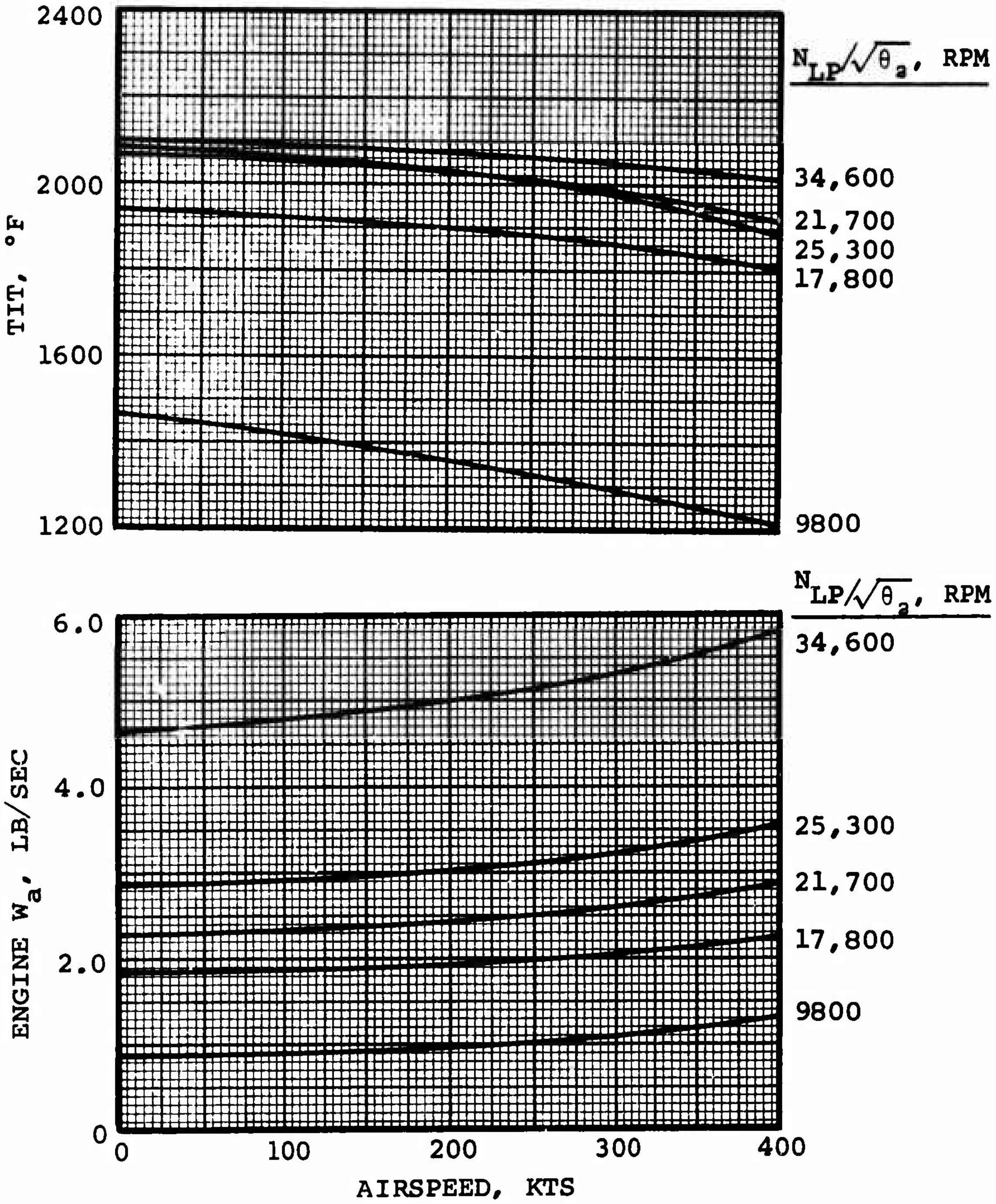

Figure 95. Engine Airflow and TIT Versus Airspeed for 3S-RF-TSE at 10,000 Feet, Standard-Day Conditions.

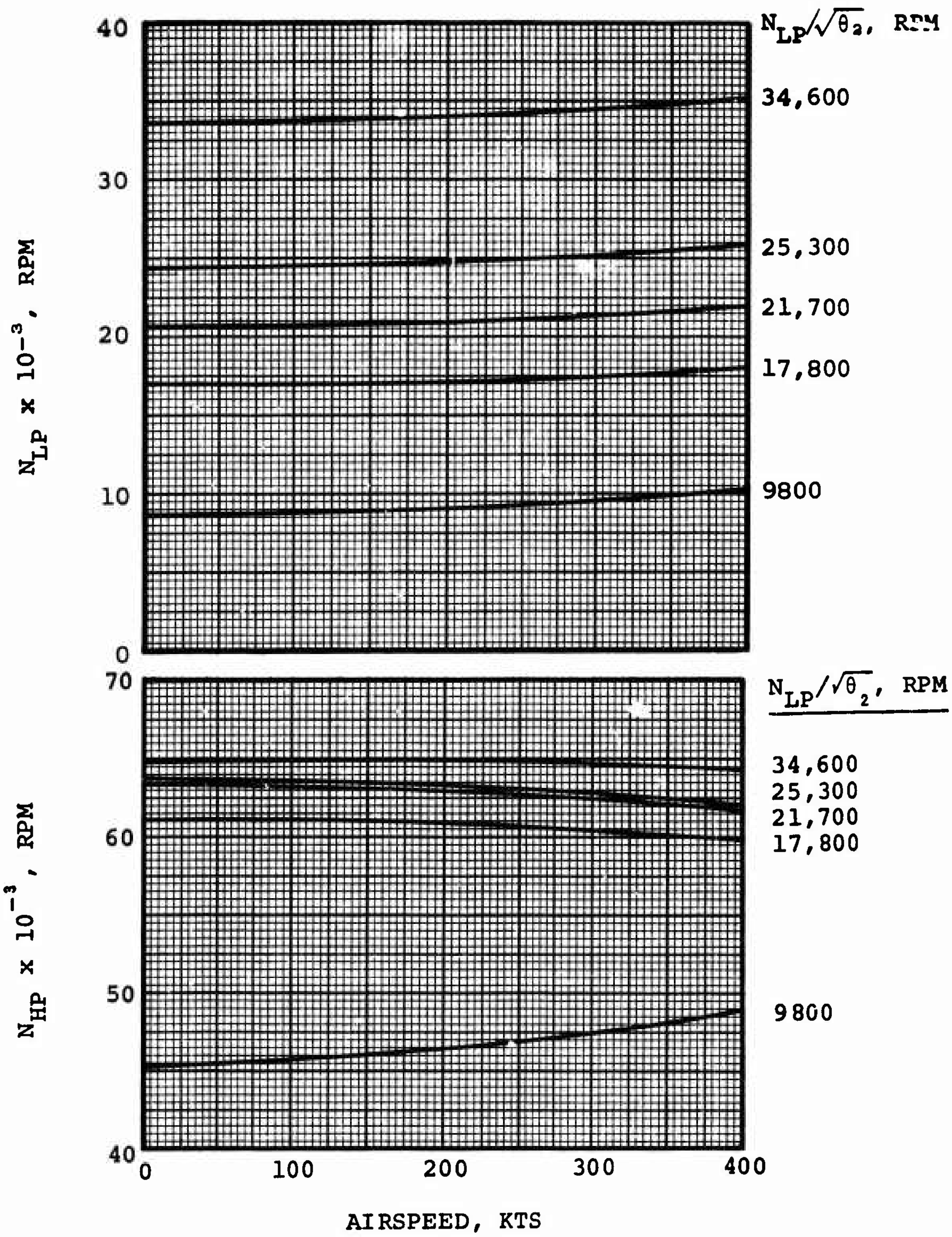

Figure 96. Airspeed Versus HP and LP Spool Speeds for 3S-RF-TSE at 10,000 Feet, Standard-Day Conditions.

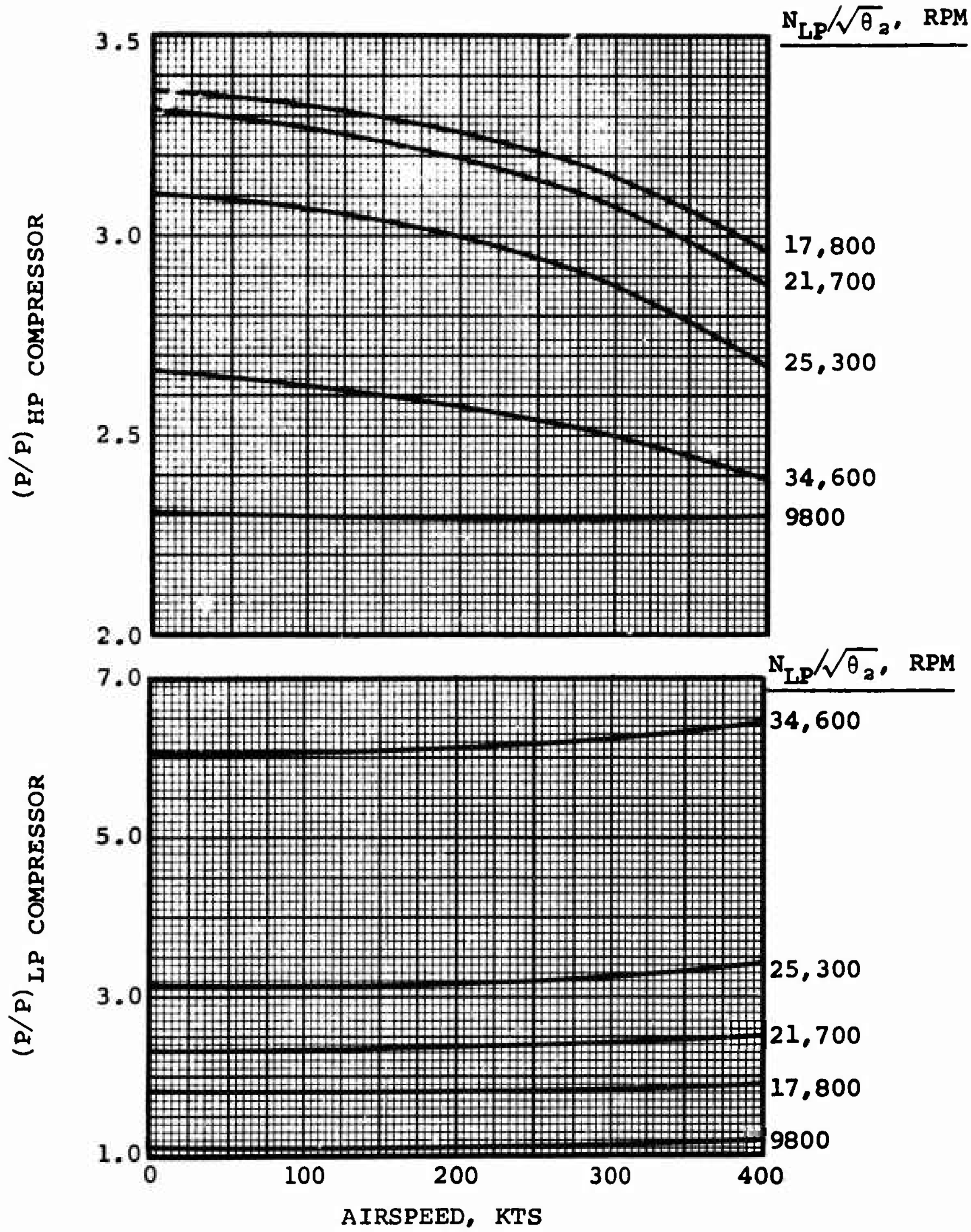

Figure 97. LP and HP Compressor P/P Versus Airspeed for 3S-RF-TSE at 10,000 Feet, Standard-Day Conditions.

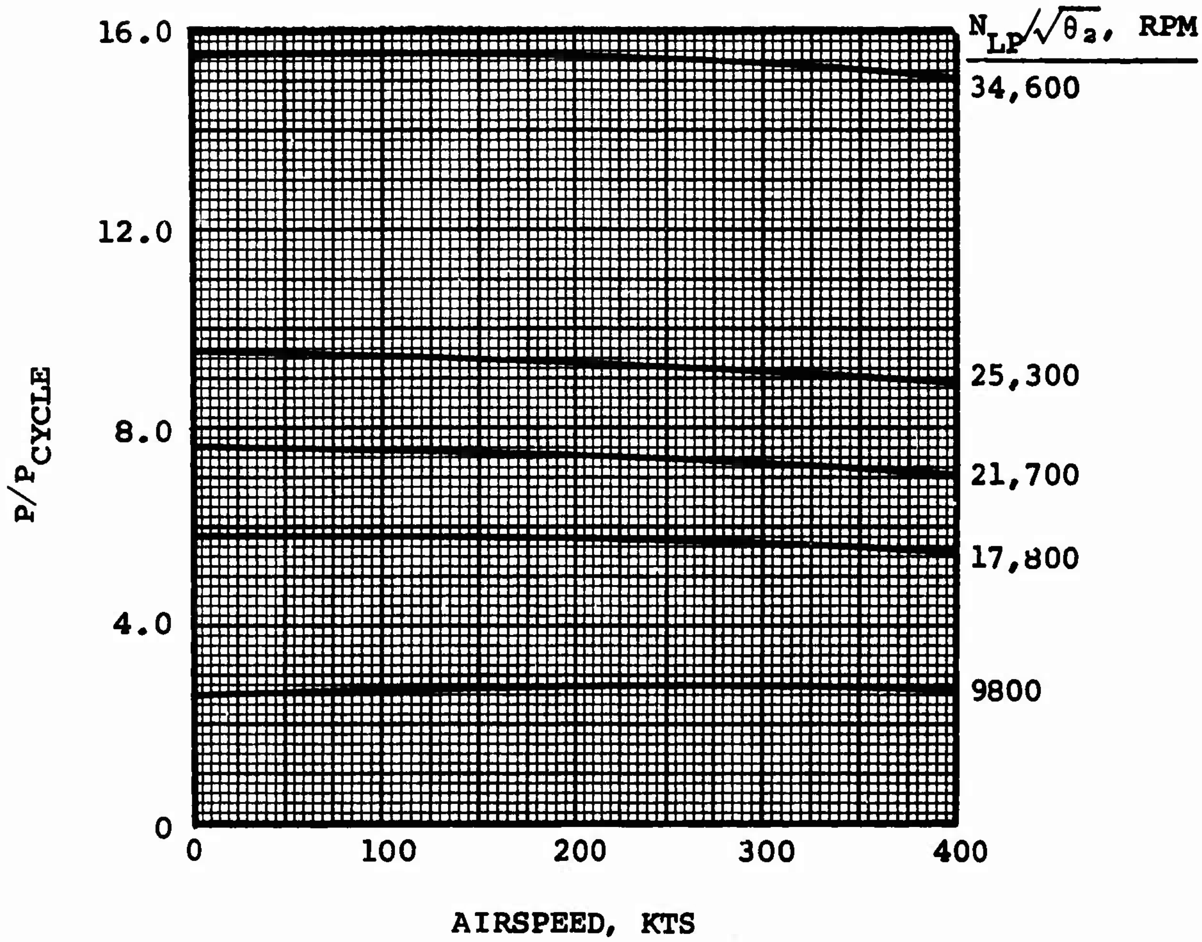

Figure 98. Cycle P/P Versus Airspeed for 3S-RF-TSE at 10,000 Feet, Standard-Day Conditions.

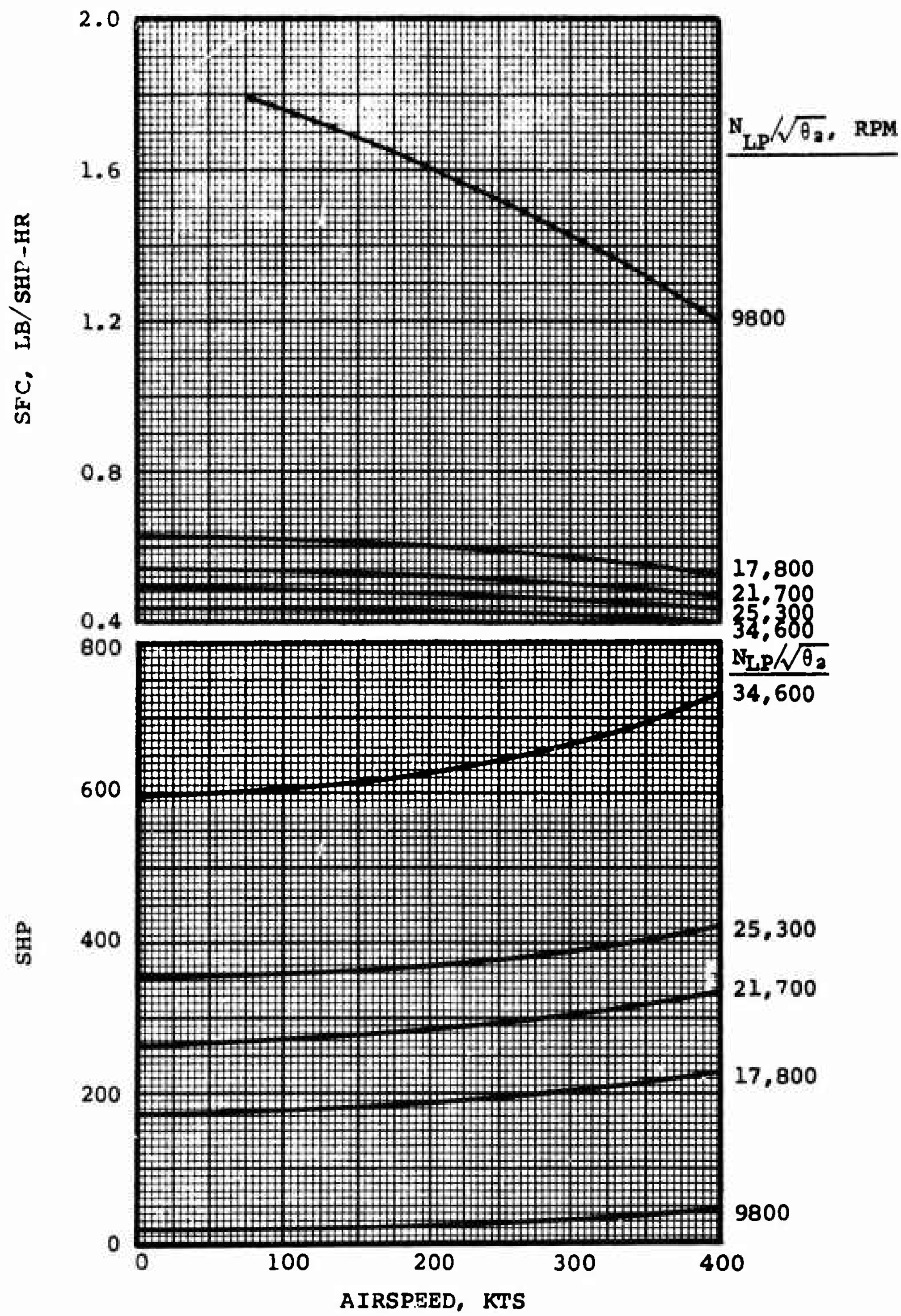

Figure 99. Shaft Horsepower and SFC Versus Airspeed for 3S-RF-TSE at 15,000 Feet, Standard-Day Conditions.

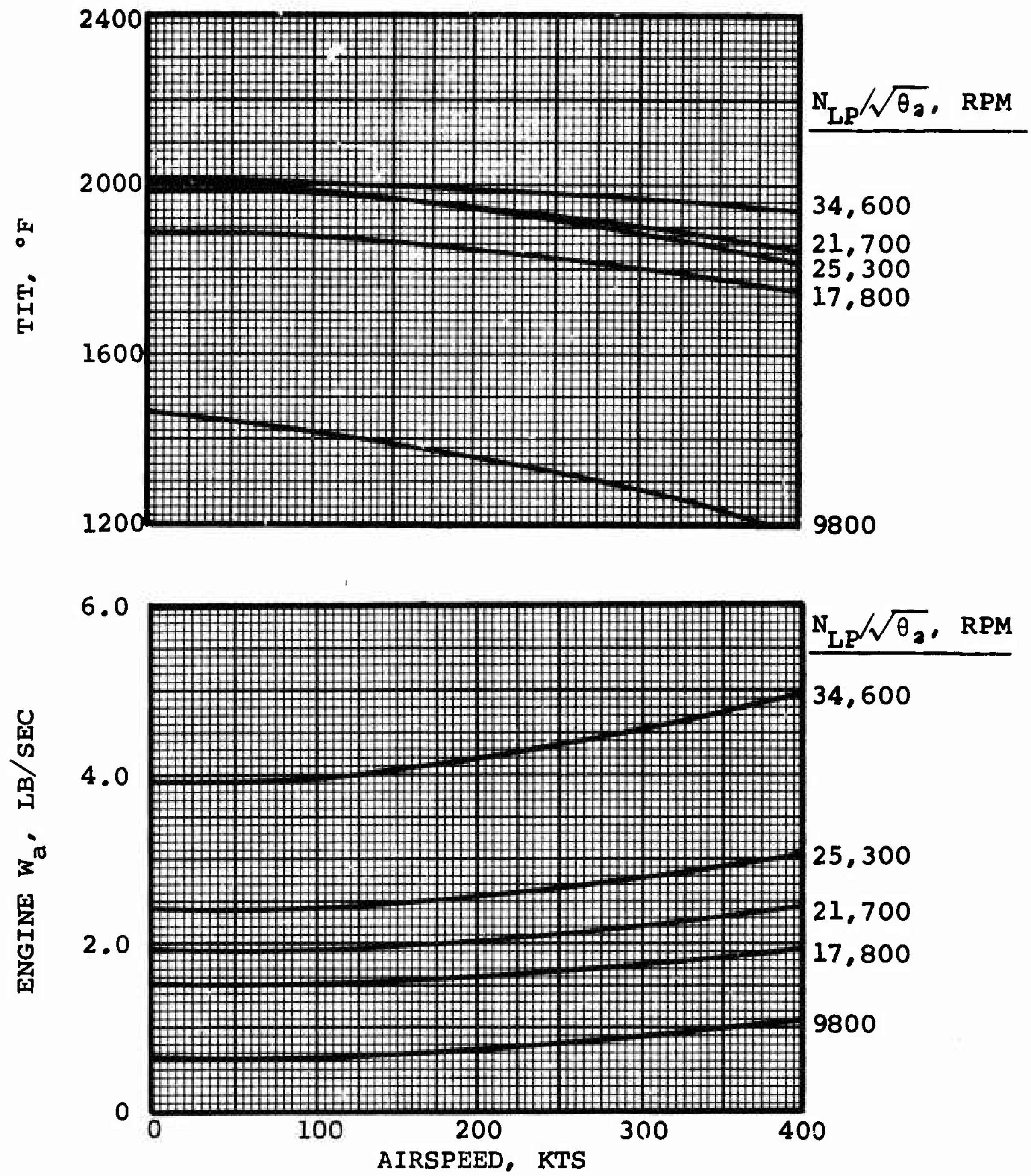

Figure 100. Engine Airflow and TIT Versus Airspeed for 3S-RF-TSE at 15,000 Feet, Standard-Day Conditions.

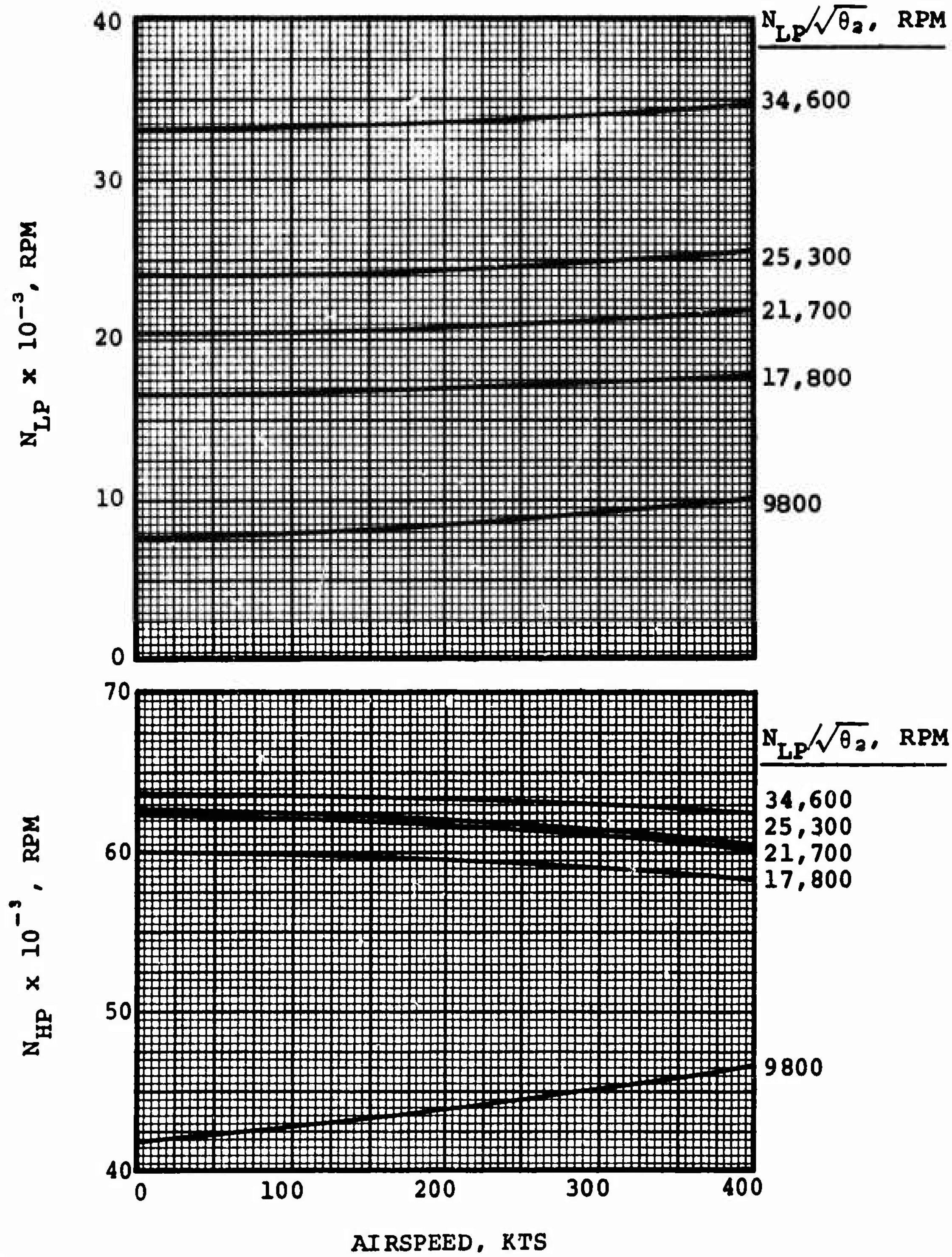

Figure 101. HP and LP Spool Speeds Versus Airspeed for 3S-RF-TSE at 15,000 Feet, Standard-Day Conditions.

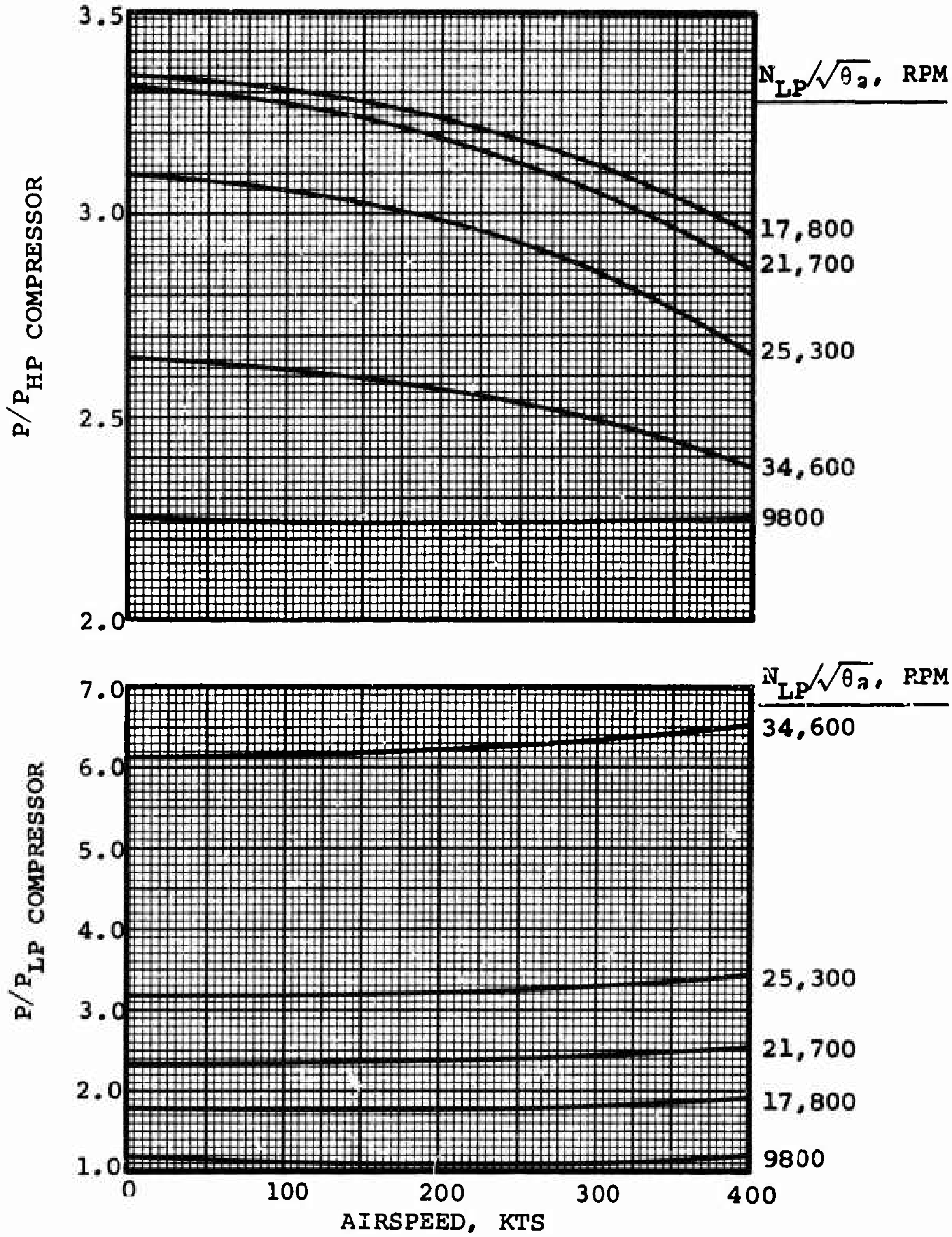

Figure 102. LP and HP Compressor P/P Versus Airspeed for 3S-RF-TSE at 15,000 Feet, Standard-Day Conditions.

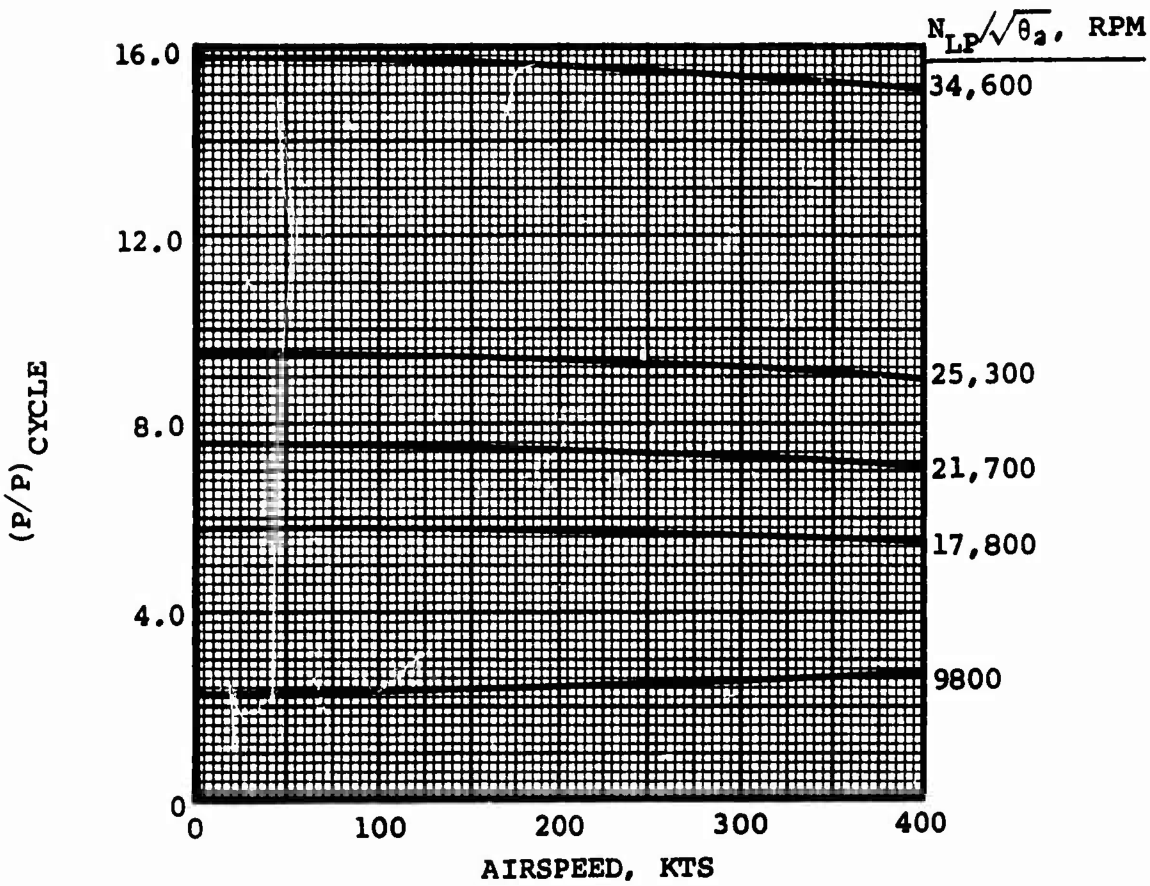

Figure 103. Cycle P/P Versus Airspeed for 3S-RF-TSE at 15,000 Feet, Standard-Day Conditions.

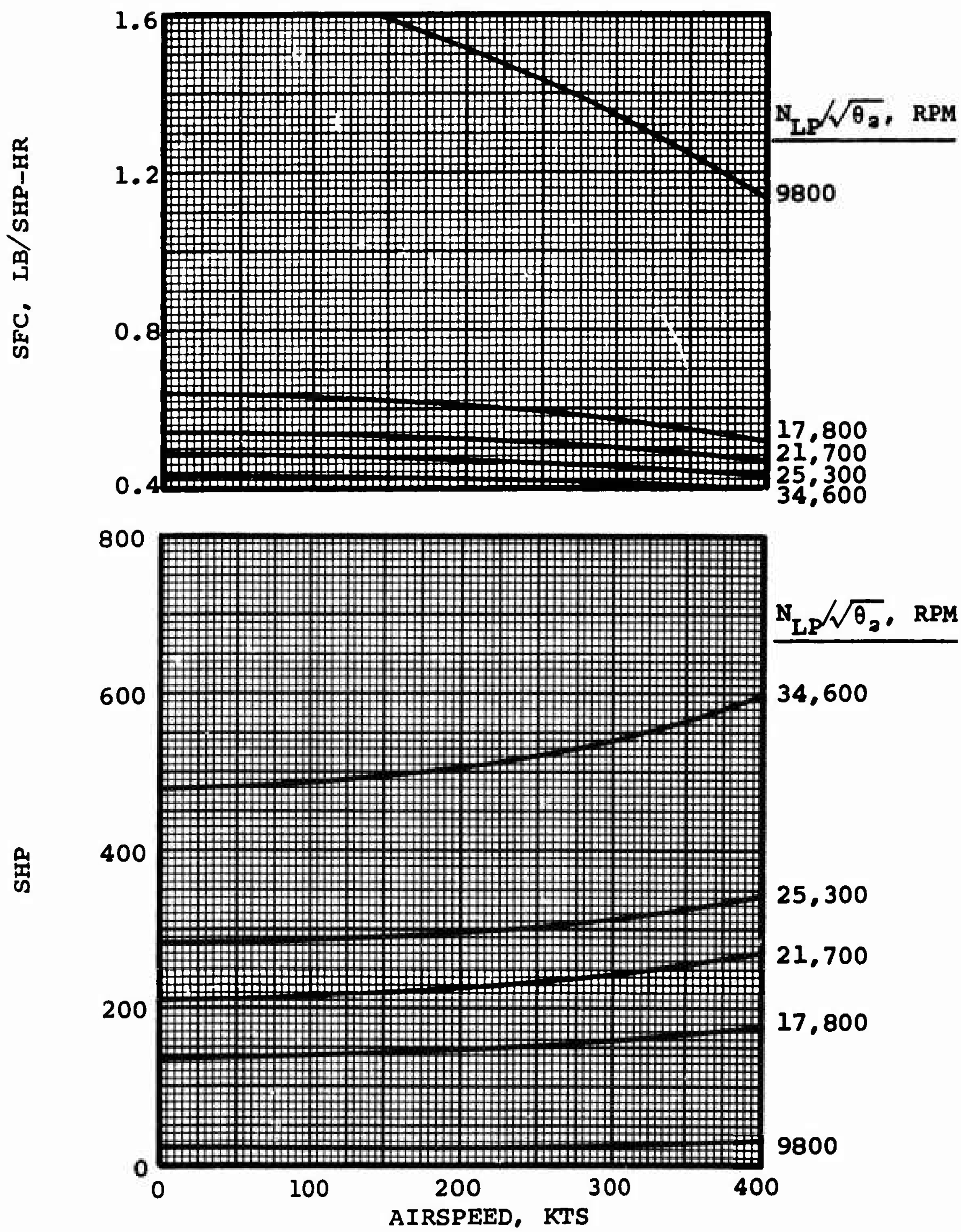

Figure 104. Shaft Horsepower and SFC Versus Airspeed for 3S-RF-TSE at 20,000 Feet, Standard-Day Conditions.

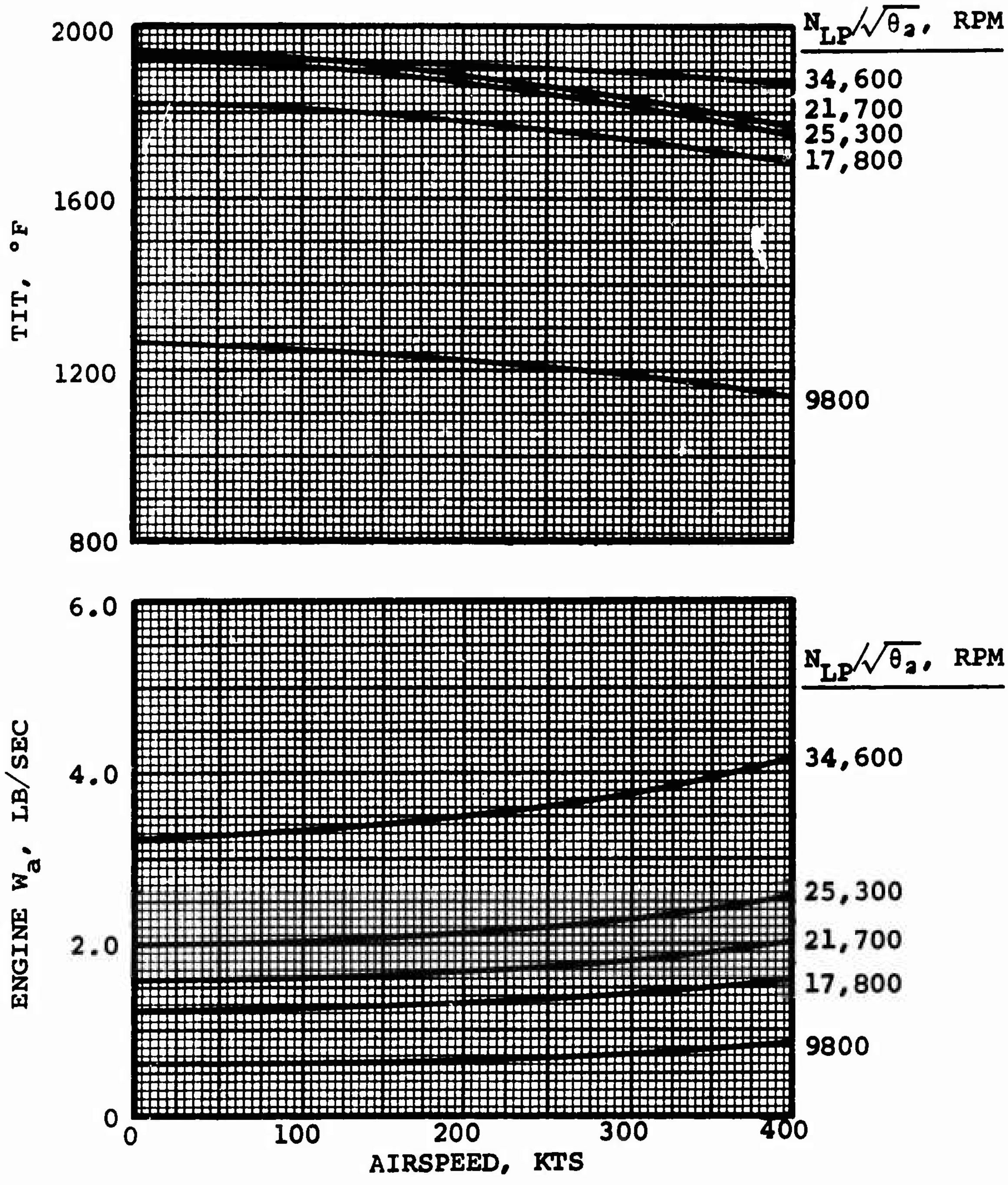

Figure 105. Engine Airflow and TIT Versus Airspeed for 3S-RF-TSE at 20,000 Feet, Standard-Day Conditions.

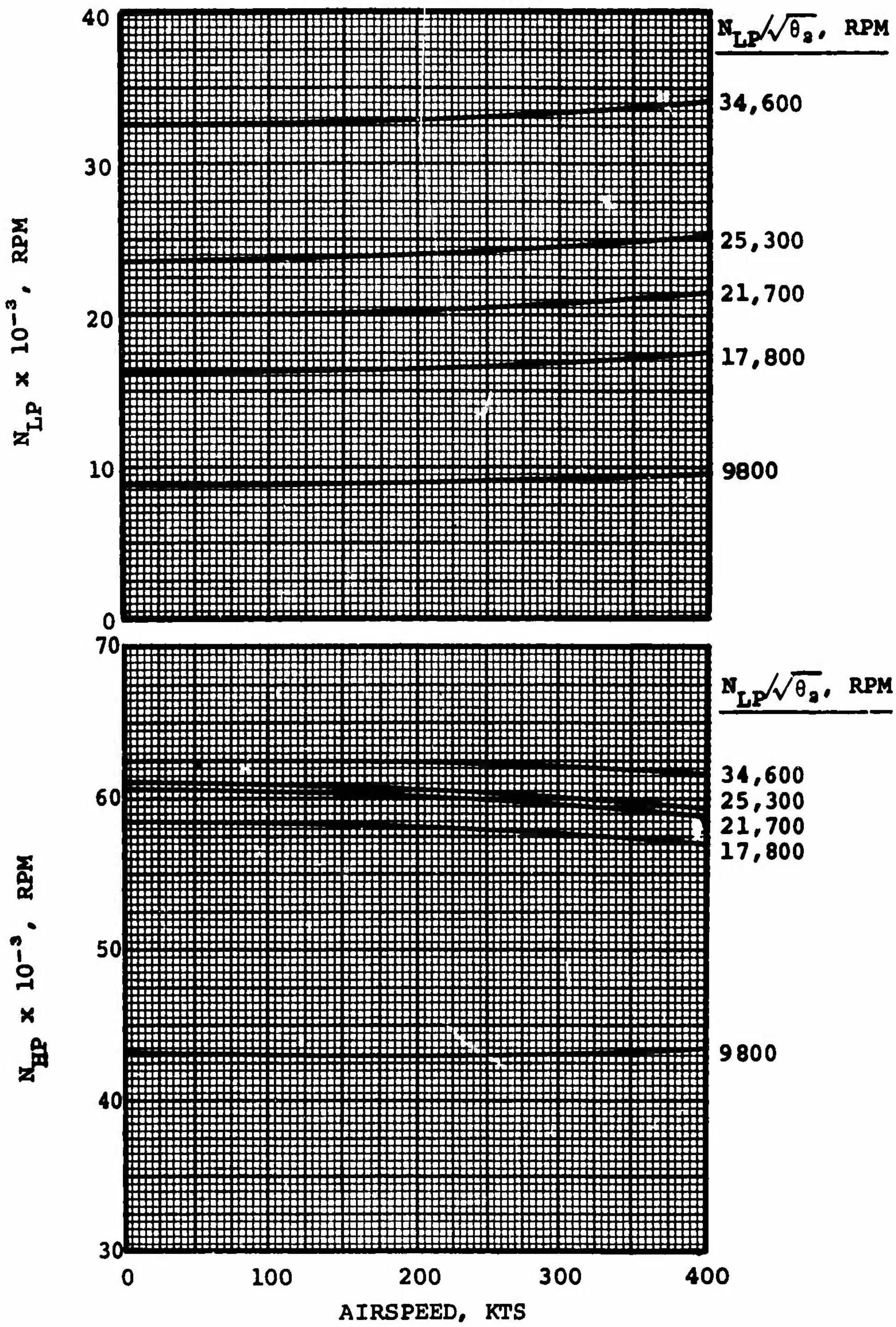

Figure 106. LP and HP Spool Speeds Versus Airspeed for 3S-RF-TSE at 20,000 Feet, Standard-Day Conditions.

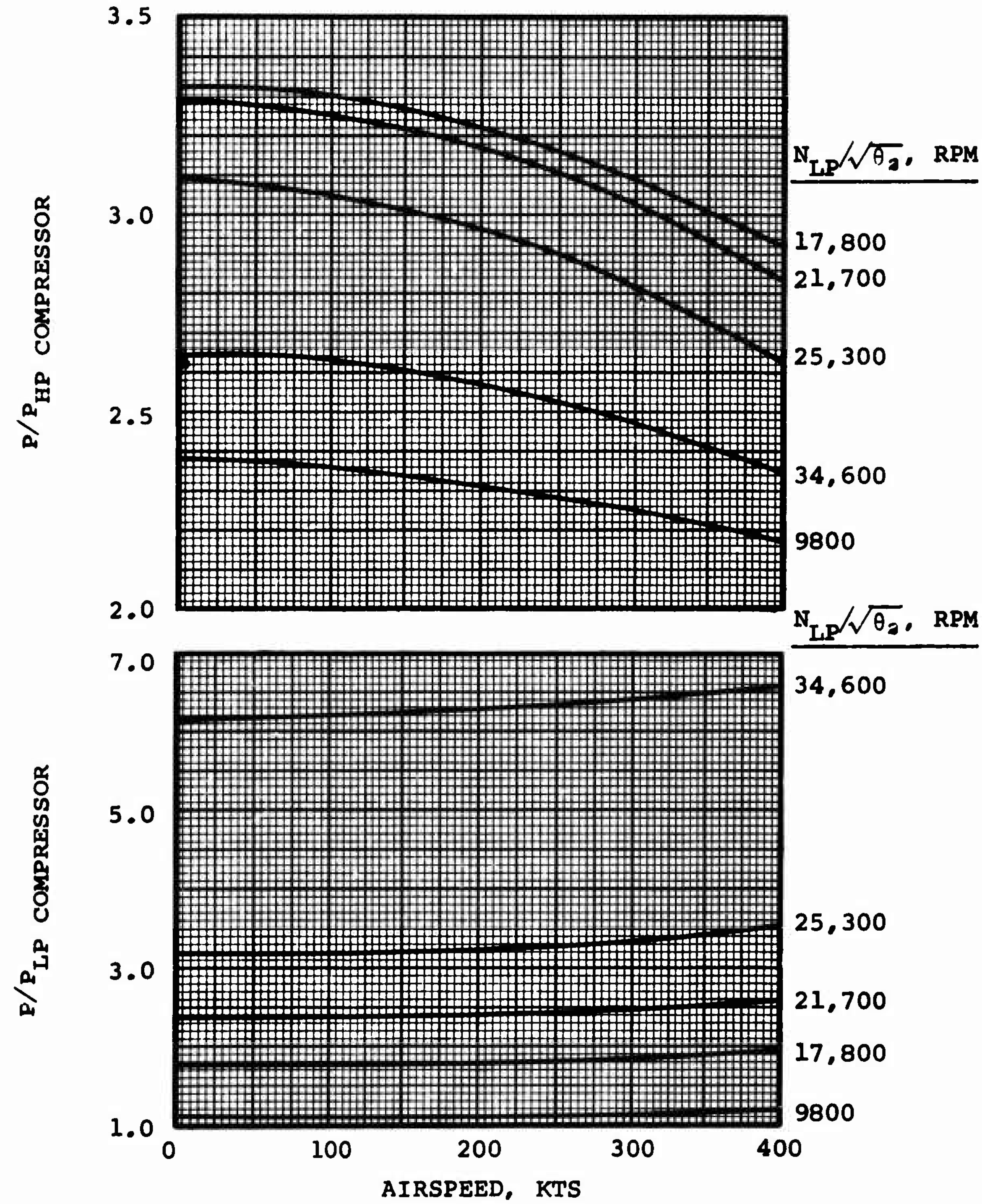

Figure 107. LP and HP Compressor P/P Versus Airspeed for 3S-RF-TSE at 20,000 Feet, Standard-Day Conditions.

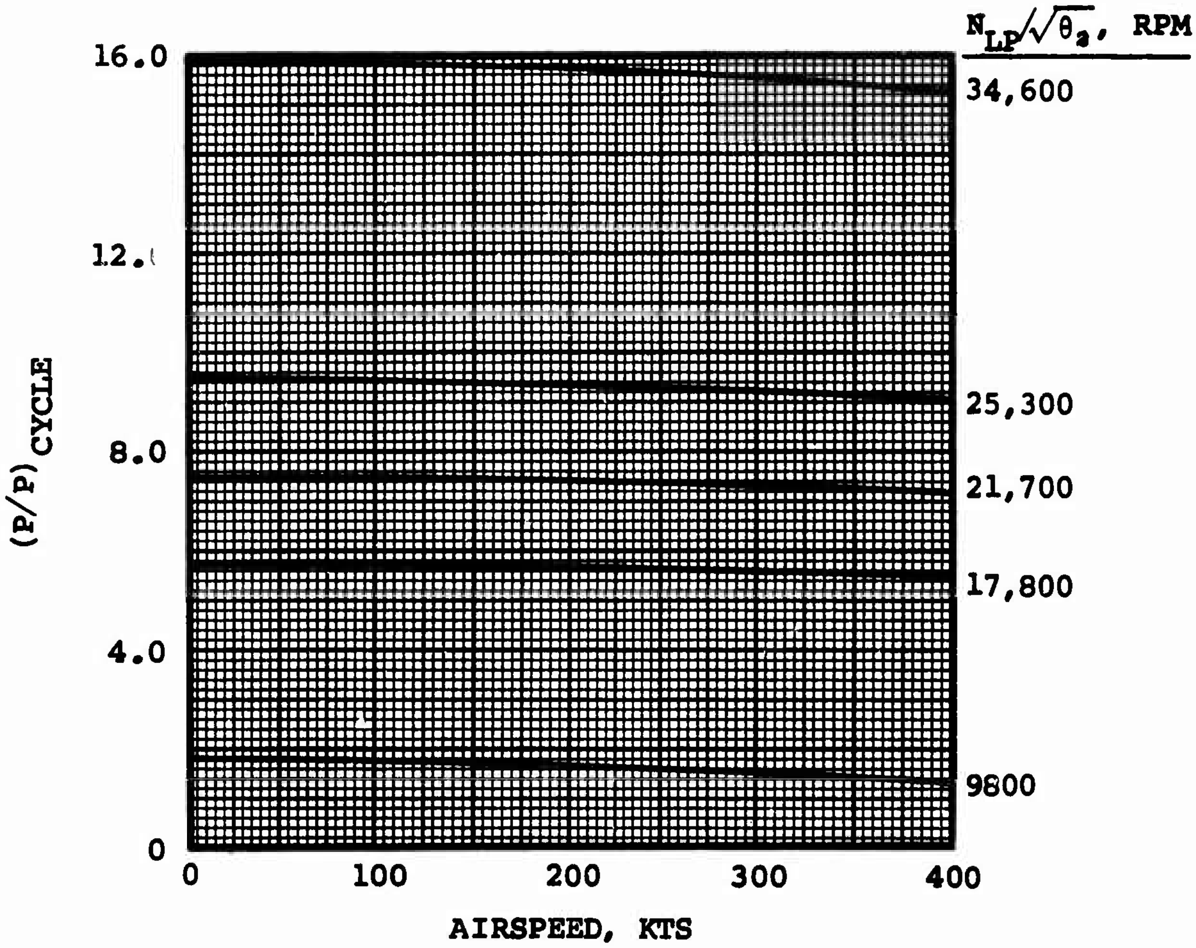

Figure 108. Cycle P/P Versus Airspeed for 3S-RF-TSE at 20,000 Feet, Standard-Day Conditions.

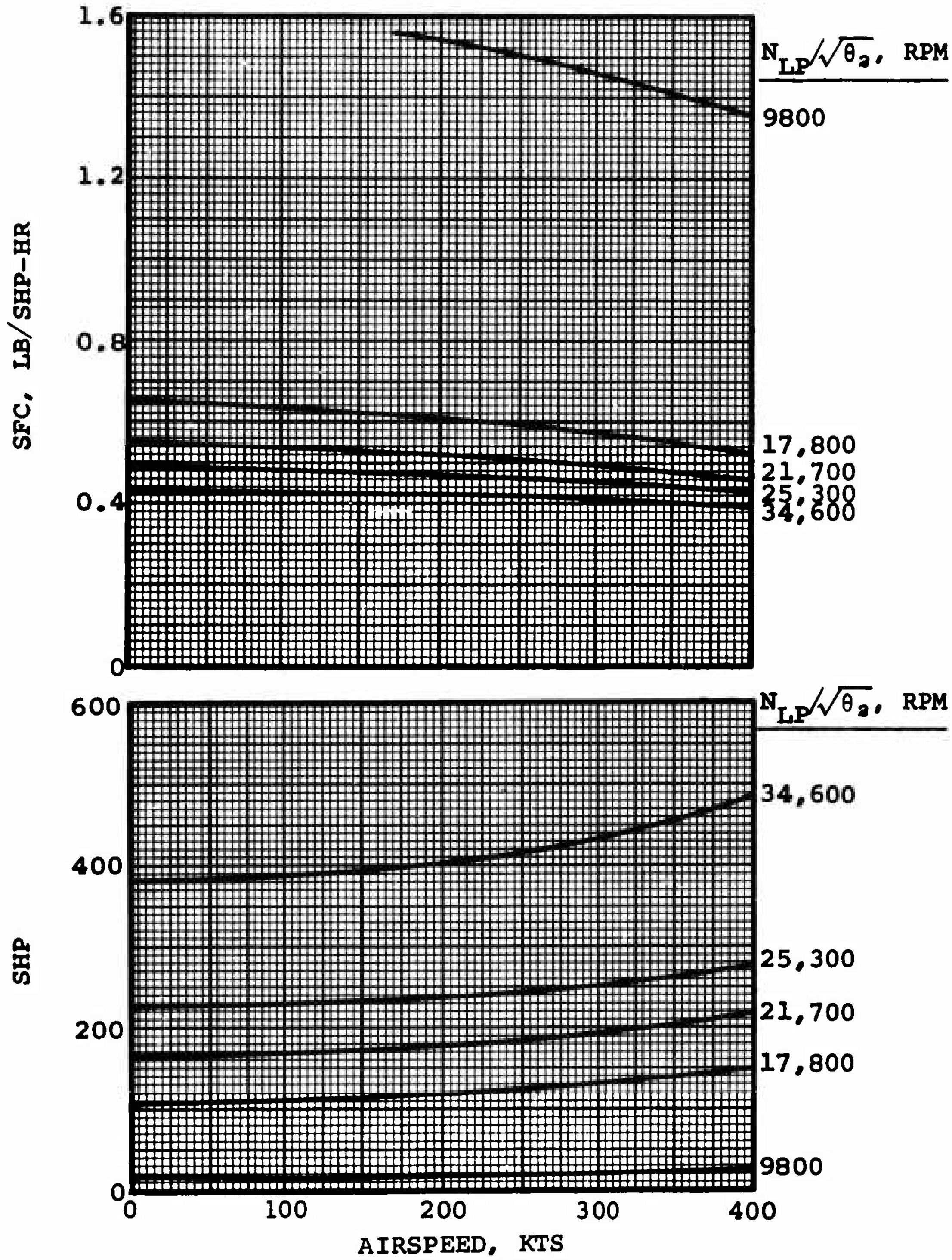

Figure 109. Shaft Horsepower and SFC Versus Airspeed for 3S-RF-TSE at 25,000 Feet, Standard-Day Conditions.

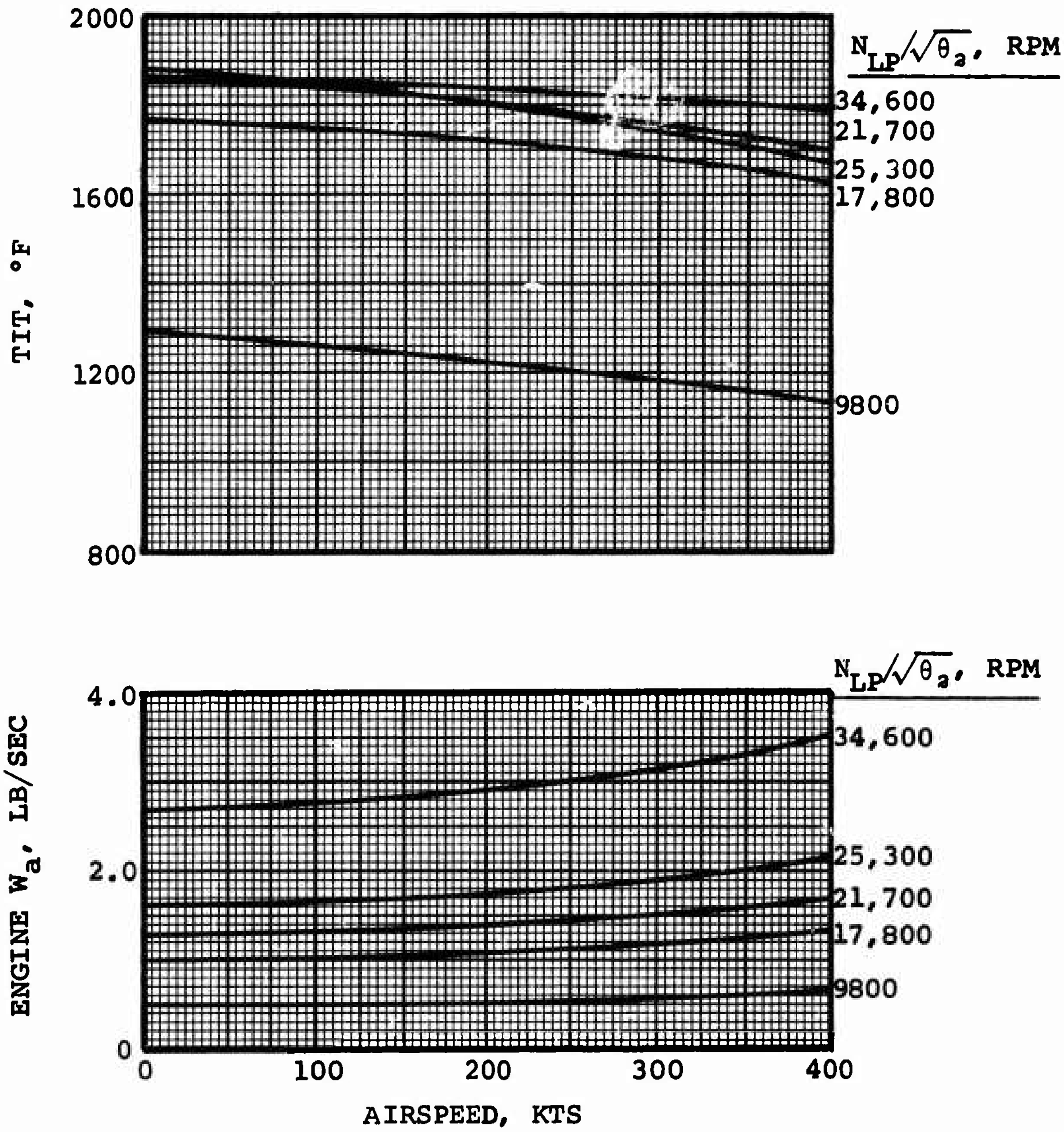

Figure 110. Engine Airflow and TIT Versus Airspeed for 3S-RF-TSE at 25,000 Feet, Standard-Day Conditions.

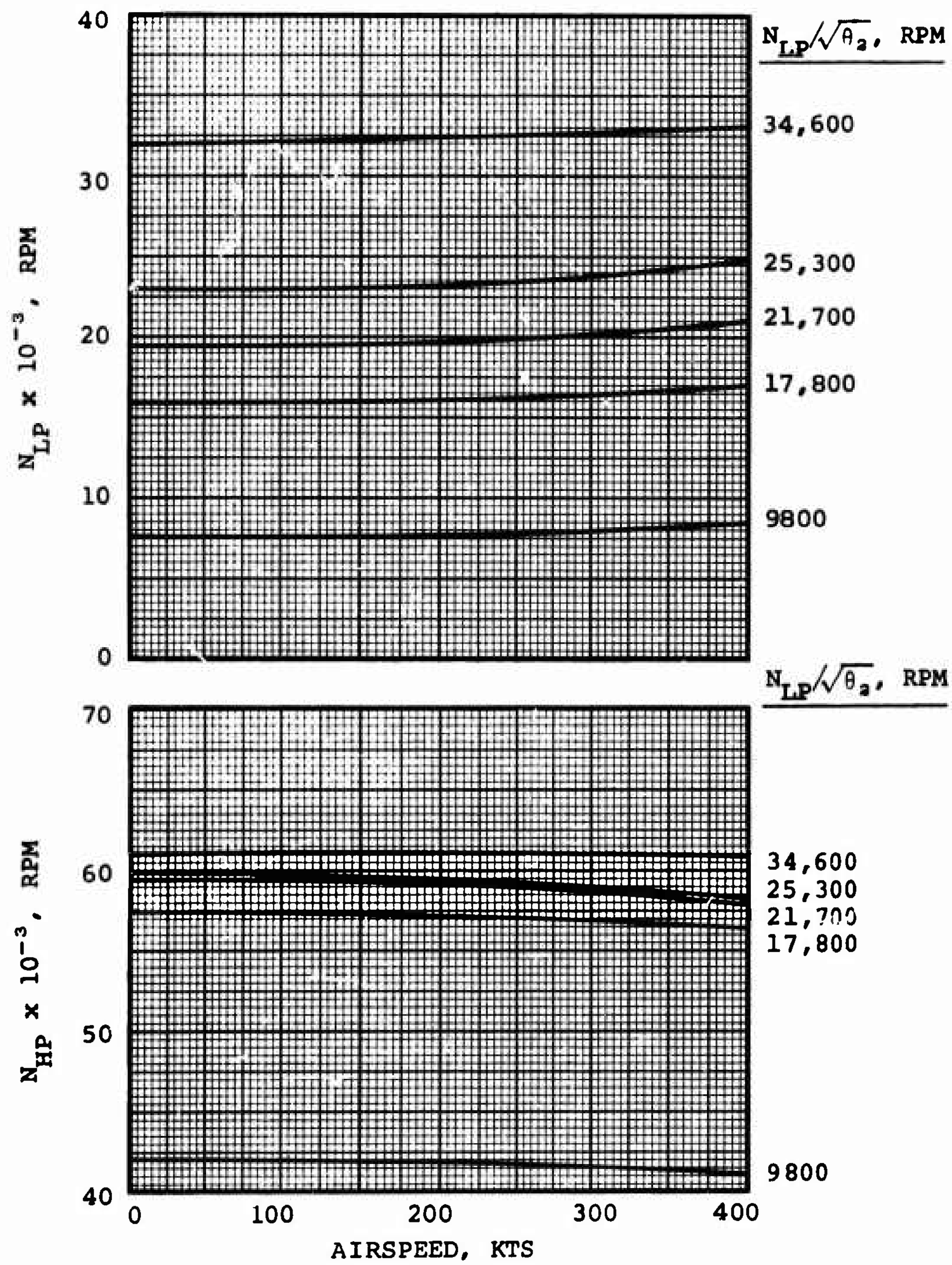

Figure 111. LP and HP Spool Speeds Versus Airspeed for 3S-RF-TSE at 25,000 Feet, Standard-Day Conditions.

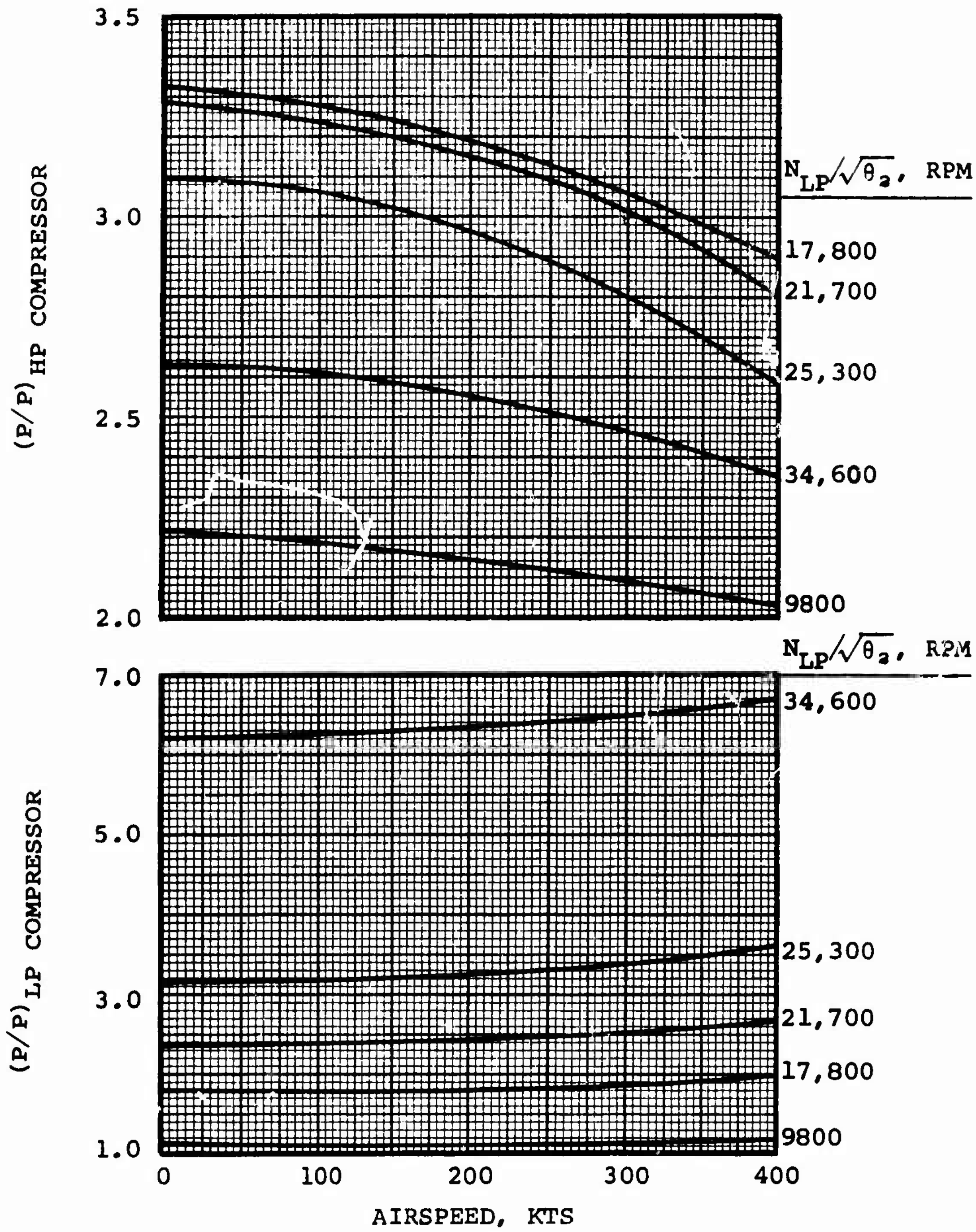

Figure 112. LP and HP Compressor P/P Versus Airspeed for 3S-RF-TSE at 25,000 Feet, Standard-Day Conditions.

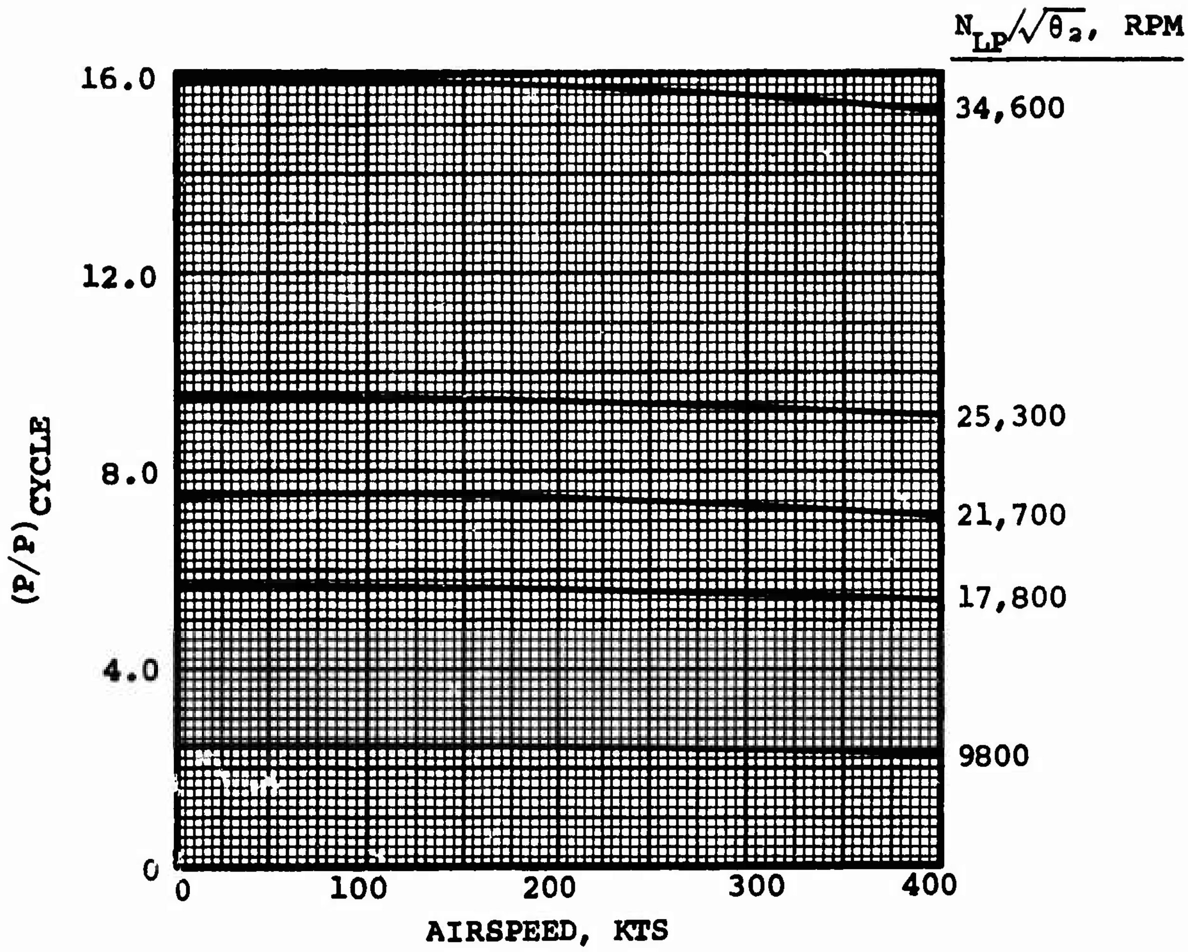

Figure 113. Cycle P/P Versus Airspeed for 3S-RF-TSE at 25,000 Feet, Standard-Day Conditions.

APPENDIX II
2S-TSE PERFORMANCE TABLE AND C''RVES

TABLE XV. 2S-TSE PERFORMANCE DATA AT 6000-FEET, 95°F, MRP

Parameter	Value
TIT	2400°F
W_a	4.804 lb/sec
Cycle P/P	14.80
W_f	393.6 lb/hr
N_{gg}	40,833 rpm
SHP	833.2 hp
SFC	0.473 lb/HP-HR

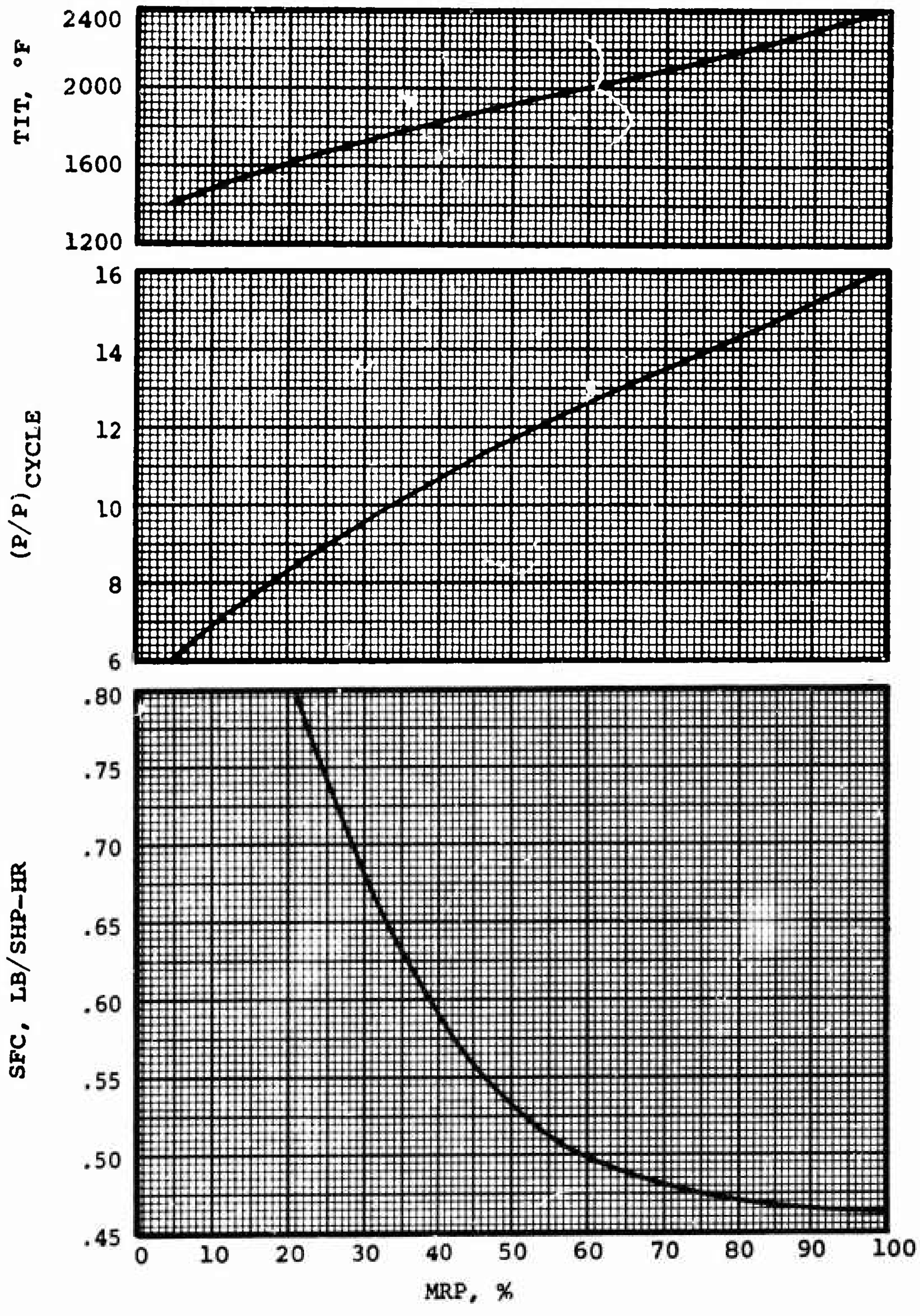

Figure 114. TIT, P/P, and SFC Versus Percent MRP for 2S-TSE at Sea-Level, Static, Standard-Day Conditions.

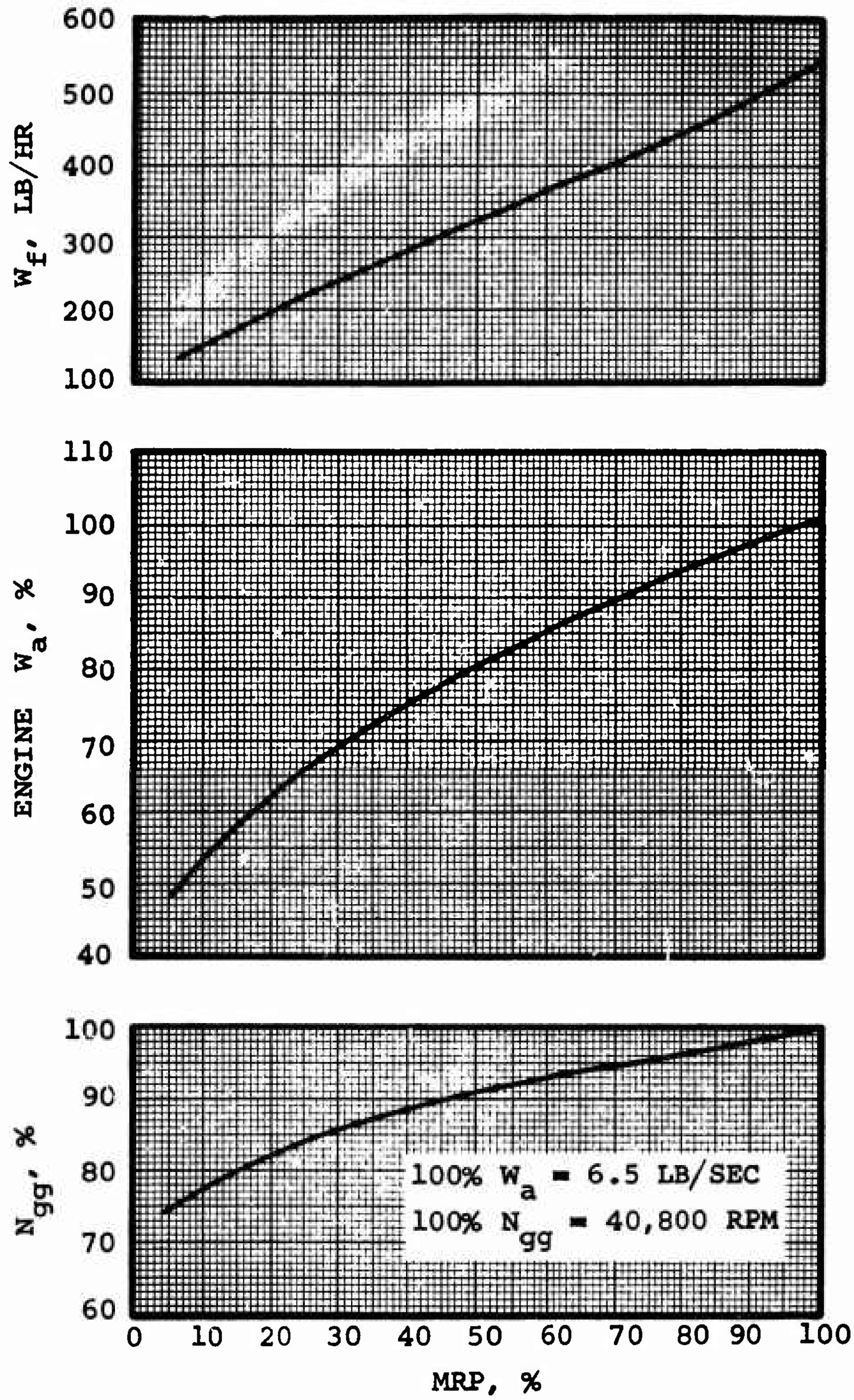

Figure 115. Fuel Flow, Airflow, and Gas Generator Speed Versus Percent MRP for 2S-TSE at Sea-Level, Static, Standard-Day Conditions.

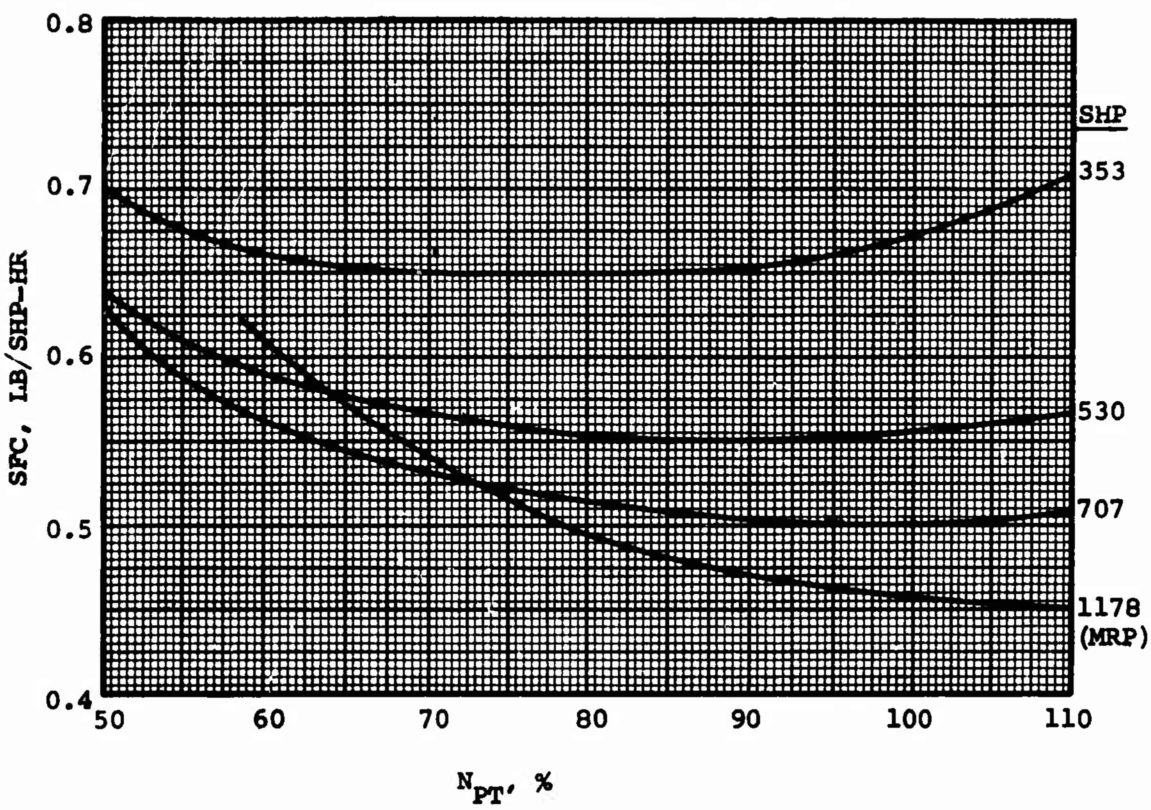

Figure 116. SFC Versus Percent Power Turbine Speed for 2S-TSE at Sea-Level, Static, Standard-Day Conditions.

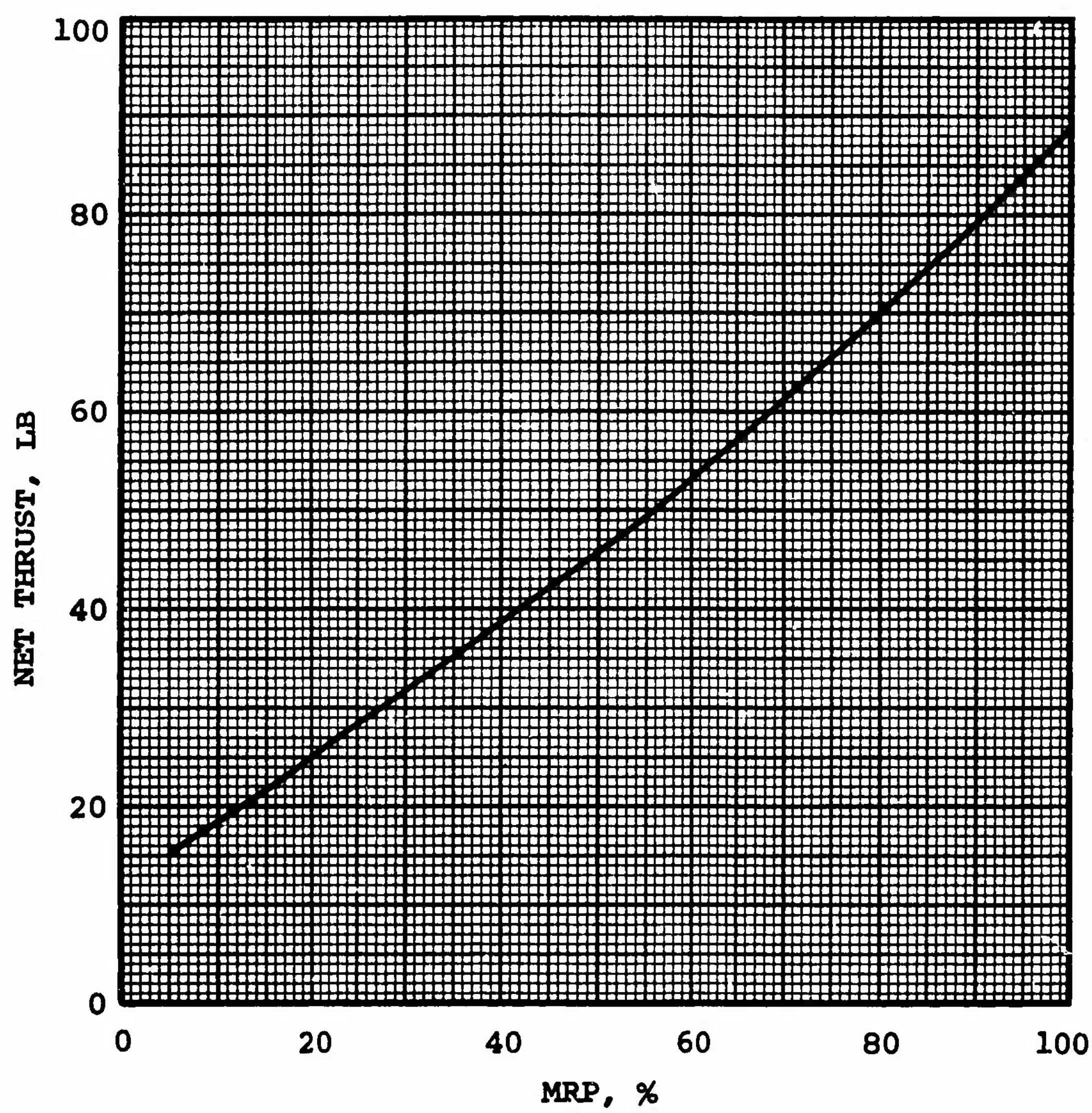

Figure 117. Net thrust Versus Percent MRP for 2S-TSE at Sea-Level, Static, Standard-Day Conditions.

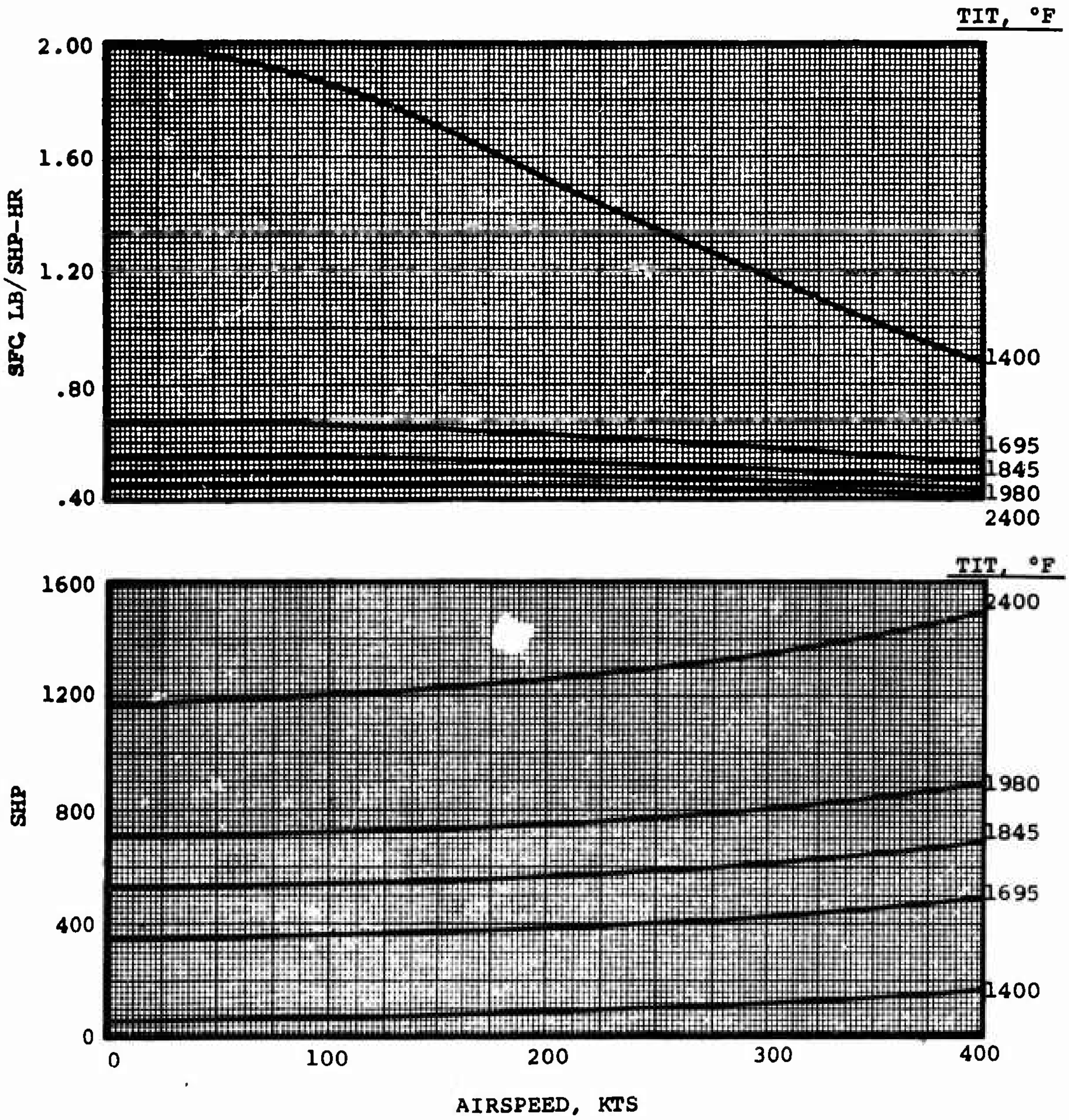

Figure 118. Shaft Horsepower and SFC Versus Airspeed for 2S-TSE at Sea-Level, Standard-Day Conditions.

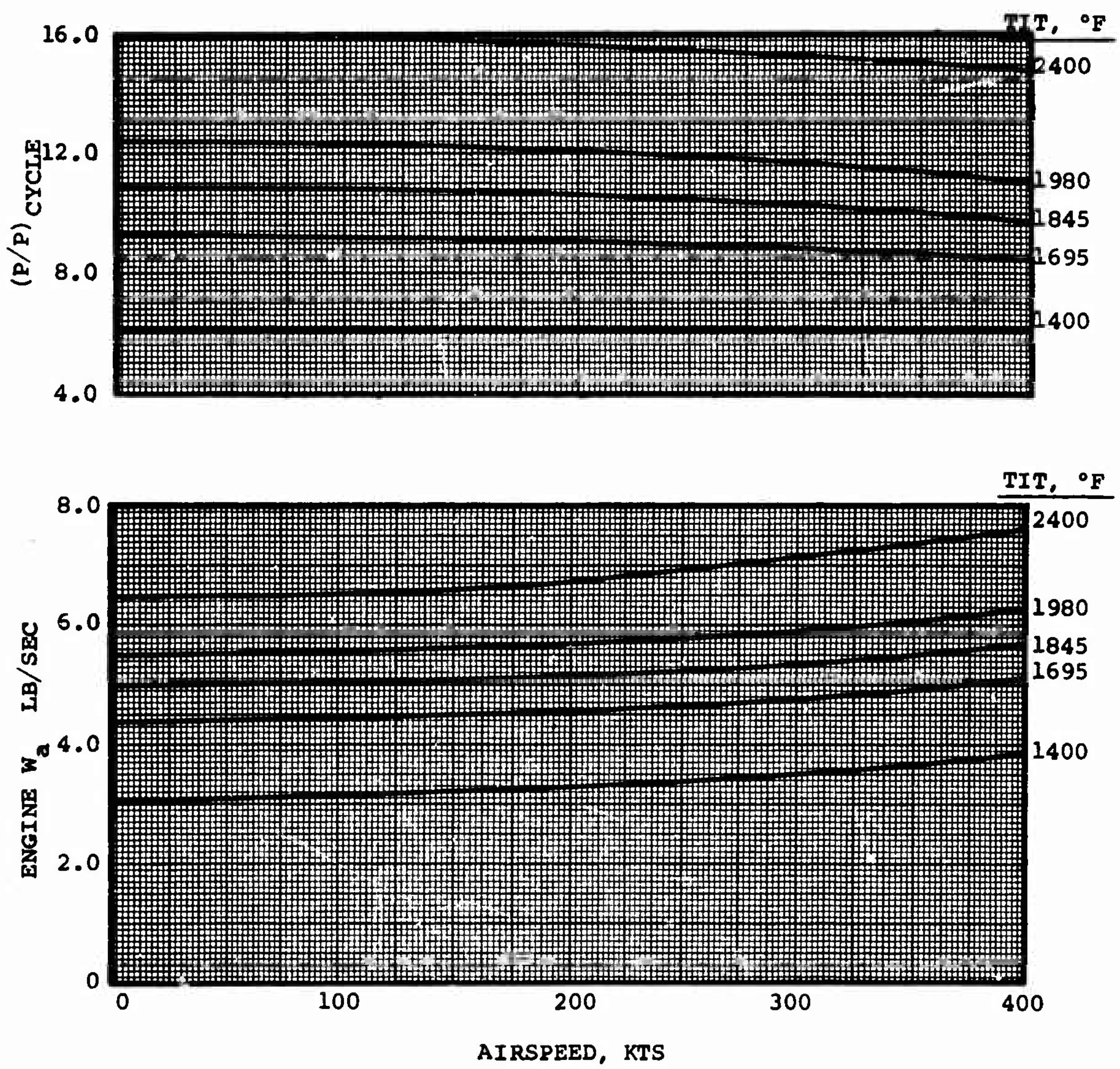

Figure 119. Engine Airflow and Cycle P/P Versus Airspeed for 2S-TSE at Sea-Level, Standard-Day Conditions.

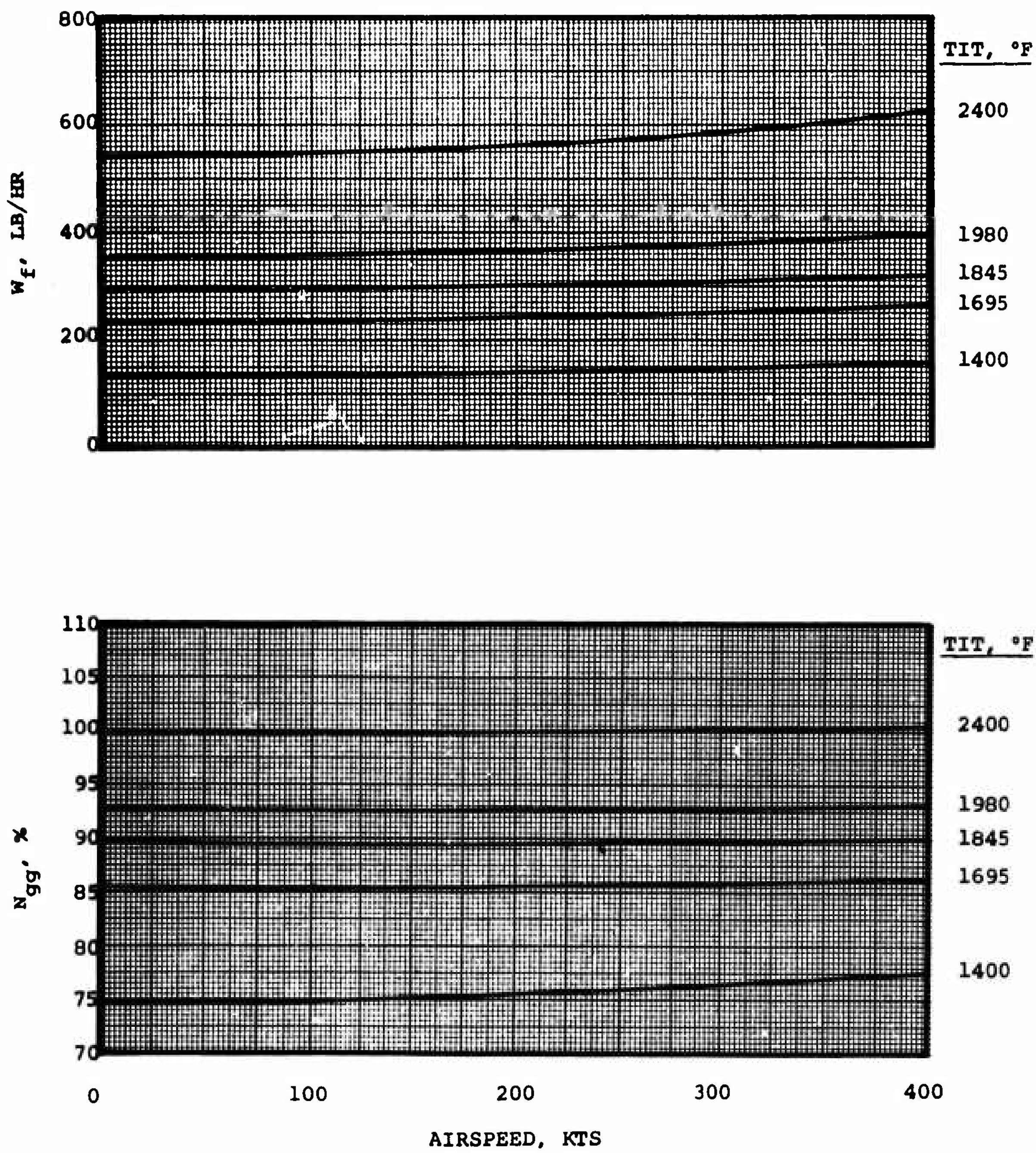

Figure 120. Gas Generator Speed and Fuel Flow Versus Airspeed for 2S-TSE at Sea-Level, Standard-Day Conditions.

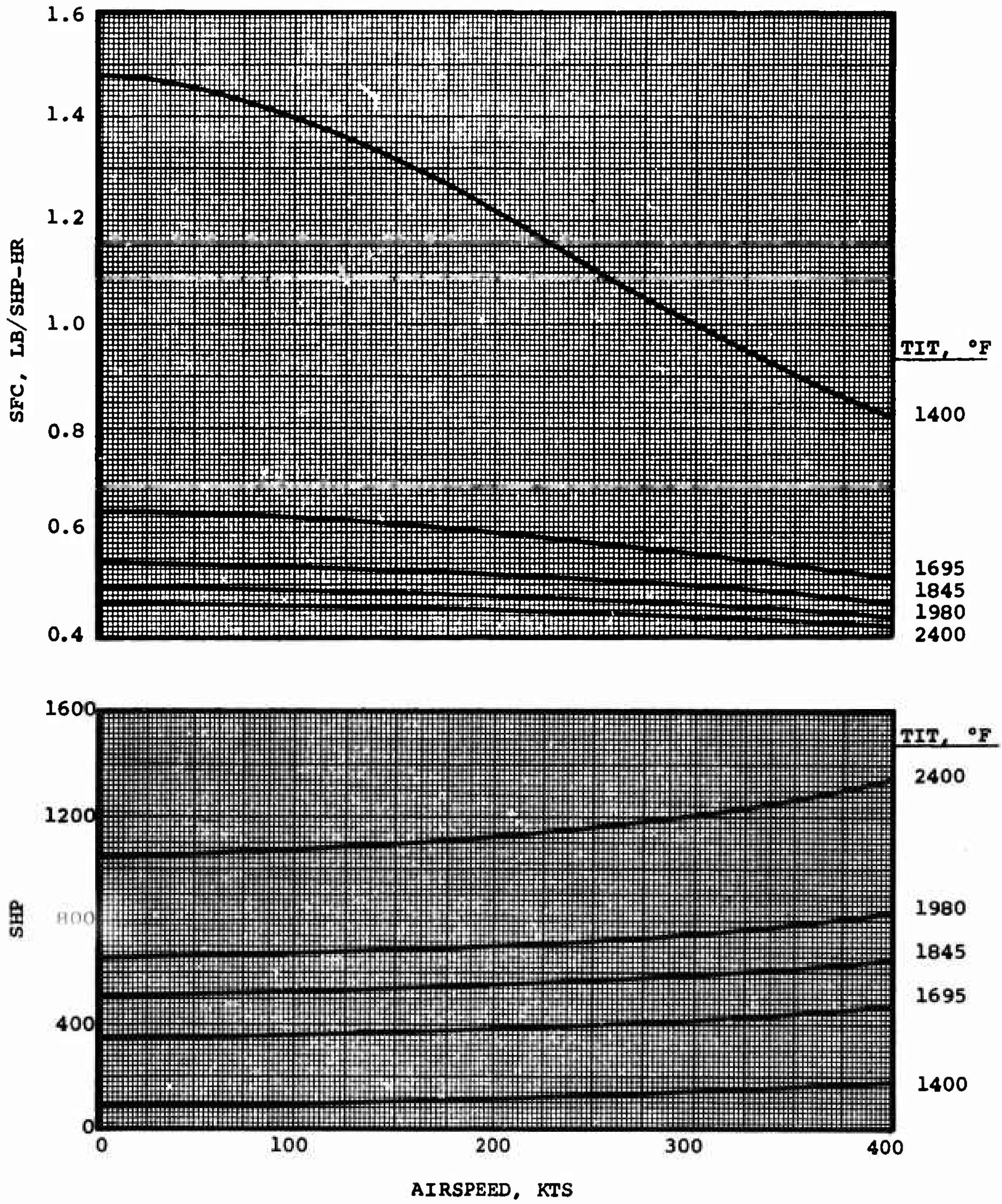

Figure 121. Shaft Horsepower and SFC Versus Airspeed for 2S-TSE at 4000 Feet, Standard-Day Conditions.

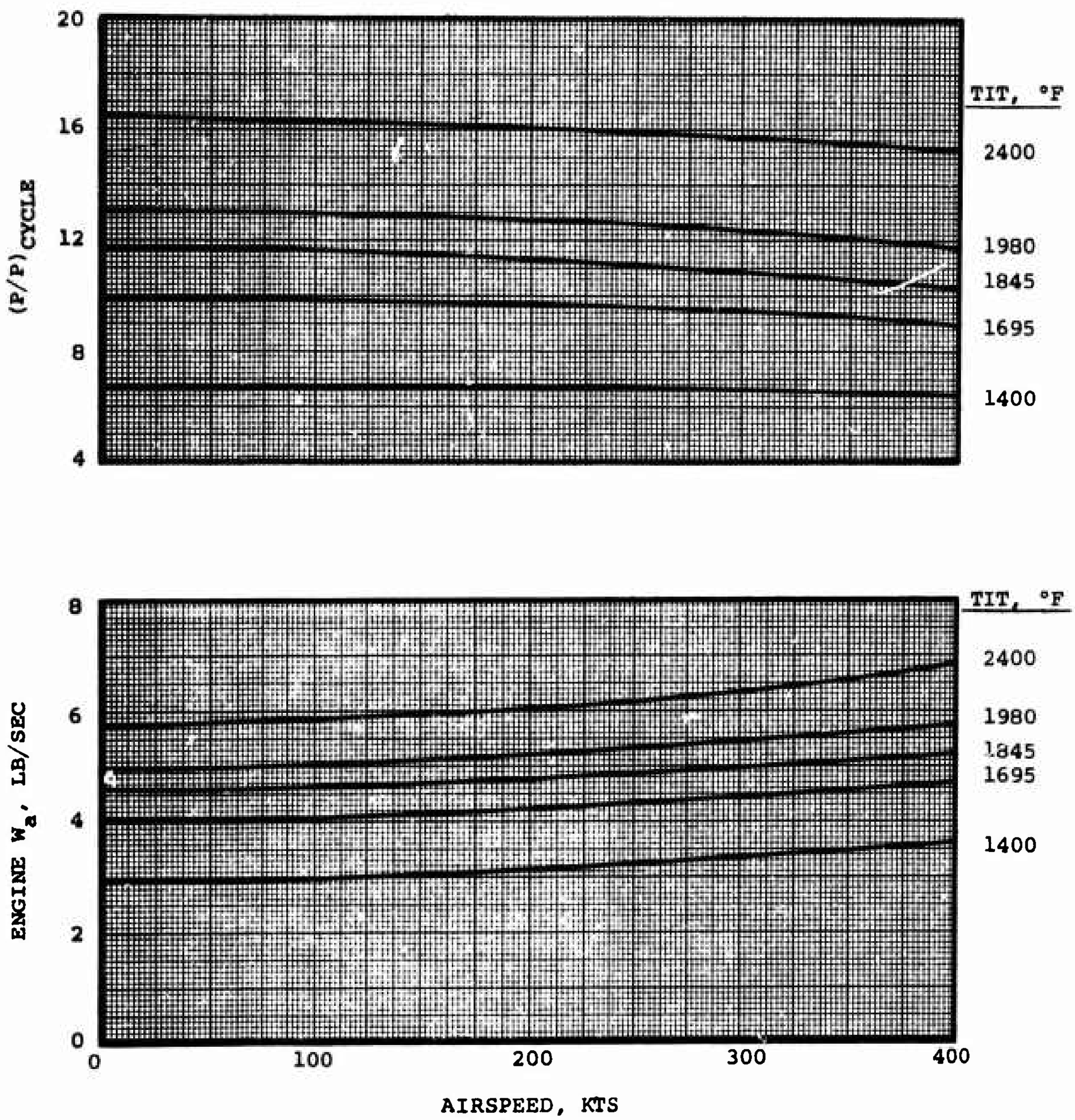

Figure 122. Airflow and Cycle P/P Versus Airspeed for 2S-TSE at 4000 Feet, Standard-Day Conditions.

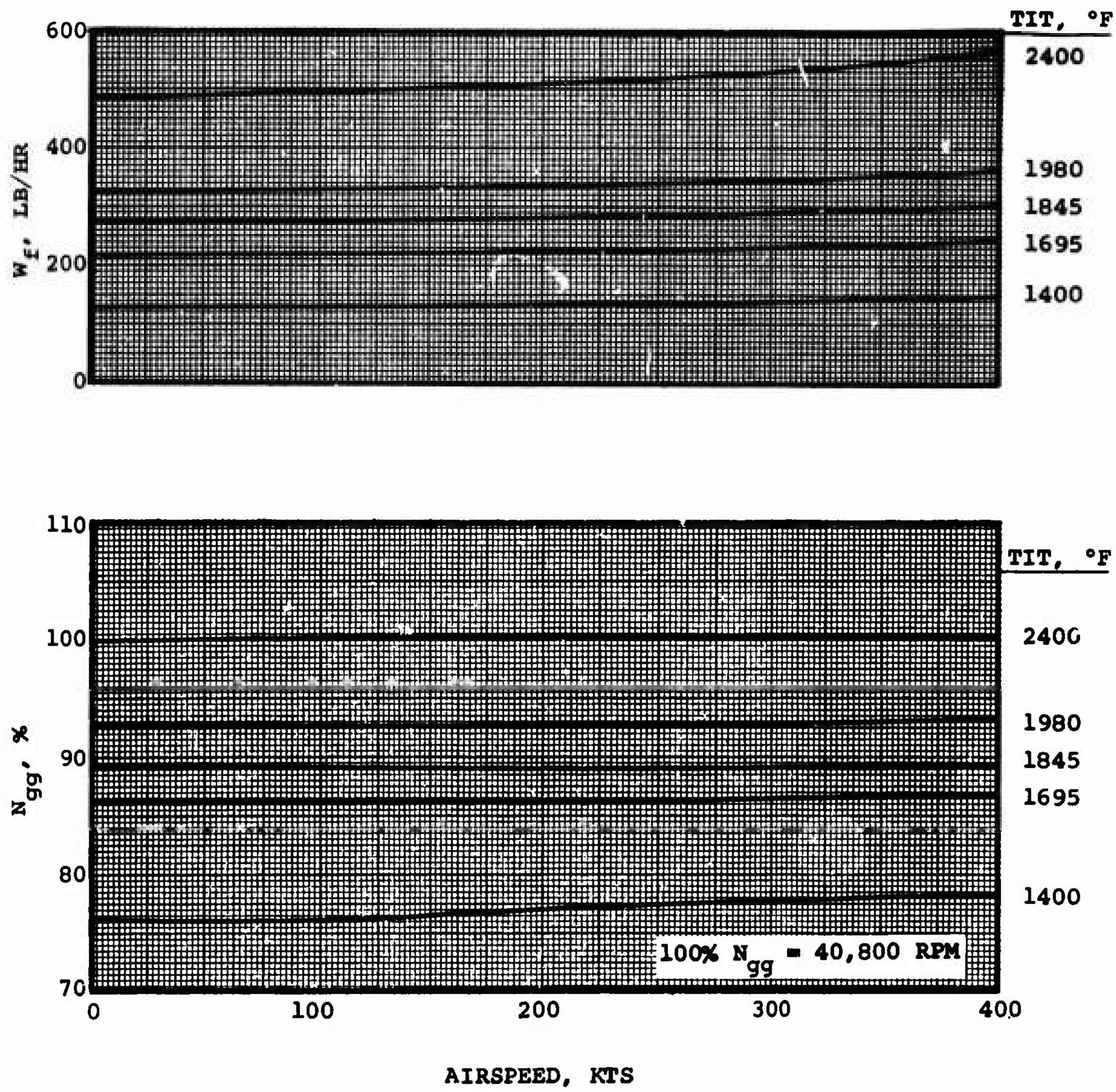

Figure 123. Gas Generator Speed and Fuel Flow Versus Airspeed for 2S-TSE at 4000 feet, Standard-Day Conditions.

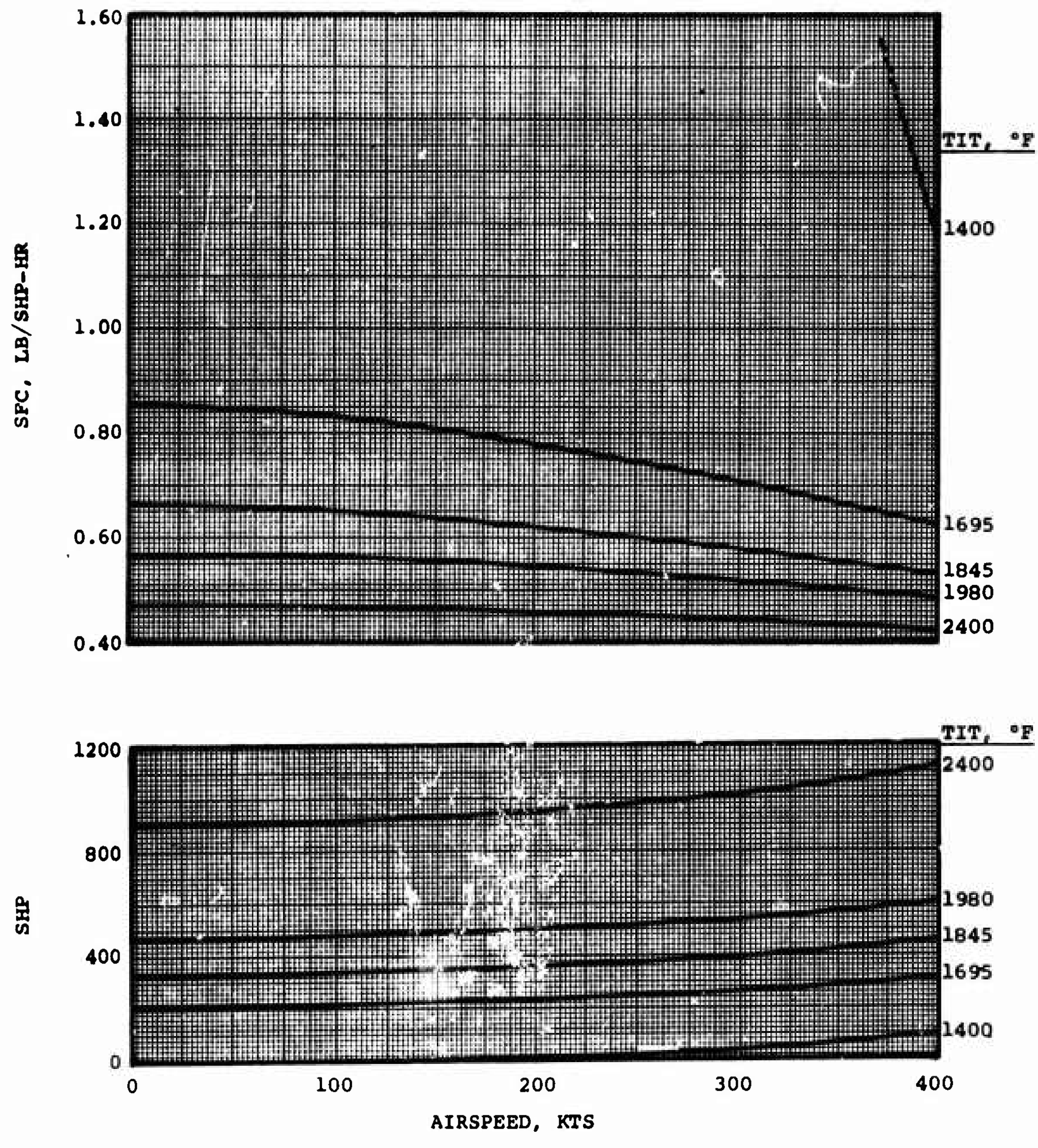

Figure 124. Shaft Horsepower and SFC Versus Airspeed for 2S-TSE at 4000 Feet, 95°F-Day Conditions.

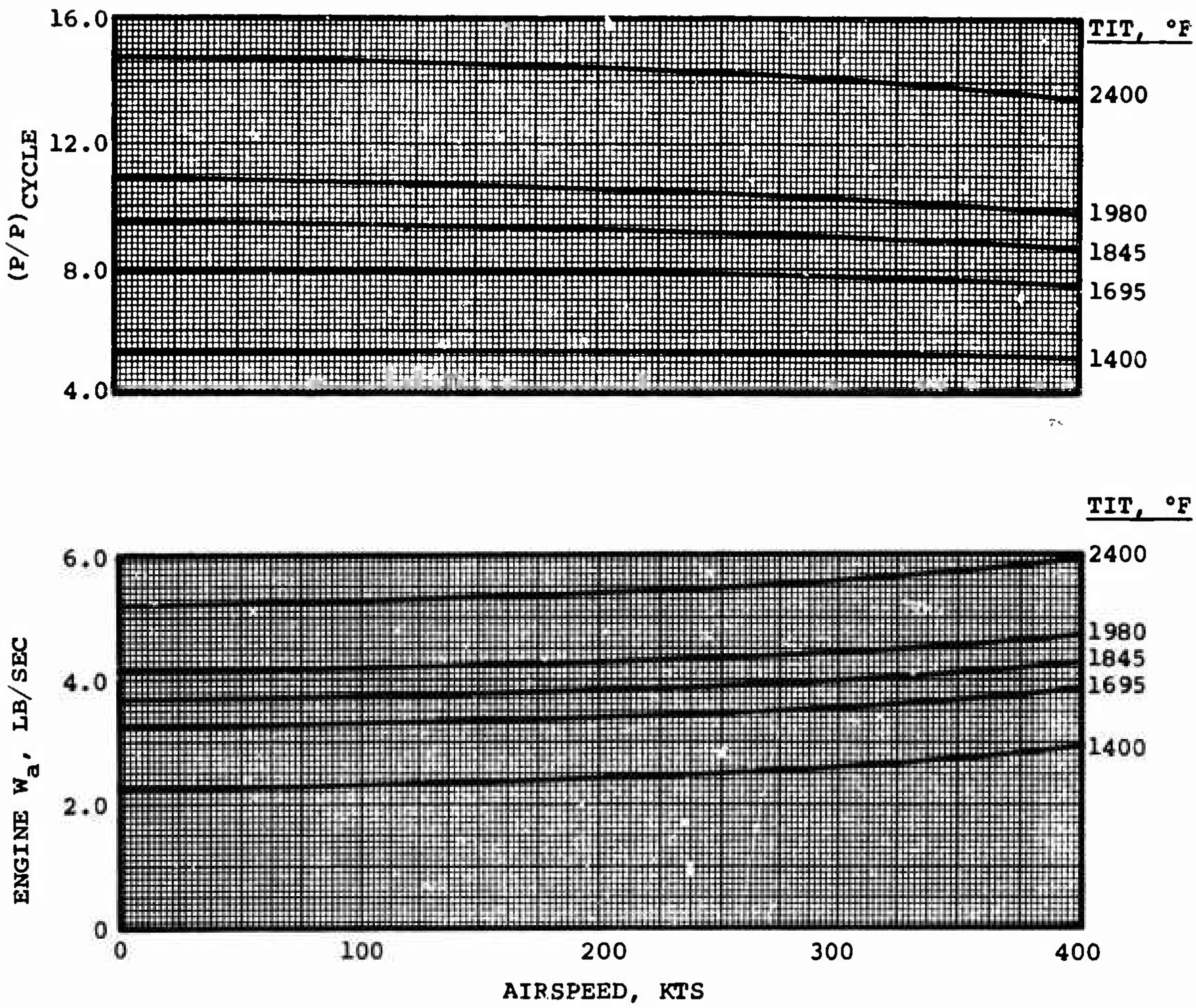

Figure 125. Engine Airflow and Cycle P/P Versus Airspeed for 2S-TSE at 4000 Feet, 95°F-Day Conditions.

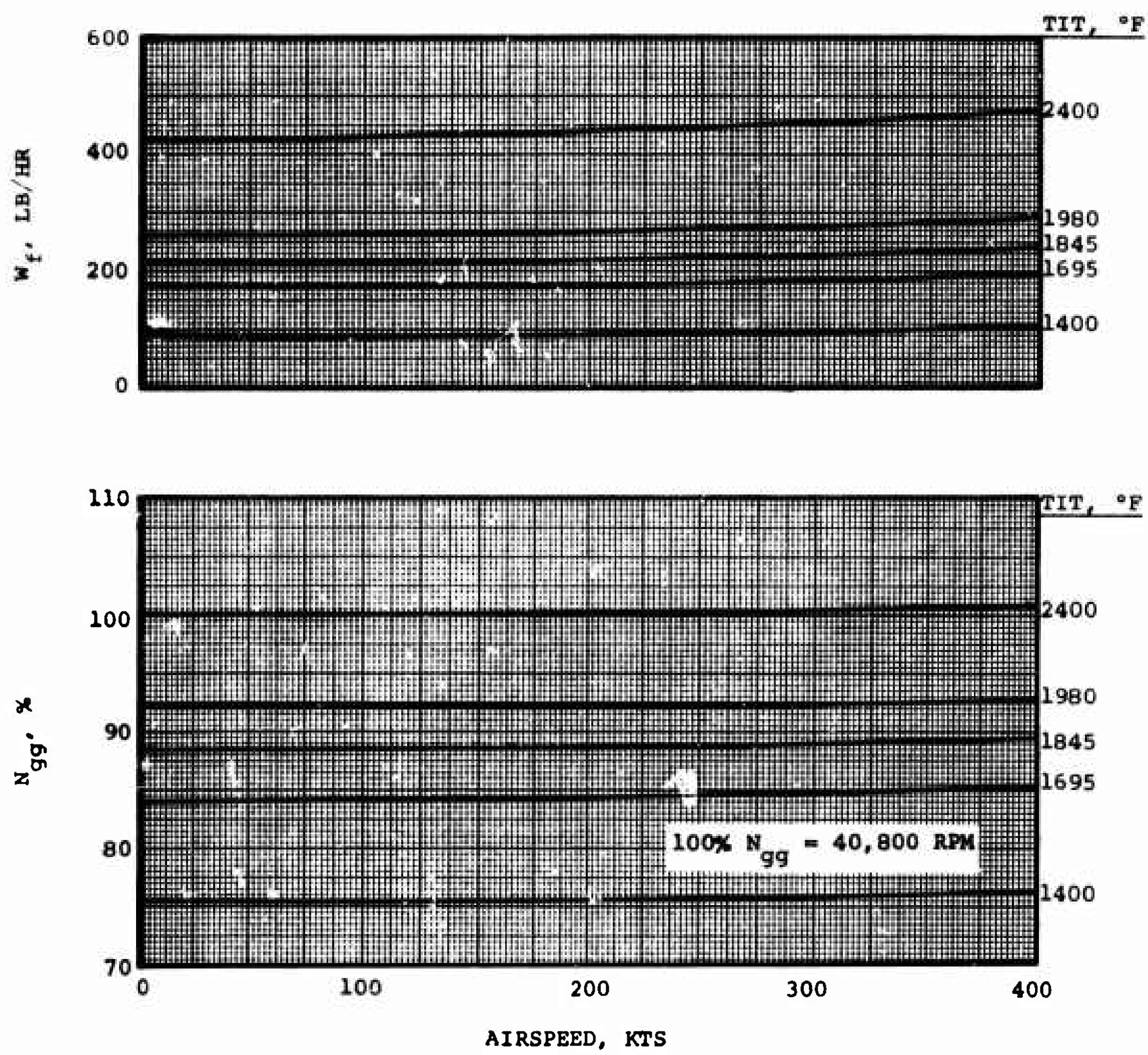

Figure 126. Gas Generator Speed and Fuel Flow Versus Airspeed for 2S-TSE at 4000 Feet, 95°F-Day Conditions.

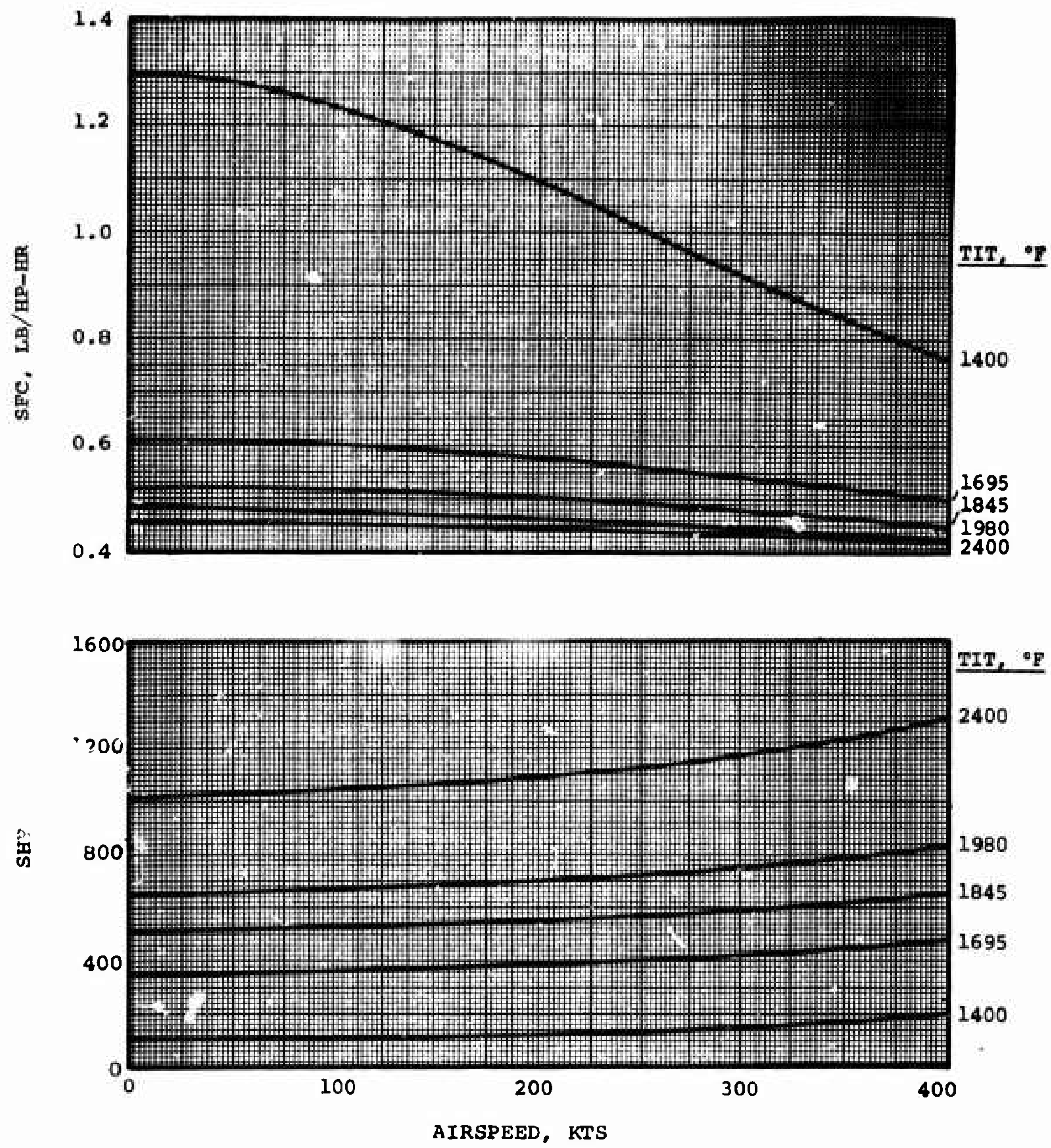

Figure 127. Shaft Horsepower and SFC Versus Airspeed for 2S-TSE at 6000 Feet, Standard-Day Conditions.

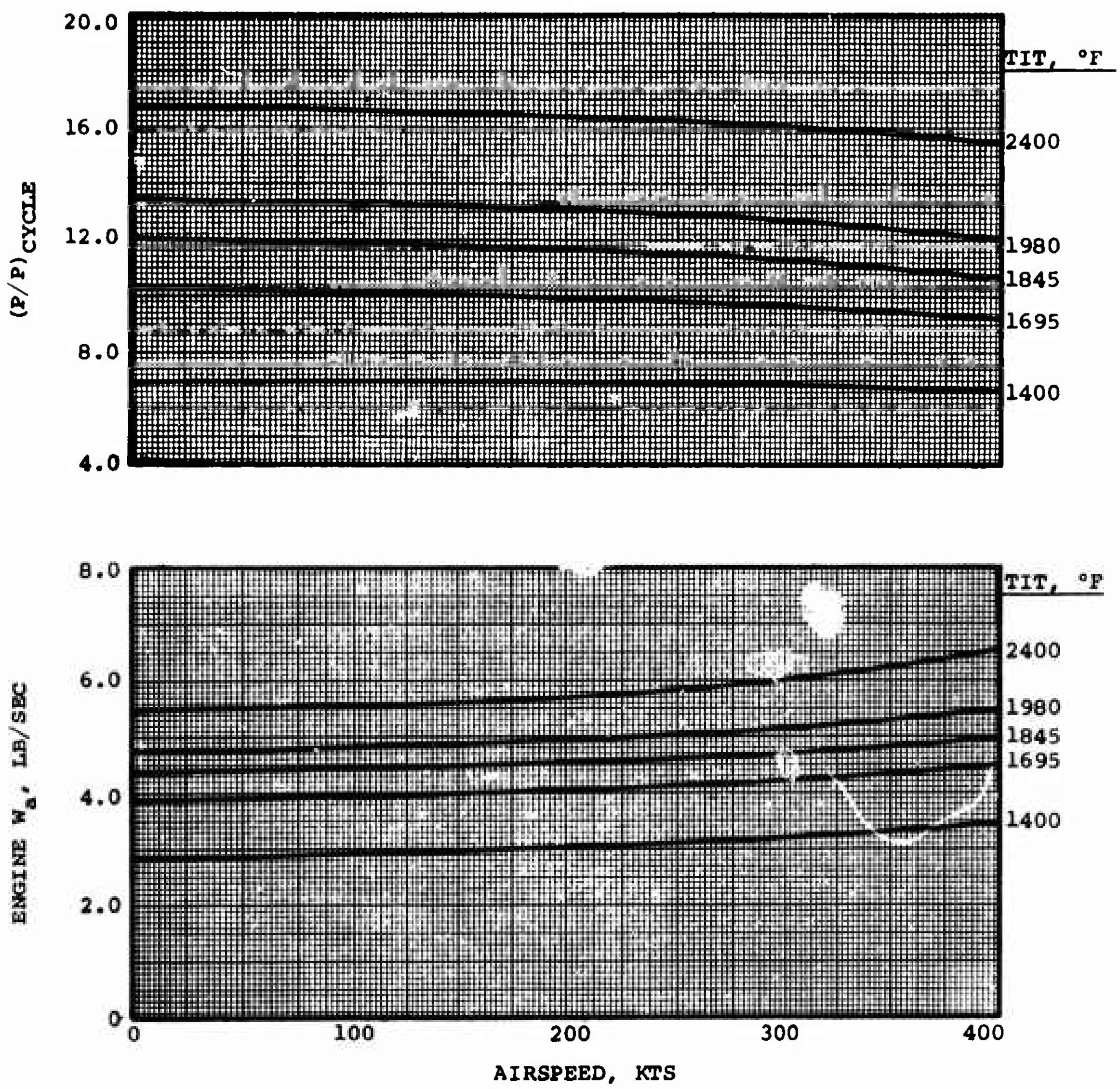

Figure 128. Engine Airflow and Cycle P/P Versus Airspeed for 2S-TSE at 6000 Feet, Standard-Day Conditions.

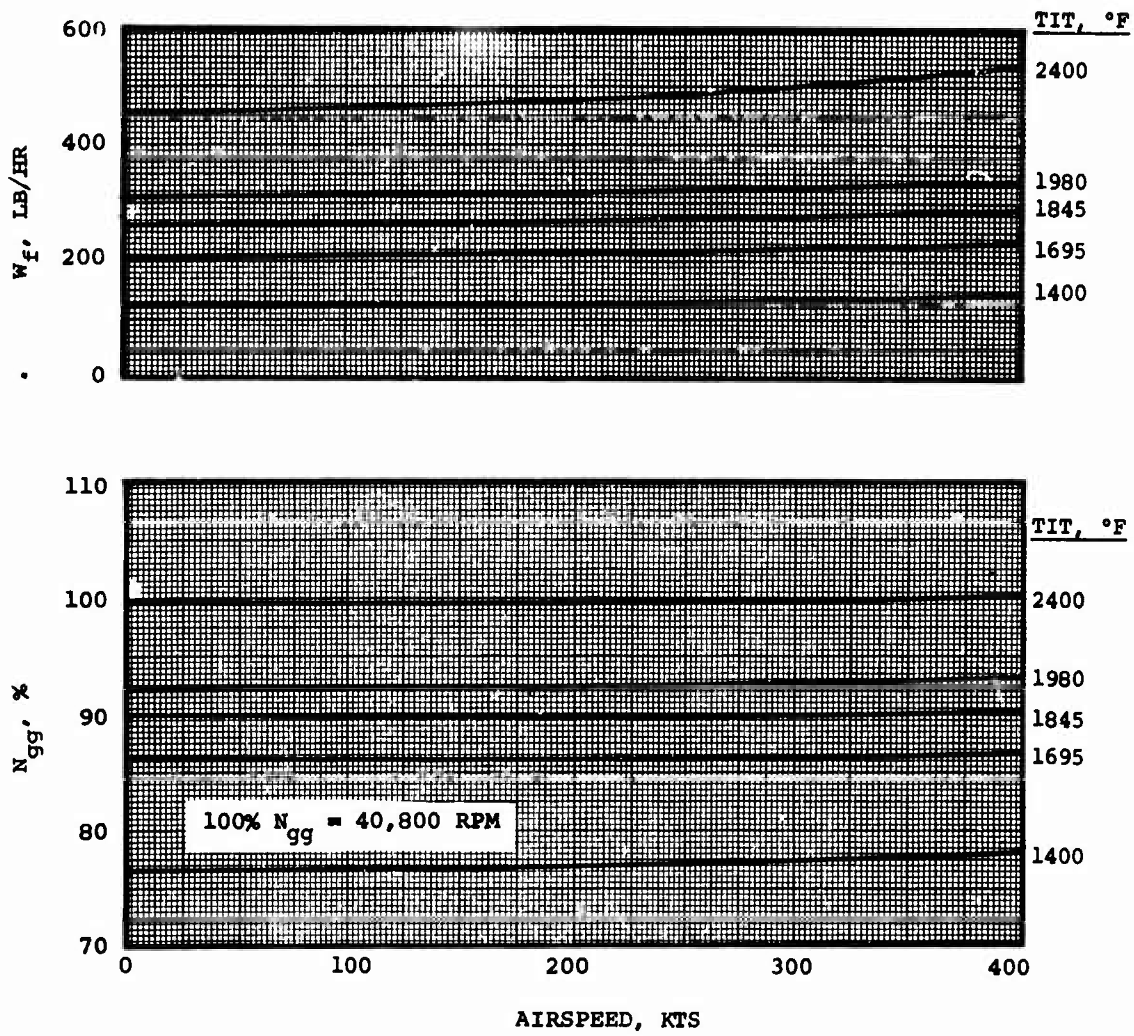

Figure 129. Gas Generator Speed and Fuel Flow Versus Airspeed for 2S-TSE at 6000 Feet, Standard-Day Conditions.

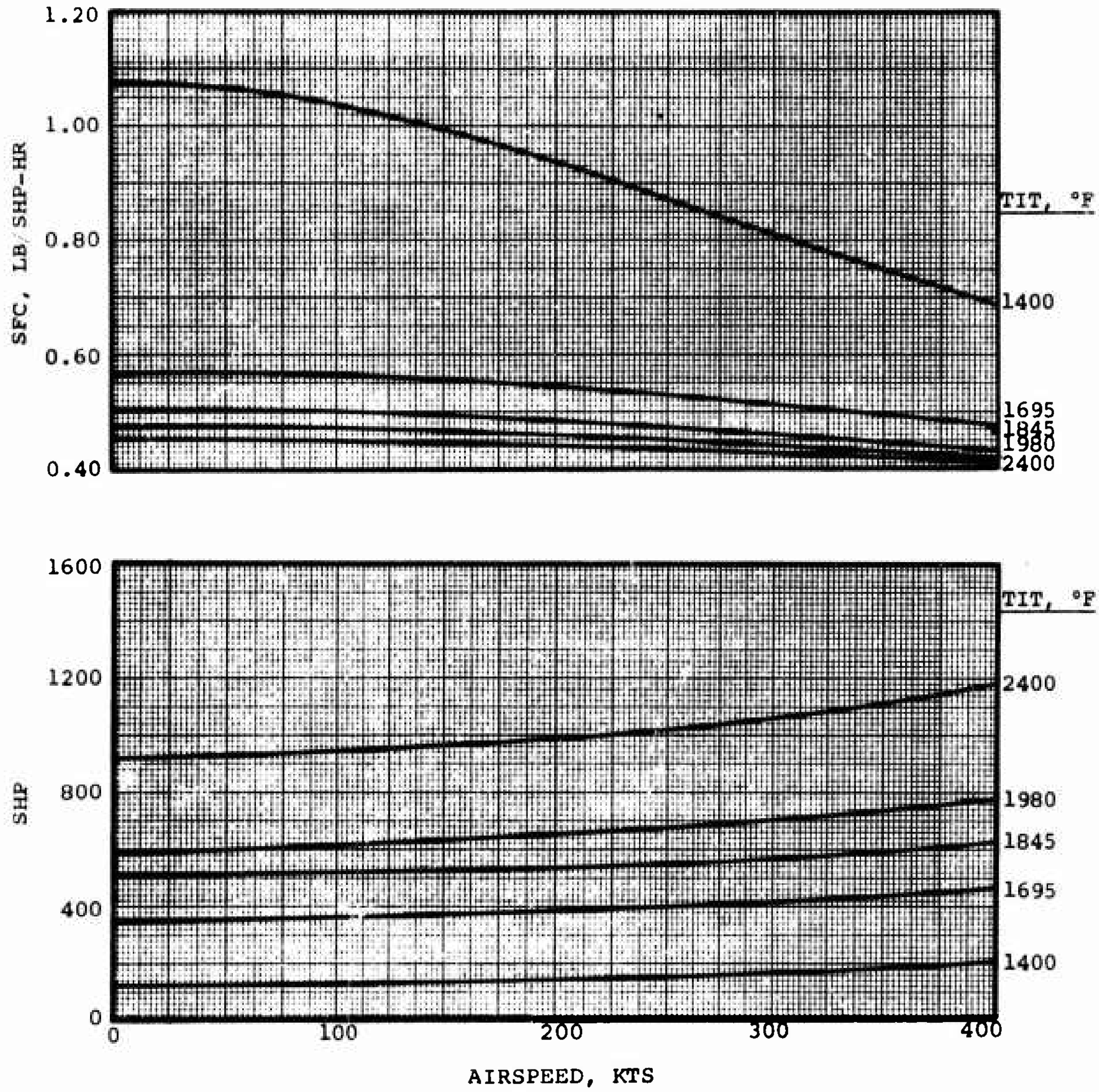

Figure 130. Shaft Horsepower and SFC Versus Airspeed for 2S-TSE at 10,000 Feet, Standard-Day Conditions.

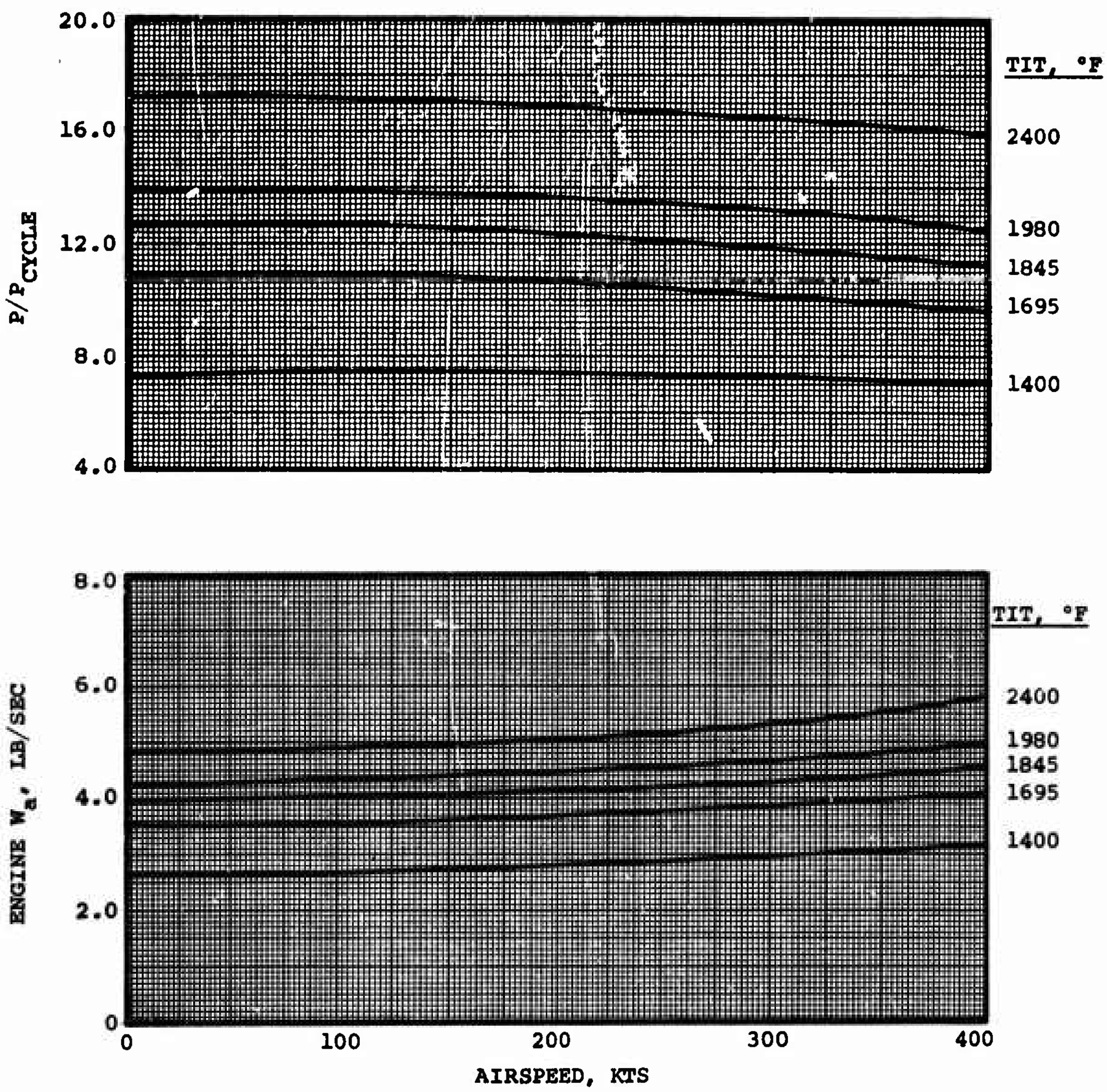

Figure 131. Engine Airflow and Cycle P/P Versus Airspeed for 2S-TSE at 10,000 Feet, Standard-Day Conditions.

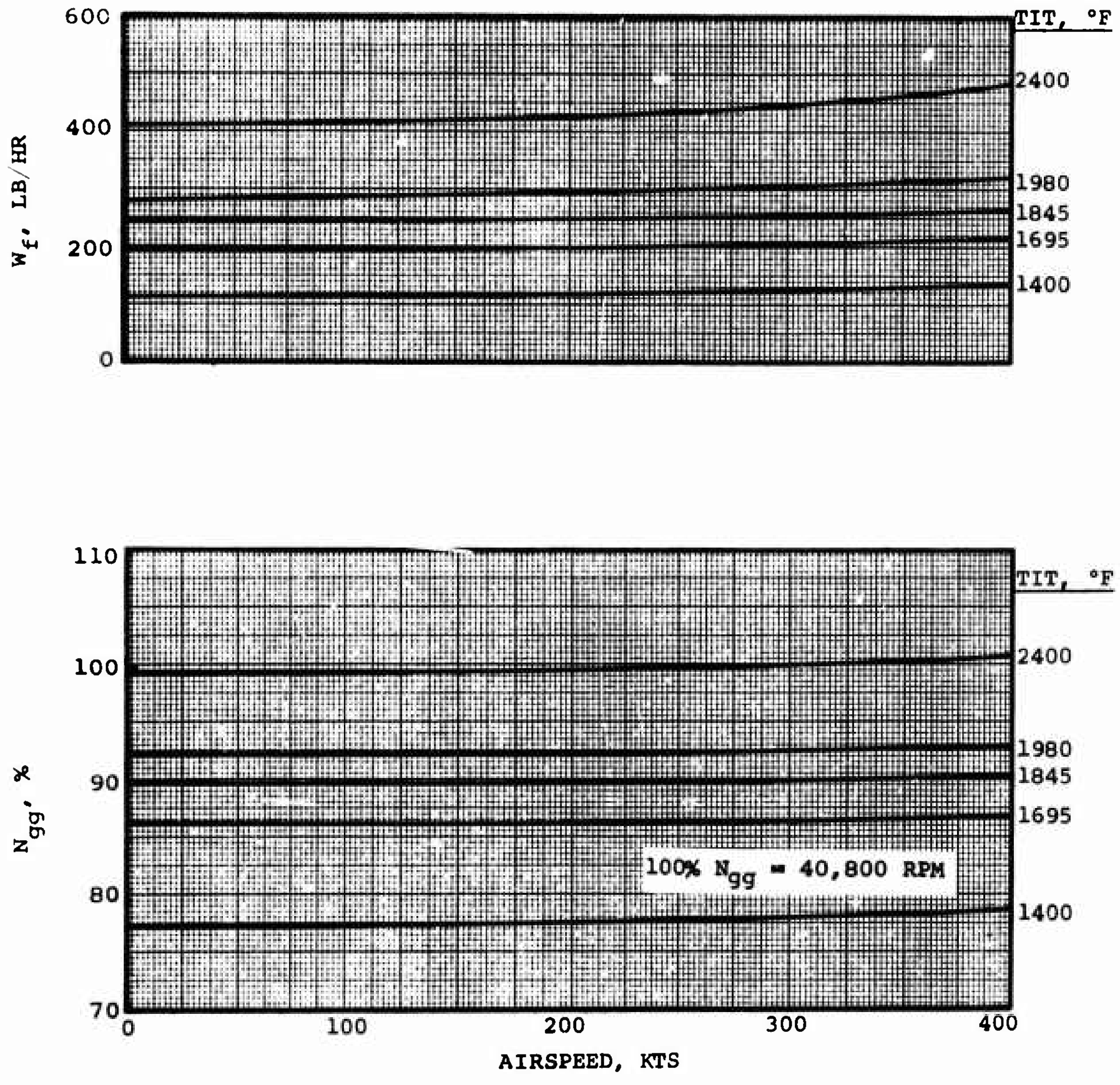

Figure 132. Gas Generator Speed and Fuel Flow Versus Airspeed for 2S-TSE at 10,000 Feet, Standard-Day Conditions.

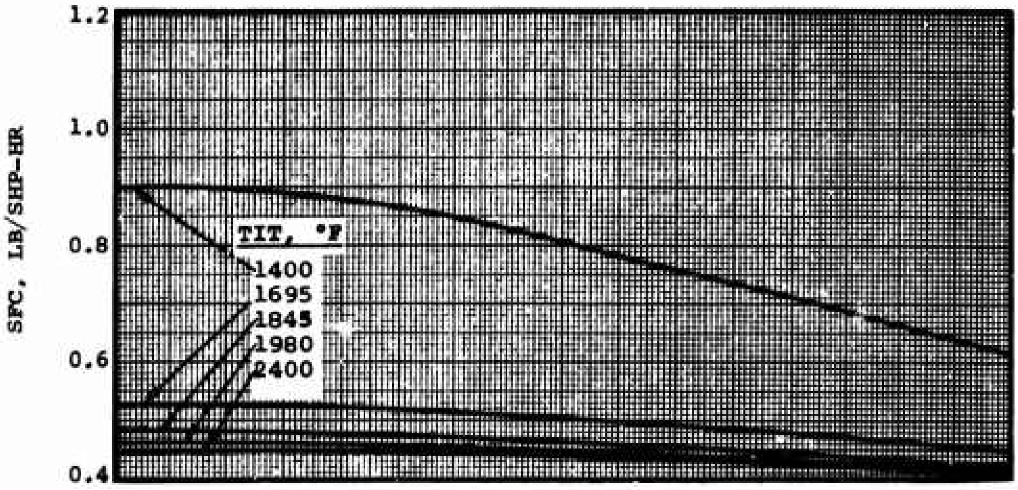

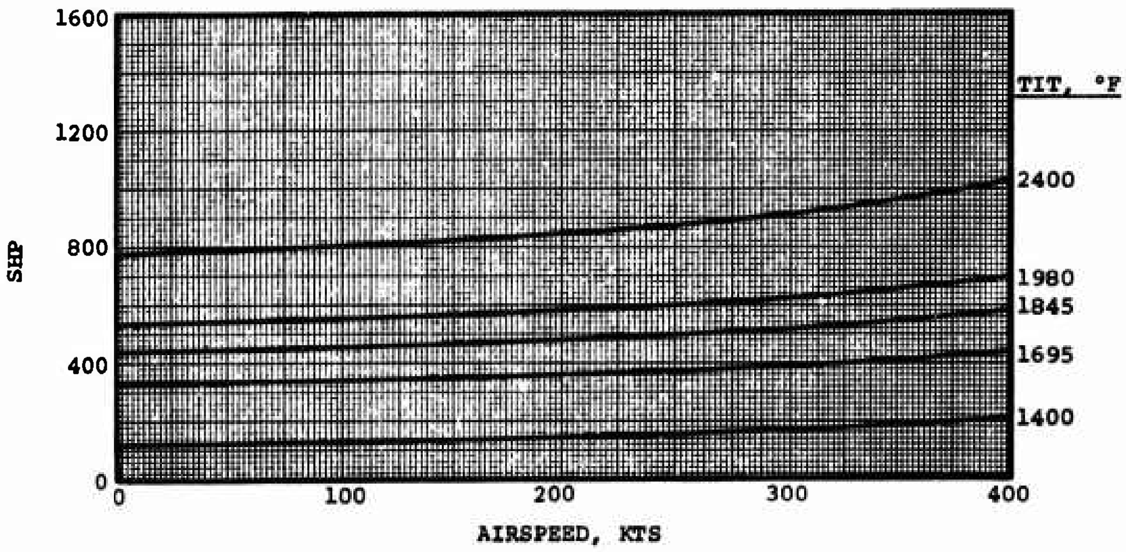

Figure 133. Shaft Horsepower and SFC Versus Airspeed for 2S-TSE at 15,000 Feet, Standard-Day Conditions.

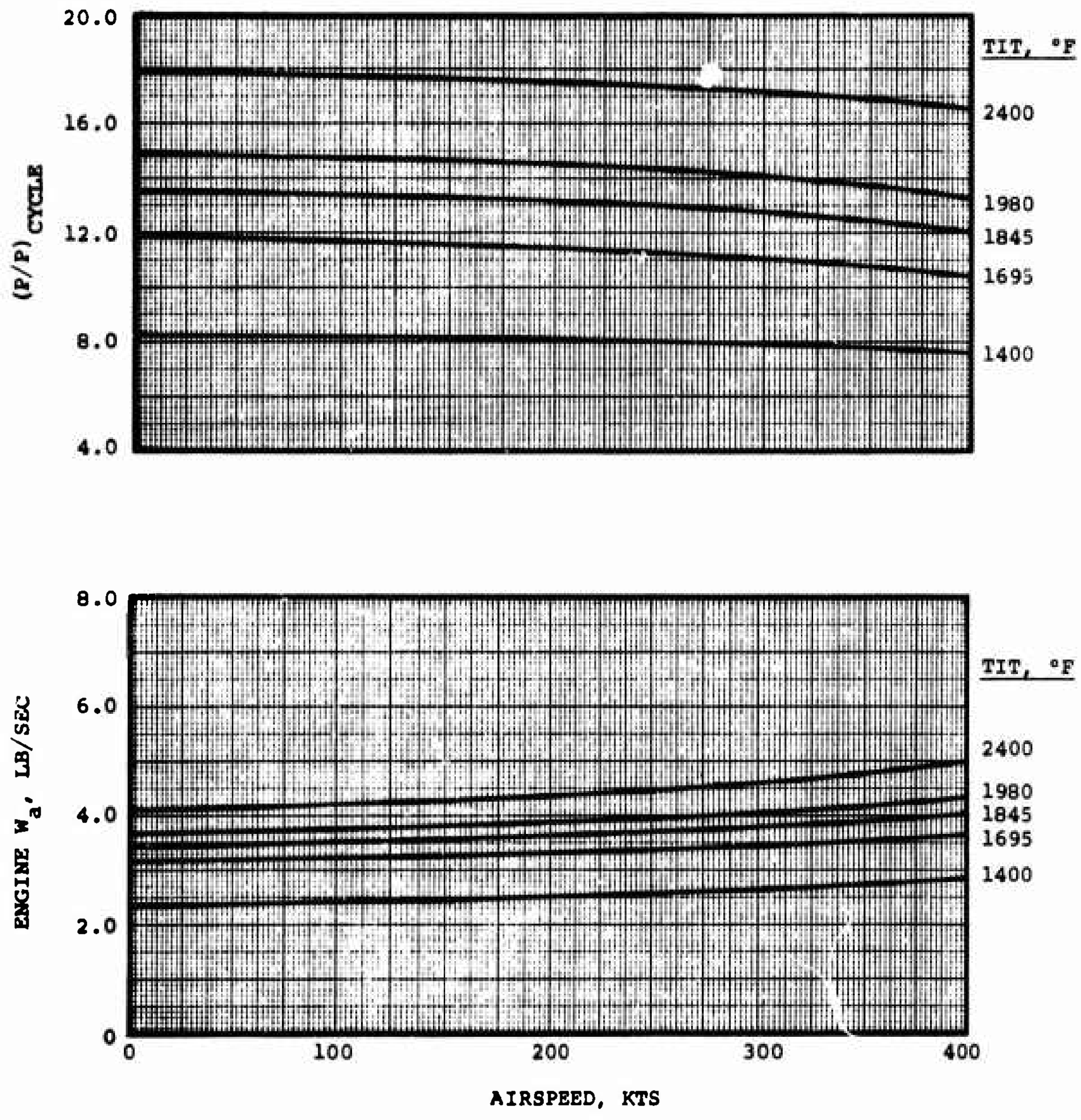

Figure 134. Engine Airflow and Cycle P/P Versus Airspeed for 2S-TSE at 15,000 Feet, Standard-Day Conditions.

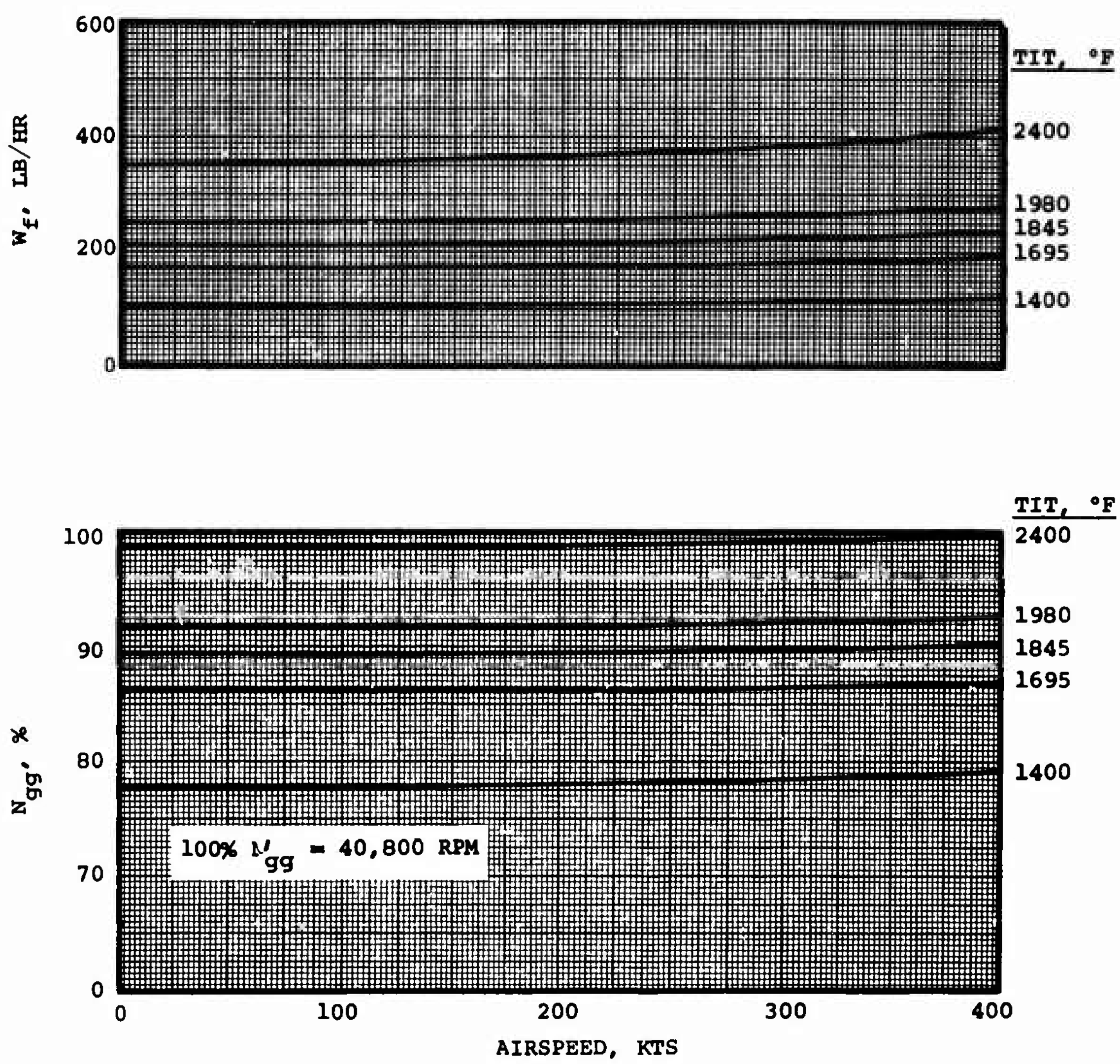

Figure 135. Gas Generator Speed and Fuel Flow Versus Airspeed for 2S-TSE at 15,000 Feet, Standard-Day Conditions.

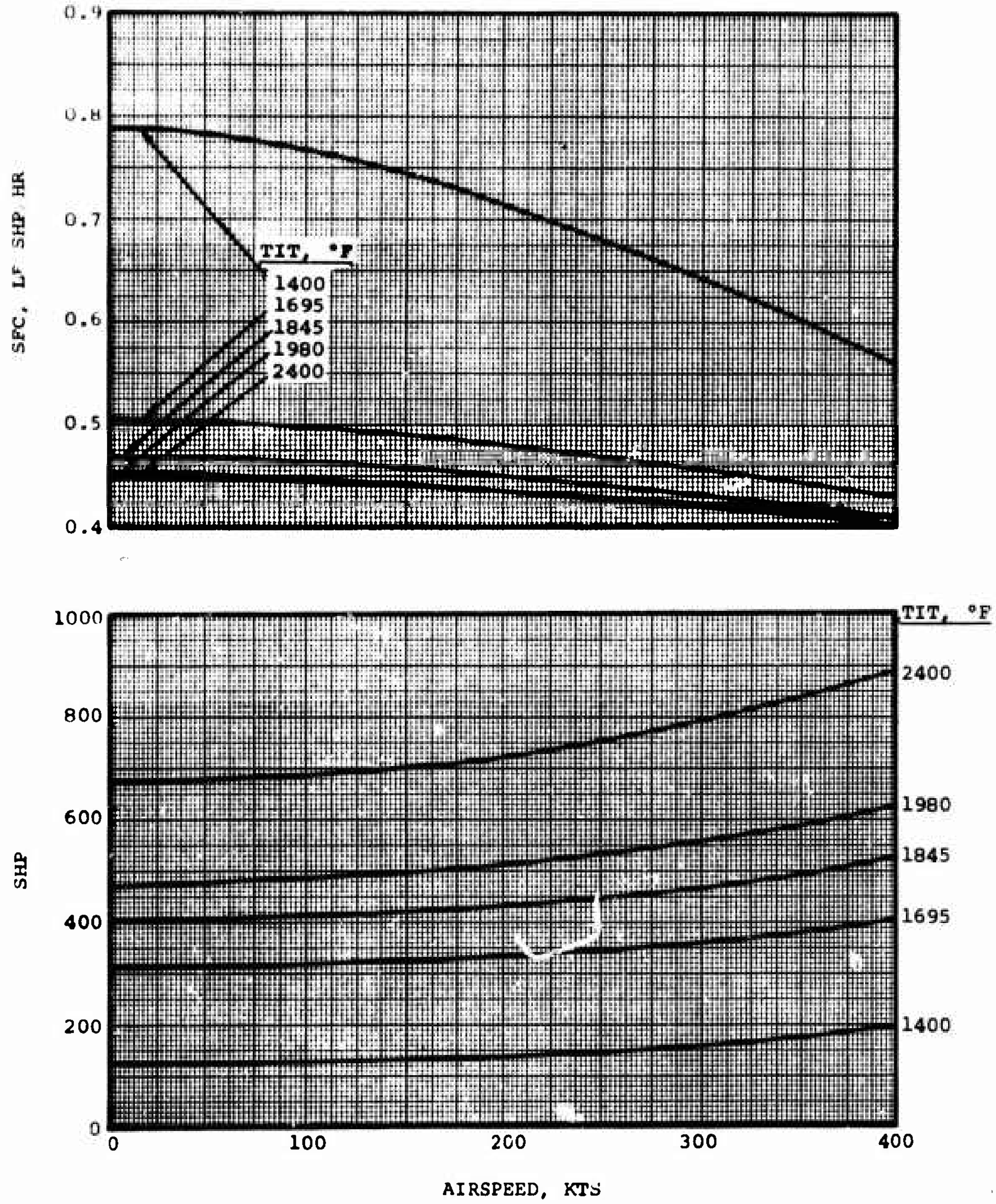

Figure 136. Shaft Horsepower and SFC Versus Airspeed for 2S-TSE at 20,000 Feet, Standard-Day Conditions.

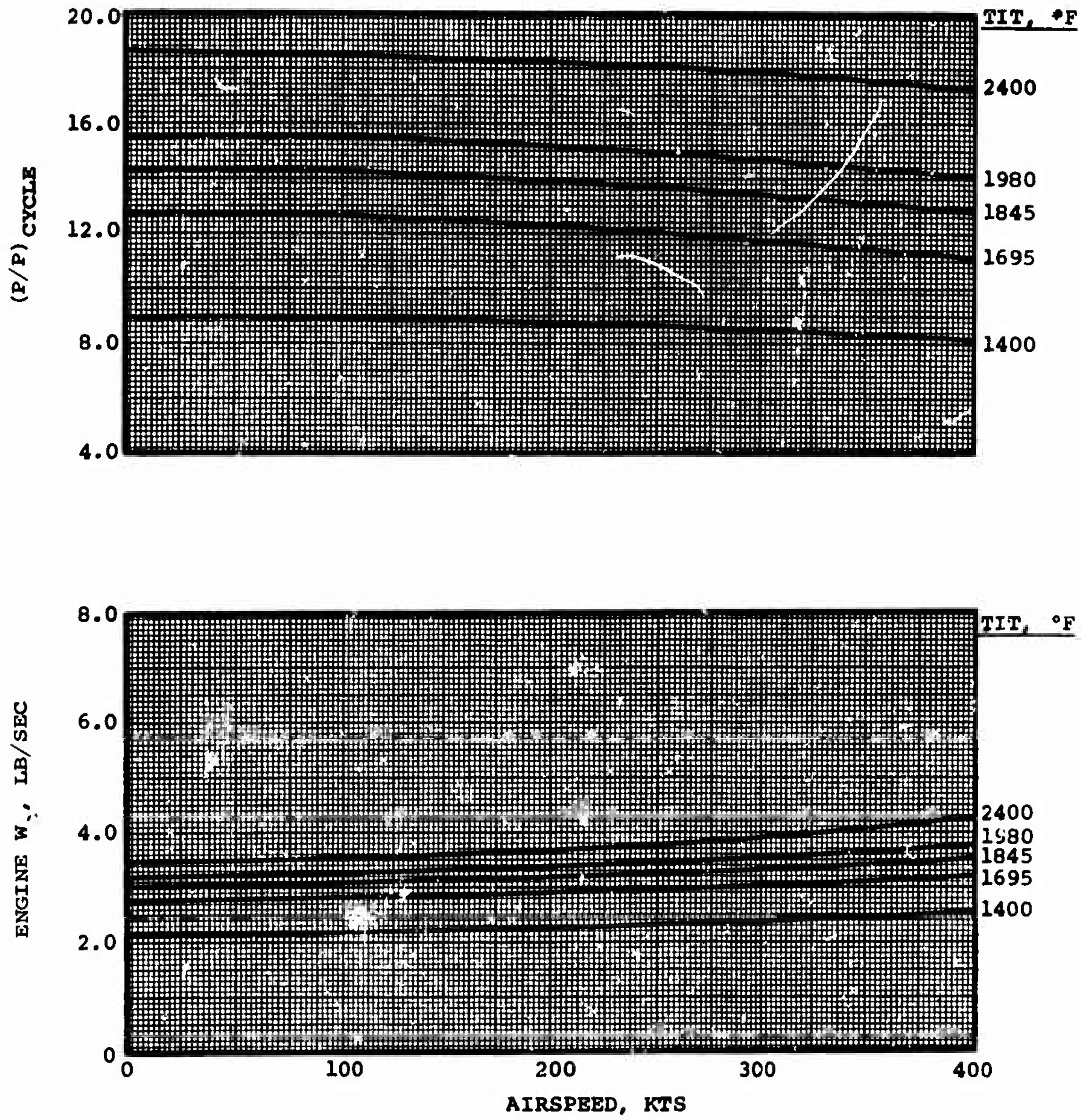

Figure 137. Engine Airflow and Cycle P/P Versus Airspeed for 2S-TSE at 20,000 Feet, Standard-Day Conditions.

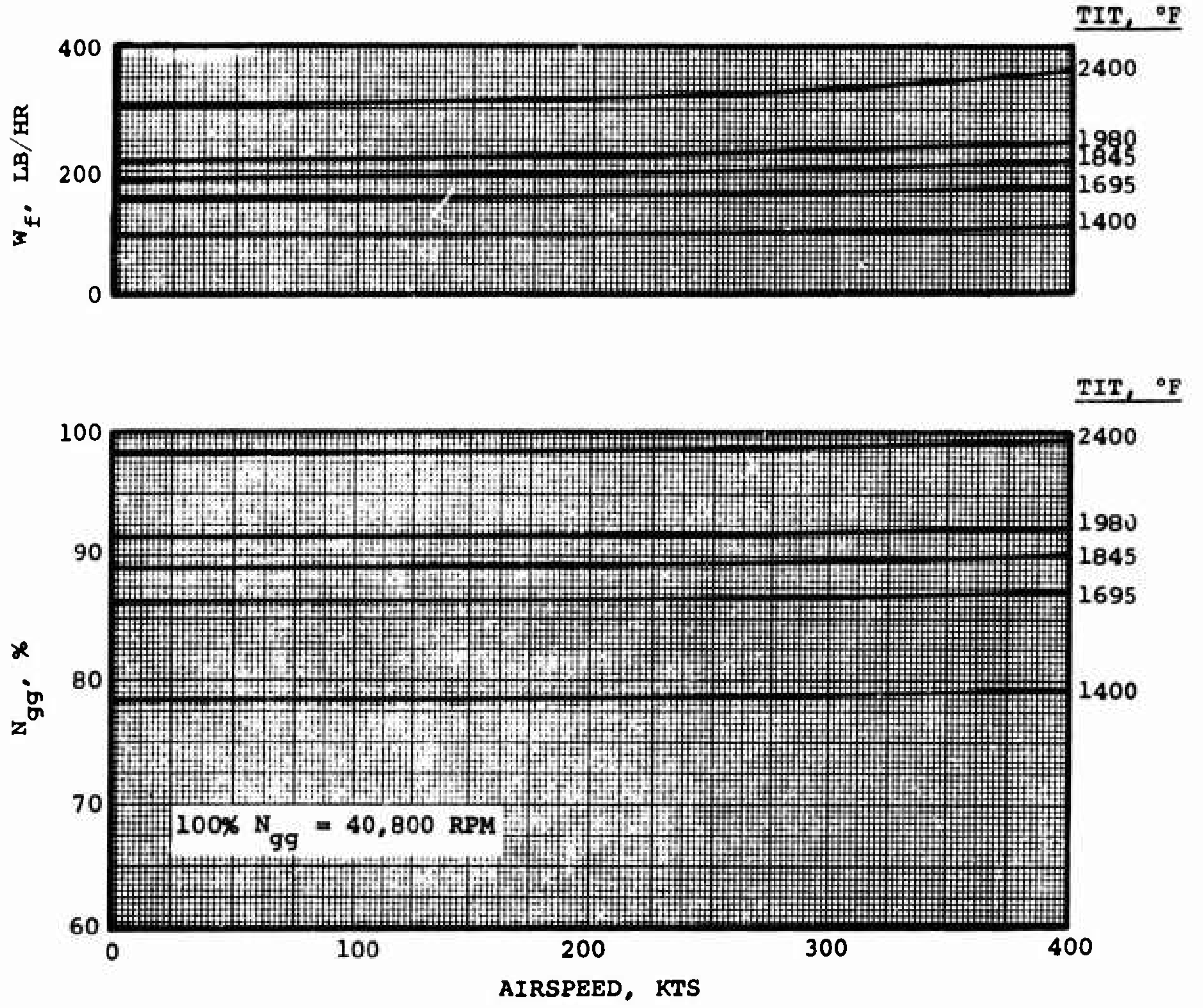

Figure 138. Gas Generator Speed and Fuel Flow Versus Airspeed for 2S-TSE at 20,000 Feet, Standard-Day Conditions.

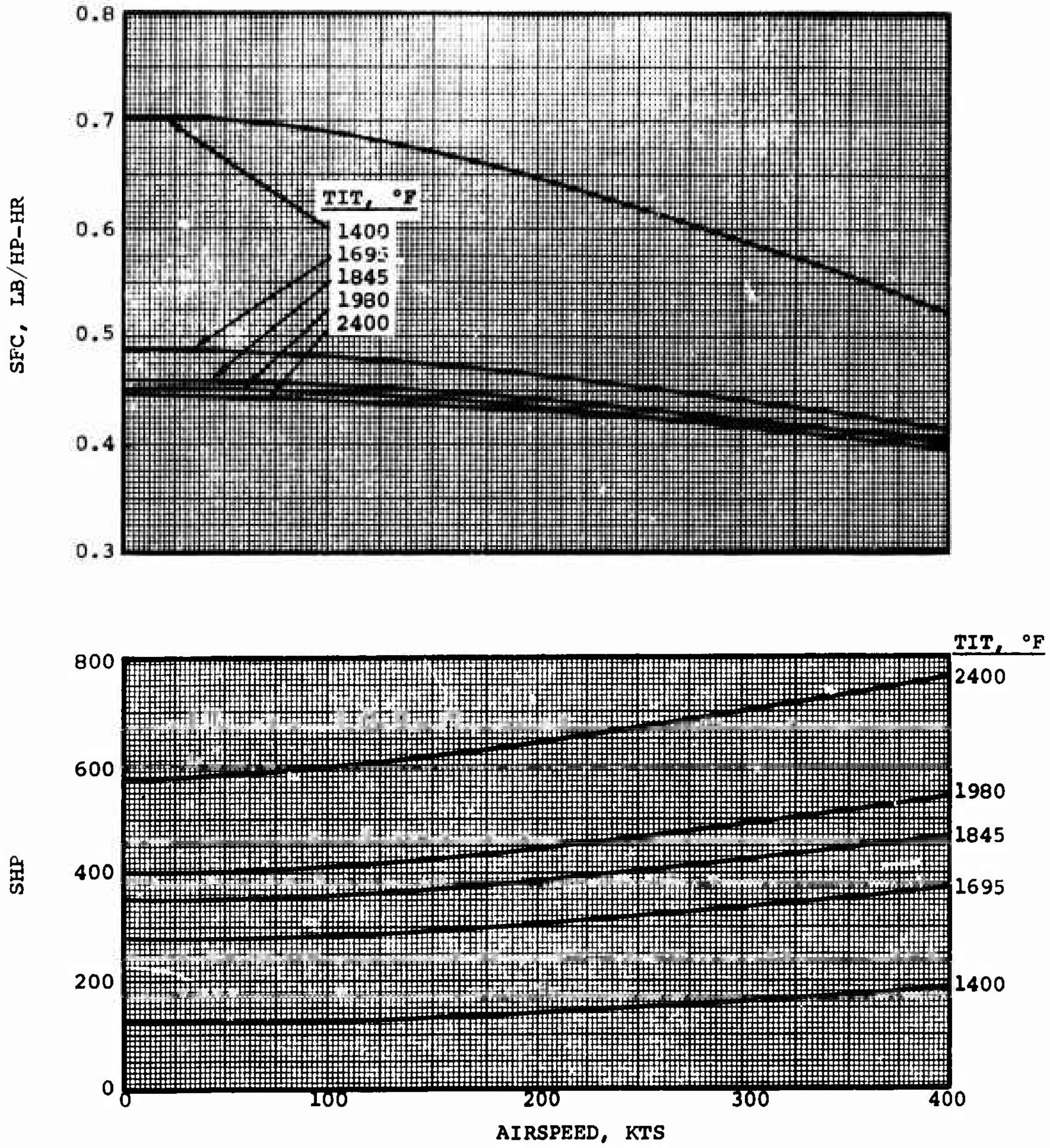

Figure 139. Shaft Horsepower and SFC Versus Airspeed for 2S-TSE at 25,000 Feet, Standard-Day Conditions.

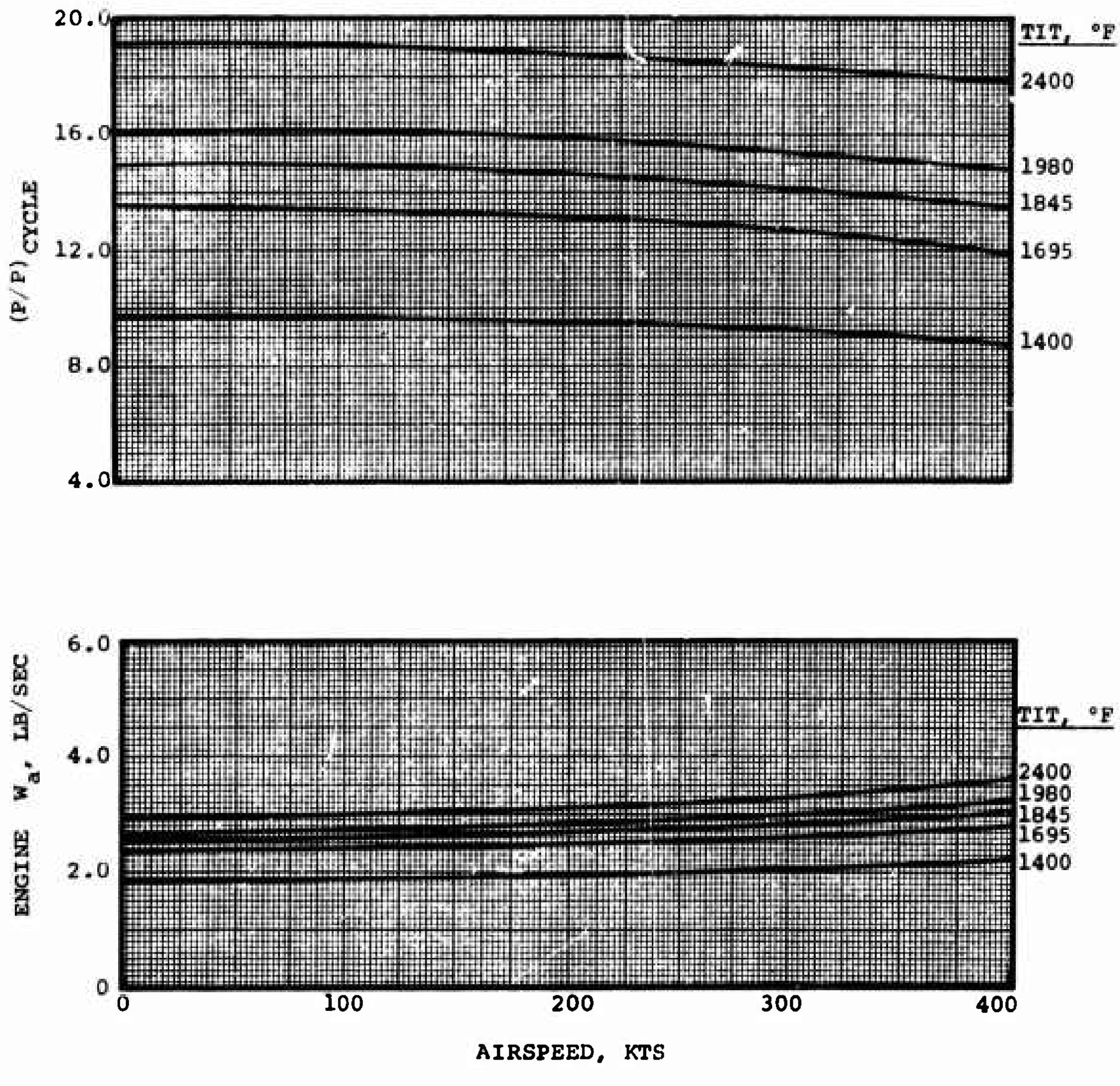

Figure 140. Engine Airflow and Cycle P/P Versus Airspeed for 2S-TSE at 25,000 Feet, Standard-Day Conditions.

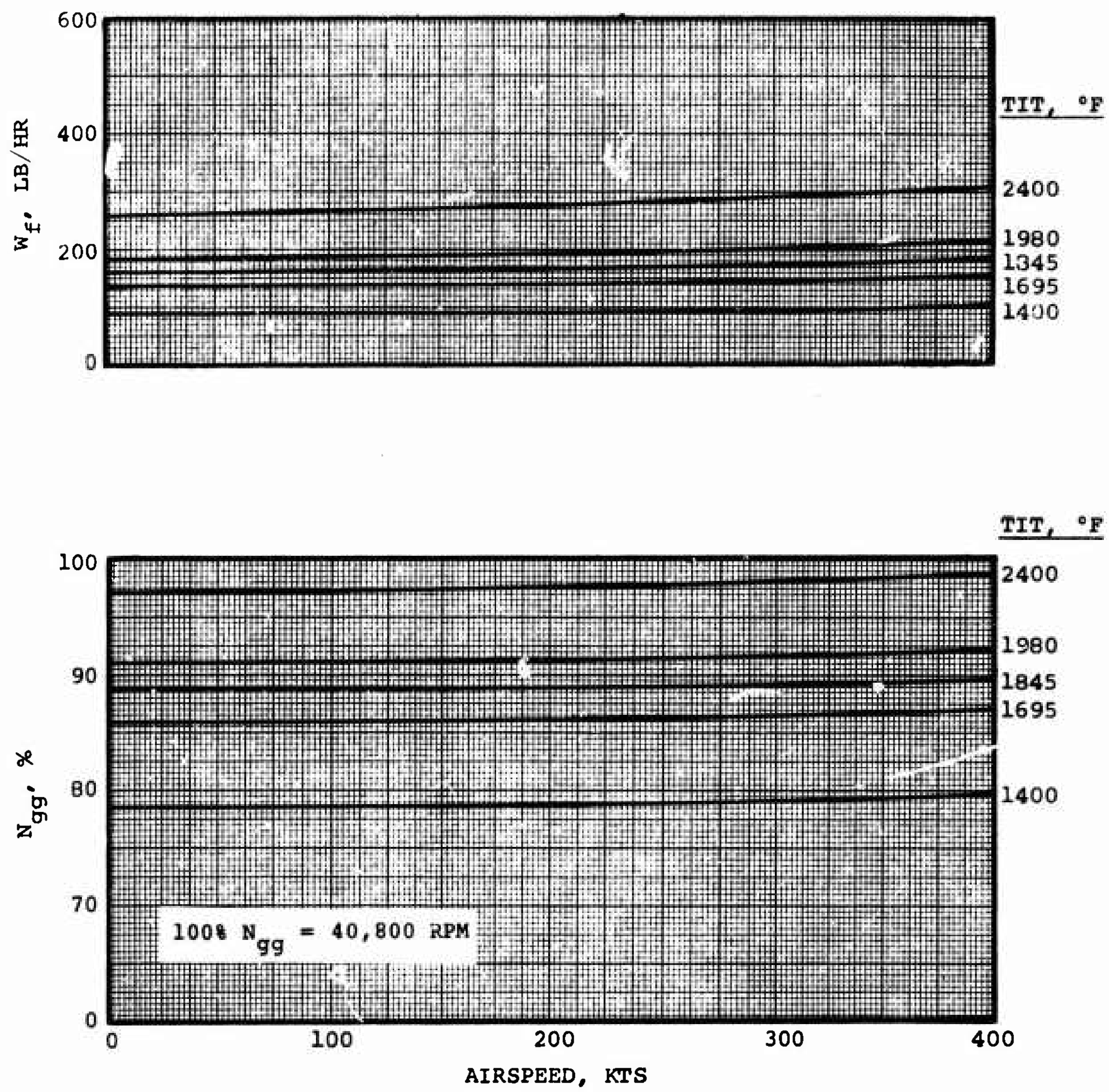

Figure 141. Gas Generator Speed and Fuel Flow Versus Airspeed for 2S-TSE at 25,000 Feet, Standard-Day Conditions.

APPENDIX III

FINAL COMPONENT PERFORMANCE SUMMARY

TABLE XVI. FINAL ENGINE CYCLE PARAMETERS AND COMPONENT PERFORMANCE AT MRP

Component Parameter	3S-RF-TSE Sea Level Std. Static	3S-RF-TSE 4000 Ft. 95°F Day, Static	2S-TSE Sea Level Std. Static	2S-TSE 4000 Ft. 95°F Day Static
INLET				
Flow, $W\sqrt{\theta}/\delta$ (lb/sec)	6.5	6.4	6.5	6.2
Pressure Drop, $\Delta P/P$ (%)	0.0	0.0	0.0	0.0
LOW-PRESSURE COMPRESSOR				
Actual Speed, N_{ACT} (rpm)	34,560	35,160	-	-
Corrected Speed, $N/\sqrt{\theta}$ (rpm)	34,560	34,000	-	-
Efficiency, η_{AD} (%)	84.0	84.1	-	-
Pressure Ratio, P/P	6.0:1	5.9:1	-	-
INNER COMPRESSOR DUCT				
Pressure Drop, $\Delta P/P$ (%)	2.9	2.9	-	-
Temperature Rise, ΔT (°F)	12.0	12.0	-	-
HIGH-PRESSURE COMPRESSOR				
Corrected Inlet Flow, $W\sqrt{\theta}/\delta$ (lb/sec)	1.45	1.45	-	-
Actual Speed, N_{ACT} (rpm)	67,000	68,900	-	-
Corrected Speed, $N/\sqrt{\theta}$ (rpm)	49,800	49,800	-	-
Efficiency, η_{AD} (%)	83.5	83.5	-	-
Pressure Ratio, P/P	2.67	2.69	-	-
COMPRESSOR (OVERALL)				
Efficiency, η_{AD} (%)	79.7	79.9	76.4	78.6
Pressure Ratio, P/P	15.5:1	15.3:1	16.0:1	14.8:1
Leakage W_1 (% W_a)	3.0	3.0	1.5	1.5
Corrected Speed, $N/\sqrt{\theta}$ (rpm)	-	-	40,800	39,500
COMBUSTOR				
Efficiency, η (%)	99.9	99.0	99.0	99.0
Pressure Drop, $\Delta P/P$ (%)	4.7	4.7	4.0	4.0
Fuel Lower Heating Value, LHV (Btu/Lb)	18,400	18,400	18,400	18,400
HIGH-PRESSURE TURBINE				
Efficiency, $\eta_{(T-T)}$ (%)	86.9	86.9	85.1	85.1
TIT, °F	2250	2400	2400	2400
Turbine Cooling Flow, W_c (%)	10.2	10.2	10.9	10.9
INTER-TURBINE DUCT				
Pressure Drop, $\Delta P/P$ (%)	2.0	2.0	2.0	2.0
POWER TURBINE				
Efficiency, $\eta_{(T-T)}$ (%)	89.7	89.6	92.2	91.7
Actual Speed, N_{ACT} (rpm)	46,000	46,000	34,450	34,450
LOW-PRESSURE TURBINE				
Efficiency, $\eta_{(T-T)}$ (%)	91.9	91.9	-	-
Corrected Speed, $N/\sqrt{\theta}$ (rpm)	18,300	18,000	-	-
TURBINE EXHAUST DUCT				
Turbine Exit Axial Mach No. M_e	0.40	0.40	0.37	0.37
Pressure Drop, $\Delta P/P$ (%)	4.10	4.10	3.80	3.80
MECHANICAL LOSSES				
Accessories, Bearings, Seals, etc., hp.	9.75	9.75	9.75	9.75
PERFORMANCE				
MRP, hp	1085	906	1178	899
SFC (lb/hp-hr)	0.445	0.452	0.459	0.471

Unclassified
Security Classification

DOCUMENT CONTROL DATA - R & D		
(Security classification of title, body of abstract and indexing annotation must be entered when the overall report is classified)		
1. ORIGINATING ACTIVITY (Corporate author) AiResearch Manufacturing Company of Arizona, Phoenix, Arizona	2a. REPORT SECURITY CLASSIFICATION Unclassified	
	2b. GROUP	
3. REPORT TITLE REVERSE-FLOW TURBOSHAFT ENGINE STUDY		
4. DESCRIPTIVE NOTES (Type of report and inclusive dates) Final Report		
5. AUTHOR(S) (First name, middle initial, last name) K. M. Johansen, W. H. Duncan		
6. REPORT DATE October 1970	7a. TOTAL NO. OF PAGES 200	7b. NO. OF REFS
8a. CONTRACT OR GRANT NO. DAAJ02-69-C-0089	9a. ORIGINATOR'S REPORT NUMBER(S) USAAVLABS Technical Report 70-48	
b. PROJECT NO. Task 1G162204A01409		
c.	9b. OTHER REPORT NO(S) (Any other numbers that may be assigned this report) PE-8134-R	
d.		
10. DISTRIBUTION STATEMENT This document is subject to special export controls, and each transmittal to foreign governments or foreign nationals may be made only with prior approval of U. S. Army Aviation Materiel Laboratories, Fort Eustis, Virginia 23604.		
11. SUPPLEMENTARY NOTES	12. SPONSORING MILITARY ACTIVITY U.S. Army Aviation Materiel Laboratories, Fort Eustis, Virginia	

13. ABSTRACT

This report presents the results of a program conducted to investigate the characteristics of a three-spool turboshaft engine having an unconventional turbine arrangement. In this engine, called a three-spool reverse-flow turboshaft engine, the combusted air passes through the high-pressure (HP) turbine, then the power turbine, and finally through the low-pressure (LP) turbine. The performance, weight, envelope, and transient characteristics of this engine were compared to those of a more conventional two-spool turboshaft engine of comparable life and component technology. In addition, the suitability of the three-spool reverse-flow turboshaft engine for recuperation was assessed.

The results of the study indicated that the three-spool reverse-flow turboshaft engine provides better part-power specific fuel consumption (SFC) than the two-spool engine. However, the engine is sensitive to ambient temperature variations, necessitating flat-rating of the engine to minimize the hot-day power lapse; is somewhat heavier; has a slightly larger envelope (length and diameter) and higher power-output speed; and requires approximately 3 seconds longer to accelerate from flight idle to 95 percent MRP.

The reverse-flow engine component arrangement appears to have its greatest potential in a recuperated configuration.

DD FORM 1 NOV 65 1473 REPLACES DD FORM 1473, 1 JAN 64, WHICH IS OBSOLETE FOR ARMY USE.

Unclassified
Security Classification

Unclassified

Security Classification

14 KEY WORDS	LINK A		LINK B		LINK C	
	ROLE	WT	ROLE	WT	ROLE	WT
Gas Turbines Aircraft Engines Propulsion Turboshaft Engines						

Unclassified

Security Classification